2011

MOLECULAR AND CHEMICAL DISSECTION OF CELLULOSE BIOSYNTHESIS IN PLANTS

Darby M. Harris
University of Kentucky, darbharris@hotmail.com

STUDENT AGREEMENT:

I represent that my thesis or dissertation and abstract are my original work. Proper attribution has been given to all outside sources. I understand that I am solely responsible for obtaining any needed copyright permissions. I have obtained and attached hereto needed written permission statements(s) from the owner(s) of each third-party copyrighted matter to be included in my work, allowing electronic distribution (if such use is not permitted by the fair use doctrine).

I hereby grant to The University of Kentucky and its agents the non-exclusive license to archive and make accessible my work in whole or in part in all forms of media, now or hereafter known. I agree that the document mentioned above may be made available immediately for worldwide access unless a preapproved embargo applies.

I retain all other ownership rights to the copyright of my work. I also retain the right to use in future works (such as articles or books) all or part of my work. I understand that I am free to register the copyright to my work.

REVIEW, APPROVAL AND ACCEPTANCE

The document mentioned above has been reviewed and accepted by the student's advisor, on behalf of the advisory committee, and by the Director of Graduate Studies (DGS), on behalf of the program; we verify that this is the final, approved version of the student's dissertation including all changes required by the advisory committee. The undersigned agree to abide by the statements above.

Darby M. Harris, Student

Dr. Seth DeBolt, Major Professor

Dr. Arthur G. Hunt, Director of Graduate Studies

MOLECULAR AND CHEMICAL DISSECTION OF CELLULOSE BIOSYNTHESIS IN PLANTS

DISSERTATION

A dissertation submitted in partial fulfillment of the
requirements for the degree of Doctor of Philosophy in the
College of Agriculture
at the University of Kentucky

By

Darby M. Harris

Lexington, Kentucky

Director: Dr. Seth DeBolt, Associate Professor of Horticulture

Lexington, Kentucky

2011

ABSTRACT OF DISSERTATION

MOLECULAR AND CHEMICAL DISSECTION OF CELLULOSE BIOSYNTHESIS IN PLANTS

Plant cell walls are complex structures that must not only constrain cellular turgor pressure but also allow for structural modification during the dynamic processes of cell division and anisotropic expansion. Cell walls are composed of highly glycosylated proteins and polysaccharides, including pectin, hemicellulose and cellulose. The primary cell wall polysaccharide is cellulose, a polymer composed of high molecular weight β-1,4-glucan chains. Although cellulose is the most abundant biopolymer on Earth, there is still a lot to learn about its biosynthesis and regulation. This research began by applying a variety of analytical techniques in an attempt to understand differences in cell wall composition and cellulose structure within the plant body, between different plant species and as a result of acclimation by the plant to different environmental conditions. Next, a number of different *Arabidopsis thaliana* lines possessing mutations affecting cell wall biosynthesis were analyzed for changes in cellulose structure (crystallinity) and biomass saccharification efficiency. One of these mutants, *isoxaben resistance1-2* (*ixr1-2*), which contains a point mutation in the C-terminal transmembrane region (TMR) of cellulose synthase 3 (CESA3), exhibited a 34% lower biomass crystallinity index and a 151% improvement in saccharification efficiency relative to that of wild-type. The culmination of this research began with a chemical screen that identified the molecule quinoxyphen as a primary cell wall cellulose biosynthesis inhibitor. By forward genetics, a semi-dominant mutant showing strong resistance to quinoxyphen named *aegeus* was identified in *A. thaliana* and the resistance locus mapped to a point mutation in the TMR of CESA1. *cesa1*^{aegeus} occurs in a similar location to that of *cesa3*$^{ixr1\text{-}2}$, illustrating both subunit specificity and commonality of resistance locus. These drug resistant CESA TMR mutants are dwarfed and have aberrant cellulose deposition. High-resolution synchrotron X-ray diffraction and ^{13}C solid-state nuclear magnetic resonance spectroscopy analysis of cellulose produced from *cesa1*^{aegeus}, *cesa3*$^{ixr1\text{-}2}$ and the double mutant shows a reduction in cellulose microfibril width and an increase in mobility of the interior glucan chains of the cellulose microfibril relative to wild-type. These data demonstrate the importance of the TMR region of CESA1 and CESA3 for the arrangement of glucan chains into a crystalline cellulose microfibril in primary cell walls.

Keywords: cell wall, cellulose microfibril, cellulose synthase, saccharification efficiency, crystallinity

Darby M. Harris

December 16, 2011

MOLECULAR AND CHEMICAL DISSECTION OF CELLULOSE BIOSYNTHESIS IN PLANTS

By

Darby M. Harris

Seth DeBolt

_____

Director of Dissertation

Arthur Hunt

_____

Director of Graduate Studies

December 16, 2011

_____

DEDICATION

In memory of my grandparents, James and Kitty Darby and Tony and Omah Harris, who were members of “The Greatest Generation” in this country and whose hard work and sacrifice have given those of my generation countless opportunities to succeed.

ACKNOWLEDGEMENTS

This dissertation was completed with the assistance and support of a number of individuals. I wish to thank the members of my Dissertation Committee: Seth DeBolt, Joe Chappell, Bob Houtz and Chris Schardl. I wish to also thank the outside examiner Czarena Crofcheck. The members of my committee provided me with guidance, encouragement, and multiple suggestions of ways in which to improve my approach to scientific research and ways to improve my dissertation.

I wish to thank the faculty of the College of Agriculture for their contributions to my professional development. More specifically, I want to thank the faculty in the Department of Horticulture, where I conducted a majority of my research. In addition to those faculty members who instructed courses I completed, I also want to thank Art Hunt, Director of Graduate Studies for the Plant Physiology Ph.D. Program.

A special thanks goes to Seth DeBolt, the director of my dissertation research, who led by example and helped greatly to raise the bar of my own research. Through his willingness to allow me freedom to explore the literature, attend conferences and participate in numerous research projects within his laboratory, I have gained the confidence necessary to step up to the next level and continue to develop my research ideas into the future.

I would also like to thank members of the DeBolt Lab for their help, encouragment and friendship over the last four years, including Jozsef Stork, Meera Nair, Kendall Corbin, Venu Mendu, Carloalberto Petti, Nihar Nayak, Ye (Summer) Xia, Mizuki Tateno, Chad Brabham, Matthew Simson and last but not least Randy Collins.

Most importantly, I thank my family. I thank my parents, Brenda and Jerry Harris, who have supported me in everything that I have done in life and who continue to show enormous excitement and offer relentless encouragement in my future adventures. I thank my sister Kate and my brother Josh who are a source of happiness and security. My wife and soulmate Isabella Jacovino, not only would I have never attempted this dissertation without her, but it would mean nothing without her by my side. We did this together and I know that we can accomplish anything set before us.

TABLE OF CONTENTS

LIST OF TABLES

LIST OF FIGURES

Chapter I

Chapter II

Chapter III

Chapter IV

Chapter V

Chapter VI

Chapter I*

The synthesis, regulation and modification of lignocellulosic biomass as a resource for biofuels and bioproducts

Most of the plant biomass is cell wall and therefore represents a renewable carbon source that could be exploited by humans for bioenergy and bioproducts. A thorough understanding of the type of cell wall being harvested and the molecules available will be crucial in developing the most efficient conversion processes. Herein, we review the structure, function and biosynthesis of lignocellulosic biomass, paying particular attention to the most important bioresources present in the plant cell wall: cellulose, hemicellulose and lignin. We also provide an update on key improvements being made to lignocellulosic biomass with respect to utilization as a second-generation biofuel and as a resource for bioproducts.

Bioenergy agriculture

Fossil fuel reserves could sustain our current energy needs well into the future (Vispute et al. 2010); but at what cost? The search for renewable forms of energy that emit less greenhouse gases relative to fossil fuels is likely to be a major challenge for the next generation of scientists and engineers. Improved efficiency and a smorgasbord of renewable 'green' technologies offer some light at the end of the tunnel (Lovins 2004). But on a case-by-case basis, the social and environmental costs associated with renewable forms of energy must be critically assessed to establish their longevity and sustainability (Fargione et al. 2008). Moreover, localized limitations for alternative energy production from low-carbon sources such as photovoltaic solar, wind, geothermal, biomass and hydroelectric will require the parallel development of various renewable energy sources. With respect to the subject of this review, the amount of land being dedicated to bioenergy crops is rapidly growing worldwide (Nass et al. 2007), and several recent analyses have suggested that the efficiency of bioenergy crops is

***This chapter is a combination of two manuscripts originally published as: Harris D and DeBolt S (2010)** Synthesis, regulation and utilization of lignocellulosic biomass. Plant Biotechnology Journal 8: 244-262 and **Harris D, Petti C, DeBolt S (2011)** The synthesis, regulation and modification of lignocellulosic biomass as a resource for biofuels and bioproducts. In *Advanced Biofuels and Bioproducts* (Lee JW, ed), New York: Springer Science+Business Media, LLC. Copyright permission was granted by the authors for inclusion in this dissertation.

overestimated (Fargione et al. 2008; Righelato and Spracklen 2007; Searchinger et al. 2008). Clearing of forested land and competition with food-based agriculture (starch and sucrose) may in fact enhance emissions from terrestrial carbon pools rather than sequester atmospheric carbon (Hill et al. 2006; Piñeiro et al. 2009). Hence, a paradigm shift towards using abandoned agricultural or nutritionally depleted land for the production of lignocellulosic (non-food) bioenergy crops to produce energy from cellulose and other cell wall polysaccharides, rather than starch from corn, is gaining momentum as a sustainable mitigation strategy (Campbell et al. 2008; Vitousek et al. 1995). Low-input bioenergy cropping systems are going to be essential to reduce impacts from pollution run-off and soil erosion (Tilman et al. 2006). To this end, plant biotechnology may have an opportunity to link with sustainability science to provide improved salt tolerance, water and nutrient use efficiency (Apse et al. 1999) and aid in enhancing the energy density of biomass species and the accessibility to otherwise recalcitrant cell wall polysaccharides. Herein, the focus is on reviewing the complexity of the plant cell wall with emphasis on cellulose and ways in which current biotechnology approaches have attempted to understand and manage its molecular architecture to improve the efficiency of lignocellulosic biofuel synthesis.

Making biofuel from plant cell walls rather than starch

To understand the process of biofuel production from lignocellulosic biomass, there are several terms to become familiar with: the term feedstock refers to the biomass crop, and these are generally warm season C4 perennial grasses, fast growing woody crops such as willow (*Salix* spp.) or poplar (*Populus* spp.) and common garden and agricultural waste. In the case of perennial grasses, the feedstock is generally allowed to senesce in the field. The biomass is harvested dry and transported to a cellulosic ethanol refinery where it is saccharified to turn the cellulose, hemicelluloses (HCs) and pectin into fermentable sugars. The term saccharification refers to the process of enzymatic bioconversion of cellulose and other wall polysaccharides into fermentable sugars. With respect to cell wall polysaccharides, cellulose represents a major source of fermentable sugars in lignocellulosic biomass and biotechnological applications directed towards the access to and biosynthetic manipulation and hydrolysis of cellulose have received significant attention. However, it is important to keep in mind that similar treatment of other cell wall polysaccharides, primarily the HCs, is relevant and important for the complete utilization of lignocellulosic biomass in the conversion process to biofuels.

Moreover, the future of hydrocarbon production from lignocellulosic biomass will shortly be realized via microbial fermentation, liquid phase catalysis and pyrolysis or gasification and has been recently reviewed (Regalbuto 2009).

The combined action of three different enzymes is required to effectively convert cellulose to glucose: endoglucanases, exoglucanases and cellobiases (Nidetzky et al. 1994). However, untreated lignocellulosic biomass is naturally very recalcitrant to enzymatic hydrolysis, and consequently, a substantial amount of enzyme would be required for efficient conversion into fermentable sugar directly. The recalcitrant nature of cellulose is attributed to many factors including the crystallinity of cellulose, accessible surface area and coating by lignin and HCs (Mosier et al. 2005) (Figure 1.1a, b). Therefore, prior to saccharification, a feedstock may be pretreated to loosen the interaction between lignin, cellulose and other wall polysaccharides and to increase the surface area for enzymes to access cellulose. There are various pretreatment regimes that can be implemented before subjecting the biomass to cellulolytic enzymes, including uncatalysed steam explosion, ammonia fibre/freeze explosion, acid- or base-catalysed hydrolysis and liquid hot water pretreatment (Mosier et al. 2005). Unfortunately, the current combined costs of hydrolytic enzymes and pretreatment processes reduce the ideal efficiency of biofuel production from cellulose, making the entire process two to threefold higher in price than production from maize grain starch (Sticklen 2008). This above-mentioned process does not include the utilization of lignin for bioenergy, in which case increasing proportional lignin content of plant biomass will be important. The chemistry involved in the thermal and chemical deconstruction of specific inter-unit linkages in lignin, as well as revealing how critical bonds in lignin can be cleaved in low-temperature oxidative processes, is central to this problem, because some inter-unit linkages are more readily cleaved, such as the β-*O*-4 linkage, which is cleaved in the pulping process (Campbell and Sederoff 1996). Hence, long-term efforts to directly manipulate the *in planta* biosynthetic processes via genetic engineering strategies will become apparent as our understanding of the cell wall biosynthetic process matures.

Key cell wall components and their functional significance

Before we examine the details of cellulose, hemicellulose and lignin biosynthesis we wish to review some additional classification terms that describe the type of cell wall. Every plant cell forms a primary cell wall (PCW) early in the cell lifecycle that is

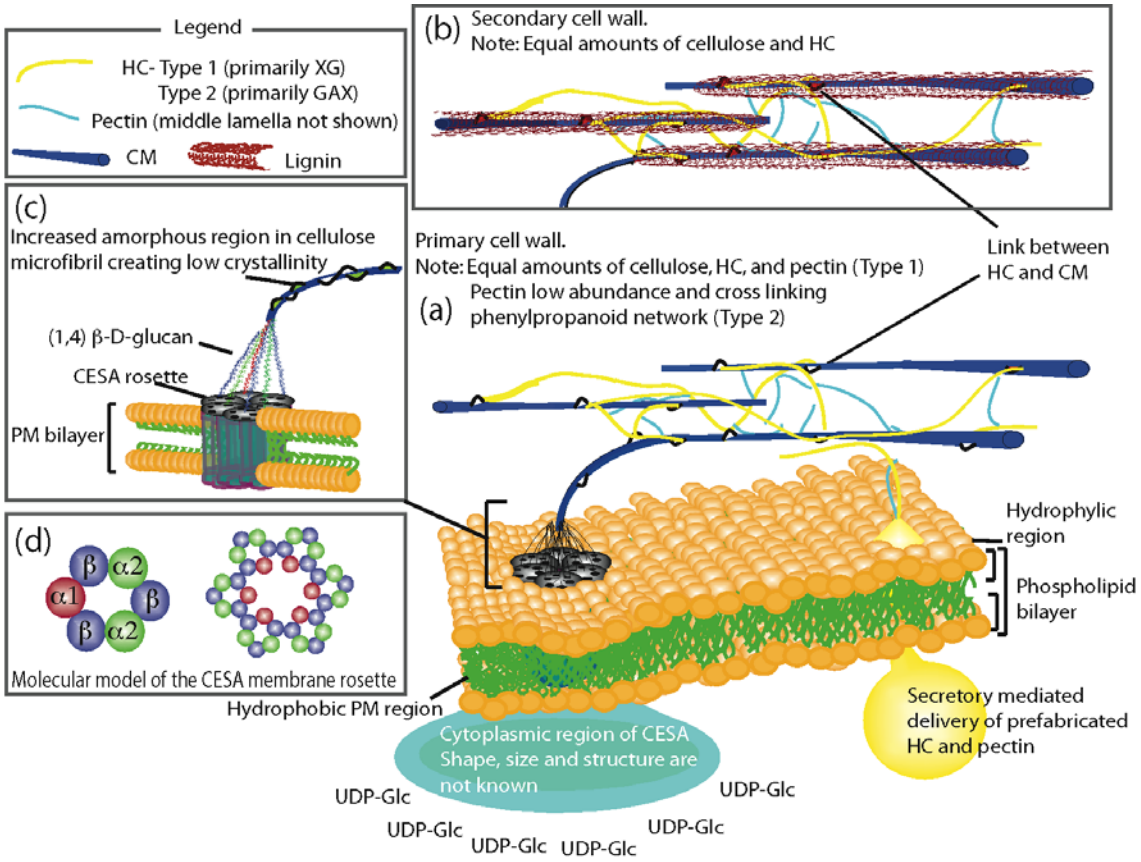

Figure 1.1. A schematic representation of the general structure of the plant cell wall matrix with emphasis on cellulose. (a) A simplified version of the primary cell wall is shown as a network of cellulose microfibrils (CMs) interlocked and coated by cross-linking hemicelluloses (HCs) which are primarily xyloglucans in Type I walls and glucuronoarabinoxylans in Type II walls. Together, CMs and HCs are embedded in a matrix of pectin (Type I) or acidic polysaccharides (Type II) with various levels of proteins (not shown) that aid in wall structure, assembly and degradation (Vergara and Carpita 2001). Cellulose is being synthesized at the plasma membrane (PM) by a symmetrical rosette of six globular cellulose synthase (CESA) protein complexes (Brown 1996; Herth 1983). The CESA rosette incorporates UDP-glucose molecules, present in the cytosol, into growing β-1,4- linked glucan chains, a total of 36 of which are produced by a single rosette which then co-crystallize to form a single microfibril (Herth 1983). Occasionally, the glucan chains are thought to form less ordered regions that structurally form amorphous zones along the length of the CM, rather than crystalline regions

(O'Sullivan 1997), which may serve as specific connection points between the cross-linking HCs and the CM (Himmel et al. 2007). The precise architecture of the CESA rosette complex and the identity of possible proteins with which it interacts at the cytosolic and extracellular PM surface have yet to be resolved. For this reason, and because most of the proteins, including the catalytic domains, extend into the cytoplasm, the CESA complex is depicted as a nebulous, ill-defined structure in the cytosol. HCs and pectin are shown being delivered, prefabricated, to the cell wall matrix through the PM via a Golgi secretory vesicle. (b) The secondary cell wall is produced by certain cell types as part of the maturation process after growth has ceased and consists primarily of CMs, HCs and lignin. Lignification results in the coating of CMs with anhydrous lignin polymers that further strengthen the cell wall but also present a major barrier in the biochemical conversion process to biofuels by blocking access and causing adsorption of hydrolytic enzymes (Mosier et al. 2005). (c) Cellulose crystallinity is another important factor contributing to the recalcitrant nature of most lignocellulosic biomass to enzymatic degradation (Mosier et al. 2005). Genetic modification of various CESA proteins has been shown to reduce the crystallinity of the lignocellulosic biomass and enhance enzymatic degradation (Harris et al. 2009). Perhaps this phenomenon occurs through the creation of more amorphous regions within the CM or by causing a proportional shift in the volume fraction of the cell wall between the cellulose, HC and lignin fractions. Here, the glucan chains produced by the different CESA protein are color-coordinated to match (d). (d) A molecular model of the CESA membrane rosette showing the molecular configuration of a single rosette subunit (left) and the complete CESA rosette (right). Each rosette subunit is identical, consisting of one molecule of α1, two molecules of α2 and three molecules of β type CESA proteins (adapted from Ding and Himmel 2006). Only three possible types of protein–protein interactions are necessary (α1-β, α2-β, and β-β) for rosette assembly in the PM or for rosette–rosette interaction to constitute the array formation seen in the parenchyma cells of maize stem pith (not shown) (adapted from Ding and Himmel 2006). Figure not to scale.

continuously produced throughout the period of cell growth. The shape and morphogenesis of plant cells are defined by the capacity of the PCW to constrain cellular turgor pressure in a directed and controlled manner thereby permitting anisotropic expansion during cell growth. All PCWs contain cellulose and a hydrated matrix consisting of hemicelluloses and pectins, with some structural proteins. Two distinctive types of PCWs, either Type I or Type II, have traditionally been described within the angiosperms based on polysaccharide composition (Carpita and Gibeaut 1993). However, accumulating evidence from other plant species, for example *Equisetum*, suggests that PCWs are best described as falling within a continuum rather than into specific classes. For the sake of general discussion on PCWs, the traditional classification can be maintained, although keeping in mind that some plant species may be found at either extreme of a particular range.

In general, Type I PCWs are present in dicots and liliaceous monocots while Type II PCWs can be found in the Poales (grasses) and related commelinid monocots (Carpita and Gibeaut 1993). The main defining feature used in describing the differences between the two wall types is the particular class of hemicelluloses (HCs) found within these walls. HCs, as will be discussed below, are heterogeneous in nature with multiple classes represented in different cell types, which is in contrast to cellulose, a homogenous polymer present in roughly the same configuration in all cell walls. Type I walls contain mostly the xyloglucan form of HCs embedded in a pectinaceous gel cross-linked to structural proteins (Carpita and Gibeaut 1993). Type II walls contain much less pectin and fewer proteins and their HCs are primarily glucuronoarabinoxylans (GAXs) and mixed-linkage (1,3), (1,4)-β-D-glucans embedded in an acidic polysaccharide network of highly substituted GAXs (Carpita and Gibeaut 1993). In addition, there is an appearance of cross-linking phenylpropanoid networks associated with HCs through the GAXs during the maturation of Type II cell walls as growth and cell expansion come to a halt (Carpita 1986; Scalbert et al. 1985). In either case, the PCW is a complex and dynamic structure that modulates cell expansion. In addition to PCWs, all plants deposit a thick secondary cell wall (SCW) around certain cell types after cell growth has ceased (Figure 1.2). These particular cell types primarily include xylem fibres and vessels in secondary xylem as well as inter-fascicular fibres and sclerids. The SCW contains cellulose, HCs predominating as either glucuronoxylans (dicots) or GAXs (grasses) and lignin with an additional acidic phenylpropanoid network present only in the walls of the

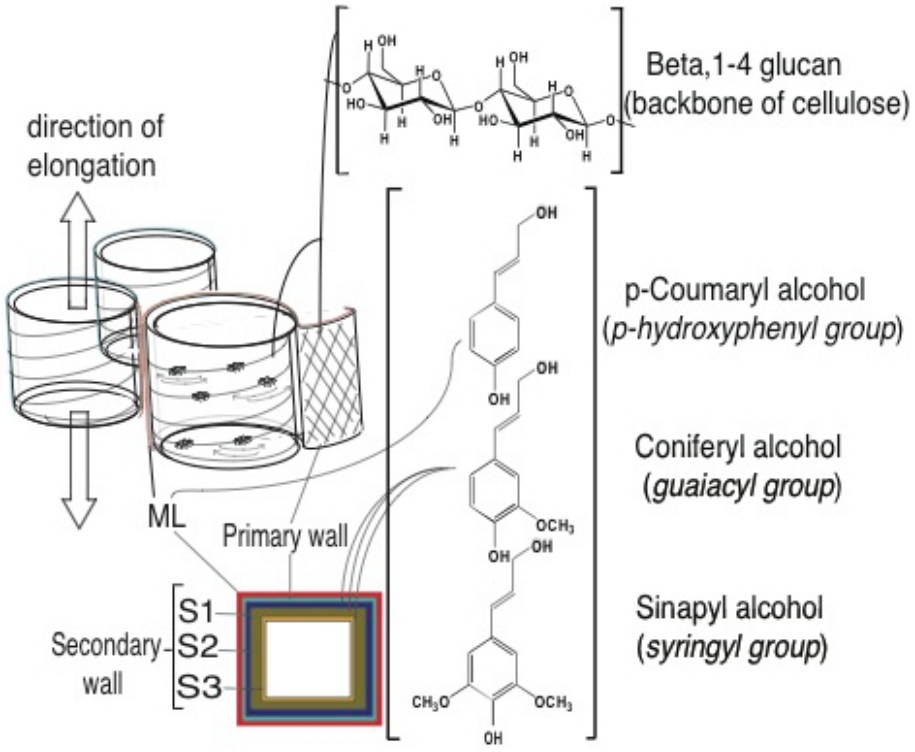

Figure 1.2. A model for cellulose and lignin after (Brett 2000) showing their location with respect to the entire cell and the structural formulae for their basic building blocks (for the most recent overview of lignin biosynthesis see: (Weng et al. 2008). Cellulose, in the form of microfibrils, is composed of multiple β-1,4 glucan chains produced from cellulose synthase rosette complexes at the plasma membrane that are shown moving perpendicular to the direction of cell elongation in the primary cell wall. Cellulose is generally enriched in the secondary cell wall (SCW) but is also heavily complexed with lignin throughout the multiple lamellae (S1, S2 and S3) of the SCW (Mellerowicz et al. 2001). Lignin is derived from three precursors: p-coumaryl, coniferyl and sinapyl alcohols and is a major constituent in all lamellae of the SCW accounting for 15%–25% of the total plant dry matter in prominent bioenergy feedstock grasses (Stork et al. 2009) but can be found to lesser extents in certain feedstocks like sorghum or to slightly greater extents in certain trees (Pauly and Keegstra 2008).

grasses (McCann and Roberts 1991). The SCW primarily contains cellulose, HCs and the polyphenolic compound lignin which provides added strength, protection and hydrophobicity to plant tissues. The SCW is also the primary component of wood cells found in trees. In typical angiosperm trees such as *Populus* spp., the SCW consists of three layers (S1, S2, and S3), which are collectively composed of approximately 45% cellulose, 25% HCs and 20-25% lignin (Andersson-Gunnerås et al. 2006) (Figure 1.2). In terms of cell type, over 50% of poplar wood is composed of xylem fibers which in turn contain most of their mass in the S2 layer of the SCW, thus making this the main area of focus in attempts to modify wood properties (Mellerowicz and Sundberg 2008). While most herbaceous plants lack woody tissue, the SCW is generally much thicker and more energy dense than the PCW in these species. Therefore, an important overall consideration for crops being used as feedstocks for bioenergy, such as grasses and fast growing woody corps, is that a majority of their cell wall polysaccharides and lignin will be bound up in the more recalcitrant SCW tissues.

In general, the cell wall can be likened to a molecular building block of the plant organism, where surrounding the cells of young plant tissue cellulose provides the structural support that is linked together by a more flexible polysaccharide matrix of HC and acidic polysaccharides or pectin which provides the flexibility for expansibility of the cell (Willats et al. 2001) (Figure 1.1a). In the walls surrounding the cells of more mature tissues in herbaceous plants or in the trunks and major limbs of trees, cellulose is surrounded by lignin that provides added strength, water resistance and pathogen protection to the plant (Campbell and Sederoff 1996) (Figure 1.1b). The molecular capital and energy for making cell wall sugars and polymers is derived from atmospheric carbon and sunlight via photosynthesis (Farquhar et al. 2001). In fact, highly efficient carbon-fixing plants, such as the hybrid *Miscanthus* x *giganteus*, can convert approximately 2% of incident solar radiation into biomass (Beale and Long 1995). Therefore, the use of cell walls as a renewable form of energy is highly attractive because plants have adapted to proliferate in nearly every biome on the planet (Wright et al. 2004). What has also become apparent in discussions involving the conversion of cell wall polysaccharides to biofuels is the heterogeneity of the potential feedstocks used in the process and how to progress towards a more complete understanding of the molecular architecture within these different feedstocks. A better understanding of the

structure and synthesis of the cell wall can facilitate the development of more sophisticated biotechnological applications for the purposes of wall deconstruction.

Synthesis and regulation of key cell wall biopolymers

Cellulose

As has been noted many times, the distinction given to cellulose as the most abundant carbohydrate found in plants also makes it the most abundant biopolymer in nature and an obvious target for bioconversion. In plant cells, cellulose exists in the form of paracrystalline microfibrils that are made up of multiple, unbranched, parallel glucan chains, which in turn are composed of (1,4) linked β-D-glucosyl residues that are alternatively rotated 180° along the polymer axis (Hermans 1949). Plants synthesize cellulose at the plasma membrane by a symmetrical rosette of six globular protein complexes, collectively called the cellulose synthase complex (CSC) and totaling 25-30 nm in diameter (Brown 1996). Each lobe of the CSC rosette contains several structurally similar cellulose synthase (CESA) subunits (Pear et al. 1996; Smith and Ennos 2003). CESAs are classified within family 2 of glycosyltransferases, which not only catalyze the addition of many glucose residues to a growing glucan chain (processive), but also invert each glucose residue to create β-linkages, thus making cellobiose the repeating unit (Richmond 2000). CESAs polymerize β-1,4-glucan chains from the activated sugar donor UDP-glucose, which is supplied by either UDP-glucose pyrophosphorylase or sucrose synthase. Several reports have suggested that sucrose synthase provides most of the UDP-glucose to CESAs due to the existence of a membrane bound form of this enzyme that is often highly expressed in tissues actively producing cellulose (Geisler-Lee et al. 2006) or by its effect on biomass production when over-expressed (Coleman et al. 2006; Coleman et al. 2009). However, it should be noted that there has not yet been any evidence to show direct physical association of sucrose synthase with the CSC and thus both sources of UDP-glucose are likely used. With regards to polymerization, although there is strong evidence to support the addition of glucosyl units to the non-reducing end of glucan chains, the molecular mechanism by which CESA create a β-1,4-glucan chain has not yet been elucidated (Koyama et al. 1997; Lai Kee Him et al. 2002) (Figure 1.1). Bioinformatic analyses have provided putative substrate binding and catalytic residues, however it is not clear whether glucan chains are synthesized by the addition of one or two glucosyl units (Richmond 2000).

The predicted CESA topology suggests the existence of 8 transmembrane helicies that anchor the protein in the plasma membrane. This even number of helices means that the N-terminal and C-terminal ends of the protein should reside on the same side of the plasma membrane. Current models have placed both termini on the cytoplasmic side of the membrane, which also allows for a cytoplasmic location for the putative substrate binding and catalytic sites. One of the hypothetical three-dimensional CESA structures suggests that the 8 transmembrane helicies form a pore in the plasma membrane through which the growing glucan chain passes to reach the cell wall (Delmer 1999). Although there is still no reported crystal structure of a plant CESA, a clearer picture of how the glucan chain is transported to the cell wall is now emerging. The recent structure determination of subunit D in the CSC of *Gluconacetobacter xylinus* (AxCeSD) in complex with a short glucan (cellopentaose), suggested that glucan chains are indeed extruded through the PM via a distinct pore (Hu et al. 2010). This study in a bacterial system bolsters the idea that the protein transmembrane helicies define the membrane pore, and in the case of plant CESAs this would include the 8 transmembrane helicies, which would therefore facilitate glucan chain extrusion. Current models of the CSC propose that each of the six protein complexes may synthesize six glucan chains, each glucan chain presumably synthesized by a single CESA protein, thus a total of 36 glucan chains are produced by a single rosette which then co-crystallize to form one microfibril (Ding and Himmel 2006; Doblin et al. 2002; Scheible et al. 2001) (Figure 1.1). The length of individual glucan chains varies depending on the cell type and plant species examined, but in general can be from 1000-8000 (PCW) to as much as 16000 (SCW) glucose molecules in length (Triplett and Timpa 1995). The formation of the crystalline structure of cellulose is highly dependent upon the hydrogen bonding of three hydroxyl groups that are present on each glucosyl residue (Nishiyama et al. 2002; Nishiyama et al. 2003). Most naturally occurring cellulose is referred to as cellulose I and maintains two co-existing phases, cellulose Iα (triclinic unit cell) and cellulose Iβ (monoclinic unit cell). Terrestrial plants contain a higher proportion of cellulose Iβ that primarily composes the more crystalline inner chains of the microfibril core, while both forms of cellulose compose the chains in the surrounding paracrystalline sheath (Qian et al. 2005; Šturcová et al. 2004). The cellulose microfibril also contains intermittent regions of less ordered glucan chains that structurally create amorphous zones along the microfibril (O'Sullivan 1997). The mechanism by which amorphous zones form is unclear other than possibly by the random exclusion of portions of glucan chains during the assembly

(crystallization) process. With regards to the mechanism by which glucan chains assemble, the sequence of amino acids that define the pore in the bacterial subunit D appear crucial for creating the proper environment for glucan chain passage (Hu et al. 2010). It has been speculated that an analogous pore structure, if present in plant CESA, may be responsible for correctly orienting the glucan chain to ensure proper hydrogen bonding to adjacent chains once it emerges from the CESA and into the cell wall environment (Harris et al. 2009). If this idea is correct, mutations within the transmembrane helicies of plant CESAs could affect the threading of the glucan chain through the membrane pore and could ultimately influence microfibril crystallization. Functionally, these amorphous zones along the microfibril are hypothesized to serve as attachment points for HCs that cross-link one microfibril to another and help strengthen the cell wall (Himmel et al. 2007). Importantly, both the degree of polymerization (glucan chain length) and degree of crystallization (inter- and intra- chain hydrogen bonding) are two intrinsic properties of cellulose that have some effect on its enzymatic hydrolysis (Mansfield et al. 1999).

In the model plant *Arabidopsis thaliana*, 10 genes (*CESA1-10*) have been identified that code for the CESA proteins (Richmond 2000). Biochemical and genetic evidence suggests that three *CESA* genes, *CESA4*, *-7* and *-8* directly interact and are necessary for cellulose deposition during SCW formation (Taylor et al. 2003; Turner and Somerville 1997). Similar evidence suggests that essential members of the PCW CSC include CESA1, -3, and a small family of CESA6-related proteins providing the third component that vary temporally and spatially (Persson et al. 2007). Spatiotemporal regulation of *CESA* genes has recently been uncovered, with *CESA9* implicated in forming the secondary cell wall in epidermal testa cells of the *A. thaliana* seed coat (Segal et al. 1959). A similar set of *CESA* genes have been identified in the genomes of many higher plants including 10 genes in (Tanaka et al. 2003), 12 genes in maize (Appenzeller et al. 2004; Holland et al. 2000), 18 genes in poplar (Djerbi et al. 2005; Joshi et al. 2004), and 8 genes in barley (Burton et al. 2004) (see Table 1.1 for a complete list of mutations in *A. thaliana CESA* genes).

Regulation of CESA activity

The fundamental mechanisms underlying the assembly, activation, guidance and termination of the CESA rosette remain unclear. There is evidence to suggest that CESA

rosette assembly initially occurs in the endoplasmic reticulum, and the complex then moves to the cisternae and vesicles of the Golgi where it is eventually supplied to the PM via the trans-Golgi network (Gardiner et al. 2003; Haigler and Brown 1986). In addition, there is also evidence suggesting that rosette assembly may occur by the homo- and heterodimerization of CESA proteins through redox-regulated disulphide bond formation between some of the cysteine residues within their N-terminal zinc-binding domain (RING-motif) present in all CESA proteins (Kurek et al. 2002). However, recent evidence has emerged regarding the interaction between SCW CESA proteins suggesting that this RING-motif is not essential for CESA interaction, but may instead enhance the interaction between CESA proteins in conjunction with non-covalent inter-molecular interactions and may also play a role in recruitment of other unknown interacting factors (Atanassov et al. 2009; Timmers et al. 2009). Furthermore, convincing evidence has been presented that many enzymes involved in cell wall polysaccharide biosynthesis, including CESA proteins, reside in lipid rafts (Niklas and Cobb 2008). Further research is needed to deduce how the sterol- /sphingolipid-rich lipid rafts support CESA, and whether they have a role in organizing the CESA complex in the PM-cell wall continuum.

Recently, CSI1 (cellulose synthase-interactive protein 1) was identified in *A. thaliana* as the first protein, other than the CESA proteins, to interact with the CSC in higher plants (Gu et al. 2010). However, a number of other proteins have been implicated in the overall process of cellulose synthesis by genetic approaches (Fagard et al. 2000; Mouille et al. 2003; Scheible and Pauly 2004; Taylor et al. 2004; Williamson et al. 2001). These include *korrigan* (*kor*) a membrane bound β-1,4-endoglucanase (Nicol et al. 1998; Sato et al. 2001; Szyjanowicz et al. 2004; Zuo et al. 2000), *cobra* (*cob*) a glycosyl-phosphatidyl-inositol anchored protein of unknown function (Roudier et al. 2005; Schindelman et al. 2001), *kobito/elongation defective 1* (*kob/eld1*) a novel plant specific membrane protein of unknown function (Brocard-Gifford et al. 2004; Lertpiriyapong and Sung 2003; Pagant et al. 2002), a katanin-like protein (Bouquin et al. 2003; Burk et al. 2001; Webb et al. 2002) and *ectopic lignin in pith* (*elp1*), a basic chitinase-like protein (Zhong et al. 2002b). In addition, research has shown that a reduction in expression of certain members of the receptor-like serine/threonine protein kinases (RLKs), specifically members of the wall-associated kinases (WAKs), leads to a loss of cell expansion and a dwarf phenotype (Lally et al. 2001; Wagner and Kohorn 2001). WAKS contain

extracellular domains that can be linked to pectin molecules in the cell wall, in addition to a transmembrane-spanning domain that crosses the PM and an intracellular kinase domain (He et al. 1996; Verica and He 2002). It has been shown that a single *wak2* mutation exhibits a dependence on sugars and salts for seedling growth (Kohorn et al. 2006). This mutation also reduces the expression and activity of vacuolar invertase, often a key factor in turgor and expansion (Kohorn et al. 2006). WAKs may thus provide a molecular mechanism linking cell wall sensing (via pectin attachment) to regulation of solute metabolism, which in turn is known to be involved in the turgor maintenance of growing cells. An RLK in a separate family from the WAK proteins, but believed to act as a cell wall sensor, is THESEUS1, which has been show to attenuate, but not completely rescue, the shortened hypocotyl phenotype of the CESA6 null mutant *procuste* (Hématy et al. 2007). Gene expression studies have revealed that CESA proteins are expressed spatially and temporally throughout plant development (Scheible et al. 2001), and particular CESA subunits are expressed in similar spatial and temporal patterns (Brown et al. 2005; Persson et al. 2005).

Transcription factors may play an important role in PCW and SCW biogenesis as evidenced by the vascular-related NAM, ATAF1/2, and Cuc2 (NAC)-domain (VND)6 and VND7 containing plant-specific transcription factors that have been shown to regulate the differentiation of tracheary elements (Kubo et al. 2005). Specifically, these authors show that overexpression of VND6 and VND7 can induce transdifferentiation of various cells into metaxylem- and protoxylem-like vessel elements in *A. thaliana* and poplar, respectively. Additional plant-specific transcription factors, designated NAC secondary wall-thickening promoting factors (NST), are responsible for secondary wall thickenings in cells other than the xylem vessels (Mitsuda et al. 2007). It has been shown that NST1 and NST2 act redundantly in secondary wall thickenings of the anther endothecium (Mitsuda et al. 2005), and that NST1 and NST3 provide a similar redundant regulation of secondary wall thickening in inter-fascicular fibres and secondary xylem (Mitsuda et al. 2007; Zhong et al. 2007b). Two members of the myeloblostosis (MYB) transcription factor family, MYB26 and MYB46, can also regulate secondary wall biosynthesis by either regulating the expression of NST1 and NST2 and thus control cell wall thickening in the anther endothecium or by serving as the direct target of NST3 and control cell wall thickening in fibres, respectively (Yang et al. 2007; Zhong et al. 2007a). Collectively, these proteins can be viewed as important transcriptional switches that turn on the

Table 1.1 Cellulose synthase (CESA) mutations in *Arabidopsis thaliana* and their source. Adapted from Daras et al. 2009.

Protein	Gene ID	Allele	Mutation	Phenotype	Cell Wall	Reference
CESA1	At4g32410	*rsw1-1*	A549V	Root swelling, stunted growth (heat, temperature sensitive)	Primary	Arioli T et al. 1998
		rsw1-2	G631S	Lethality		Gillmor et al. 2002
		rsw1-10	T-DNA	Root swelling, stunted growth		Fagard et al. 2000
		rsw1-20	D780N	Swollen root, abnormal dark morph., reduced root and hypocoty growth		Beeckman et al. 2002
		rsw1-45	E779K	Swollen root, abnormal dark morph., reduced root and hypocoty growth		Beeckman et al. 2002
		ags1-2	A903V	Semidominant resistance to quinoxyphen, mild growth phenotype		DeBolt unpublished
		cesa1	T-DNA	Gametophytic lethality, deformed and sterile pollen grains		Persson et al. 2007
CESA2	At4g39350	*cesa2*	Ds	MT orientation, abnormal cell expansion, leaf cell wall defects	Primary	Chu et al. 2007
		cesa2	T-DNA	Short etiolated hypocotyl		Desprez et al. 2007; Persson et al. 2007
CESA3	At5g44030	*ixr1-1*	G998D	Semidominant resistance to isoxaben	Primary	Scheible et al. 2001
		ixr1-2	T942I	Semidominant resistance to isoxaben, mild growth phenotype		Scheible et al. 2001
		cev1	G617E	Stunted root growth, induction of defense responses		Ellis et al. 2002
		eli1-1	S301F	Swollen root and hypocotyl, stunted growth, induction of defense response		Caño-Delgado et al. 2003
		eli1-2	A522V	Swollen root and hypocotyl, stunted growth, induction of defense response		Caño-Delgado et al. 2003
		rsw5	P1056S	Root swelling, stunted growth at permis. temperature		Wang et al. 2006
		than	P578S	Root swelling, stunted growth at permis. temperature, semidom., lethality		Daras et al. 2009
		repp3	P578L	Shorten, swollen root, short etiolate hypocotyl in *PIN2::PIN1-HA;pin2* bkgd		Feraru et al. 2011
		cesa3	T-DNA	Gametophytic lethality, deformed and sterile pollen grains		Persson et al. 2007
CESA4	At5g44030	*irx5-1*	Ds	Irregular xylem vessels	Secondary	Taylor et al. 2003
		irx5-2	W995Stop	Irregular xylem vessels		Taylor et al. 2003
		irx5-3	Q263Stop	Irregular xylem vessels		Taylor et al. 2003
CESA5	At5g64740	*cesa5*	T-DNA	Reduced mucilage deposition on seed coat	Primary	DeBolt unpublished
CESA6	At5g64740	*ixr2*	R1064W	Semidominant resistance to isoxaben	Primary	Desprez et al. 2002
		prc1-1	Q720Stop	Swollen and stunted roots and dark-grown hypocotyls, many alleles		Fagard et al. 2000
				Root hair phenotype		Singh et al. 2008
		cesa6	T-DNA	Subtle growth phenotypes		Persson et al. 2007

Continued on the following page.

CESA7	At5g17420	*irx3*	W859Stop	Collapsed xylem, weak stem	Secondary	Taylor et al. 1999
		fra5	P557T	Fragile fibers, weak stem, extremely thin fiber walls, semidominant		Zhong et al. 2003
		mur10-1	W444Stop	Reduction in growth and dark-green coloration of aerial parts		Bosca et al. 2006
		mur10-2	H734Y	Reduction in growth and dark-green coloration of aerial parts		Bosca et al. 2006
CESA8	At4g18780	*irx1-1*	D683N	Weak stem, collapsed xylem vessels	Secondary	Taylor et al. 2000
		irx1-2	S679L	Weak stem, collapsed xylem vessels		Taylor et al. 2000
		fra6	R362K	Reduced fiber wall thickness		Zhong et al. 2003
		lew2-1	W217Stop	Tolerant to osmotic stress, more severe than *irx1*		Chen et al. 2005
		lew2-2	L792F	Tolerant to osmotic stress, more severe than *irx1*		Chen et al. 2005
CESA9	At2g21770	*cesa9*	T-DNA	Depleted secondary cell wall seed coat testa cells	Primary/Secondary	Stork et al. 2010

developmental program of secondary wall biosynthesis during the development of fibres, vessels and anther endothecium (Zhong and Ye 2007). Interestingly, it has been shown that under appropriate growth conditions, hypocotyls of *A. thaliana* had a very similar structure to secondary xylem (wood) (Chaffey et al. 2002). There was complete suppression of secondary wall formation in the secondary xylem (except for the xylem vessels) of the hypocotyls in the *nst1-1*/*nst3-1* double knockout mutants of *A. thaliana* (Mitsuda et al. 2007). In addition, there are putative homologues of NST1 and NST3 in the genome of poplar, suggesting that a common mechanism for the control of wood formation exists in herbaceous and woody plants, and that NSTs may play an important role in secondary wall synthesis during wood formation. Taking into consideration the fact that fibres are the most abundant secondary wall-containing cell type in dicot wood, the identification of these genes could provide important tools for the genetic manipulation of wood quality and production in the feedstocks of biofuels. But even further levels of transcriptional regulation are likely; this was recently determined by (Held et al. 2008), who showed that small interfering RNAs (siRNA) targeted a region of CESA and were up-regulated during the spatio-temporal phase of cell elongation in barley (*Hordeum vulgare*). This exploration of *cis*-antisense pairs offered a snapshot of a precise regulatory system for cell wall biosynthesis that initiates from regulated silencing of CESA genes and not from the CESA-like (CSL) genes. Deeper mining of the siRNA pool and exploration of trans-antisense transcripts may also identify further CESA regulation by siRNA.

Another intriguing aspect of cellulose biosynthesis regulation surrounds the half-life of rosette complexes in the PM, which has been shown to be <30 min, at least for SCW CESA complexes, suggesting a turnover rate far higher than that of the average membrane protein (Jacob-Wilk et al. 2006). This evidence is consistent with the observation made by (Paredez et al. 2006) showing PCW CESA6 particles linked to yellow fluorescent protein (YFP::CESA6), appearing at the PM and moving almost immediately (within a minute) after arrival and continuing at a constant rate in the PM for at least 15 min. To better understand the regulation of cellulose synthesis, further study will be needed on the mechanisms involved in rosette assembly, rates of glucan chain synthesis and reasons for rapid turnover in both PCW and SCW rosette complexes. It is plausible that post-translational modifications play an active role in many of these processes (Nühse et al. 2004). One hypothesis is that CESA protein turnover is

Table 1.2 Additional mutations and genes in *Arabidopsis thaliana* implicated in cellulose biosynthesis.

Protein	Gene ID	Allele	Mutation	Phenotype	Cell Wall	Reference
CSI1	At2g22125	*csi1*	T-DNA	Swollen root, etiolate hypocotyl, small aerial orgs, 6 alleles	Primary	Gu et al. 2010
CTL1	At1g05850	*elp1*	W181Stp	Swollen root, etiolate hypocotyl, stunted, more root hairs	Primary	Zhong et al. 2002
		pom1	T-DNA	Shorten swollen root under high sucrose conds., many alleles		Hauser and Benfey 1993
KOBITO	At3g08550	*kob1-1*	T-DNA	Swollen root, etiolate hypocotyl, stunted, sterile	Primary	Pagant et al. 2002
	kob1-2	G2795A*		Swollen root, etiolate hypocotyl, stunted, sterile		Pagant et al. 2002
		eld1-1	W426Stp	Shortened root, hypocotyl, severely stunted, sterile, lethality in soil		Lertpiriyapong & Sung 2003
		eld1-2	T-DNA	Shortened root, hypocotyl, severely stunted, sterile, lethality in soil		Lertpiriyapong & Sung 2003
		abi8	5 bp del	Shortened root, severely stunted growth, male sterile		Brocard-Gifford et al. 2004
KORRIGAN	At5g49720	*kor1-1*	T-DNA	Reduced hypocotyl and root, mild growth phenotype	Primary	Nicol et al. 1998
		kor1-2	T-DNA	Reduced hypocotyl and root, strong growth phenotype		Zuo et al. 2000
		irx2-1	P250L	Collapsed xylem	Secondary	Szyjanowicz et al. 2004
		irx2-2	P553L	Collapsed xylem		Szyjanowicz et al. 2004
		rsw2-1	G429R	Reduced hypocotyl and root (heat, temperature sensitive)	Primary	Lane et al. 2001
		rsw2-3	S183N	Reduced hypocotyl and root (heat, temperature sensitive)		Lane et al. 2001
		rsw2-4	G344R	Reduced hypocotyl and root (heat, temperature sensitive)		Lane et al. 2001
COBRA	At5g60920	*cob-1*	G167R	Reduced hypocotyl, swol. root (sucrose sens.), idem *cob-2*	Primary	Schindelman et al. 2001
		cob-3	W55R	Reduced hypocotyl, swollen root (sucrose sens.)		Schindelman et al. 2001
		cob-4	T-DNA	Severely reduced hypocotyl, swol. root, aerial org. (sucrose sens.)		Roudier et al. 2005
KINESIN-LIKE	At5g47820	*fra1*	84 bp del	Fragile fiber, stunt. inflores. stem, idem *fra1-2*, *fra1-3*	Primary/Second.	Zhong et al. 2002
		fra1-4	99 bp inst.	Fragile fiber, stunted inflorescence stem		Zhong et al. 2002
KATANIN1-p60	At1g80350	*fra2*	1 bp del	Fragile fiber, stunt. Inflores. stem and aerial orgs.	Primary/Second.	Burk et al. 2001
		bot1	EMS/T-DNA	Shorten hypocotyl, root, stem and aerial orgs., many alleles		Bichet et al. 2001
		erh3-1	H353Y	Short, swollen, hairy roots	Primary	Webb et al. 2002
		erh3-2	G274R	Severely short, swollen, hairy roots		Webb et al. 2002
		erh3-3	A406V	Short, swollen, hairy roots		Webb et al. 2002
		lue1	NS394	Decreased stem elongation in response to GA, impaired apical hook		Bouquin et al. 2002
THESEUS1	At5g54380	*the1-1*	G37D	Partially restores hypocotyl elongation in *prc1-1*	Primary	Hématy et al. 2007
		the1-2	E150K	Partially restores hypocotyl elongation in *prc1-1*		Hématy et al. 2007
		the1-3	T-DNA	Partially restores hypocotyl elongation in *prc1-8*		Hématy et al. 2007
WAK2	At1g21270	*wak2*	cTAP**	Severely stunted inflorescence stem and aerial organs	Primary	Kohorn et al. 2009

*Nucleotide representing mutation at the splice acceptor site of the third intron resulting in a truncated protein

**Dominant negative allele created by the fusion of a tandem affinity tag (TAP[32]) on the C-terminus of WAK2

regulated through phosphorylation, by which phosphorylated proteins become targets for proteolytic degradation (Nühse et al. 2004; Taylor 2007). Data supporting this thesis showed that CESA7 is phosphorylated in vivo on two serine residues within the hyper-variable region of the protein, between the two putative catalytic domains (Taylor 2007). This data also show that phosphorylation of CESA7 leads to its degradation via a proteosome-dependent pathway, suggesting a mechanism for the regulation of the relative levels of individual CESA proteins that are active in a rosette complex (Taylor 2007). Interestingly, another study analysing the turnover rate of just the CESA zinc-binding domain concluded that this domain, taken from a SCW CESA in cotton, was primarily susceptible to a cysteine protease and not the ubiquitin/proteosome pathway (Jacob-Wilk et al. 2006). This study combined with the data showing that dimerization of CESAs in the Golgi and degradation at the PM may be controlled by the redox state of the zinc-binding domain within the CESA, shows that there may be multiple mechanisms to control CESA turnover (Kurek et al. 2002). The YFP::CESA6 particles visualized in confocal microscopy images are also observed to disappear from the PM, suggesting the simultaneous turnover of the entire rosette complex and thus a further level of regulation that terminates CESA activity. It is possible that CESA deactivation/activation is regulated by PM-localized kinases and phosphatses, such as has been shown for chitin synthase, which is activated at the PM after travelling from the Golgi (Valdivia and Schekman 2003). A further question that remains unclear is whether a CESA rosette is completely endocytosed after making a microfibril or whether they remain labile, and/or await reactivation in or around the PM? Understanding the mechanism by which plants regulate the turnover of CESAs and other proteins involved in cellulose synthesis may lead to the manipulation of this process and the ability to increase cellulose production. (See Table 1.2 for a complete list of genes associated with cellulose biosynthesis in *A. thaliana*).

Feedback between CESA and the cortical microtubule array

The orientation in which the cell lays down CMs is central to cell shape and morphogenesis. The guidance model for movement of CESA proteins suggests that CESA complex directionality is guided by the orientation of the underlying microtubules (Delmer and Amor 1995; Hepler and Newcomb 1964). The ability to detect CESA complexes in live cells allowed for assay of cellulose biosynthesis at the level of individual CESA complexes in single cells and was successful in demonstrating the

coordination of CESA with cortical microtubules (Paredez et al. 2006) (Figure 1.3). These tools were applied to resolving the alignment hypothesis of cellulose deposition and exactly what role microtubules play in dictating the trajectory of CESA rosettes as they lay down newly formed CMs. YFP::CESA6 proteins are visible as a series of discreet particles at the PM that co-localize with and move along linear paths coincident with underlying cortical microtubules (Paredez et al. 2006). If a dark-grown *A. thaliana* seedling expressing a microtubule marker (e.g. tubulin alpha-5 (TUA5::YFP) (Shaw et al. 2003) is exposed to light, then the cortical microtubule array will reorient from transverse to longitudinal. This rapid reorientation of the microtubule array in response to light also mimics the reorganization of the CESA array (Paredez et al. 2006). Although Paredez et al. show compelling evidence for a strong functional association between the CESA complex and cortical microtubules, their results also show that in the absence of cortical microtubules, the movement of CESA complexes does not appear to be random. Further analysis of the trajectory and rate of movement showed that CESA complexes move at exactly the same velocity regardless of the presence of microtubules (DeBolt et al. 2007a). This phenomenon may result from an intrinsic capacity of CESA rosettes to self-organize, or there is an additional intrinsic factor other than cortical microtubules that promotes CESA rosette organization. These observations are supported by previous studies which show that CMs were continually deposited transverse to the long axis of the root even after prolonged disruption of cortical microtubule arrays and additionally even when the transverse template of previously synthesized microfibrils was also perturbed (Himmelspach et al. 2003; Sugimoto et al. 2003). Until recently, analysis of the interaction between SCW CESA complexes and microtubules was unclear. A YFP::IRX3 (IRREGULAR XYLEM 3) fusion was used to observe the coordinate dynamics of SCW CESA motility coincident with a transverse banding pattern of microtubules (Wightman et al. 2009; Wightman and Turner 2008). These studies also revealed a subcellular compart- ment labelled with CESA cargo that appears to localize preferentially to microtubules, but it is unclear whether this compartment is secretory or endocytic in nature.

While these live-cell imaging results support the microtubule alignment hypothesis for cellulose deposition, the relationship between cytoskeletal organization, cell wall biosynthesis and cell morphogenesis remains a highly complex problem with many unanswered questions. Two recent molecular genetic studies have made further inroads

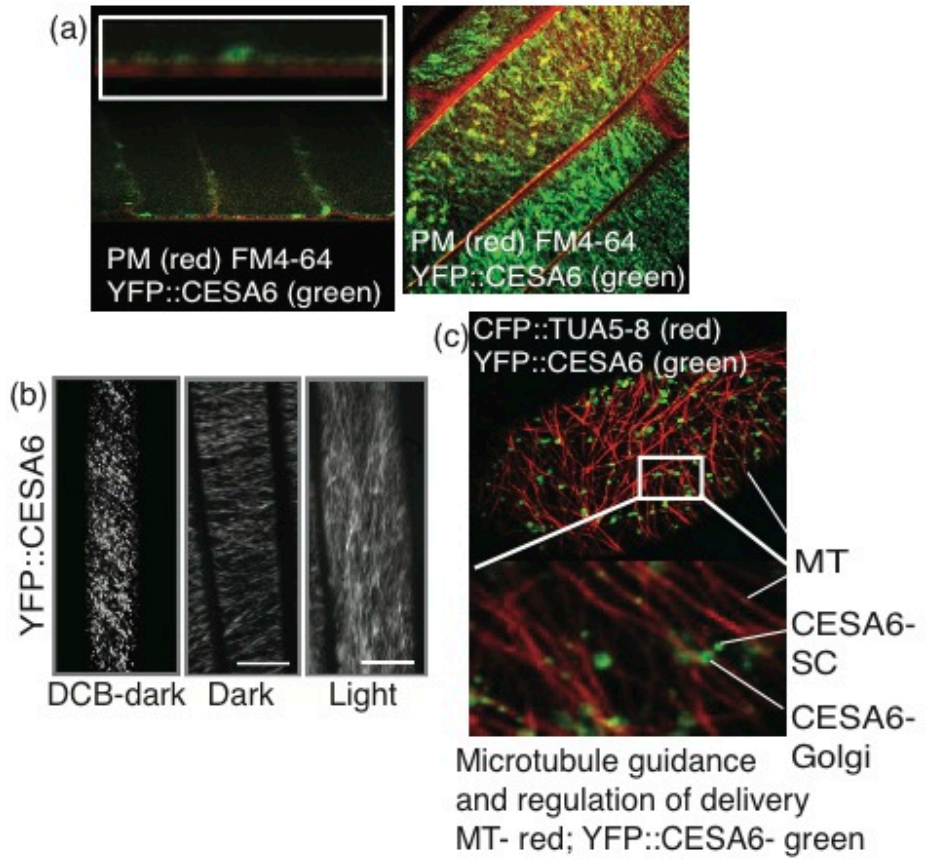

Figure 1.3. The dynamic cellulose array visualized using a functional YFP::cellulose synthase (CESA)6 translational fusion protein via laser confocal microscopy. (a) Shows the plasma membrane (PM) labelled with FM4-64 dye and CESA proteins labelled with green in a transverse oriented array. The inset (top, left) reveals YFP::CESA6 coincident with the FM4-64-labelled PM (DeBolt S., unpublished data). (b) The effect of the herbicide dichlorobenzonitrile on complexes in a time average of 61 frames shows that the CESA particle movement is arrested (DeBolt et al. 2007b), compared with (a, left) representing the transverse YFP::CESA6 array of a dark-grown seedling in the upper hypocotyl using a time average of 61 frames and (c) shows a YFP::CESA6 particle (green) tracking along a cortical microtubule (CFP::TUA5-6) (red). The image also shows a series of distinct YFP::CESA6-labelled complexes, being the membrane complex, the Golgi stacks and an additional secretory compartment (CESA6-SC), which has recently been described as facilitating the delivery of CESA cargo to the PM (Gutierrez et al. 2009).

into these problems; first (Paredez et al. 2008) have shown that feedback between microtubules and CESA goes both ways. Specifically, chemical inhibition of cellulose biosynthesis causes rapid changes in the dynamics of the microtubule array, providing evidence for a negative feedback loop. These authors discovered altered microtubule array dynamics in a genetic background where both *korrigan* and *procuste* were ablated. Hence, it was evident that negative feedback between the health of CESA and the microtubule array exists establishing an exciting area for further study. Secondly, many models have proposed a molecular link between the cortical microtubules and CESA (DeBolt et al. 2007a; Paredez et al. 2008). Discovery of a novel microtubule-associated protein in hybrid poplar (*Populus tremula* L. x *tremuloides*) named MAP20, which is inhibited by the cellulose synthesis inhibitor dichlorobenzonitrile (DCB) (Rajangam et al. 2008), provides the first tangible link and evidence for a biochemical intermediate-dictated CESA interaction with microtubules. DCB has been shown to inhibit cellulose biosynthesis by stopping the movement of CESA complexes and causing an increased number of complexes to build up and produce amorphous cellulose at the PM (Bowling and Brown 2008; DeBolt et al. 2007b; Herth 1983). Rajangam et al. (2008) found that DCB specifically bound to MAP20 and when fluorescently tagged MAP20::YFP was localized to the cortical microtubules. Hence, if in fact MAP20 is the sole targeted element for DCB, then it plays an intriguing role in cell morphogenesis and will be an exciting protein for further study. MAP20 gene expression was highly spatially and temporally co-expressed with the SCW CESA genes (Rajangam et al. 2008), beckoning the question of whether distinct MAP20 paralogues confer function in PCW versus SCW cellulose biosynthesis.

Hemicellulose

Plant cell walls also contain a heterogeneous group of polysaccharides termed the hemicelluloses (HCs) that make up 20-40% of total wall carbohydrates. Depending on the plant species, HCs may contain the pentose sugars β-D-xylose and α-L-arabinose; the hexoses β-D-mannose, β-D-glucose and β-D-galactose and/or the uronic acids α-D-glucuronic, α-D-4-*O*-methylgalacturonic and α-D-galacturonic acids. The assumed role of HCs in the cell wall is to interact with other polymers to ensure the proper physical properties of the wall. This interaction is most important with regards to the coating and tethering of cellulose microfibrils, which aids greatly in strengthening the cell wall. Of all the HCs identified, the synthesis of mannans are best understood and characterized

(Liepman et al. 2007). However, the only mannans present in the vegetative tissue of plants at any significant amount are the galactoglucomannans (GGMs) found in the SCW of the softwood angiosperms species such as conifer, with most mannans found as storage carbohydrates in the seeds of many plants (Gírio et al. 2010). The structure and synthesis of xyloglucans are perhaps the next most characterized HC, while present in the PCWs of most plants (as much as 25% in dicots), their minor presence in the SCW makes them less valuable as a source for bioenegy or biochemicals. It is the xylans that are the most abundant HCs, representing the major HC component of SCWs in the hardwoods and grasses (20-30% of total biomass) (Scheller and Ulvskov 2010) (Figure 1.1). Although the xylans are a diverse group of polysaccharides, one common feature is a backbone of (1,4) linked β-xylose residues (Scheller and Ulvskov 2010). The two sub-groups of xylans most prominent within the cell walls of bioenergy feedstocks include the glucuronoarabinoxylans (GAXs) and the glucuronoxylans (GXs) (Ebrigenova 2006). The GAXs make up most of the HCs in the lignified tissues of grasses and cereals with di-substituted arabinofuranosyl residues on the xylopyranan backbone. The GXs represent the main HC component of the SCW in hardwoods and are linear polymers with substitution in position 2 by α-D-glucuronic acid (GA) and/or its O-4-methyl-derivative (MeGA). Therefore, because xylans are the major HC component of the SCW, their biosynthesis will be detailed further.

In general, plants synthesize HCs quite differently to that of cellulose, forming these polymers in the Golgi apparatus and then secreting them via Golgi vesicles across the plasma membrane and into the cell wall. The HC biosynthetic pathway is currently only partially resolved thereby the feasibility of altering their content in the cell walls is still limited. It still seems wide open how secretion is influenced by the cytoskeleton and localized membrane lipid environments. With respect to xylans biosynthesis, the pathway leading to UDP-xylose synthesis has been the object of numerous studies (Seifert 2004) UDP-xylose is formed from the decarboxylation of its immediate precursor, UDP-glucuronic acid (Harper and Bar-Peled 2002), however there are two known pathways that lead to UDP-glucuronic acid synthesis. The pathway generally considered the most important is the conversion of UDP-glucose into UDP-glucuronic acid by UDP-glucose dehydrogenase, which accounts for approximately 50% of the UDP-glucuronic acid pool (Pieslinger et al. 2010). The second pathway, known as *myo*-inositol oxygenation, involves the conversion of *myo*-inositol into glucuronic acid, which

is subsequently converted, through an intermediate step, into UDP-glucuronic acid. The intermediate step is catalysed by a glucuronokinase which has been recently characterised and the *myo*-inositol pathway fully elucidated (Pieslinger et al. 2010).

The structure of GXs suggests that various glycosyltransferases (GTs) are required for the genesis of the GX-backbone and backbone substitution. As many as 25 GTs were shown to be expressed during SCW synthesis in poplar and the FRAGILE FIBER8 (*FRA8*) implicated in normal xylem fiber development (Zhong et al. 2005). In addition, IRREGULAR XYLEM8 (*IRX8*) and IRREGULAR XYLEM9 (*IRX9*) are *A. thaliana* homologs to three GTs from poplar expressed during SCW synthesis. A recent study showed that *IRX8* and *IRX9* are primarily expressed during fiber cell wall thickening and that they are targeted to the Golgi where GX biosynthesis occurs (Peña et al. 2007). Single and double mutant analysis showed that the irx8/irx9 double had a reduction of GX content in the inflorescence stems, *IRX9* is essential for the normal elongation of GX chains and that *FRA8* and *IRX8* are needed for the formation of the characteristic glycosyl sequence 1 (β-D-Xyl-(1-3)-α-L-Rha-(1-2)-α-D-GalA-(1-4)-D-Xyl-repeated 4 times) at the reducing end of GX as well as for a normal amount of GX chains (Peña et al. 2007). The glycosyl sequence 1 was shown to be a primer for GX synthesis and the backbone is extended by adding xylose to the non-reducing end of the growing polysaccharide chain (Peña et al. 2007). A mutation in the gene *PARVUS* leads to an almost complete disappearance of the glycosyl sequence 1 and it has been suggested that *PARVUS* is involved in the first transfer of the reducing xylose residue of the tetrameric sequence 1 to an unknown acceptor at the ER (Lee et al. 2007). In another recent study, a close homolog of the *FRA8* gene, the *F8H* gene, was shown to have complete functional redundancy with *FRA8*, with no phenotypical alteration of the SCW thickening in the *F8H* knockout, while the *fra8*/*f8h* double mutant showed severe growth retardation and failure to bolt (Lee et al. 2009). Two closely related genes, *IRX10* and *IRX10-L*, were recently characterised as being important for cell wall thickening and shown to have functional relevance in GX backbone elongation (Wu et al. 2009). The single mutants showed no significant differences from the wild-type, however the double mutant was severely affected in size and cell wall thickening. The close relationship between these proteins suggested a partial redundancy that was shown by complementation studies. However, depending on which was the mutant acting as pollen donor or pollen receptor, in the generation of the double mutant, rescue was not

bi-directionally equivalent. *IRX10* was more efficient at rescuing thereby indicating greater functional importance than *IRX10-L* and demonstrating a lack of complete redundancy (Wu et al. 2009). Further investigation of gene duplication in the GA pathway brought to evidence *IRX9-L* and *IRX14-L*, which acted as partially redundant to their similar counterpart *IRX9* and *IRX14* (Wu et al. 2010). The only single mutant that showed stunted growth was *irx9,* whereas none of the *irx9-L1*, *irx9-L2* or *irx14* or *irx14-L* has a recognizable phenotype. On the contrary, gene-paired-double mutants showed a severe stunted phenotype and very little, if any, SCW formation (Wu et al. 2010). Functional complementation studies showed that each pair of genes acted interchangeably and that they were all involved in xylan backbone elongation. However, when *irx9* was complemented by *IRX10* or *IRX14* and *vice versa* for each possible combination, rescue was not possible and the wild-type phenotype was not restored thereby clearly indicating that *IRX9, IRX10* and *IRX14* are not interchangeable (Wu et al. 2010). Despite the recent isolation of several mutants with reduced backbone, the mechanisms of GX synthesis and substitution is still unclear. Recently two Golgi-localized putative glycosyltransferases, GlucUronic acid substitution of Xylan (GUX)-1 and GUX2 that are required for the addition of both GA and MeGA branches to GX in *A. thaliana* stem cell walls were identified (Weimer et al. 1995). The *gux1/gux2* double mutants showed loss of xylan glucuronyltransferase activity and lacked almost all detectable xylan substitution, but showed no change in xylan backbone quantity, indicating backbone synthesis and substitution can be uncoupled. More importantly, although the weakened stems did not show collapsed xylem vessels thus allowing the plants to grow to normal size, the xylans from these plants were more readily extracted, were composed of a single monosaccharide, and required fewer enzymes for complete hydrolysis (Weimer et al. 1995). These results demonstrate the potential for manipulating and simplifying the structure of xylan to improve the properties of lignocellulose for bioenergy use.

The dissection of the arabinoxylan pathway was enhanced by a study showing the presence of arabinoxylan arabinosyltransferase activity in the microsomal and Golgi membranes isolated from wheat seedlings. The enzyme was further characterised but it was not possible to unequivocally correlate the transfer of arabinose to the arabinoxylan backbone (Porchia et al. 2002). (Zeng et al. 2008) showed the presence of glucuronyltransferase activity in wheat Golgi-enriched microsomes that is further

increased by the presence of UDP-xylose in the reaction medium and results in the genesis of GAX chains thereby suggesting involvement in GAX biosynthesis. GAXs have been implicated in the formation of cross-linkages between ferulate residues in the cell wall of grasses that contributes to the intrinsic difficulty in the enzymatic accessibility of cellulose and HCs. The genes involved in feruloylation are still unknown, however Mitchell et al. (2007) used a novel bioinformatic approach to propose a putative candidate gene family in rice, which encompass 12 members responsible for feruloylation of arabinoxylans. Members of this family were down-regulated by a general multi-gene RNAi approach. Two constructs were designed, one to target subgroup I and II and the other to target III and IV, which led to a general down-regulation of the transcript levels of diverse members of the gene family. A significant reduction of cell wall-ester-linked ferulic acid was observed for some of the most effectively down-regulated genes pointing these out as strong candidates involved in feruloylation (Piston et al. 2010).

Lignin

Lignin is a complex aromatic heteropolymer deposited within the SCWs of all vascular plants, and accounts for approximately 30% of the terrestrial organic carbon fixed annually in the biosphere, placing it second to cellulose as the most abundant biopolymer on earth (Boerjan et al. 2003). Lignification aids the plant by providing added strength to xylem fibers that give support for upright growth, by waterproofing tracheary elements that make up the vascular system and by helping increase the resistance of plants to pathogen attack (Boerjan et al. 2003) (Figure 1.1). Lignin content can vary with environmental factors, but in general comprises around 13-19% of the biomass in switchgrass (*Panicum virgatum*) (Lynd et al. 1999; Stork et al. 2009), 22-25% in Miscanthus (*Miscanthus* x *giganteus*) (Brosse et al. 2009; Sorensen et al. 2008), and around 20% in big bluestem (*Andropogon gerardii*) and eastern gamagrass (*Tripsacum dactyloides*) (Stork et al. 2009), all of which are C4 grass species that have potential as bioenergy feedstocks. In addition, lignin accounts for approximately 25-30% of the dry weight of potential hardwood bioenergy tree crops like poplar and can be even higher in softwood species (Pauly and Keegstra 2008). The prominence of lignin in a majority of plant tissues has been recognized by reference to the non-starch or non-sugar components of the plant body as simply ‘lignocellulosic’ biomass. Traditional research attention was given to lignin with respect to chemical pulping and forage digestibility, but

recently interest has intensified concerning conversion processes to biofuels and biochemicals. Much of the focus has centered on the fact that the cellulose microfibrils of the SCWs are embedded in a meshwork of HCs and lignin that create a barrier for cellulase enzymes and decrease saccharification efficiency. However, from a thermochemical conversion prospective, the association of lignin with cellulose is not a major issue and more important is the fact that lignin contains structural units that are more chemically reduced and energy dense than any of the cell wall carbohydrates and thus could serve as a source of hydrocarbon fuels and high-value chemicals, if means can be found to free those structural units from the polymer.

The ultimate source of lignin in the plant is the amino acid phenylalanine (Phe), which is derived from the shikimate biosynthesis pathway in the plastid (Rippert et al. 2009). Current evidence suggests that through the general phenylpropanoid and monolignol-specific pathways located on or near the cytosolic side of the ER membrane, Phe is deaminated to form cinnamic acid, followed by a series of ring hydroxylations, O-methylations and side-chain modifications culminating in the production of the *p*-hydroxycinnamyl alcohol monomers (monolignols) coniferyl and sinapyl alcohol and to a lesser extent *p*-coumaryl alcohol (Li et al. 2008). Upon incorporation into the lignin polymer, these monomers are referred to as guaiacyl (G), syringyl (S) or *p*-hydroxyphenyl (H) units respectively (Ralph et al. 2004). In general, angiosperm dicot lignins are composed of G- and S-units, while gymnosperms, with a few notable exceptions, are composed almost entirely of G-units with minor amounts of H-units (Vanholme et al. 2010). Most if not all of the enzymes required for monolignol biosynthesis are known and include: phenylalanine ammonia lyase (PAL), the three ER membrane bound cytochrome P450 monooxygenases cinnamate 4 hydoxylase (C4H), coumarate 3-hydroxylase (C3'H) and ferulate 5-hydroxylase (F5H), the two methyltransferases caffeoyl-CoA 3-O-methyltransferase (CCoAOMT) and caffeic acid/5-hydroxyferulic acid O-methlytransferase (COMT), the two oxidoreductases cinnamoyl-CoA reductase (CCR) and cinnamyl alcohol reductase (CAD) as well as two enzymes 4-coumarate-CoA ligase (4CL) and shikimate hydroxycinnamoyl transferase (HCT) that are involved in the generation of pathway intermediates (Coleman et al. 2008a; Coleman et al. 2008b; Gross et al. 1973; Koukol and Conn 1961; MacKay et al. 1997; Raes et al. 2003; Weng et al. 2008).

Although it is uncertain how the newly synthesized monolignols are translocated to the apoplast (cell wall), once there most evidence suggests that the single electron oxidation of the monolignol phenol by wall-bound peroxidases and/or laccases followed by combinatorial radical coupling commences formal lignin polymerization (Boerjan et al. 2003). Presumably, the coupling of two monolignols with one another initiates polymerization. Most likely due to the lack of steric hindrance, coupling between monolignols is favored at the central β carbon of their side chain, resulting in the most common β-β dimer, however β-*O*-4 and β-5 linked dimers can and do occur (Vanholme et al. 2010). In order for polymerization to continue, the lignin dimer must be dehydrogenated once more to a phenolic radical before it can couple with the next monomer radical. Bond formation is again favored at the central β carbon of the monolignol side chain and depending on the bond configuration and the subunit composition of the dimer, the end-wise coupling process can produce either more β-*O*-4, when a monomer adds to S- and G-units (most common), or β-5 bonds that occurs only when adding to G-units (Bonawitz and Chapple 2010). If only the three previously mentioned bonds contributed to lignin polymerization, then the lignin polymer would form a relatively straight linear chain. However, two oligolignol radicals with G-unit ends can also react to form 4-*O*-5 or 5-5 couplings that generate a branch-like quality to the polymer structure. In fact, lignin containing a high proportion of G-units is more highly cross-linked than lignin rich in S-units, which may contribute to the more rigid and hydrophobic character of G-unit lignin (Bonawitz and Chapple 2010). Therefore, the relative proportion of a given lignin monomer dictates the relative abundance of the inter-unit linkage present in the lignin polymer. Interestingly, the β-*O*-4 linkage is not only the most common linkage found in plants (Freudenberg et al. 1965), but it is also the easiest of all the linkages to chemically cleave and increasing this linkage could potentially enhance the efficiency of conversion processes (Harris and DeBolt 2010). It should also be noted that an alternative hypothesis with regards to lignin polymerization suggests that lignin monomers are coupled with absolute structural control by proteins in the cell wall bearing arrays of dirigent sites, however there has been no genetic data yet produced to support this claim (Vanholme et al. 2010). Additional evidence supporting the predominant radical coupling model of lignification has shown that all phenolic compounds, monolignols or otherwise, that enter into the region of the cell wall where oxidation and radical coupling occurs have the potential to be radicalized and incorporated into the lignin polymer, suggesting a very flexible process not likely

mediated by ligand specific enzymes (Vanholme et al. 2010). This phenomenon may also allow for a strategy of designing lignins for industrial applications, specifically by regulating the influx and species of monolignol or other phenolic compound into the cell wall (Grabber et al. 2008). And finally, regarding the global control of lignification, several transcription factors belonging to the MYB and NAC gene families, similar to those responsible for SCW biogenesis, have been shown to play a key role in regulating the expression of many of the genes in the monolignol biosysnthesis pathway (Zhong et al. 2006; Zhou et al. 2009).

Modification of cell wall structure and synthesis to overcome biomass recalcitrance

A further understanding of the synthesis and regulation of the three major cell wall molecules (cellulose, hemicellulose and lignin) will further clarify targets for genetic modification. However, the current understanding of plant cell wall biosynthesis is already allowing for intriguing results through approaches that use genetic modification combined with the latest conversion technologies. To begin, a great deal of research to date has focused on methods to improve the biochemical conversion efficiency of plant biomass with specific focus on how cellulose can be degraded by microbial enzymes into glucose for subsequent production of biofuels. The most mature conversion technology uses carbohydrate chemistry and fermentation technology for alcohol production. Other methods of processing the carbohydrates currently in development include fermentation by genetically altered microbes to various hydrocarbon products or the production of a targeted range of hydrocarbons for fuels and chemicals through the use of solid-phase catalysts under carefully controlled conditions (Regalbuto 2009). Regardless of how the sugars are processed, the efficiency of the cellulose saccharification process is critical to making many of these types of bio-based production processes economically viable. Although there is still debate in the literature about the relative importance of all the factors that contribute to the recalcitrant nature of cellulose, the most studied aspects include the effect of coating by lignin and hemicelluloses, the degree of microfibril crystallinity and polymerization, and the accessible surface area of the microfibrils (Mosier et al. 2005). In spite of this debate, there is a general consensus that in order for cellulases to efficiently hydrolyze cellulosic substrates, the enzymes must first be able to access the individual glucan chains of the tightly packed and coated microfibril (Mansfield et al. 1999). Traditionally, pretreatment

of the lignocellulosic biomass has been employed to loosen the interactions of the microfibril with the other cell wall components, thus increasing access for the enzymes (Mosier et al. 2005). However, research centered on making genetic modifications *in planta* to produce cellulose that is more accessible to these enzymes and perhaps reduce or eliminate many pretreatment techniques has also developed.

A long-standing paradigm in forage quality and production states that as lignin content decreases, forage digestion rates for ruminant livestock increase, which in turn improves the ratio of food intake to weight gain (Sullivan 1955). This paradigm translates perfectly to the hydrolysis step of the biochemical conversion process with the net result allowing for a decreased enzyme load while obtaining an increased breakdown rate of the biomass. The reason for this phenomenon not only concerns the increased access of the hydrolytic enzymes to the cellulose microfibrils due to the decreased lignin coat, but there is also a reduction in the nonproductive binding (adsorption) and inactivation of cellulases by the lignin component, thus resulting in less enzymes required to degrade the biomass (Berlin et al. 2005). Therefore, for the purpose of accessing the sugars within the wall, while much of the research in this area has traditionally focused on using pretreatment technology to eliminate lignin post-harvest, reducing or modifying the lignin content in biomass is beginning to show great promise (Coleman et al. 2008a; Coleman et al. 2008b; Ragauskas et al. 2006). The genetic modification of the enzymes involved in lignin biosynthesis has gained a lot of momentum in recent years through the use of model plants to dissect the biosynthetic pathway (Chen et al. 2006; Nakashima et al. 2008; Ralph et al. 2006; Ralph et al. 2008; Weng et al. 2008). Successful examples include the down regulation of certain lignin biosynthetic pathways that has led to more digestible forage and better pulping efficiency for paper processing processing (O'Connell et al. 2002; Reddy et al. 2005). Of particular interest for conversion technology was a study performed on transgenic alfalfa lines in which six lignin biosynthesis genes were independently down regulated by antisense technology resulting in the identification of two transgenic lines (*HCT, C3'H*) that showed a significantly greater saccharification efficiency of their untreated biomass compared to that of the pretreated biomass controls (Chen and Dixon 2007) (Figure 1.4a). This study lends further and more specific evidence to the suggestion that genetic reduction of lignin content can effectively overcome cell wall recalcitrance to saccharification using enzymatic hydrolysis and that these techniques could potentially preclude the need for

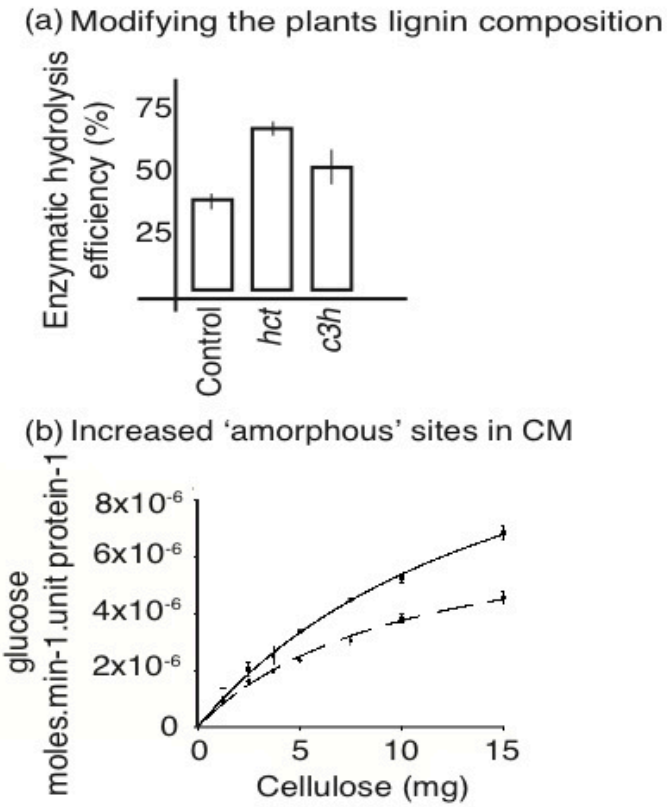

Figure 1.4. A summary of two examples showing lignin and cellulose modifications to improve saccharification efficiency. (a) Genetic modification of lignin biosynthesis in alfalfa results in higher saccharification efficiency (Chen and Dixon 2007). Specifically, the saccharification efficiency of the untreated hydroxycinnamoyl transferase and coumaroyl shikimate 3-hydroxylase down-regulated lines was significantly greater than that of the pretreated biomass control (Chen and Dixon 2007). (b) The result of the mutations proposed by Harris et al. (2009) showed the initial kinetic rate of sugar release from semi-purified cellulose by a cellulase enzyme mixture as a function of cellulose concentration. Wild-type *A. thaliana* biomass has closed circles and dashed line; *ixr1-2* mutant biomass has closed squares and solid line (error bars n = 3).

acid pretreatment (Chen and Dixon 2007). In addition, it has been recognized that many lignin mutants have a reduced growth phenotype, as was the case in this study, although remarkably, the 40% reduction in overall biomass of the *HCT* mutant was offset by a 166% increase in sugar production, thus reflecting a significant theoretical improvement in fermentable sugar production on a per plant basis (Chen and Dixon 2007).

A caveat with regards to lignin regulation states that partial elimination of lignin from tree crops like poplar has the potential to dramatically reduce their water use efficiency and hydraulic conductivity as well as increase xylem cavitation (Coleman et al. 2008b). Therefore, developing a plant with less recalcitrant cell walls by significantly reducing lignin content may require either additional bioengineering or a completely alternative approach that attempts to modify or shift lignin to a more benign composition with respect to conversion processes, yet still allow normal plant development. Research into lignin 'redesign' has shown that supplementation of coniferyl ferulate, a simple methoxylated analog of the natural conjugate coniferyl p-coumarate, into maize cell walls during the lignification process increased lignin extractability by up to 2-fold in aqueous NaOH pretreatment and increased cell wall hydrolysis and sugar release in pretreated and untreated cells (Grabber et al. 2008). In another study, the expression of a transgene encoding a high tyrosine-content peptide in the lignifying tissues of hybrid poplar resulted in a higher polysaccharide release after treatment of the biomass with hydrolytic enzymes (Liang et al. 2008). Analysis is currently underway to determine if the tyrosine-rich peptides actually cross-linked with phenolic hydroxyl groups in the lignin to modify the lignocellulosic structure of the transgenic biomass. In a related but different approach, this time targeting the UDP-xylose pathway, a mono-specific UDP-glucose dehydrogenase, a dual-specific ADH-like UDP-glucose dehydrogenase and several UDP-glucuronate decarboxylases were cloned and expressed in xylogenic tobacco cells (Bindschedler et al. 2005). It was hypothesized that a lowering of xylan production in these cell lines, by the down-regulation of the UDP-glucuronate decarboxylase, might lead to alterations in lignin biosynthesis, a change in cellulose extractability and perhaps offer insights into how lignin is coupled to hemicelluloses in dicots (Bindschedler et al. 2007). Interestingly, despite the lower xylan content of the antisense lines, the lignin content and composition remained relatively unchanged, however the delignification properties were actually lower (lignin was harder to remove) and less cellulose was extracted than in control lines. Thus, it appears that the level of xylan relative to lignin

may be an important factor in delignification properties and cellulose extractability, in this case reduced xylan may lead to a closer association between cellulose and lignin (Bindschedler et al. 2007).

Regarding the potential for reducing cell wall recalcitrance through a reduction in cellulose crystallinity, one of the earliest discoveries was that of naturally occurring proteins that have the unique property of disrupting cellulose crystallinity. Upon analysis of various microbial carbohydrate-active enzymes, it was realized that many possess a contiguous sequence of amino acids termed a carbohydrate-binding module (CBM) that produces a discrete fold imparting carbohydrate-binding activity (Shoseyov et al. 2006). Further research showed that microbial enzymes possessing CBMs, such as cellulases and chitinases, are brought into close and prolonged contact with their recalcitrant substrates and have increased rates of substrate hydrolysis (Shoseyov et al. 2006). Interestingly, some CBMs expressed alone without the catalytic portion of the enzyme have displayed an ability to disrupt the corresponding substrate. This phenomenon was initially shown to disrupt the structure of cellulose microfibrils *in vitro* (Din et al. 1991) and then later during heterologous expression in plant systems where the CBM was targeted to the cell wall (Shoseyov et al. 2006). Many of these heterologous expression studies with CBMs have noted that the reduction in cellulose crystallinity caused by the disruption effect of the CBM often coincides with an increase in cellulose biosynthesis and thus an overall increase in plant biomass. It has been postulated that this occurs through a physicomechanical mechanism by which the CBM molecule slides between the glucan chains as they are extruded from the CSC before they begin hydrogen bonding to adjacent chains, thus separating them in a wedge-like action which essentially uncouples the polymerization step from the crystallization step of cellulose biosynthesis (Levy et al. 2002).

In addition to CBMs from microbial sources, a group of pH-dependent wall-loosening plant proteins with close homology to CBMs, known as expansins, have been shown to be activated during the acid growth response of plant cells and to stimulate PCW enlargement by disrupting the non-covalent binding between wall polysaccharides (Cosgrove 2005). Capitalizing on the ability of expansins to weaken networks of cellulose microfibrils (McQueen-Mason and Cosgrove 1994), a recent study has shown that when added to a cellulase mixture, the protein swollenin (an expansin-like protein

from *Trichoderma reesei*, Saloheimo et al. 2002) can enhance the degradation of crystalline cellulose into glucose providing an improvement for bioconversion technology (Chen et al. 2010b). Other plant proteins of interest include the endo-β-1,4-glucanases (EGases), especially the relatively new subclass of the α-EGases that contain a functional and modular CBM conferring binding to crystalline cellulose (Urbanowicz et al. 2007). The presence of a CBM in this plant EGase suggests that it may have a role in cellulose degradation which could include functions as diverse as cell wall disassembly during fruit softening and organ abscission, hydrolysis of polysaccharide chains at the cellulose microfibril periphery, or even cell wall assembly by regulating cellulose crystallinity crystallinity during biosynthesis (Urbanowicz et al. 2007). In addition, the binding of xyloglucans to cellulose microfibrils also suggests that these molecules may be involved in the *in muro* modification of cellulose. Xyloglucan *endo*-transglycosylases (XETs) are a group of enzymes able to carry out rearrangement of xyloglucans by cleavage and re-ligation that may occur in conjunction with other enzymes such as EGases. By using XETs specifically as the receptor anchor for chemical groups, chemical functionality and other modifications have been made to cellulose (Zhou et al. 2006; Zhou et al. 2005; Zhou et al. 2007). Taken together, the genetic manipulation of endogenous plant enzymes for the controlled growth and degradation of lignocellulosic biomass is an important avenue of research towards improving biomass processing of biofuel and biochemical feedstocks.

Another method that may hold promise for increasing the access of enzymes to cellulose and thus decreasing the need for pretreatment is that of increasing the more soluble amorphous zones within the cellulose microfibril (Himmel et al. 2007). In search of mutations that may cause an increase in enzymatic conversion efficiency, a recent study screened a majority of the available PCW mutants in *A. thaliana* and found that a number of previously generated mutant plants yielded significantly more fermentable sugar than wild-type plants (Harris et al. 2009). This study also measured the biomass crystallinity of these plants and discovered that two of the best enzymatic conversion mutants, *isoxaben resistance1-2* and *2-1* (*ixr1-2*, *ixr2-1*), had lower relative crystallinity index (RCI) values than wild-type plants. This evidence suggests that there may be fundamental changes in the orientation, size or density of the cellulose crystallites composing the cellulose in these mutants, although further analysis of the cellulose is still needed to confirm this possibility (Harris and DeBolt 2008; Harris et al. 2009).

Regarding the nature of the *ixr1-2* and *ixr2-1* mutants, previous research has shown that these single point mutations reside in or near a transmembrane spanning domain in the C-terminus of CESA3 and CESA6 respectively (Desprez et al. 2002; Scheible et al. 2001). Speculating on the reasons for the increased saccharification efficiency and reduced RCI, perhaps these mutations alter the structure of the CESA protein, changing its orientation either within the plasma membrane or with respect to neighboring CESAs in the CSC. An unstable or improperly positioned CESA, even to a slight degree, could alter the path of the glucan chain during polymerization and effect its subsequent incorporation into the crystallizing microfibril either through poor proximity with the other glucan chains or through unstable hydrogen bonding angles. The overall effect could be an increase in the amorphous zones along the fibril length that might explain the increased saccharification and reduced RCI. An additional hypothesis for this data is that the altered cellulose array results in a proportional shift in the volume fraction of cellulose, hemicellulose and lignin in the cell wall that could result in an increased availability of cellulose to hydrolytic conversion. Whatever the case may be, it is also interesting to note that the conversion process for these plants required less enzyme loading and less overall reaction time to that of wild-type, suggesting two areas of cost reduction for biofuel production (Harris et al. 2009).

In addition to the need for pretreatment of biomass to facilitate enzymatic breakdown of the recalcitrant cell walls, another costly step in the biochemical conversion process is the production of the hydrolytic enzymes (cellulases, xylanases, etc.) generally via microbial bioreactors. In fact, the combined costs of pretreatment and enzyme production can greatly reduce the ideal efficiency of biofuel production from lignocellulosic biomass, making the entire process two to threefold more expensive than production from maize grain starch (Sticklen 2008). To address the enzyme production question, it has been noted that plants are already used for the production of many industrial and pharmaceutical products, including enzymes and other proteins. Therefore, why not produce plant cell wall hydrolytic enzymes in the very bioenergy feedstock crops that they will be used to degrade? Research in this area has already shown that a biologically active heterologous thermostable endo-1,4-β-endoglucanase (E1) enzyme from *Acidothermus cellulolyticus* can be expressed in *A. thaliana* (Ziegler et al. 2000), potato (*Solanum tuberosum* L.) (Dai et al. 2000) and tobacco (*Nicotiana* sp.) (Ziegelhoffer et al. 2001) plants. Initially, when combined with pretreatment processes

such as ammonia fibre/freeze explosion (AFEX), approximately two-thirds of the activity of the heterologous E1 was lost (Teymouri et al. 2004). However, further research has demonstrated that expressing the E1 enzyme in corn (Biswas et al. 2006) and rice (Oraby et al. 2007) followed by enzyme extraction from the dry transgenic biomass in a total soluble protein (TSP) preparation and then re-introduction to the biomass after AFEX pretreatment, led to successful conversion of some of the corn stover and rice straw into glucose (Oraby et al. 2007; Ransom et al. 2007). Continued research is focused on improving the heterologous expression process primarily by increasing the variety of hydrolytic enzymes that can be expressed as well as by increasing the levels of *in planta* enzyme production and the biological activity of these enzymes post extraction (Sticklen 2008). It is well known that in order to get near complete levels of cellulose and hemicellulose degradation from pretreated biomass, a number of cellulase (endoglucanase, exoglucanase, and β-glucosidase) and hemicellulase (endo-xylanases and exo-xylanses) enzymes must work synergistically to promote the solubilization and hydrolysis of these carbohydrates into their principle monosaccharide constituents (Zhang and Lynd 2004). Hence, attempts are currently being made to express all the required enzyme components for cell wall carbohydrate degradation, thus reducing the need for external supplementation. In addition to enzyme variety, the amount of enzyme produced is also critical. The *A. cellulolytius* E1 enzyme has been produced in rice at amounts around 5% and in maize at 2% of plant TSP, however it has been estimated that levels need to be around 10% TSP to avoid the need for additional enzymes (Sticklen 2008). Strategies being used to increase the level of enzyme production include genetically engineering the chloroplast genome instead of the nuclear genome, better subcellular targeting of the enzymes after expression such as localization to the ER, apoplast or chloroplast, and the better matching of enzyme pH requirements with that of the subcellular compartment targeted for localization (Sticklen 2008).

Modification of cell wall structure and synthesis to increase biomass quantity and energy density

It is entirely possible that energy density may be the measure of the ideal energy plant rather than a less recalcitrant cell wall, in which case larger or more energy dense biomass crops will be preferred and traditional combustion or thermochemical-/catalytic-based conversions that can lead directly to liquid fuels will be used (Regalbuto 2009). In fact, technology is already being developed to allow for industrial-scale conversion of

biomass directly to liquid hydrocarbons via pyrolysis or gasification (NSF 2008). Determining all the factors that will comprise energy density in plants is still taking shape, however it is certain that engineering plant cells to grow larger and accumulate greater amounts of energy dense macromolecules will be an important goal. In addition, although there is still a great deal to learn at a fundamental level about the sensing and signaling mechanisms that alter carbon assimilation, carbon storage and growth rate within the plant (Smith and Stitt 2007), research in this area has already uncovered useful modifications which increase plant biomass. These studies vary in approach, from the modification of plant growth regulators such as brassinosteriods in *A. thaliana* (Choe et al. 2001) or gibberellins in poplar (Eriksson et al. 2000) to the gaining of a better understanding of the synchronization of the circadian clock and external light-dark cycles that can also result in improved plant growth (Dodd et al. 2005). Other studies have shown an increase in growth by the overexpression of heterologous enzymes in the cellulose biosynthesis pathway. Examples include yeast-derived invertases (Canam et al. 2006) and the *A. thaliana* family A sucrose phosphate synthase (Park et al. 2008), both expressed in transgenic tobacco. More specifically, the substrate ratios of cellulose biosynthesis have also been targeted, such as the overexpression of sucrose synthase (SuSy) and UDP-glucose pyrophoshorylase, targeted for their role as the only known suppliers of UDP-glucose to the CESA enzymes (Coleman et al. 2006). A good example has shown that the expression of cotton (*Gossypium hirsutum*) SuSy in hybrid poplar (*Populus alba* x *grandidentata*) affects carbon partitioning leading to an increase in cellulose production in the SCW without increasing plant growth, thus representing a good strategy to increase energy density in the plant (Coleman et al. 2009). Other studies such as the deregulation of ADP-glucose pyrophosphorylase, a key starch biosynthesis enzyme in rice (Smidansky et al. 2003) and the overexpression of purple acid phosphatase in tobacco (Kaida et al. 2009) both show promising results for increasing plant biomass and cellulose synthesis respectfully. However, the authors of these last two studies have only speculated at the possible mechanism of action that produces the increases, thus reminding researchers of the difficulties inherent in elucidating the details of plant growth and regulation. For example, with regard to purple acid phosphatase, it was suggested that the enhanced activity of the CESAs was due to their activation by phosphorylation (Kaida et al. 2009). Indeed, several putative cytoplasmic phosphorylation sites have been identified in the CESAs of *A. thaliana* using a phosphoproteomics approach (Nühse et al. 2004). Additional support for this

hypothesis has shown that CESA7 is phoshorylated *in vivo* on two serine residues within the hyper-variable region of the protein, between the two putative catalytic domains and that this leads to its degradation via a proteosome dependent pathway (Taylor 2007). However, while there is increasing evidence to suggest phosphorylation/dephosphorylation as a mechanism for the regulation of the relative levels and activity of individual CESA proteins in a CSC, other mechanisms for CESA turnover, such as cysteine proteases (Jacob-Wilk et al. 2006) have also shown support. What these and other studies suggest is that there are many complex factors involved in the regulation of plant growth and cellulose biosynthesis and that perhaps a thorough understanding of what encompasses 'normal' regulation is most important, followed by the continued identification of mutants with altered growth phenotypes and cellulose quality.

Recent discoveries that have added great insight into the molecular mechanisms involved in the biogenesis of the SCW include identification of several NAC domain transcription factors that all belong to one particular phylogenetic subgroup and are key transcriptional activators of SCW formation (Shen et al. 2009). The NAC transcription factors identified to date include VND1-VND7 (vascular-related NAC-domain) that regulate differentiation of tracheary elements (Kubo et al. 2005) and NST1 and NST3 (also known as SND1) (NAC SCW thickening promoting factor) that promote secondary thickening in xylem fiber cells (Mitsuda et al. 2007; Zhong et al. 2006; Zhong and Ye 2007). As this transcriptional network for regulation of the SCW has been further resolved, it has been shown that these NACs regulate a cascade of downstream transcription factors that in turn activate SCW biosynthetic genes (Demura and Ye 2010). Three members of the MYB transcription factor family, MYB26, MYB83 and MYB46, can also regulate secondary wall biosynthesis by either regulating the expression of NST1 and NST2 and thus control cell wall thickening in the anther endothecium or by serving as the direct target of NST3 and control cell wall thickening in fibers (McCarthy et al. 2009; Yang et al. 2007; Zhong et al. 2007a). Another potentially important study regarding these transcriptional switches showed that under appropriate growth conditions, hypocotyls of *A. thaliana* had similar structure to the secondary xylem (wood) found in trees (Chaffey et al. 2002). In the *nst1*-1/nst3-*1* double knockdown mutants of *A. thaliana*, there was nearly complete suppression of SCW formation within secondary xylem fibers of the hypocotyls (Mitsuda et al. 2007). Interestingly, there are

putative homologs of *NST1* and *NST3* in the poplar genome, therefore a common mechanism for the control of wood formation may exist in herbaceous and woody plants and *NST*s along with other NACs could play an important role in SCW biosynthesis during wood formation. The further characterization of NAC genes could provide important tools for the genetic manipulation of fiber cells and thus modification of wood quality and production that could positively impact feedstocks for biofuels.

In response to gravity, many angiosperm trees significantly alter the normal development of the SCW on the upper surface of their branches and leaning trunks by forming tension wood (TW). The formation of TW results in wood cells with a SCW devoid of an S3 and most of an S2 layer and replaced by a gelatinous layer (G-layer) consisting of highly crystalline cellulose with a high degree of tensile strength due to the parallel orientation of the microfibrils (Andersson-Gunnerås et al. 2006). The TW benefits the tree by exerting a tensile force that can pull a tree trunk vertical or hold a large branch horizontal thus keeping the leaves in an optimal position for gathering sunlight (Bowling and Vaughn 2008). The potential interest in TW for bioconversion technology resides in the fact that the G-layer, present in both the xylem and the phloem fibers, is 98% crystalline cellulose and virtually devoid of lignin and hemicelluloses, thus representing the purest form of cellulose occurring in woody tissues and increasing the overall cellulose content of the wood by about 10-20% (Andersson-Gunnerås et al. 2006; Joshi 2003). The process of TW formation can be experimentally induced and has therefore been a valuable model system to understanding the process of cellulose biosynthesis in trees. It has already been shown that orthologs to the CESA genes involved in SCW synthesis in *A. thaliana* are upregulated during TW formation in aspen trees, including specific NAC genes (Bhandari et al. 2006). In addition, a global analysis of the differential expression in transcripts and fluctuations in metabolites during TW formation in poplar identified many molecular players involved in the change in carbon flow into various cell wall components and mechanisms important for the formation of the G-layer (Andersson-Gunnerås et al. 2006). A study of this type has provided a roadmap of sorts for the further functional analysis of genes involved in G-layer biosynthesis in TW and identification of areas for future genetic manipulation. An understanding of the molecular mechanism of highly crystalline cellulose production during TW generation in trees could provide a mechanism for the production of ectopic TW in trees and other plant species, resulting in an increase in overall cellulose content (Gomez et al. 2008; Joshi 2003).

As was mentioned previously, the expression and localization of CBMs to the plant cell wall can reduce cellulose crystallinity through the process of uncoupling cellulose polymerization with crystallization (Shoseyov et al. 2006). Interestingly, many of these same studies also report an increase in cellulose production with concomitant increases in plant biomass, presumably by the same uncoupling phenomenon (Shoseyov et al. 2006). Growth acceleration has also been shown for expansin-expressing transgenics of *A. thaliana* (Cho and Cosgrove 2000), poplar (Gray-Mitsumune et al. 2008) and rice (Choi et al. 2003). In the same respect, the overexpression of EGases has been shown to cause enhanced plant growth, most likely due to their proposed role in PCW loosening. For example, poplar trees developed longer internodes and enhanced growth by the overexpression of the *A. thaliana* EGase *cel1* (Shani et al. 2004). Likewise, lignin down regulation not only increases biomass digestibility, but it can also result in an increase in cellulose content (Jouanin et al. 2000; Li et al. 2003). This phenomenon is most likely caused by a compensatory response by the plant to maintain the structural integrity of the cell wall and sustain directional growth. The combination of these two factors could be very beneficial for numerous different conversion processes to biofuels and platform chemicals, as the plant would have an increased concentration of more digestible cellulose. Research in this area has shown that transgenic poplar plants transformed with antisense constructs of the lignin biosynthesis gene *Pt4CL* result in trees with a 45% decrease in lignin and a 15% increase in cellulose content (Jouanin et al. 2000; Lapierre et al. 1999). As referred to earlier, directing the plant's energy and carbon storage into cellulose rather than lignin may result in compromising SCW strength, water conductivity and an increase in the susceptibility to pathogens (Weng et al. 2008). Interestingly, classic plant breeding programs to lower lignification, primarily for improvement in forage quality, have been pursued extensively for many plant species over a number of years, including various Bermuda grasses (*Cynodon dactylon*) (Akin 2007), and the *brown midrib* class of cell wall mutants in maize (*bm*) and sorghum (*bmr*). Recently, a study showed that these maize and sorghum mutants not only show a clear reduction in lignin composition but also have improved fermentable sugar yields after enzymatic saccharification (Vermerris et al. 2007). Equally important is the fact that although initially most of the *brown midrib* mutants had compromised growth characteristics similar to those seen with some of the transgenic lignin mutants, these traits have been largely eliminated by conventional breeding methods (Pedersen et al.

2005). Therefore, the genetic resources available from these plants may provide a model to define cell wall and gene abnormalities that can be copied to accelerate the breeding program in bioenergy feedstocks.

The fact that lignin is the second most abundant biopolymer on earth after cellulose also makes it a potential target for direct conversion into biofuels. However, due to the nature of lignin biosynthesis, non-enzymatic conversion technologies will be needed to produce fuels and chemicals and currently there is a lack of selective and cost-efficient processes available for lignin conversion. This fact has lead to the current use of the lignin residue produced from biorefining as a fuel that is burned to generate power, most often to run the biorefinery itself (DeBolt et al. 2009). Yet there are many strategies, old and new, in development that could lead to the efficient extraction and depolymerization of lignin into its monomeric substituent groups, which in turn can be upgraded into hydrocarbons (reviewed in Zakzeski et al. 2010). Of these numerous methods, one of the newer more attractive strategies includes the use of thermolytic ionic liquids, which are essentially non-volatile molten salts with a melting point less than 100ºC (Holbrey and Seddon 1999), that recent studies have indicated are suitable as solvents for the dissolution of lignocellulosic materials (Fort et al. 2007; Kilpeläinen et al. 2007; Pu et al. 2007). The use of ionic liquids to dissolve lignocellulosic biomass may also pair quite well with the subsequent fermentation of the liberated carbohydrates into biofuels as the process can occur at near-ambient temperatures and pressures with the use of a very limited set of ionic liquid substructures. An alternative strategy to disassemble lignin also under development is Baeyer-Villiger oxidation, which involves the cleavage of carbon-carbon bonds adjacent to a carbonyl that can convert the aromatic rings in lignin to carboxylic acids and their lactones, thus taking advantage of the plethora of reactive sites present in lignin polymers (Pan et al. 1999). The oxygenates that result from this oxidative deconstruction can then be deoxygenated via process like hydrodeoxygenation, to give hydrocarbons. Unfortunately, the high number of functional groups also means that a large number of reactions can take place at different sites in the polymer, producing small molecules, degraded polymer residues, and crosslinked polymers. In addition, the oxidation process can catalyze the hydrolysis of carbohydrates, especially the hemicellulose constituents, which can reduce yields for carbohydrate fermentation (Tan et al. 2009). Therefore, research is focusing on improving oxidation methods that avoid cleaving the hemicelluloses as well as strategies to genetically alter lignin biosynthesis in

plants to increase the more easily cleaved β-*O*-4 linkages. A third developing technology that shows strong potential is the thermal decomposition of lignocellulosic biomass via fast pyrolysis. This process results in the depolymerization and fragmentation of cellulose, hemicellulose and lignin producing a dark brown, free-flowing liquid known as bio-oil (Czernik and Bridgwater 2005). Upon water addition to the bio-oil, fractionation of the liquid occurs, with the light oxygenates derived from the carbohydrates forming the water-soluble upper layer, and the lignin-derived oligomeric (aromatic) compounds settling in the lower water-insoluble layer (Czernik and Bridgwater 2005). The purity of the lignin-derived fraction can be further improved through the use of additional solvent fractionation methods (Chum and Black 1990). Applications for the two fractions include the production of calcium salts as environmentally friendly road deicers via the neutralization of carboxylic acids present in the water-soluble fraction and the replacement of phenol in phenol-formaldehyde resins using the water insoluble fraction. Although the lignin-derived aromatics are less reactive than phenol, 30-50% of the phenol can be replaced, producing high quality resins (Czernik and Bridgwater 2005). Most recently, a process termed catalytic fast pyrolysis has developed that introduces zeolite catalysts into the pyrolysis process and leads to the conversion of oxygenated compounds generated by pyrolysis of the biomass into gasoline-range aromatics (Carlson et al. 2008). It is likely that advances in understanding the chemistry of catalytic fast pyrolysis materials, which are specifically designed for biomass conversion, will lead to further process improvements (Carlson et al. 2008; Vispute et al. 2010).

Chapter II*

The use of small molecules to dissect cell wall biosynthesis and manipulate the cortical cytoskeleton

Plant cell walls are composed of highly glycosylated proteins and polysaccharides, including pectin, hemicelluloses and cellulose, which form a complex and dynamic extracellular matrix that modulates cell expansion. The principal cell wall polysaccharide is cellulose and it stands as the most abundant biopolymer in the world. Although genetic screens have identified a handful of genes that participate in cellulose biosynthesis, the complexity of events contributing to activation of the cellulose synthase A (CESA) at the plasma membrane that includes its motility and interaction with other polymers and proteins suggests that the list of players is far from complete. This chapter examines the use of chemical genetics to dissect and extend our understanding of cellulose biosynthesis in plants.

The plant cell wall is a complex and dynamic extracellular matrix that surrounds every plant cell. The wall provides a number of different yet simultaneous functions to allow for plant survival including mechanical support for upright growth, facilitation of cell shape and morphogenesis as well as roles in signaling during pathogen defense and abiotic stress response (Carpita and Gibeaut 1993). The primary cell wall in particular has a necessary rigidity that maintains cell growth anisotropy while also remaining highly dynamic and metabolically active for its crucial roles in cell division and differentiation (Farrokhi et al. 2006). The polymer networks present within cell walls that allow for these various processes to occur consist principally of a cellulose/hemicellulose network, a coextensive heterogeneous pectic polysaccharide network, some glycoproteins, and in mature non-growing cells with a secondary cell wall, a network of polyphenolic compounds such as lignin (Carpita and Gibeaut 1993). Due to this complexity, the biosynthesis of plant cell wall polymers involves numerous enzymes that catalyze a wide range of reactions. The completion of the *Arabidopsis thaliana* genome sequence led to

***This chapter was originally published as: Harris D and DeBolt S (2011)** The use of small molecules to dissect cell wall biosynthesis and manipulate the cortical cytoskeleton. In *Plant Chemical Biology* (Overvoorde P & Audenaert D, eds), John Wiley & Sons, Ltd, Chichester, UK. (In press). Copyright permission was granted by the authors for inclusion in this dissertation.

the prediction that about 15% of plant genes may be involved in the biosynthesis and metabolism of the plant cell wall (Somerville et al. 2004). One example of an important family of enzymes with members from viruses, bacteria, fungi, algae and all higher plants (Richmond 2000) is the processive glycosyltransferases (synthases) of which there are several hundred genes putatively annotated in *A. thaliana* (Coutinho and Henrissat 1999), however the function of only a limited number have been thoroughly characterized. This is also the case for many other genes that encode important enzymes for wall synthesis such as non-processive transferases, transglycosylases, and enzymes involved in the inter-conversion of nucleotide-sugars and nucleotide-sugar transporters. Therefore, because of the large number of currently uncharacterized enzymes, understanding the details of cell wall polysaccharide biosynthesis represents a major challenge in plant biology (Somerville et al. 2004).

The power of molecular genetics in the study of cell walls

The identification and characterization of mutants with altered cell wall structure have provided significant insights into the molecular players and mechanisms involved in cell wall biosynthesis. Through the use of forward and reverse genetic approaches, a number of cell wall mutants have been revealed, especially in *A. thaliana* (Farrokhi et al. 2006; Somerville et al. 2004). Successful forward genetic screens include primary wall sugar compositional analyses that have lead to the identification of mutants with altered pectic polysaccarides and xyloglucans (Reiter et al. 1993; Reiter et al. 1997; Zablackis et al. 1996). In addition, screens that detect changes in the secondary cell wall have identified mutants with an irregular xylem phenotype that results from reduced cellulose biosynthesis (Turner and Somerville 1997) and abnormal glucuronoarabinoxylan content (York and O'Neill 2008). A number of reverse genetic approaches have made use of the publicly available *A. thaliana* lines with T-DNA insertions to identify additional proteins involved in wall biosynthesis and metabolism (Alonso et al. 2003; Farrokhi et al. 2006; Somerville 2006).

Although molecular genetics is a powerful approach, problems such as loss-of-function lethality and gene redundancy have remained a challenge in plant systems. Altering the function of an essential gene can often result in embryonic or post-embryonic lethality making the study of the gene function very difficult (Meinke 1985). A good example in

cell wall research is found in the study of the cellulose synthase A (CESA) genes and in particular *CESA1* and *CESA3* of *A. thaliana* that show gametophytic lethality when completely knocked out. Homozygous *cesa1* and *cesa3* null mutants have never been recovered and when analyzed in the heterozygote state their progeny were shown to produce 50% deformed pollen grains that were devoid of cellulose and incapable of producing a pollen tube (Persson et al. 2007). Therefore, traditional genetic studies have often relied on conditional mutations to circumvent the problem of lethality, however a conditional mutant, when available for a gene of interest, often requires a substantial change in the environment of the organism to generate a phenotype. Such an example can be found with temperature sensitive alleles, where an increase in temperature results in the destabilization of the corresponding protein and a resulting phenotype. A good example in cell wall research is the *A. thaliana* temperature-sensitive mutant *rsw1* that harbours a point mutation in the essential primary cell wall CESA1 enzyme. This mutant was selected by a root radial swelling phenotype at the restrictive temperature (Arioli et al. 1998). The identification of CESA1 was the first strong genetic evidence to suggest that this particular subfamily of processive glycosyltransferases are involved in cellulose biosynthesis in plants. In fact, the identification of other conditional mutants has proved quite useful in plant cell wall research, as many forward genetic screens have used a conditional approach (Baskin et al. 1992; Benfey et al. 1993; Reiter et al. 1993). However, changes in the growth environment invariably alter the expression of many other genes as was shown in yeast when a temperature shift from 25°C to 37°C resulted in the change in expression of 854 heat-responsive genes, 50% of which had unidentified function (Causton et al. 2001). Therefore, care must be taken when evaluating phenotypes resulting from a screen of this nature, so as not to inaccurately assign a phenotypic role to a mutation under investigation.

Another challenge with the traditional genetic approach is gene redundancy, as is quite common in plants, that can mask the phenotype of an altered gene by causing the up-regulation of other genes with analogous function thereby rescuing the loss of the altered gene (Byrne et al. 2002). The *A. thaliana* genome sequence shows that there is a high level of gene redundancy, with only 35% of genes classified as unique and with 37% of genes belonging to families with five or more members (*Arabidopsis* Genome Initiative, 2000). A common example in plant cell wall research is found in the redundancy of genes involved in the biosynthesis of hemicelluloses such as xyloglucans

(Scheller and Ulvskov 2010). The xyloglucans are a critical component required for cross-linking cellulose microfibrils in the primary walls of many plants. However, many of the genes encoding proteins involved in the synthesis of xyloglucans, such as members of the *mur* class of mutants in *A. thaliana* (Reiter et al. 1997), show little (Madson et al. 2003) to no visible phenotype (Perrin et al. 1999) and require generation of double or triple mutants to create xyloglucan deficient plants (Cavalier et al. 2008; Dick-Pérez et al. 2011; Zabotina et al. 2008b). Gene redundancy likely represents an evolutionary advantage to safeguard the proper making of cell walls, however, overcoming redundancy of gene function and the proteins for which they encode in the cell wall biosynthetic process has posed a significant research challenge.

Why use chemical genetics to study plant cell walls?

The chemical genetics approach is complementary to traditional genetic studies. Instead of relying on genetic mutations to disrupt protein activities within a signalling or metabolic network, a screen for small cell-permeable molecules that alter a process of interest is used. There are several advantages of chemical genetics over the traditional genetic approach. Small molecules can be used to address the loss-of-function lethality problem because the timing and location of the application can be controlled, which mimics a conditional mutation (Robert et al. 2008). Important with respect to the inhibition of biosynthetic enzymes of the plant cell wall, temporal knockouts can be created at different points in development due to the relative flexibility of the inhibition process, which is rapid and reversible in most cases (Zabotina et al. 2008a). Often a small molecule that binds to and alters the function of one protein will also bind to closely related members of that protein family which can frequently alleviate the problem of gene redundancy. In addition, small molecule effects are often tunable allowing gradient phenotypes to be observed by varying the concentration of the small molecule, which can add confidence to the apparent biological effect of the small molecule probe (Spring 2005).

The use of chemical genetics in cell wall research

Cellulose is the most abundant carbohydrate found in plants and is also the main load-bearing component of cell walls, which makes it an effective target for small-molecule inhibitors of cell wall formation. Cellulose exists as *para*-crystalline microfibrils that are made up of multiple, unbranched, parallel glucan chains, which in turn are composed of

(1,4) linked β-D-glucosyl residues that are alternatively rotated 180° along the polymer axis (Hermans 1949). Plants synthesize cellulose at the plasma membrane by a symmetrical rosette of six globular protein complexes, collectively called the cellulose synthase complex (CSC) and totaling 25-30 nm in diameter (Brown 1996). Each lobe of the CSC rosette contains several structurally similar cellulose synthase A (CESA) subunits (Pear et al. 1996). The predicted membrane topology of a typical plant CESA suggests a cytoplasmic N-terminal region containing zinc-finger domains followed by two transmembrane domains (TMDs), then a large cytoplasmic domain containing the catalytic motifs and finally a cluster of six more TMDs at the C-terminus (Delmer 1999). Hypothetical three-dimensional models based on this topology all suggest that the eight TMDs anchor the protein in the plasma membrane and form a pore, either as a single polypeptide or as a CESA dimer, through which the growing glucan chain passes to reach the cell wall (Carpita 2011; Delmer 1999). Current molecular models of the CSC propose that each of the six protein complexes may synthesize as many as six glucan chains, each glucan chain presumably synthesized by a single CESA protein, thus a maximum of 36 glucan chains could be produced by a single rosette which then co-crystallize to form one microfibril (Ding and Himmel 2006; Doblin et al. 2002; Scheible et al. 2001) (Figure 2.1). Live-cell imaging of transgenic *A. thaliana* plants carrying a yellow fluorescent protein (YFP)-labeled CESA6 have recently been used to show that CSCs move at a constant velocity at the plasma membrane via a microtubule (MT) guidance mechanism. However, when MTs are completely depolymerized, YFP-CESA6 velocity remains unchanged (DeBolt et al. 2007a; Paredez et al. 2006), suggesting that the force of glucan chain polymerization is responsible for movement rather than MT motor proteins. In *A. thaliana*, 10 *CESA* genes have been identified (Richmond and Somerville 2000). A combination of genetic and biochemical analyses has revealed that three distinct CESA proteins are required to form the CSC; CESA4, 7 and 8 in the secondary cell wall (Taylor et al. 2003) and CESA1, 3 and 6 or the CESA6-related proteins CESA2, 5 and 9 in the primary cell wall (Persson et al. 2007). There is currently no reported crystal structure of a plant CESA protein, nor the complete purification of a functional CSC *in vitro*, therefore the precise mechanism of glucan chain polymerization or CESA subunit interaction within the CSC remains unresolved.

Some of the first examples of the use of small molecules as tools to study cell wall assembly were through the use of previously characterized chemicals and herbicides

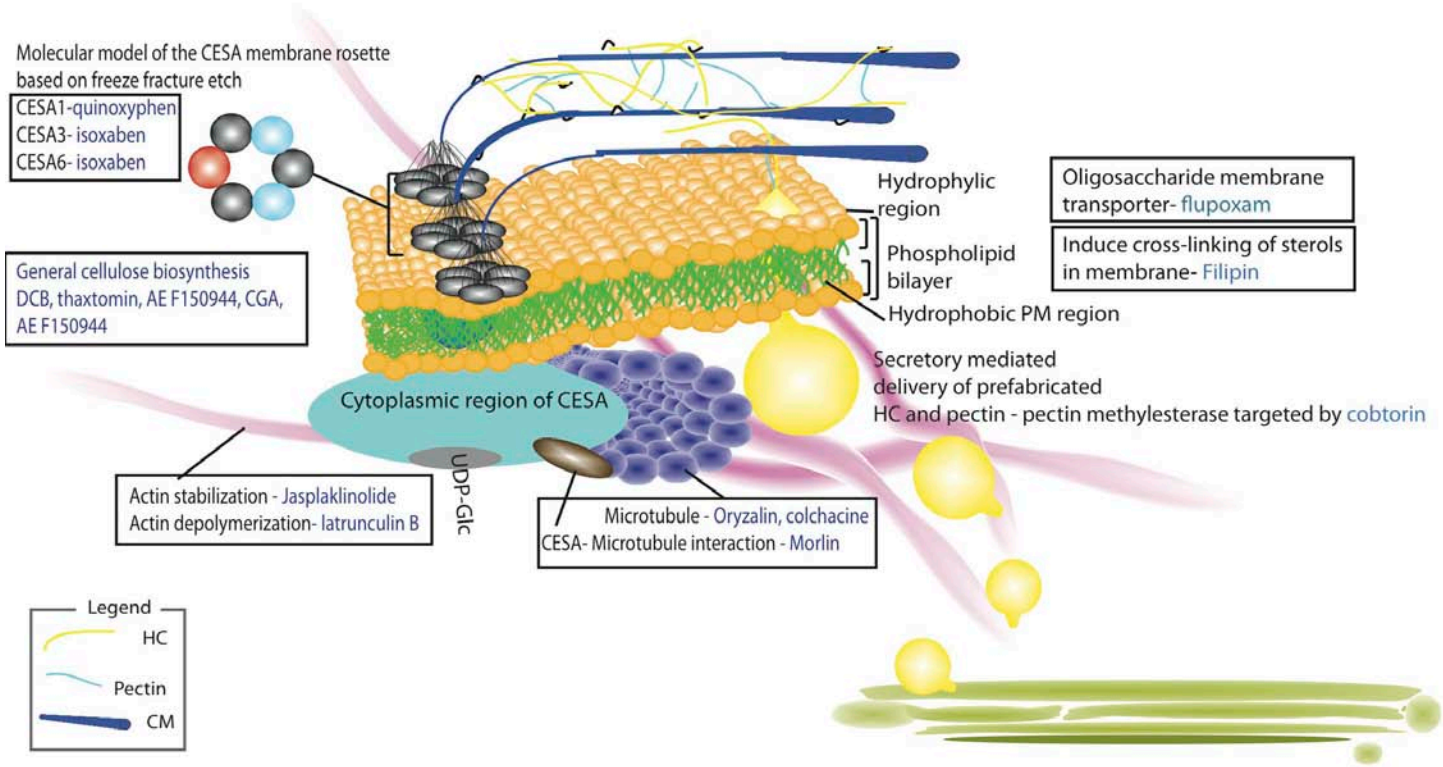
Molecular model of the CESA membrane rosette based on freeze fracture etch
CESA1-quinoxyphen
CESA3- isoxaben
CESA6- isoxaben
General cellulose biosynthesis
DCB, thaxtomin, AE F150944, CGA, AE F150944
Hydrophylic region
Phospholipid bilayer
Hydrophobic PM region
Oligosaccharide membrane transporter- flupoxam
Induce cross-linking of sterols in membrane- Filipin
Secretory mediated delivery of prefabricated HC and pectin - pectin methylesterase targeted by cobtorin
Cytoplasmic region of CESA
UDP-Glc
Actin stabilization - Jasplaklinolide
Actin depolymerization- latrunculin B
Microtubule - Oryzalin, colchacine
CESA- Microtubule interaction - Morlin
Legend
HC
Pectin
CM

Figure 2.1. The chemical toolbox for dissecting cellulose biosynthesis. Numerous cellulose biosynthesis inhibitors have been classified and some have been mapped to a target gene by forward chemical genetics such as isoxaben (*CESA3* and *CESA6*) or quinoxyphen (*CESA1*). Others, such as DCB, CGA 325'615, thaxtomin A and AE F150944 have not been mapped to a target gene, although DCB is proposed to interact with a microtubule-associated protein (MAP) (Rajangam et al. 2008). Morlin putatively targets the interaction between MTs and cellulose synthase (DeBolt et al. 2007a). Oryzalin and colchicine are MT-targeting compounds and have been used to illustrate the molecular rail hypothesis for guidance of cellulose synthase (Paredez et al. 2006). Actin depolymerization by latrunculin B has been used to show the requirement for actin mediated trafficking in placing cellulose synthase uniformly at the plasma membrane (Gutierrez et al. 2009). Stabilization of actin by jasplaklinolide reveals functional association between MTs and actin, which has yet to be examined in context of cellulose biosynthesis (Sampathkumar et al. 2011). Cobtorin, another cellulose biosynthesis inhibitor (Yoneda et al. 2007) was examined genetically using FOX lines and resistance was gained via mutations in a lectin family protein, a pectin methylesterase (AtPME1) and a putative polygalacturonase (Yoneda et al. 2010). Furthermore, examining the plasma membrane cell wall continuum in relation to cellulose synthase may utilize tools such as the plasma membrane-specific fluorescent dye filipin or the drug flupoxam, which appears to target an oligosaccharide membrane transporter (Austin et al. 2011).

that either inhibit cellulose biosynthesis or effect the cortical cytoskeleton by inhibiting MT or actin dynamics. Isoxaben (N-[3(1-ethyl-1-methylpropyl)-5-isoxazolyl]) (Table 2.1A) is a preemergence, broad leaf herbicide that inhibits cellulose biosynthesis (Heim et al. 1990b). Following a forward genetic screen for isoxaben resistant (*ixr*) mutants (Heim et al. 1989; 1990a), the *A. thaliana* loci conferring resistance to isoxaben were identified by map-based cloning and found to be *cesa3*^{ixr1} and *cesa6*^{ixr2} (Desprez et al. 2002; Scheible et al. 2001). This result is significant because at the time the only known components of the CSC were the CESA enzymes, although conclusive biochemical analysis was still lacking. Interestingly, the mutations conferring resistance to isoxaben are not found near the putative active site for either CESA3 or CESA6. Rather, the mutations are located in the C-terminal transmembrane spanning domains of both enzymes. In addition, not only does isoxaben cause a reduction in the amount of acid insoluble cell wall material, but also live-cell imaging of the rapidly elongating cells of *A. thaliana* etiolated hypocotyls expressing YFP-CESA6 has shown that the YFP signal disappears from the plasma membrane shortly after treatment with isoxaben (Paredez et al. 2006). This indicates that the mode of action of isoxaben in cellulose biosynthesis inhibition could be to prevent CESAs from coming together to form the CESA rosette complex that appears necessary for crystalline cellulose microfibril assembly. Therefore, it is possible that isoxaben may act directly through the physical disruption of protein-protein interactions or indirectly by blocking the putative pore that these transmembrane domains form to extrude the glucan chain into the cell wall. The use of isoxaben has also been helpful in supporting the premise that the CESA6-related proteins CESA2 and CESA5 both compete for the same binding site as CESA6 within the CSC. The isoxaben resistant mutant *cesa6*$^{ixr2-1}$ displays a lower isoxaben resistance compared with *cesa3*^{ixr1}, however isoxaben resistance is increased in *cesa6*$^{ixr2-1}$ when it is crossed with *cesa2* or *cesa5* and is even higher in the triple mutant. This suggests that all three CESA6-related isoforms are isoxaben targets, which explains the lower resistance of *cesa6*$^{ixr2-1}$ compared to *cesa3*^{ixr1}, because CESA3 does not appear to compete with other isoforms for its positions in the CSC (Desprez et al. 2007). Therefore, isoxaben has been a very useful tool to help evaluate gene redundancy issues among primary cell wall CESA enzymes and has provided a basis for the selection of a non-conditional mutation in the essential *CESA3* gene. However, concerning a resistance mechanism, ultimately the absence of a crystal structure for the CESA enzymes or an *in vitro* assay makes it difficult to fully resolve how isoxaben interferes with cellulose biosynthesis.

There are other cellulose biosynthesis inhibitors that appear to cause similar cellular phenotypes to that of isoxaben. AE F150944 (N2-(1-ethyl-3-phenylpropyl)-6-(1-fluoro-1-methylethyl)-1,3,5-triazine-2,4-diamine) (Table 2.1B) and CGA 325'615 (1-cyclohexyl-5-(2,3,4,5,6-pentafluorophenoxyl)-1λ4,2,4,6-thiatriazin-3-amine) (Table 2.1C) are both experimental herbicides developed by Bayer CropScience and Novartis (Syngenta) respectively, while thaxtomin A (4-nitroindol-3-yl-containing 2,5-dioxopiperazine) (Table 2.1D) is a phytotoxin produced by several species of the gram-positive filamentous bacteria in the genus *Streptomyces* that cause scab disease in potato and other taproot crops (Kiedaisch et al. 2003; Peng et al. 2001; Scheible et al. 2003). AE F150944 appears to inhibit crystalline cellulose synthesis by destabilizing plasma membrane rosettes (Kiedaisch et al. 2003). Freeze-fracture electron microscopy showed that the plasma membrane below the patterned thickenings of AE F150944-treated tracheary elements in mesophyll cells of *Zinnia elegans* was depleted of cellulose-synthase-containing rosettes, which appeared to be inserted intact into the plasma membrane followed by their rapid disaggregation (Kiedaisch et al. 2003).

Likewise, CGA 325'615 and thaxtomin A were also shown to inhibit the synthesis of crystalline cellulose and live-cell imaging shows that the green fluorescent protein (GFP)-labeled CESA3 signal in etiolated *A. thaliana* hypocotyls disappears from the plasma membrane shortly after treatment with either chemical (Bischoff et al. 2009; Crowell et al. 2009). Interestingly, while there has not been a resistant mutant identified for AE F150944 or CGA 325'615, a forward resistance screen to thaxtomin A in *A. thaliana* identified the gene *TXR1* that encodes a novel small protein most likely involved in the regulation of a transport mechanism and thus may provide resistance by reducing the uptake of thaxtomin A by the plant (Scheible et al. 2003). Specifically, N- and C-terminal GFP fusions to TXR1 were localized in the cytoplasm of tobacco leaf protoplasts and consistent with the lack of predicted transmembrane domains in the TXR1 protein, suggest that the protein acts as a cytosolic regulator of a membrane protein rather than being a permanent component of a transporter complex. The focus of future studies will be to determine whether the GFP fusions correctly reflect the localization of TXR1 and with which proteins TXR1 interacts (Scheible et al. 2003). The identification of mutants of this nature are good examples of how resistance to a small molecule does not always require the mutation of a molecular target of the molecule, but may occur through mutations to mechanisms that metabolize, modify or in this instance

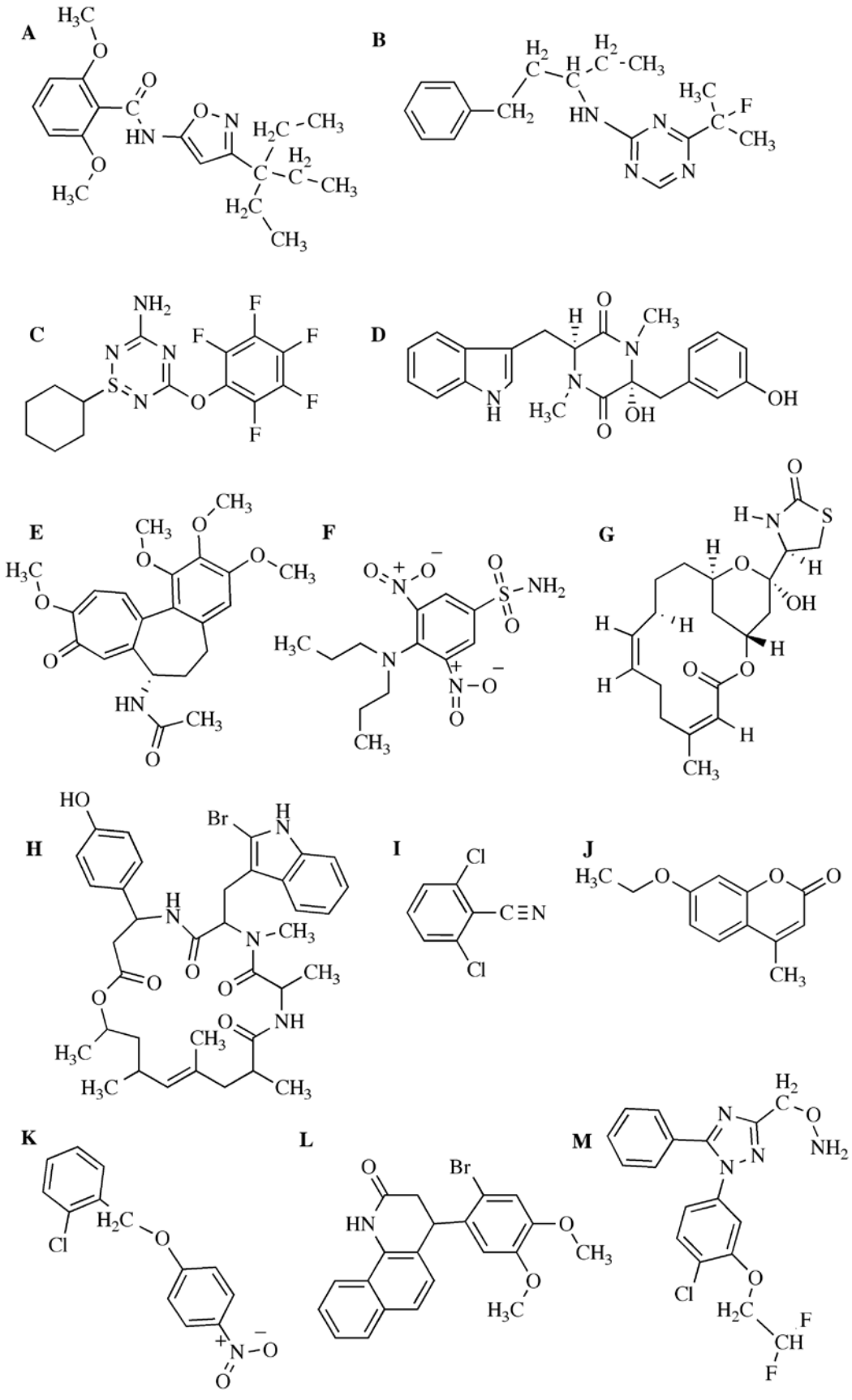
A
B
C
D
E
F
G
H
I
J
K
L
M

Table 2.1. Chemical structures for molecules described in the text. (A) Isoxaben, N-[3(1-ethyl-1-methylpropyl)-5-isoxazolyl], (B) AE F150944, N2-(1-ethyl-3-phenylpropyl)-6-(1-fluoro-1-methylethyl)-1,3,5-triazine-2,4-diamine, (C) CGA 325'615, 1-cyclohexyl-5-(2,3,4,5,6-pentafluorophenoxyl)-1λ4,2,4,6-thiatriazin-3-amine, (D) Thaxtomin A, 4-nitroindol-3-yl-containing 2,5-dioxopiperazine, (E) Colchicine, N-[(7*S*)-1,2,3,10-tetramethoxy-9-oxo-5,6,7,9-tetrahydrobenzo[*a*]heptalen-7-yl]acetamid, (F) Oryzalin, 4-(dipropylamino)-3,5-dinitrobenzenesulfonamide, (G) Latrunculin-B, 4R-[(1R,4Z,8Z,10S, 13R,15R)-15-hydroxy-5,10-dimethyl-3-oxo-2,14-dioxabicyclo[11.3.1]heptadeca-4,8-dien-15-yl]-2-thiazolidinone, (H) Jasplakinolide, 7-[(2-bromo-1H-indol-3-yl)methyl]-4-(4-hydroxyphenyl)-8,10,13,15,17,19-hexamethyl-1-oxa-5,8,11-triazacyclononadec-15-ene-2,6,9,12-tetrone, (I) DCB, 2,6, dichlorobenzonitrile, (J) morlin, 7-ethoxy-4-methyl chromen-2-one, (K) Cobtorin, 4-[(2-chlorophenyl)-methoxy]-1-ntirobenzene, (L) Quinoxyphen, 4-(2-bromo-4,5-dimethooxy-phenyl)-3,4-dihydro-1H-benzo-quinolin-2(1H)-one, (M) Flupoxam, 1-[4-chloro-3-[(2,2,3,3,3-pentafluoro-propoxy)methyl]phenyl]-5-phenyl-1H-1,2,4-triazole-3-carboximide.

cause reduced uptake of the molecule. In the future, if forward resistance screens are successful towards AE F150944 or CGA 325'615, it will be interesting to learn whether the resistance loci map to CESA or to new molecular players in cellulose biosynthesis.

Understanding the association between cellulose deposition and cortical MTs has been investigated for a number of years (Green 1962; Ledbetter and Porter 1963). In the typical plant cell, MTs are positioned just under and parallel with the plasma membrane and constitute the majority of the plant interphase cortical cytoskeletal array (Ehrhardt and Shaw 2006). In fact, the discovery of interphase MTs was stimulated in part by the observation that the mitotic spindle-disrupting drug colchicine (N-[(7*S*)-1,2,3,10-tetramethoxy-9-oxo-5,6,7,9-tetrahydrobenzo[*a*]heptalen-7-yl] acetamid) (Table 2.1E), a small molecule that traditionally has been used as a medicine for humans, also caused giant algal cells to swell in a radial pattern (Green 1962). It was then observed in subsequent studies that cellulose microfibril deposition in the walls of growing plant cells tended to be parallel to, and were often coincident with, the subjacent MTs (Ehrhardt and Shaw 2006). Other groups of anti-MT compounds seem to be specific to plant MTs and are ineffective against vertebrate MTs, making them effective herbicides with widespread use (Morejohn 1991). The dinitroaniline classes of small molecules such as oryzalin (4-(dipropylamino)-3,5-dinitrobenzenesulfonamide) (Table 2.1F) are agriculturally important herbicides commonly used to control the emergence of annual grasses and certain broadleaf weeds. Oryzalin has been shown to bind to the maize tubulin dimer to form a tubulin–oryzalin complex, which is then thought to co-polymerize with unliganded tubulin and to slow further MT assembly (Hugdahl and Morejohn 1993). Interestingly, as the different hypotheses on the alignment of cellulose microfibrils by cortical MTs have developed (Baskin 2001), the use of both anti-cellulose and anti-MT small molecules have indicated that the relationship between the cortical MTs and cell morphogenesis is more complicated than early models predicted. For example, it is possible to observe uncoupling of MT and cellulose microfibril orientation and to see order appear in one array when the other array is experimentally disrupted (Paredez et al. 2008; Paredez et al. 2006; Wasteneys and Galway 2003). MT depolymerization via oryzalin was also used to dissect trafficking of cellulose synthase to the plasma membrane (Crowell et al. 2009; Gutierrez et al. 2009). Here, a cellulose synthase rich vesicle tracks on the depolymerizing end of cortical MTs. It was also shown that effective trafficking of cellulose synthase required an intact actin cytoskeleton using the actin

depolymerizing drug latrunculin-B (4R-[(1R,4Z,8Z,10S,13R,15R)-15-hydroxy-5,10-dimethyl-3-oxo-2,14-dioxabicyclo[11.3.1]heptadeca-4,8-dien-15-yl]-2-thiazolidinone) (Table 2.1G) (Gutierrez et al. 2009). Pharmacological stabilization of actin by jasplakinolide (7-[(2-bromo-1H-indol-3-yl)methyl]-4-(4-hydroxyphenyl)-8,10,13,15,17,19-hexamethyl-1-oxa-5,8,11-triazacyclononadec-15-ene-2,6,9,12-tetrone) (Table 2.1H), a cyclo-depsipeptide produced by an Indo-pacific sponge, *Jaspis johnstoni* (Senderowicz et al. 1995) has more recently been used to show interdependence between the MT and actin cytoskeletons (Sampathkumar et al. 2011). It will be intriguing to use jasplakinolide to dissect the role of actin and more generally actin mediated trafficking in cellulose synthase delivery to the plasma membrane in plant cells.

DCB (2,6, dichlorobenzonitrile) (Table 2.1I), marketed since the 1960s under various trade names, is another synthetic herbicide that is known to inhibit cellulose biosynthesis (Hogetsu et al. 1974), but its mode of action appears to be different than that of isoxaben. Although DCB has been shown to interfere with the assembly of the linear terminal complexes implicated in cellulose biosynthesis in the alga *Vaucheria hamata* (Mizuta and Brown 1992) and to cause changes in the number of intact rosettes at the plasma membranes of moss (*Funaria hygrometrica*) and wheat (*Triticum aestivum*) (Herth 1987; Rudolph et al. 1989), more recent live-cell imaging results have shown DCB to cause simultaneous accumulation and cessation of CESA mobility within localized regions at the plasma membrane of *A. thaliana* (DeBolt et al. 2007b). This suggests that DCB does not block the interaction of CESA proteins during CSC formation, however the mechanism by which this small molecule prevents β-1,4-glucan polymerization and thus CESA mobility is still uncertain. An early clue towards the molecular function of DCB was that is was shown to bind to small proteins of 12kD from suspension-cultured tomato cell extracts and of 18 kD from cotton fiber extracts, the amount of which seemed to increase significantly at the onset of secondary cell wall synthesis in the cotton fibers (Delmer et al. 1987). In addition, DCB induces changes in the cortical MT networks in the fucoid alga *Pelvetia compressa* and *A. thaliana* roots (Himmelspach et al. 2003), which suggest that the DCB binding protein might be associated with MTs (Bisgrove and Kropf 2001). Recently, a target for DCB was identified in hybrid aspen (*Populus tremula* x *tremuloides*) using a biochemical approach and found to be MICROTUBULE-ASSOCIATED PROTEIN20 (MAP20) a protein that was also shown to bind with MTs (Rajangam et al. 2008). The assembly, bundling, and

stability of MTs have a strong dependence on the activity of various MAPs and their regulatory kinases and phosphatases (Sedbrook 2004; Wasteneys and Yang 2004). MAPs have been shown to play a role in the synthesis of the secondary cell walls in *A. thaliana*, as the FRAGILE FIBER1 (FRA1) and FRA2 proteins both affect the patterning of cellulose microfibrils in the inner wall of interfascicular fibers (Burk et al. 2007; Zhong et al. 2002a). However, MAP20 may be one of the first examples of a direct link between a specific MAP and cellulose biosynthesis and provides a possible explanation for the action of DCB.

Several other forward chemical genetic screens for compounds affecting cell wall synthesis and morphology have been conducted. To identify new chemical inhibitors of cell wall synthesis, a screen utilizing a library of 20,000 compounds from the DIVERSet collection (ChemBridge, San Diego, CA) was conducted and the coumarin derivative morlin (7-ethoxy-4-methyl chromen-2-one) (Table 2.1J) was indentified by a swollen root phenotype in *A. thaliana* (DeBolt et al. 2007a). Further analysis using live-cell imaging of fluorescently labeled MAP4 (microtubule associated protein-4) and CESA revealed that morlin caused a defect in cytoskeleton organization and its functional interaction with CESA. The identification of the target(s) for morlin may provide further insight in the mechanisms of cortical MT interaction with the cell membrane and cellulose biosynthesis. Likewise, in a smaller but similar screen looking for a swollen cell phenotype in tobacco BY-2 cells, the compound cobtorin (4-[(2-chlorophenyl)-methoxy]-1-ntirobenzene) (Table 2.1K) was identified (Yoneda et al. 2007). Further analysis showed that the effect of cobtorin was to perturb the parallel alignment of pre-existing cortical MTs and nascent cellulose microfibrils, thus the target for this molecule is likely to have an important role in the relationship between MTs and microfibrils (Yoneda et al. 2007). Recently, as a method for screening for genetic resistant mutants to cobtorin, these same authors employed the *A. thaliana* FOX hunting library, an activation tagging technology that makes use of full-length cDNAs that create gain-of-function mutants (Yoneda et al. 2010). From approximately 13,000 FOX lines, three cobtorin-resistant lines were identified. Interestingly, the genes that were overexpressed in the three FOX lines corresponded to a lectin family protein, a pectin methylesterase (AtPME1) and a putative polygalacturonase. This study goes on to show some important features of pectin in relation to the formation and orientation of cellulose microfibrils, which depend on the methylation ratio of pectin and its distribution (Yoneda et al. 2010), and which has

recently been experimentally characterized by ^{13}C solid-state magic-angle-spinning NMR (Dick-Pérez et al. 2011).

As additional chemical screens are completed and new molecules are identified that target the cell wall, it is certain that many will be followed up with successful forward resistance or hypersensitive screening and new molecular players in cell wall biosynthesis will be identified at an ever increasing efficiency. An example of the former is a drug classified as a quinolin derivative named quinoxyphen (4-(2-bromo-4,5-dimethooxy-phenyl)-3,4-dihydro-1H-benzo-quinolin-2(1H)-one) (Table 2.1L), that seems to mimic isoxaben in its cellular phenotype by causing the disappearance of YFP::CESA6 at the plasma membrane in *A. thaliana*, however the resistant locus for this drug was determined through a map-based approach to be *CESA1* (Harris and DeBolt, unpublished). The fact that quinoxyphen affects YFP-CESA6 while apparently targeting CESA1 further supports the previous evidence gained from studies with isoxaben and *rsw1* indicating that these proteins interact with each other to form a functional CSC during primary cell wall cellulose biosynthesis. The quinoxyphen resistant mutant also shows a growth phenotype only slightly reduced to that of wild-type, thus representing the first fully viable, non-conditional mutant in CESA1. An example of a recent chemical genetic hypersensitivity screen was that of an EMS-mutagenized population of *A. thaliana* hypersensitive to the cellulose biosynthesis inhibitor flupoxam (1-[4-chloro-3-[(2,2,3,3,3-pentafluoro-propoxy)methyl]phenyl]-5-phenyl-1H-1,2,4-triazole-3-carboximide) (Table 2.1M) (Austin et al. 2011). Two mutants were identified, *flupoxam hypersensitive 1 and 2* (*fph1, fph2*) and through the use of NGM technology the loci were identified as *ECTOPIC ROOT HAIR3* (*ERH3*) for the *fph1* locus and *OLIGOSACCHARIDE TRANSMEMBRANE TRANSPORTER* (*OST3/OST6)* for the *fph2* locus. Neither *ERH3/FPH1* nor *OST3/OST6/FPH2* encode cell wall biosynthetic enzymes and consequently this screen did not identify new biosynthetic enzymes involved in *de novo* synthesis of cell walls, but rather for regulators of cell wall composition (Austin et al. 2011).

Chapter III*

Tools for cellulose analysis in plant cell walls

Cellulose is intimately associated with multiple facets of human civilization: central to clothing, shelter, heat, medicine and food, there are few moments in the average human life that are not spent in direct contact with cellulose or a by-product of its composition. It should come as no surprise then that a considerable amount of time and energy have been spent, and a couple of Nobel prizes awarded, in research involved with the analysis of cellulose structure and metabolism from various sources. As the understanding of this important biomacromolecule has developed, numerous analytical techniques have been put to use to decipher cellulose biosynthesis, structure and function within the plant cell wall. Content of this update is designed to introduce the reader to current and developing tools for cellulose characterization. To begin, 'a brief history on the analysis of cellulose' describes how many of the modern analytical techniques used to determine cellulose structure came into use. This leads into the various imaging techniques that interrogate cellulose biosynthesis especially those that have arisen since the identification of the CELLULOSE SYNTHASE A (CESA) genes. We then turn our attention to recent *in vitro* biochemical studies of CESA and in this context we discuss the relationship between CESA and detergent-resistant fractions of the plasma membrane (PM), which have the opportunity to shine new light on the PM-cell wall continuum.

Characterization of cellulose using integrated analytical tools: A brief history

Cellulose was named by the French Academy over 171 years ago (Brongniart et al. 1839) subsequent to its characterization in various plant tissues by the famous French plant scientist Anselme Payen (Payen 1838). His use of different treatments based on sodium hydroxide, potassium hydroxide or nitric acid to extract and partially digest cellulose from oak and beech wood revealed an element composition comparable to that of starch (Payen 1838). Classical organic chemistry then allowed for the determination of the β-(1$\rightarrow$4) linkage that separates glucose residues in the cellobiose unit (reviewed

*** This chapter was originally published as: Harris D, Bulone V, Ding S-Y, Debolt S (2010)** Tools for cellulose analysis in plant cell walls. Plant Physiology 153: 420-426. Copyright permission was granted by the authors for inclusion in this dissertation.

in (Hon 1994). The remarkable nature of cellulose as a polymer of repeating glucose (cellobiose) units (Haworth 1932; Staudinger 1926) contributed greatly to the 1937 and 1953 Nobel Prize's in Chemistry. Today it is understood that cellulose fibrils from many natural sources result from individual glucan chains of cellulose aggregating via hydrogen bonds and Van der Waals forces to form a long thread-like paracrystalline structure termed the microfibril. The route that led to a sophisticated model of cellulose structure began with X-ray diffraction (XRD) studies. The first XRD patterns of cellulose fibers were generated from wood, hemp and bamboo samples, and although detailed structural data was not initially obtained, it was determined that the crystallites were of a rod-like shape (Nishikawa and Ono 1913). However, cellulose in a majority of higher plants forms crystalline domains that are not large enough to produce high-resolution crystallographic structure determination (Lai Kee Him et al. 2002; Muller et al. 2002). Therefore, many of the early molecular models developed for the monoclinic unit cell (Meyer and Misch 1937) and triclinic unit cell (Honjo and Watanabe 1958) of cellulose were based on algal or tunicate (animal) model systems (Fischer and Mann 1960). In addition, modern XRD data have been collected at even higher resolution than before by using a synchrotron light source and can be paired with the separate analytical technique of neutron diffraction, which in combination with specific deuteration, has greatly increased the power to locate hydrogen atoms involved in the inter- or intra-molecular hydrogen bonding of the cellulose microfibril (Nishiyama et al. 2002; Nishiyama et al. 2003).

Simultaneous to the development of XRD methods, (Rowen et al. 1947) analyzed cellulose from cotton (*Gossypium hirsutum* L.) by Infrared (IR) absorption spectroscopy and later (Marrinan and Mann 1956) recognized that algae (*Valonia*) and bacterial cellulose yielded IR spectra that were different from those of tunicates, cotton, or ramie (*Boehmeria nivea*). Eventually, in the early 1980s the spectroscopic technique of solid-state ^{13}C cross-polarization (CP) magic-angle spinning (MAS) nuclear magnetic resonance (NMR) spectroscopy was able to resolve this issue by showing that native cellulose I diffraction data from many natural sources were a composite of diffraction from the two crystalline allomorphs Iα (triclinic unit cell) and Iβ (monoclinic unit cell) (Atalla and VanderHart 1984). ^{13}C-NMR spectroscopy would not only confirm that the crystalline structure of the cellulose microfibril in most plants was a composite of Iα and Iβ crystalline forms (Viëtor et al. 2002), but in combination with Fourier transform infrared

spectroscopy (FTIR) spectra, it suggested that the more crystalline inner chains of the microfibril core are composed primarily of cellulose Iβ, while both forms of cellulose compose the chains in the surrounding paracrystalline sheath (Šturcová et al. 2004).

Collectively, these early crystallographic and spectroscopic studies laid the foundation for elucidation of the native cellulose structure in plant cell walls. Simultaneously, microscopic analyses showed that cellulose microfibrils were dimensionally different in different cell types of the plant (Balashov and Preston 1955; Roelofsen and Houwink 1953). Malcolm Brown and coworkers revealed, first in the green alga *Oocystis* (Brown and Montezinos 1976) and then in higher plants (Mueller and Brown 1980), that the ends of nascent cellulose microfibrils were often associated with globular structures designated as terminal complexes (TCs) embedded in the plasma membrane. The freeze fracture of the plasma membrane was imaged on the P-fracture face by transmission electron microcopy (TEM), showing a structure with a six-fold symmetry (rosette), and remains to this day a fundamental piece of evidence suggesting that this type of structure is involved in cellulose synthesis in plants (Mueller and Brown 1980). Further, in the study by Kimura and co-workers (Kimura et al. 1999), TEM was used in combination with an immunoaffinity probe to show that the catalytic subunit of cellulose synthase is associated with the rosette complex in vascular plants. Despite the disadvantages of extensive and often destructive sample preparation, and the inability to study live specimens, TEM is unsurpassed in its resolution and has been the method of choice for ultra-structure analysis of the cell wall. Newer techniques in TEM sample preparation are being developed to reduce sample destruction along with the use of promising new affinity tools to be used in conjunction with TEM, such as carbohydrate-binding modules (CBMs), that will most likely provide enhanced molecular resolution imaging of the cellulose microfibril network (reviewed in Sarkar et al. 2009).

Integrated with the abovementioned analytical tools of IR, NMR, XRD, and TEM, the relatively new imaging technique of atomic force microscopy (AFM) has the capacity to provide atomic level resolution of the cellulosic matrix in the cell wall of fresh tissue. Therefore, beyond the compositional structure of cellulose, AFM can offer a spatial view of cellulose microfibril orientation in the polylaminate cell wall. AFM is based on scanning probe microscopy (SPM) (Binning and Rohrer 1986), and uses a physical tip to scan the surface of a specimen to determine its topography, physical properties and chemical

structure (Drake et al. 1989). AFM operates by driving a cantilever with a sharp tip mounted at its end to allow raster scanning across the specimen surface. AFM images are the result of convolutions of the tip and the "true" structure of the specimen at an atomic resolution. Plant cell walls were one of the first biological samples that were examined by AFM (Kirby et al. 1996; van der Wel et al. 1996). The motivation of using AFM for characterizing cell walls is obvious: plant cell walls are relatively stiff and flat, and the molecular features of the microfibril network occur at the nanometer scale. Ideally, AFM could be used to answer some of the key questions regarding the nanostructures within plant cell wall cellulose (Davies and Harris 2003; Engel et al. 1999; Kirby et al. 1996; Morris et al. 1999; Thimm et al. 2000; van der Wel et al. 1996) beyond that defined by the previously mentioned analytical techniques.

To take full advantage of AFM and reduce interference by artifacts, an approach with minimized sample preparation is ideal. Greatest success has used hand-cut sections of fresh or naturally aged dry tissue while operating the AFM in tapping mode and imaging the inner surface of the native cell wall (Ding and Himmel 2006; Himmel et al. 2007). Using this strategy, it was possible to image primary and secondary cell walls from maize (*Zea mays* L.). AFM imaging of dry primary cell walls documented microfibril dimensions precisely measured at 3-5 nm (Ding and Himmel 2006), consistent with the 36-glucan chain model of cellulose elementary fibril (CEF) biosynthesis. In addition, cellulose macrofibrils, consisting of a bundle of CEFs that split at the end to form smaller bundles and eventually single CEFs, were also observed by AFM (Ding and Himmel 2006). Each microfibril observed in mature primary cell walls contained only a single CEF with non-cellulosic polymers associated with its surface (Ding and Himmel 2006; Himmel et al. 2007). AFM images of maize cell walls from fresh cells further confirmed these observations (Figure 3.1A and B). AFM images of 3-day old developing maize coleoptiles (Figure 3.1A) showed macrofibrils of 50-100 nm in diameter with rather clean surface features, which contained multiple CEFs. By contrast, 4-week old maize stem piths containing mature parenchyma (Figure 3.1B) displayed 2 distinguishable layers. In the upper layer, the fibrils appeared to be small macrofibrils with diameters of 7-10 nm, and single CEFs with diameters of 3-5 nm. In the posterior layer, all microfibrils of 3-5 nm diameter were arranged in a parallel orientation (Figure 3.1B). Furthermore, in the mature cell walls (Figure 3.1B) particle-like features decorated the macrofibrils that may

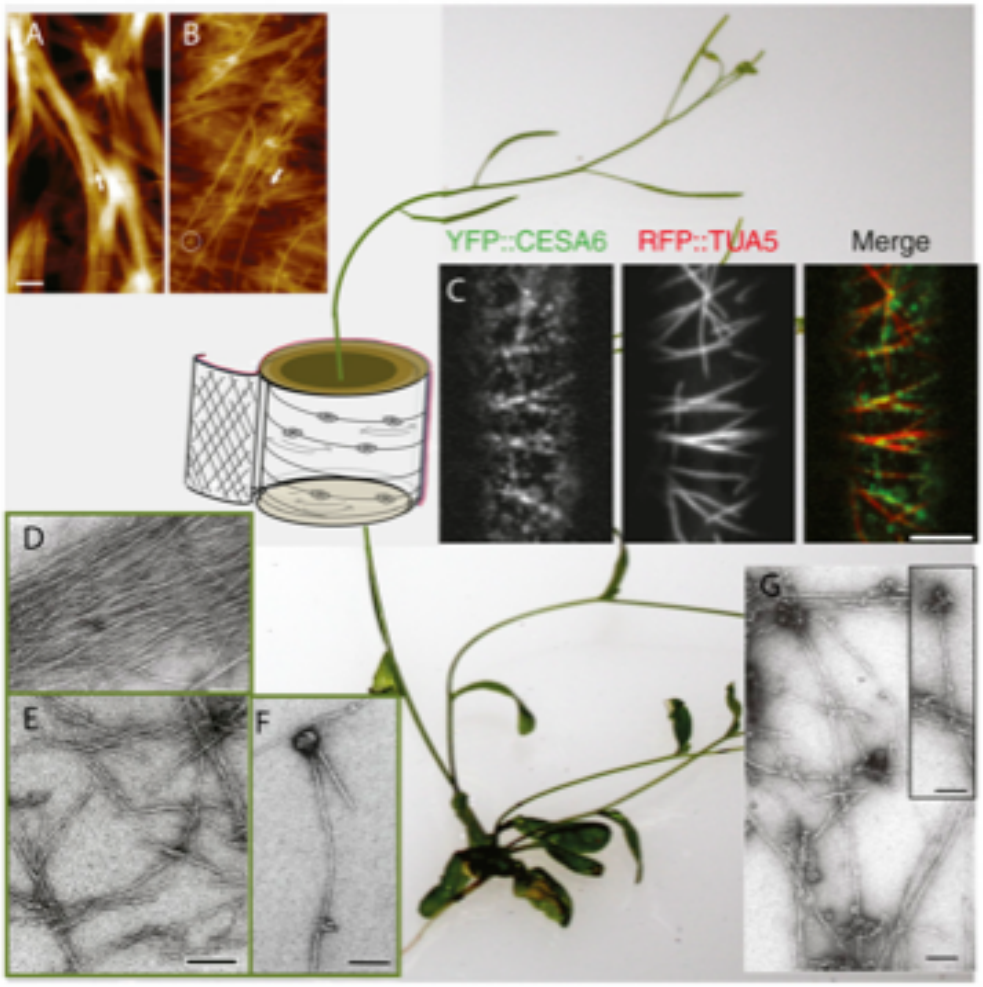

Figure 3.1. Emerging tools for cellulose analysis in plant cell walls. The background is set with the model plant *Arabidopsis thaliana*; a simple schematic is overlaid on the stem to indicate various facets of cell wall cellulose synthesis. AFM height image of fibril structures in the elongating primary cell wall of maize contained primarily macrofibrils that split at the end (indicated by the arrow)(A). The mature primary cell wall contained both small macrofibrils in the upper most layer that can also split at the end (indicated by the arrow) and parallel-arranged single elementary fibrils (B). Particle-like features were clearly seen and were typically associated with the macrofibrils (indicted by the circle) (B). Scale bar = 100 nm. Confocal image of upper hypocotyl cells of transgenic plants expressing YFP::CESA6, RFP::TUA5 (tubulin) and the overlay of the two compatible fluorophors in a merged imaged reveals the coincidence of CESA with microtubules(C). Scale bar = 5 μm. Electron micrographs of cellulose microfibrils extracted from primary walls of blackberry (*R. fruticosus*) cells (D and E) and of cellulose synthesized *in vitro* (F)

using detergent extracts as a source of enzyme. The cellulose from cell walls was observed before (D) and after (E) treatment with the Updegraff reagent (Lai Kee Him et al. 2002). A cellulose microfibril synthesized *in vitro* associated to a globular particle, which most likely corresponds to the enzyme complex (not treated with the Updegraff reagent) (F). Electron micrograph of cellulose microfibrils (G) synthesized *in vitro* by DRMs isolated from hybrid aspen cells grown as suspension cultures (negative staining with 2% uranyl acetate). Insert: magnification of putative DRM structures that carry the active cellulose synthase machinery and from which cellulose microfibrils are being formed. Scale bars in E, F and G = 0.1 μm.

have been formed by hemicelluloses, proteins or other cell wall polymers (Ding and Himmel 2006) and were not observed in the macrofibrils of elongating cells (Figure 3.1A). A plausible explanation for these differences among cell types is a delay between cellulose biosynthesis and incorporation of other cell wall polymers into the cell wall. Ultimately, AFM imaging representing the native structure of cellulose provides an enormous opportunity to better understand molecular architecture in dermal cell layers, particularly when combined with confocal live-cell imaging described below.

As an analytical tool, confocal microscopy has rapidly evolved from being a challenging technique with limited accessibility to a high throughput tool providing quantitatively precise localization data for 30% of the proteome in the model plant *Arabidopsis thaliana* (Chalfie et al. 1994; Cutler et al. 2000; Heazlewood et al. 2007; Tian et al. 2004). The capacity to visualize a protein relies on excitation of an autofluorescent protein (AFP), such as the green fluorescent protein (GFP) derived from the jellyfish *Aqueora victoriae*, fused to a plant protein of interest. Despite the most famous AFP being the GFP characterized 16 years ago (Chalfie et al. 1994), there are now numerous forms of AFP including blue (BFP), cyan (CFP) and yellow (YFP) fluorescent proteins (Goodin et al. 2007). Designing an AFP expression fusion can still be a daunting task given the numerous expression vectors available, the choice of where to fuse the AFP, what promoter to use, and whether to use stable or transient expression of the chimeric protein fusion (reviewed in Goodin et al., 2007). Live-cell imaging of CESA has led to a remarkable increase in our understanding of the enzyme's subcellular localization, regulation, trafficking and guidance in growing cells during primary cell wall synthesis (Crowell et al. 2009; DeBolt et al. 2007a, 2007b; Desprez et al. 2007; Gutierrez et al. 2009; Paredez et al. 2006, Persson et al. 2007) and in vascular tissue during secondary cell wall synthesis (Wightman and Turner 2008). Labeling of the primary wall complex with YFP::CESA6 or GFP::CESA3 in *A. thaliana* hypocotyl cells, revealed discrete particles at the focal plane of the PM. The observation that these particles moved along linear trajectories at constant velocity (av. 270 $nm.min^{-1}$: Paredez et al. 2006) suggests they represent actively synthesizing complexes. The majority of labeled CESA, however, resides in the cytoplasm, located in Golgi stacks (confirmed by colocalization with labeled β-mannosidase, a Golgi-resident protein) and in a heterogenous population of smaller compartments (Crowell et al. 2009; Gutierrez et al. 2009; Paredez et al. 2006)

In vivo visualization of cellulose synthase was initially used to investigate the dynamic interaction between CESA complexes and the underlying cortical microtubule array (Paredez et al. 2006), first described nearly 40 years ago (Hepler and Newcomb 1964). It was long believed that the microtubule cytoskeleton guided CESA complexes and thus cellulose deposition; however, the mechanism for this guidance was not known. Time-lapse confocal microscopy showed that CESA trajectories were coincident with labeled microtubules, indicating that microtubules act as molecular rails rather than passive barriers to CESA movement (Figure 3.1C) (Paredez et al. 2006). More recently, the microtubule array was found to participate in the delivery of CESA complexes to the PM (Crowell et al. 2009; Gutierrez et al. 2009). Analysis of individual delivery events indicated that complexes are preferentially delivered to sites that are coincident with cortical microtubules (Gutierrez et al. 2009). Interestingly, small CESA-containing compartments have been shown to associate with the cortical microtubule array (Crowell et al. 2009; Gutierrez et al. 2009). Taken together, these observations suggest that microtubules may position CESA delivery to the PM by interacting with secretory compartments in the cytoplasm.

Recent work has also revealed that CESA motility is coincident with microtubule arrays during secondary cell wall synthesis (Wightman and Turner 2008). Importantly, these authors also deduced that actin filaments are instrumental in rapid intracellular trafficking of CESA, which is necessary for cell wall thickening (Wightman and Turner 2008). The actin cytoskeleton is also required for proper CESA trafficking during primary cell wall synthesis: application of the actin-depolymerizing drug latrunculin B disrupts the global distribution of CESA at the PM (Gutierrez et al. 2009). Further details have been gleaned from careful observation of time-lapse imaging, for instance it was observed that after arriving at the PM focal plane, the YFP::CESA6 began to move almost immediately (within a minute) after arrival (Paredez et al. 2006). From this, a tentative deduction would be that the CESA complex is activated and begins making cellulose very soon after arrival at the PM. Particles also are observed to disappear from the PM, suggesting a further level of regulation that terminates CESA activity. However, it has not been possible to track a PM localized CESA particle from the initiation of its lifespan to termination. One reason for this is that the inevitable curvature of the epidermal cell being imaged makes it difficult to conclude that a particle has not simply moved out of the focal plane rather than disappeared from the PM. Indeed, many questions remain

unanswered for the budding microscopist and will require future improvements in confocal resolution.

Small effector molecules have been invaluable in dissecting aspects of cellulose biosynthesis by live-cell imaging. For instance the inhibitor of microtubule polymerization, oryzalin, was useful in demonstrating that the CESA insertion and directional motility were independent of microtubules (DeBolt et al. 2007b; Paredez et al. 2006). As mentioned above, inhibiting actin polymerization using latrunculin B showed the requirement for actin in CESA trafficking (Gutierrez et al. 2009; Wightman and Turner 2008). Assessing the localization behavior of CESA after treatment with inhibitors of cellulose biosynthesis such as isoxaben (*N*-[3(1-ethyl-1-methylpropyl)-5-isoxazolyl]; Heim et al., 1989), DCB (2,6, dichlorobenzonitrile; (Montezinos and Delmer 1980), CGA (1-cyclohexyl-5-(2,3,4,5,6-pentafluorophenoxyl)-1λ4,2,4,6-thiatriazin-3-amine; (Peng et al. 2001) and thaxtomin (Loria et al. 2006) have allowed for the study of the mechanisms of action for these drugs. For instance, CGA, thaxtomin and isoxaben cause clearance of CESA from the PM, and therefore either secretion of CESA is compromised or CESA is unable to assemble once at the PM (Bischoff et al. 2009; Crowell et al. 2009; Paredez et al. 2006). By contrast, DCB does not stop complexes from forming at the PM, but once there, CESA movement ceases and CESA hyper-accumulates (DeBolt et al. 2007b). Interestingly, DCB has been shown recently to bind to a microtubule-associated-protein in hybrid aspen, further supporting an action of the drug on the movement of CESA (Rajangam et al. 2008). New inhibitors of cellulose biosynthesis have been screened and identified using live-cell imaging, a good example being morlin (DeBolt et al. 2007a), which inhibits both microtubule dynamicity and CESA, further demonstrating the intimate association between these processes. Obtaining the protein targets of all these small molecule inhibitors presents an enormous opportunity to define new players or interactions in cell wall cellulose biosynthesis.

Biochemical analyses of cellulose biosynthesis

Despite all the previous evidence presented, the biochemical analysis of the CESA rosettes has been a major challenge in the field of plant cell wall biosynthesis. The enzyme complex is highly unstable and this has limited the possibility of purifying it and studying its biochemical properties *in vitro*. Detergent extractions of proteins from plant plasma membranes typically lead to the loss of the β-(1→4) glucosyltransferase activity

of cellulose synthase (Bessueille and Bulone 2008; Delmer 1999). In addition, further complication is due to the unavoidable concomitant extraction of callose synthase from the plasma membrane. This enzyme uses the same substrate as cellulose synthase (UDP-glucose) and exhibits high activity *in vitro* (Colombani et al. 2004; Lai Kee Him et al. 2001; Lai Kee Him et al. 2002; Okuda et al. 1993), even though callose is normally a minor cell wall component that forms transiently at the cell plate prior to cell division, or in specialized cells (*e.g.* pollen tubes) or cell structures (*e.g.* plasmodesmata) (Stone and Clarke 1992). Thus, the formation of β-(1→3) glucan by callose synthase is typically prevalent in *in vitro* reactions, and this has further complicated the detection of the highly unstable and low cellulose synthase activity. In addition, due to non-rigorous polysaccharide characterization, the incorporation of glucose from UDP-glucose into ethanol-insoluble β-(1→3) glucans has sometimes been wrongly associated to cellulose biosynthesis reviewed in (Bulone 2007; Colombani et al. 2004). It has been proposed that callose and cellulose formation might be catalyzed by the same enzyme (Delmer 1999), but the isolation of different genes encoding the presumed catalytic subunits of callose and cellulose synthases is contradictory with this hypothesis reviewed in (Bessueille and Bulone 2008). However, one may still argue that experimental evidence demonstrating that the products of the *CESA* genes cannot catalyze the formation of callose, and *vice versa*, is still missing. The definitive answer to this question will be obtained when an active cellulose synthase preparation devoid of callose synthase activity becomes available. The first successful *in vitro* synthesis of cellulose from plant cell free extracts was achieved using cotton fiber and mung bean enzymes (Kudlicka and Brown 1997; Kudlicka et al. 1995; Kudlicka et al. 1996). However, it was only several years later that the amount of cellulose synthesized *in vitro* was significantly improved by the careful selection of detergents that allow the extraction of enzyme complexes in an intact form (Lai Kee Him et al. 2002). The use of taurocholate and Brij 58 to extract cellulose synthase from plasma membranes of cell suspension cultures of blackberry (*Rubus fruticosus*) allowed the synthesis of cellulose in mg amounts. This made possible the complete and unequivocal characterization of the cellulose synthesized *in vitro* (Lai Kee Him et al. 2002). Interestingly, the microfibrillar cellulose formed in the *in vitro* reactions was 10-15% more crystalline than the cellulose extracted from the primary walls of the same cells, as measured by XRD analysis (Lai Kee Him et al. 2002). This was further supported by the fact that cellulose from primary walls was sensitive to the Updegraff (Updegraff, 1969) reagent (Figure 3.1D and E) while the *in*

vitro synthesized microfibrils were not (Lai Kee Him et al. 2002). When the samples were not treated with this reagent, the individual microfibrils synthesized *in vitro* were associated with globular structures that most likely correspond to the enzyme complex responsible for their formation (Figure 3.1F). Since this significant progress, the method has been optimized in other plant systems such as hybrid aspen (Colombani et al. 2004) and tobacco BY2 cells (Cifuentes et al. 2010) for which digitonin was selected as the best detergent. It seems that the type of detergent used for enzyme extraction needs to be determined for different plant species, which perhaps reflects different lipid environments. As for the blackberry cellulose synthase (Lai Kee Him et al. 2002), higher levels of activity were obtained with the detergent-extracted cellulose synthase from hybrid aspen when the cells were harvested at their stationary phase, with up to 50% cellulose and 50% callose synthesized *in vitro* (Colombani et al. 2004). To date, this represents the highest proportion of cellulose to callose reported in *in vitro* synthesis experiments. But despite these important advances, it remains that the *in vitro* assays need to be systematically combined with careful analyses of the *in vitro* product to determine the extent of β-(1→4) linkages formed. This can be performed routinely using highly specific cellulases that are not contaminated by β-(1→3) glucanase activities, which is not always the case for commercial enzymes. Typically, the biochemical evidence of the *de novo* synthesis of cellulose is provided by the sensitivity of the polymer synthesized in the presence of radioactive UDP-glucose to the specific cellulases. If needed, more complete characterization can be performed, for instance by GC/MS analysis after derivatization of the glucans (methylation analysis), electron and/or XRD analysis, TEM and NMR reviewed in (Bulone 2007). However, for XRD and NMR analyses, the scale-up of the *in vitro* reactions is required to obtain enough polymer for the characterization. Solid-state NMR is particularly demanding in terms of amount of polysaccharide (typically at least 10 mg), but a sensitive method based on the use of UDP-glucose in which the glucose is enriched in ^{13}C has been developed and allows the analysis of *in vitro* glucans with as low as 100 μg of polysaccharide (Fairweather et al. 2004). The analysis of the cellulose synthesized *in vitro* can be further facilitated by dissolving the β-(1→3) glucan that is co-synthesized with cellulose in NaOH solutions. Indeed, crystalline cellulose such as that synthesized *in vitro* by the detergent-extracted enzyme from blackberry is not soluble in NaOH (Lai Kee Him et al. 2002). However, it is important to keep in mind that some poorly crystalline β-(1→4) glucan may be synthesized and lost by dissolution in NaOH. In summary, the tools to

assay cellulose synthase *in vitro* and unequivocally characterize the cellulose formed are currently available. This opens a great opportunity to perform detailed biochemical analysis of the cellulose synthase complex when a purified preparation can be obtained. To date, this has been extremely challenging, but important progress has been made recently in this area with the purification of complexes from *A. thaliana* using dual epitope tagging and the specific corresponding purification steps (Atanassov et al. 2009). However, it was not possible in this work to search for enzymatic activity because the purification procedure was not efficient enough. The enzymatic assays and sensitive tools mentioned above for the characterization of cellulose synthesized *in vitro* will be most useful also for the biochemical analysis of recombinant individual catalytic subunits of cellulose synthase, which may be possible in the near future with the development of more efficient expression systems for membrane-bound proteins.

Owing to the availability of these tools and of specific anti-cellulose synthase antibodies, it was recently demonstrated that callose and cellulose synthases are located in detergent-resistant structures exhibiting similar biochemical properties as lipid rafts in animal cells (Bessueille et al. 2009). The preparations were active *in vitro* and able to synthesize microfibrillar glucans that were identified as callose and cellulose (Bessueille et al. 2009). The glucan sample identified as cellulose, shown in Figure 3.1G, was not treated with any procedure prior to observation. This allowed for the preservation of the detergent-resistant membrane microdomains (DRMs), which are visible as globular structures or aggregates of globular structures (Figure 3.1G). It was not determined though whether both callose and cellulose synthases are located in the same or different sub-populations of DRMs (Bessueille et al. 2009). The relationship between DRMs and lipid rafts is debated (Hancock 2006; Lichtenberg et al. 2005), essentially because the experimental conditions used for DRM isolation may artificially induce the formation of such structures (Lichtenberg et al. 2005). It remains nonetheless that the extractions of DRMs reflect differential affinities of specific sets of membrane proteins to various lipid environments (Lichtenberg et al. 2005). Thus, the isolation of DRMs is a valuable tool for understanding the interactions of callose and cellulose synthases with the lipids that co-segregate with them and that consist of a higher relative proportion of sterols and sphingolipids than the total plasma membranes (Bessueille et al. 2009). In addition, DRMs represent a form of isolated carbohydrate synthases that can be further fractionated using detergents or other compounds such as chaotropic agents that disrupt

interactions between specific lipids and proteins. This approach, combined with the enzymatic assays available and the detailed proteomics analysis of the sub-fractions recovered after treatment with chaotropic agents, represents a promising strategy to identify proteins that interact directly with the enzyme complexes.

Chapter IV*

Relative Crystallinity of Plant Biomass: Studies on Assembly, Adaptation and Acclimation

Structural and morphological diversity is a striking feature of land plants. Lignin and a group of carbohydrate polymers (pectin, hemicelluloses and cellulose) form the scaffolding of the cell wall, which in turn are the building blocks for cell shape and morphogensis (Brown 2004). The crystalline nature of cellulose has been one of the central problems studied by polymer scientists. Cellulose microfibrils are the main structural component of plant cell walls and are formed of (1-4) linked β-D-glucosyl residues that are alternatively rotated by 180° along the polymer axis to form ribbon-like chains (Hermans 1949). It has been established that each glucosyl residue has three hydroxyl groups, one of which is a hydroxymethyl group. The tight bonding capacity of the hydroxyl groups via hydrogen bonding are critical to determining how the crystal structure of cellulose forms and also in directing important physical properties of cellulose materials (Nishiyama et al. 2002). The chains of glucosyl residues in the fibril periodically fail to coalesce into an ordered crystalline structure; these amorphous zones along the fibril length are recognized as possibly serving the association between hemicellulose and cellulose fibrils (Gomez et al. 2008). In elongating plant tissue, cellulose deposition is generally considered to occur perpendicular to the axis of elongation, constraining lateral swelling (due to turgor pressure) and allowing longitudinal or anisotropic cell expansion (Mutwil et al. 2008). A surprising gap in our understanding concerns fibril length and what controls it, with current estimates ranging from 300 to 15,000 glucan units (Brett 2000). Another unresolved question regarding cellulose biosynthesis is whether cellulose fibril orientation, length or crystallinity may provide differential biomechanical properties to certain cell and tissue types and how this may correspond to a specific ecological niche?

Study of the overall variation in plant function have largely focused on traits such as foliar stoichiometry (Vitousek et al. 1995), specific leaf area (Niklas and Cobb 2008),

*** This chapter was originally published as: Harris D and DeBolt S** (2008) Relative crystallinity of plant biomass: studies on assembly, adaptation and acclimation. PLoS ONE 3: e2897. Copyright permission was granted by the authors for inclusion in this dissertation.

seed and seedling characteristics (Wright et al. 2000), leaf area/dry mass (specific leaf area) (Vile et al. 2005), wood specific gravity (Woodcock and Shier 2003), stem diameter (Niklas and Cobb 2008) and the relationship between stem and branch wood specific gravity (Swenson and Enquist 2008). This building number of key functional traits is aimed at providing botanists with the ability to characterize the differential body plan and biomass allocation of plants with respect to their ecological niche (Graham et al. 2000). Do plants adapt to environmental stimuli by regulating the density, orientation and/or biomechanical properties of cellulose fibrils in differentiated tissues? Recent studies of cellulose biosynthesis have shown that the upper hypocotyls of dark-grown *A. thaliana* seedlings expressing a functional YFP tagged cellulose synthase 6 (CESA6) have a transverse oriented CESA array. Yet, when this array is exposed to light the array rapidly changes (within 20 min) to a longitudinal array (Paredez et al. 2006) suggesting that elongating plants that are searching for light are very rapidly able to alter the biomechanics of their cellulose array. The orientation of CESA motility (Paredez et al. 2006; DeBolt et al. 2007a) appears to be guided by underlying cortical microtubules. Moreover, the site of CESA insertion at the plasma membrane occurs in a non-random pattern suggestive of regulation (DeBolt et al. 2007b). It has recently been found that the plant may have a cell wall sensing mechanism, *THESEUS1,* to provide transcriptional feedback on the integrity of the cell wall (Hématy et al. 2007). Recent discoveries at the cellular level suggest much is to be learnt about the regulation and plasticity of cellulose synthesis and its contribution to morphogenesis. The necessary body plan and biomass allocation properties of plants that proliferate under certain selection pressures such as growing at a rainforest floor have been found to differ dramatically from those that adapted to the upper canopy environment (Wright et al. 2007). Land plant ecology on the basis of functional traits would thus suggest that plants adapt their biomechanical structure (Read and Stokes 2006; Smith and Ennos 2003); this hypothesis was to be addressed in the current study with respect to the structure of cellulose.

Experiments described herein were designed to determine whether relative crystallinity of plant biomass samples was capable of responding to environmental cues. A central tool for polymer scientists studying the structure of cellulose polymorphs has become X-ray diffraction (Segal et al. 1959; Weimer et al. 1995), which has been shown to reflect the degree of polymerization (Puri 1984) as well as structure (Andersson et al. 2003; Andersson et al. 2000; Andersson et al. 2004; Honjo and Watanabe 1958; Sarén et al.

2001; Teeäär et al. 1987). Adopting published methods for the calculation of a relative crystallinity index (RCI, Weimer et al. 1995) as well as results gathered using synthetic cellulose (Simacell, Weimer et al. 1995 or Avicel, Andersson et al. 2004), RCI was determined using X-ray diffraction (XRD) in various plant samples. RCI determination can be influenced by the preferred orientation of cellulose crystallites in a sample (Andersson et al. 2004) or the size and surface area of the cellulose crystallites (Yoshida et al. 2008). Hence it is important to note that the RCI parameter is relative to the portion of crystalline cellulose in the sample, thus defined as crystallinity of the sample rather than absolute crystallinity of the cellulose itself. Problems in crystallinity determination for wood samples from Norway spruce and Scots pine by transmission X-ray diffraction suggest that cellulose properties of size, orientation and crystalline:amorphous ratios are important considerations when assessing diffractogram differences (Andersson et al. 2004). Plant response to abiotic physical stresses such as wind was assessed by RCI and in more detail etiolation was assessed by X-ray diffraction, YFP::CESA6 experiments and FTIR analysis. RCI was measured in a study of 35 diverse plant species, spanning liverworts to several C4 grasses. The RCI values of root, shoot and leaf were compared to assess differences among plant assembly components. Finally, these results are discussed with respect to technical challenges and ecological and biomechanical context.

Materials and Methods

Chemicals All chemicals and reagents used were of analytical grade or higher. Authentic samples of organic acids and their salts were obtained from Sigma Aldrich, FMC BioPolymer, Fisher Scientific, Riedel den Haan and BDH as applicable.

Statistical analysis Hierarchical clustering, frequency distribution analysis (histogram) and analysis of variance were performed in the freeware statistical program *R* (Auckland, NZ).

Plant Material and Sampling Foliar samples from non-*Arabidopsis thaliana* plants were from plants grown in Lexington Kentucky at the University of Kentucky Arboretum on the University of Kentucky campus and an Agricultural Experimental Station research farm. Samples from 35 different plant specimens were used in experiments were as follows: *Marchantia polymorpha, Sphaeopterus cooperi, Asparagus setaceus, Sedum*

morganianum, Podocarpus macrophyllus, Cycas circinalis, Araucaria araucana, Equisetum hyemale, Epiphyllum oxypetalum, Aspidistra elatior, Drosera adelae, Arabidopsis thaliana, Pisum sativum, Panicum virgatum (Cave in Rock, Alamo, Trailgrazer)*, Arundo donax, Miscanthus giganteus, Miscanthus sinescens, Miscanthus saccharifolia, Cyanodon tactylon*, *Phalaris arundinacea L., Eragrostis tef, Eragrotis curvula, Tripsacum dactyloides* (PMK24, Meade Co and Jackson), *Festuca arundinacea, Spentina pectinaria, Chasmanthium latifolium, Sorghastrum nutans (Cheyenne and Rumsey), Muhlenbergia shreberi, Andropogon gerardii* (KYAG9601 and KAW) and *Sorghum bicolor.* Sampling occurred during 2007-2008 and leaf samples for the study of RCI were batch samples of 15 leaves. *Arabidopsis thaliana* cv. Columbia plants were analyzed as whole plants samples or divided into roots, shoots and leaves. These plants were grown at 22°C under a 16 h light 8 h dark regime in 3 batches of 50 plants and harvested as plant biomass. The transgenic plants expressing YFP::CESA6 were slightly different than those previously published (DeBolt et al. 2007a; DeBolt et al. 2007b; Hématy et al. 2007) in that we extensively re-screened the T1 generation of the transformation described by Paredez et al. (2006) to isolate a homozygous allele that complemented the procuste (CESA6) mutant since the previous allele was heterozygous. We selected the homozygous allele that had functional and bright expression of the YFP.

Characterization of Natural Variation in Relative Crystallinity by X-ray Scattering

Samples were prepared by oven drying biomass at 60°C for 36 hours. Alternative temperatures for the drying regime were used, such as 37°C for 7 days or 80°C for 12 hours followed by 110°C for two hours, neither of which altered the RCI value measured in *A. thaliana* tissue. Tissue was then homogenized using as Arthur H Thomas Co Scientific grinder (Philadelphia, PA) equipped with a 1 mm sieve. For experiments testing finely ground biomass, homogenization was achieved by ball milling into fine powder. Biomass samples were then contained in a custom built sample holder of pressed boric acid. In brief, plant material was placed into a mold, containing a sleeve and hand pressed with a solid metal plug forming a disk shape. The sleeve and plug were removed and a boric acid (Fischer, Madison, WI) base was then formed by pouring the boric acid over the bottom and sides of the sample and applying 40,000 psi of pressure to the 40X40 mm mold using a Carver Autopellet Press (Wabash, IN). Samples were pressed to create an even horizontal surface. A Bruker-AXS Discover D8

Diffractometer (Bruker-AXS USA, Madison, WI) was used for wide angle X-ray diffraction with Cu Ka radiation generated at 30 mA and 40 kV. The experiments were carried out using Bragg-Brentano geometries (symmetrical reflection). Diffractograms were collected between 2º and 70º or 2º and 40º (for samples with little baseline drift), with 0.02º resolution and 2 s exposure time interval for each step (run time, 2 h). Sample rotation to redirect the X-ray beam diffraction site was achieved per replicate. *A. thaliana* material was grown under both greenhouse and growth chamber for analysis. The data analysis was carried out using the calculation for relative crystallinity index (22) of: RCI=I_{002}-I_{am}/I_{002} x 100, where I_{002} is the maximum peak height above baseline at approximately 22.5º and I_{am} is the minimum peak height above the baseline at ~18º. For assessment of experimental accuracy, the pressed samples were examined using reflective geometries at 22.5º 2-theta with the sample scanned rotationally (360º) and in an arc (90º) to obtain an intensity/spatial orientation plot of a sample for which the RCI had already been established. The range of reflective intensities was then used to estimate the accuracy of the RCI determination using a 95% cutoff across the plot range. Diffractograms were collected in Diffrac-Plus-XRD Commander software (Bruker-AXS, Karlsruhe, Germany) and minimally processed (baseline identification, noise correction, 3D display and cropping of RCI signature region) using the EVA and TexEval (Bruker-AXS Karlsruhe, Germany) software.

Etiolation and high wind experiments *Pisum sativum* (pea) was chosen for etiolation experiments. Changes in the cellulose relative crystallinity index were tested in hypocotyls of pea plants grown under light and dark conditions. Approximately 100 pea seedlings were germinated in soil and identical flats were halved and either grown in darkness to encourage etiolated hypocotyls or in light (16:8 light: dark) conditions for 7 days. Whole plants were then harvested, cleaned with Millipore water and leaf and root tissue removed and discarded. Hypocotyls were then pooled and oven dried to complete dryness at 80°C for 36 hours and pressed and packed in custom-built boric acid base as described above for measurement of relative crystallinity by X-ray diffraction. For high wind experiments, *Arabidopsis thaliana* Columbia plants were germinated and grown for 7 days under no wind conditions and then either exposed to wind produced by a fan at a constant average air velocity of 4.6 meters per second for a period of 14 days. All plants were container grown under growth room conditions of 16:8 light: dark for both treatments and watered regularly to avoid dehydration. Stem tissue and leaf tissues

were separated and independently dried at 80°C for 36 hours prior to processing and XRD analysis as described above. Static and video imaging was performed using a Kodak M863 camera (8.2 MegaPixel) (Eastman Kodak Company, Rochester, NY).

Leaf Mass/Area and Leaf Length Measurements Correlated With RCI Leaf mass per unit area (LMA) measures the dry mass investment per unit of light intercepting the leaf area deployed and leaf length of all leaves was measured from the beginning of the leaf blade to the axial tip of the leaf (cm). All measurements were plotted against the RCI values in Excel (Microsoft) software.

Confocal Microscopy. Seeds were germinated on 0.5 X MS agar for 2–4 d in darkness at 21°C by wrapping in aluminum foil. Seedlings were mounted in water between a slide and a cover slip. Once mounted, specimens were imaged in darkness, then exposed to light for 5 min and then imaged again 30 minutes later. Imaging was performed on an Olympus FV1000 laser scanning confocal microscope using a 63X N.A 1.4 oil-immersion objective. The microscope is equipped with lasers for excitation wavelengths ranging from 405-633 nm and EYFP was excited using the EYFP setting in the Olympus Fluoview software (Olympus). All image processing was performed by using Olympus Fluoview software (Olympus) and ImageJ (W. Rasband, National Institutes of Health, Bethesda, MD) software.

FTIR Spectroscopy For Fourier Transform Infrared analysis (FTIR), pre-cleaned by solvent extractions and dried pea material were pooled and homogenized by excessive milling. The powder was mixed with KBr, and pressed into 7-mm pellets. Four FTIR spectra for each line were collected on a Thermo Nicolet Nexus 470 spectrometer (ThermoElectric Corporation, Chicago, IL) over the range 4,000–800 cm^{-1} (Kacuráková et al. 2000). For each spectrum, 200 scans were co-added at a resolution of 8 cm^{-1} for Fourier transform processing and absorbance spectrum calculation by using OMNIC software (Thermo Nicolet, Madison, WI). Spectra were corrected for background by automatic subtraction and saved in JCAMP.DX format for further analysis. Using win-das software (Wiley, New York), spectra were baseline-corrected and were normalized and analyzed by using the analysis covariance matrix method. Figures were processed using Adobe Illustrator.

Cellulose determinations Cellulose contents were measured spectrophotometrically according to the protocol of (Updegraff 1969) on homogeneous samples of ground biomass. Spectrophotometry was performed on a ThermoFischer Biomate3 (Madison, WI).

Results

Determining crystallinity index for plant biomass

Previous methods for estimating the crystallinity of cellulose (Andersson et al. 2003; Andersson et al. 2000; Andersson et al. 2004; Honjo and Watanabe 1958; Puri 1984; Sarén et al. 2001; Segal et al. 1959; Teeäär et al. 1987; Weimer et al. 1995). were adapted to plant biomass samples (Figure 4.1A and B, Methods and Materials). Initially, synthetic cellulose (Avicel) was pressed into a custom-built boric acid base using 40,000 pounds per square inch (psi) and analyzed using Bragg-Brentano reflective geometries. X-ray diffraction pattern (Figure 4.1A) showed consistent signature peak distribution with previous published reports (Andersson et al. 2003; Andersson et al. 2000; Andersson et al. 2004; Honjo and Watanabe 1958; Puri 1984; Sarén et al. 2001; Segal et al. 1959; Teeäär et al. 1987; Weimer et al. 1995) and an average relative crystallinity index for synthetic crystalline cellulose of 65.8 ± 8.12%. The experimental accuracy was approximated by determining the noise in the diffractogram using a *Phi* and *Chi* scan (360° rotational by 90° in an arc) of the sample, creating a intensity/ spatial orientation plot at 22.5° 2-theta (Figure 4.1B). However, this value does not take into account the possibility that texture of the sample influences RCI. It was found to be extremely challenging to use the leaf and non-woody biomass samples for the analysis of transmission geometries. Most technically challenging was mounting the sample, X-ray penetration through the sample and orientation of the fiber axis (some of which is random in leaf cells). Our attempts centered on the use of pressed potassium bromide (KBr) into a 7 mm diameter mold to create an opaque disk with the sample embedded, but maintaining any control over fiber orientation was not achieved. Also, the X-rays were not penetrating the disk well enough to provide enough intensity of the symmetrical transmission geometries (even at 110 and 200 A our peaks were very low intensity with rocking in the 110 A range required to create peak resolution). A lack of texture analysis in the samples by transmission geometries does not allow us to predict the preferred orientation of crystallites within the samples, nor the size or density of crystallites. Rather, RCI provides relative value for the reflective geometry of sample crystallinity.

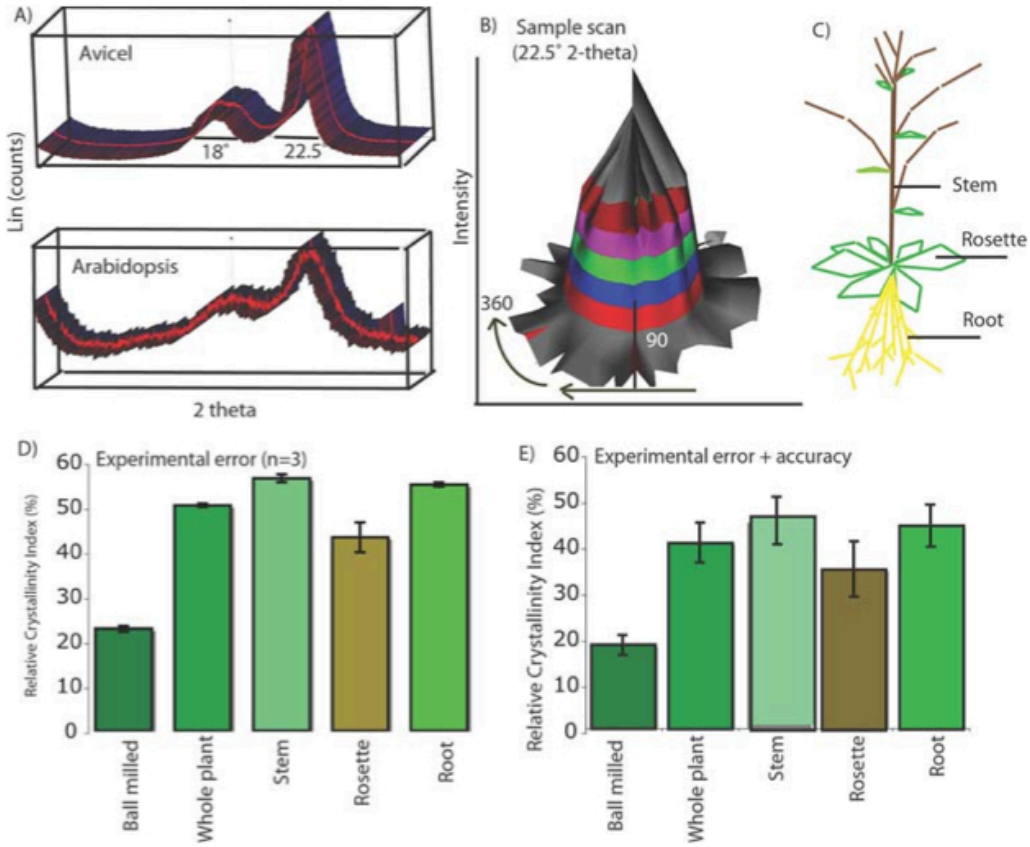

Figure 4.1. X-ray diffraction and plant ontogeny. A) Synthetic crystalline cellulose (Avicel) displayed a diffractogram pattern consistent with diffractogram from plant biomass derived from *A. thaliana* whole plant biomass (B) Schematic of the sample scan used to estimate the experimental accuracy of pressed biomass at 22.5u 2-theta. Experimental accuracy was determined to be 8.99% (C) Roots, leaves and shoots from *A. thaliana* plants were sub-sampled and analyzed by XRD showing variability of RCI between tissues. (D) RCI values for ball milled samples, whole plant sample and stem, rosette (leaf) and root values. *Rosette RCI was significantly lower than stems or roots (P,0.001, ANOVA) whereas stems and roots were not significantly different. (E) RCI values for ball milled samples, whole plant sample and stem, rosette (leaf) and root values with experimental accuracy included.

Experimental samples were packed and analyzed in triplicate and the error estimated between sample replicates was added to the estimated accuracy error. *A. thaliana* whole plant samples were measured in 12 independent samples and the value remained between 47.5% and 49.8%, suggesting that the relative estimate was reproducible, but only provided a relative crystallinity value of the sample not absolute crystallinity. Nonetheless, total error may still be underestimated, considering the results of (Andersson et al. 2004) who found that texture considerably affected determination of the experimental accuracy.

RCI measurement of root, stem and rosette tissue in *Arabidopsis thaliana*

Whole plant *Arabidopsis thaliana* Columbia tissue from a combined 50 plant crop grown at 22°C under 16:8 light: dark cycle demonstrated that the average crystallinity of cellulosic biomass was 48.49 % with a total RCI error of 4.71, which gave a total error of 9.47%. These data were consistent in several independently grown crops and gathered from 12 experimental replicates. Treatment of sample with three hot ethanol (70%) washes to remove chlorophyll and other cellular debris did not alter the RCI measurement nor did the drying samples at 37° C for 7 days compared with drying at 80° C (data not presented). *Arabidopsis thaliana* Columbia plants grown to maturity (at which time siliques had filled out containing mature seed) were harvested and divided into roots, stems and leaves (Figure 4.1C). Average RCI value for 3 independent measurements for stem was 54.79% ± 0.83, leaf (rosette RCI = 41.99% ± 3.21) and root (RCI = 53.42% ± 0.42) (Figure 4.1D). However, taking into consideration the experimental accuracy the total error was considerably greater with stems (54.79% ± 5.76), leaf (rosette RCI = 41.99% ± 6.98) and root (RCI = 53.42% ± 5.22) (Figure 4.1E). Relative crystallinity index of the *A. thaliana* leaf tissue was 23.6% and 21.4% lower that shoot and root tissue respectively (Table 4.1). The volume fraction of cellulose in the leaf tissue (22% of total biomass) was approximately 36% lower than both stems (35%) and roots (32%).

Crystallinity index among a spectrum of land plants

Foliar samples of 35 different plants were collected, oven dried and the RCI measured by XRD (Table 4.1, Figure 4.2A and B). It was evident that crystallinity measurements varied greatly among species assayed. The grasses had the highest RCI (58.5%) of all

Table 4.1 Plant species analyzed within this study

Common Name	Botanical Name	Emergence	Tissue	RCI (avg)	St. Dev	Exp Rep #	Exp Accy	Total Error	Total Error %
Avicel			Synthetic Cellulose	65.80	2.20	2	1.97	4.17	6.3
Liverwort	*Marchantia polymorpha*	Ordovician	Leaf	18.18	0.89	2	0.91	1.80	9.9
Lance leaf sundew	*Drosera adelae*	Cretaceous	Leaf	31.75	1.04	2	1.59	2.63	8.3
Monkey puzzle	*Araucaria araucana*	Jurassic	Leaf	33.33		1	1.67	1.67	5.0
Buddhist pine	*Podocarpus macrophyllus*	Permian	Leaf	33.93		1	1.70	1.70	5.0
Australian tree fern	*Sphaeopterus cooperi*	Mid-Devonian	Leaf	35.24	0.76	2	1.76	2.52	7.2
Horsetail	*Equisetum hyemale*	Carboniforous	Leaf	37.50	0.45	2	1.88	2.33	6.2
Burro tail	*Sedum morganianum*	Carboniforous	Leaf	40.00	0.49	2	2.00	2.49	6.2
Cyad Queen Sago	*Cycas circinalis*	Jurassic	Leaf	41.11	0.89	2	2.06	2.95	7.2
Cyrus spp	*Epiphyllum oxypetalum*	Cretaceous	Leaf	41.76		1	2.09	2.09	5.0
Plumosa fern	*Asparagus setaceus*	Cretaceous	Leaf	46.15		1	2.31	2.31	5.0
Arabidopsis	*Arabidopsis thaliana*	Devonian/ Carboniforous	Whole Plant	48.94	0.31	12	2.45	2.76	5.6
Cast iron plant	*Aspidistra elatior*	Cretaceous	Leaf	48.75		1	2.44	2.44	5.0
Switchgrass Kan Low	*Panicum virgatum*	Cretaceous	Leaf	55.54	0.64	3	2.78	3.42	6.2
Switchgrass Cave in Rock	*Panicum virgatum*	Cretaceous	Leaf	55.54	0.40	3	2.78	3.18	5.7
Sweet Sorghum	*Sorghum bicolor*	Cretaceous	Leaf	55.54		1	2.78	2.78	5.0
Arundo donax	*Arundo donax*	Cretaceous	Leaf	53.57		1	2.68	2.68	5.0
Giant Miscanthus	*Miscanthus giganteus*	Cretaceous	Leaf	57.90		1	2.90	2.90	5.0
Sweet Mischanthus	*Miscanthus saccharifolia*	Cretaceous	Leaf	52.20		1	2.61	2.61	5.0
Flame Mischanthus	*Miscanthus sinescens*	Cretaceous	Leaf	55.20		1	2.76	2.76	5.0
Eastern gamagrass PMK24	*Tripsacum dactyloides*	Cretaceous	Leaf	55.70		1	2.79	2.79	5.0
Eastern gamagrass Meade	*Tripsacum dactyloides*	Cretaceous	Leaf	55.90		1	2.80	2.80	5.0

Continued on the following page.

Eastern gamagrass Jackson	*Tripsacum dactyloides*	Cretaceous	Leaf	56.30		1	2.82	2.82	5.0
Indian gamagrass Cheynne	*Sorghastrum nutans*	Cretaceous	Leaf	52.10		1	2.61	2.61	5.0
Big Bluestem KAW	*Andropogon gerardii*	Cretaceous	Leaf	58.50		1	2.93	2.93	5.0
Big Bluestem KYAG09	*Andropogon gerardii*	Cretaceous	Leaf	55.60		1	2.78	2.78	5.0
Arabidopsis	*Arabidopsis thaliana*	Cretaceous	Ball Milled	22.14	0.22	2	1.11	1.33	6.0
Arabidopsis	*Arabidopsis thaliana*	Cretaceous	Whole plant (Grind)	48.94	0.36	3	2.45	2.81	5.7
Arabidopsis	*Arabidopsis thaliana*	Cretaceous	Stem (Mature)	54.79	0.83	3	2.74	3.57	6.5
Arabidopsis	*Arabidopsis thaliana*	Cretaceous	Rosette (Mature)	41.99	3.21	3	2.10	5.31	12.6
Arabidopsis	*Arabidopsis thaliana*	Cretaceous	Root (Mature)	53.42	0.42	3	2.67	3.09	5.8
Arabidopsis	*Arabidopsis thaliana*	Cretaceous	Stem +wind (3 wk)	52.08	1.23	3	2.60	3.83	7.4
Arabidopsis	*Arabidopsis thaliana*	Cretaceous	Stem –wind (3 wk)	55.80	0.38	3	2.79	3.17	5.7
Arabidopsis	*Arabidopsis thaliana*	Cretaceous	Leaf +wind (3wk)	42.02	0.88	3	2.10	2.98	7.1
Arabidopsis	*Arabidopsis thaliana*	Cretaceous	Leaf –wind (3 wk)	42.64	0.98	3	2.13	3.11	7.3
Pea	*Pisum sativum*	Cretaceous	Hypocotyl Dark (7d)	23.07	1.54	3	1.15	2.69	11.7
Pea	*Pisum sativum*	Cretaceous	Hypocotyl Light (7d)	26.86	1.18	3	1.34	2.52	9.4

Common and botanical names, evolutionary emergence, tissue used in analysis, relative crystallinity index (RCI), number or sample replicates, standard error among replicates where applicable, experimental accuracy and total error.

species tested and liverwort (*Marchantia polymorpha),* had the lowest RCI (18.8%). Of a collection of 22 grass species, the range in RCI was determined to be 51.1% to 58.5%, which was higher than leaves from all other species and more similar to values acquired from the stem of *A. thaliana*. Other noteworthy observations were the similarity of RCI values for *Podocarpus macrophyllus* and *Araucaria araucana,* which are both of the pinophyta phylum. *Cycas circinalis* (Cycad)*, Sedum morganianum* (Burro tail)*, Equisetum hyemale* (horsetail) and *Epiphyllum oxypetalum* (Orchid) also displayed a similar RCI value ranging from 37.5 to 41.7%. The carnivorous plant *Drosera adelae* (lance leaf sundew) measured the second lowest RCI of 31.8%. Indeed, other plants with a similar morphology to the lance leaf sundew but very different metabolism such as *A. thaliana* displayed higher RCI values (Table 4.1, Figure 4.2).

Relative crystallinity, analysis of cellulose reorientation using YFP::CESA6 in dark to light conditions and FTIR spectral analysis of etiolated versus light-grown pea hypocotyls

Dark-grown versus light-grown seedlings invest a greater proportion of cellular energy into seeking light (elongation) and maximizing, capturing and transmitting light (Mandoli and Briggs 1982). Shade conditions have also been shown to increase Young's modulus in petioles resulting in greater tensile strength (Liu et al. 2007). Because the plant modified its body plan under dark growing conditions, this provided an opportunity to test whether RCI changed. Seven-day-old, dark-grown etiolated pea (*Pisum sativum*) seedlings displayed no pigmentation of hypocotyls and the tissue geometry and morphology were perpendicular to the growth media horizontal surface. Seedling heights were variable as demonstrated by the average height frequency graph (Figure 4.3A and 3B). The average height of dark-grown seedlings (9.5 ± 2.8 cm) was significantly greater than light-grown seedlings (3.7 ± 1.2 cm $P<0.001$, Wilcoxan Ranked Signed Test). Leaf and root tissue was separated and discarded and light and dark-grown hypocotyls were then oven dried, pressed and packed into boric acid for analysis by XRD. The corresponding RCI measurement of dark-grown hypocotyls was 23.07 ± 1.54% (n=3) with an estimated experimental accuracy of 2.07 (total was 3.61 or 15.64%). Based on sample replicates, this value was significantly lower ($P<0.05$, ANOVA) than measurements made in light-grown hypocotyls 26.86 ± 1.17%, however considering the level of experimental accuracy measured using a scan of the sample (Figure 4.1B), the

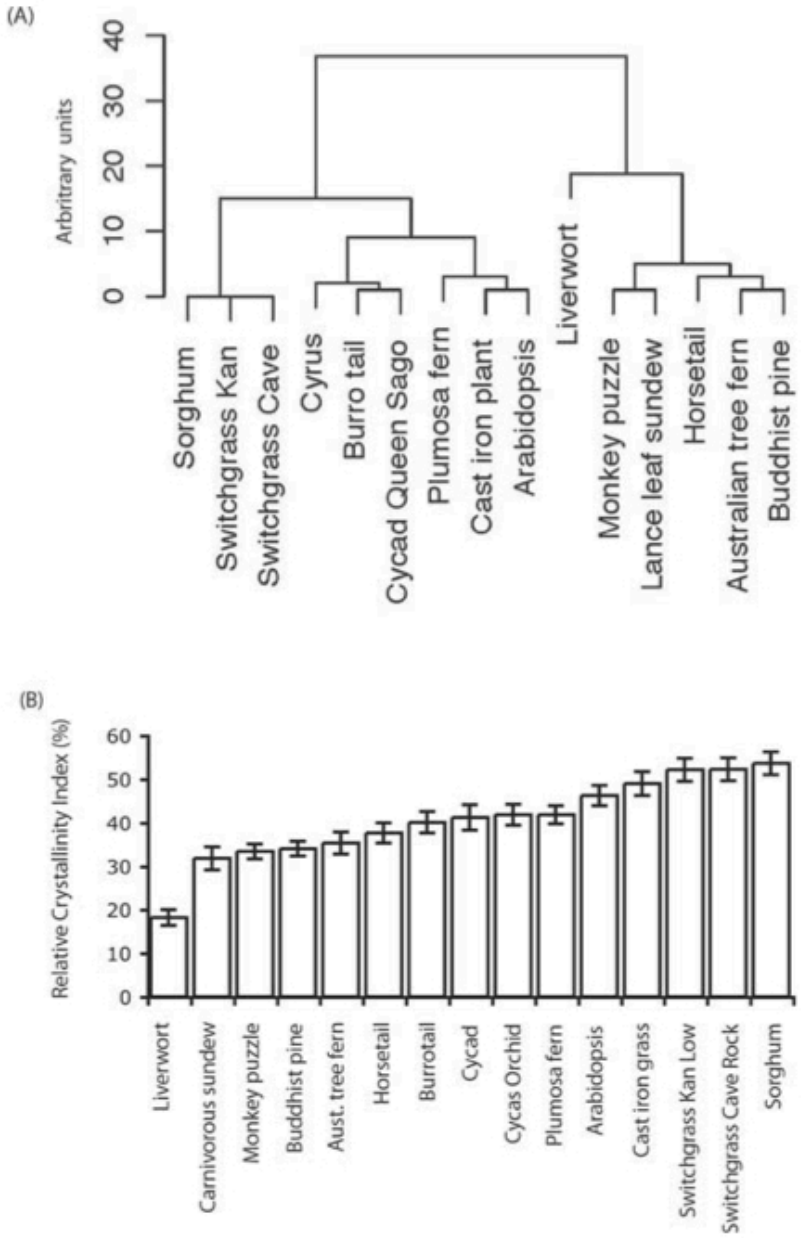

Figure 4.2. RCI values and their hierarchical cluster dendogram for foliar samples from diverse range of species indicates a large degree of variability. A) Samples were clustered based on values for their RCI (B).

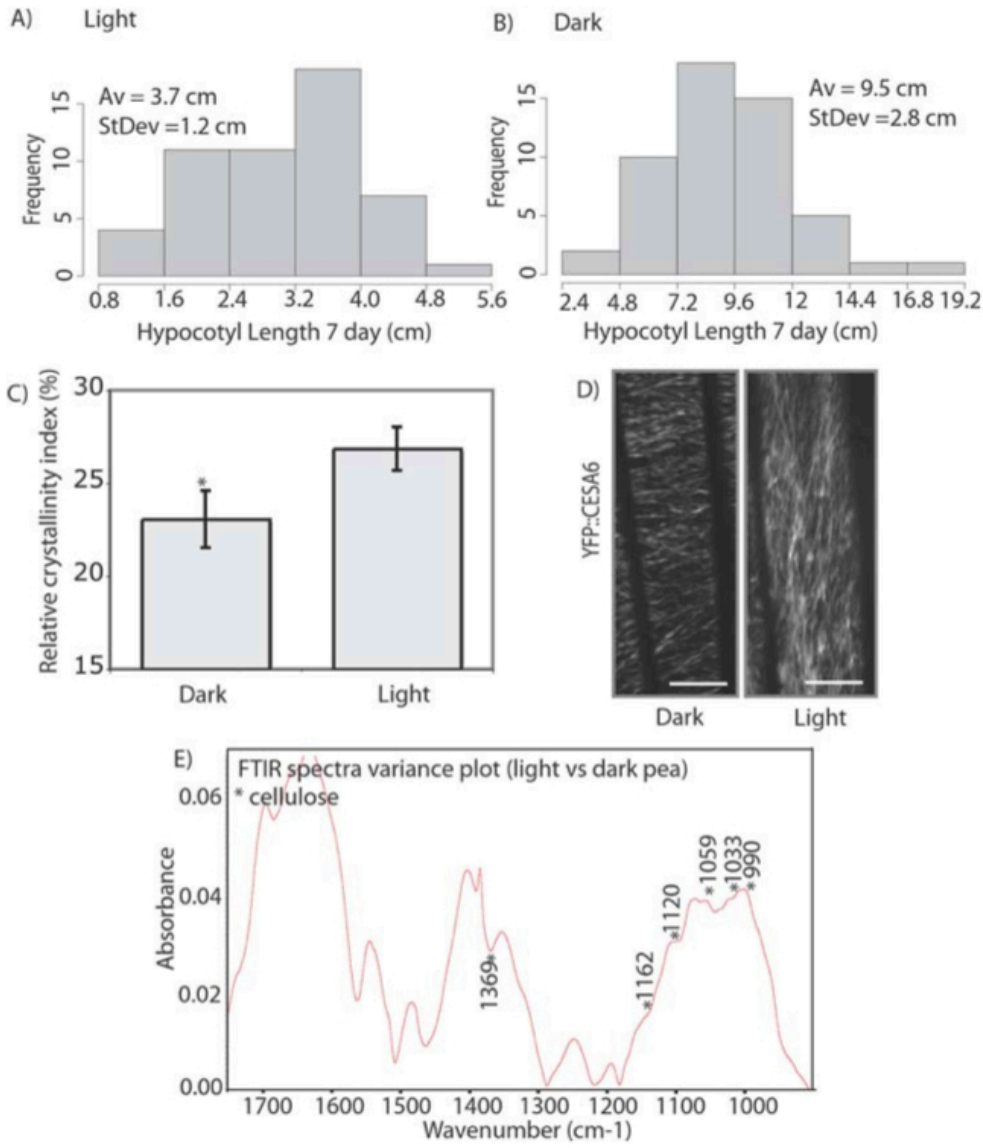

Figure 4.3. Hypocotyl lengths and RCI of etiolated pea (*Pistum sativum*) seedlings compared with light-grown seedlings were significantly different. (A) Histogram of hypocotyl length for light-grown and (B) dark-grown. Dark-grown hypocotyls had a significantly lower RCI that light-grown (C) (*P,0.001, ANOVA). (D) *A. thaliana* plants expressing YFP::CESA6 displayed a transverse orientation under dark conditions and longitudinal array under light conditions, images are time averages of 61 frames taken 10 sec apart for 10 min. Maximal linear trajectories particles was 14.66 mm for dark and 26.8 mm for light-grown. Scale bar = 10 mm (E) FTIR spectral variance plot of light versus dark-grown pea plant samples.

determination of significance was not substantiated (Figure 4.1C and D, Figure 4.3C, Table 4.1).

Because it is postulated that each visible YFP::CESA6 puncta represents an intact cellulose synthase rosette, we performed measurements of the YFP::CESA6 dynamics before and after light exposure. Dark-grown seedlings were exposed to a light source for 5 min and then reimaged 30 minutes later (Figure 4.3D). Firstly, we confirmed orientation shift from within the range of 180º ± 20 to 90º ± 20 (Paredez et al. 2006). Secondly, measurement of particle velocity of membrane bound YFP::CESA6 particles between transverse (dark) and longitudinal (light) oriented arrays were not significantly different (274 $nm.min^{-1}$ ± 34 and 268 $nm.min^{-1}$ ± 41, Wilcoxan Ranked Signed Test). Thirdly, average track lengths in the transverse array were 11.33 ± 1.46 μm compared with 14.1 ± 2.9 μm (P>0.05, ANOVA) for the longitudinal array. Maximum track lengths were 14.66 μm in the transverse array compared with 26.8 μm after exposure to the light in the longitudinal array. The combined length of a cellulose track in a given time consists of multiple particles in a 61 frame time lapse image. Fourth, the number of individual CESA puncta in a given track were compared by the calculation: $CesA_D = T_L / P_n$ where $CESA_D$ is CESA density along a track, T_L is the track length over 61 frames (μm) and P_n is the average particle number along that track. An average of 12.02 ± 2.92 particles per strand (n=47 strands) were counted in transverse arrays compared with 13.36 ± 4.30 particles per strand (n=47 strands) in longitudinal arrays (P>0.05, Wilcoxan Ranked Signed Test). Average CESA density (particles. μm^{-1}) along a single track was lower in the transverse array (0.86 ± 0.08 particles.μm^{-1}) than the longitudinal array (1.05 ± 0.13 particles. μm^{-1}) but again not significantly lower (P>0.05, ANOVA). Hence, orientation was the only significant change in the cellulose array. The FTIR spectra from the cell walls showed a clear separation of the light-grown pea hypocotyls compared with dark-grown seedlings using an analysis of variance spectra generated from four replicates. Spectral variance in the FTIR data (Figure 4.3E) within thepolysaccharide fingerprint region was difficult to assign to a single cell wall polymer and was more likely a reflection of cell wall reorganization. In the variance spectrum, there were distinct peaks in the FTIR spectrum that have been defined as arising from cellulose (Kacuráková et al. 2000) (990, 1033, 1059, 1120, 1152 and 1369 cm^{-1}) (Figure 4.3E). In addition, amide-I absorption peak at 1673 cm^{-1} (Figure 4.3E) may reflect higher protein content.

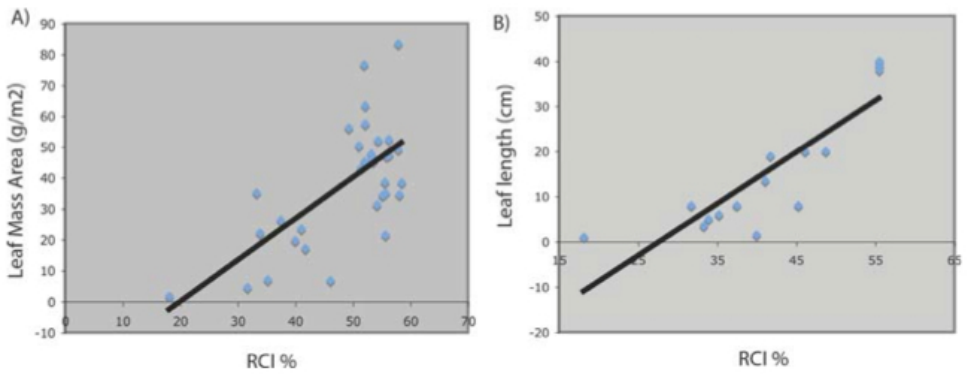

Figure 4.4. Pairwise comparison of foliar traits with RCI. (A) RCI versus leaf mass per unit area. (B) RCI versus leaf length.

Relative crystallinity under artificial high wind conditions in the stems and leaves of *Arabidopsis thaliana*

Plant responses to the effect of high wind have been well reported (reviewed in Smith and Ennos 2003). In particular wind treatment is known to decrease Youngs modulus (Wright et al. 2007). Cellulose is the main structural component of the cell wall, yet effects of high wind on the crystalline physical properties of plant samples by XRD have not been established. A constant flow of wind energy was passed over 7-day-old *A. thaliana* plants in a crude wind tunnel within a growth chamber. Plants exposed to constant high wind conditions were dwarfed and leaf area decreased consistent with previous reports (Read and Stokes 2006). The RCI values for stems tissue sampled from plants exposed to high wind (4.3 $m.sec^{-1}$)(RCI = 52.08 ± 1.23%) were significantly lower (among experimental replicates ($P<0.001$, ANOVA) than stems from plants not exposed to wind (RCI = 55.8 ± 0.38%) (Table 4.1). Yet again, given the estimated experimental accuracy of 11.2 and 9.52 % respectively, a conclusion regarding the significance of these results cannot be substantiated. Particularly since in leaves the RCI measure under wind exposure was not significantly lower than from those no wind experiments based just on sample replicates alone ($P>0.05$, ANOVA).

Leaf Mass Per Unit Area and Leaf Length Measurements Correlated With RCI

Species analyzed in this by RCI study were correlated against measurements of leaf mass per unit area (LMA) and leaf length. The correlation between RCI and LMA demonstrated the as LMA increased, so did the value for the RCI of the biomass sample (Figure 4.4A). Individual pairwise analysis of measurements of leaf length with RCI also showed positive correlation between these traits (Figure 4.4B).

Discussion

All plant cells are surrounded by a rigid cell wall that constrains internal turgor pressure and yet must yield in a controlled and organized manner to allow the cell to grow and acquire a specific shape (Brown 2004). The major load-bearing constituent of the higher-plant cell wall is cellulose, which forms crystalline fibrils that are often highly organized with respect to cell shape and growth pattern (Brown 2004). Yet, microfibril chains are thought to periodically fail to coalesce into an ordered crystalline structure and thus may have variation in the frequency of amorphous regions within the crystalline fibrils (Gomez et al. 2008). These less crystalline regions are postulated to functionally serve to link

fibrils with other wall components and thus may alter the wall structure and biomechanics. Biomechanical properties of various plant tissues under various conditions have been examined using primary shearing force, punch and dye testing or tensile strength (Read and Stokes 2006; Smith and Ennos 2003). The aims of this study were to explore the technical limitations and responses of the relative crystallinity measure to ecosystem level processes using X-ray diffraction (Andersson et al. 2003; Andersson et al. 2000; Andersson et al. 2004; Honjo and Watanabe 1958; Puri 1984; Sarén et al. 2001; Segal et al. 1959; Teeäär et al. 1987; Weimer et al. 1995). RCI analysis was overlaid with plant species diversity, response to abiotic community boundaries and endemic plasticity. These combined data showed marked variability of relative sample crystallinity in plants across these ecological niches, but detailed quantitative determination of cellulose crystallite size, orientation and density of samples remained elusive.

Care must be taken when correlating the RCI index against plant samples. A series of detailed studies on the properties of wood cellulose have shown that RCI for pure cellulose samples is directly related to the cellulose crystallinity, but in plant samples that contain a matrix of amorphous polymers in addition to cellulose, the RCI represents the volume fraction of crystalline cellulose within the given sample (Andersson et al. 2000; Puri 1984; Sarén et al. 2001). The central problem in interpreting the diffractograms by the RCI value is the preferred orientation of the crystallites (texture) contributing to change in RCI (Andersson et al. 2000; Andersson et al. 2004). Therefore, RCI values as measurement of the absolute crystallinity *per se* are comparable only if the samples have the same texture, which can be altered by orientation and size of crystallites (Andersson et al. 2000; Puri 1984; Sarén et al. 2001; Yoshida et al. 2008). It is postulated that even within the cell wall of a single cell, considerable variability in the cellulose length, orientation and absolute crystallinity may exist. Despite the problems with using X-ray diffraction to analyze plant materials (Andersson et al. 2004), determination of RCI has the capacity to distinguish changes in the volume fraction of cellulose as the crystallinity of a sample. Further, established covariance of any trait against the complexity of a biological system, in particular the relatively uncharted plant biomechanical system poses many challenges. Therefore, RCI was examined in three definable experimental categories; 1) comparison of leaves, stems and roots (assembly) 2) acclimation to abiotic stress in hypocotyls, stems and leaves and 3) adaptation of RCI

in leaves of a diverse group of land plants. Are results for different samples comparable? Analysis of 12 different *A. thaliana* sample replicates showed very high similarity of RCI between replicates (approx. 2%, Table 4.1). Moreover, upon examination of grasses, several wild grown Switchgrass species were analyzed from different sites and growing seasons and were not significantly different from the previous analysis. However, when defining RCI, we cannot guarantee that samples are comparable other than the determined RCI parameter is related to the proportion of crystalline cellulose in the foliar sample.

Within the body plan of a single plant (*A. thaliana*) there was significant variability in RCI values between the roots or stems and rosettes (Figure 4.3A and 4.3B), but not between roots and stems, suggestive of the different biomechanical architecture underlying ontogeny. For example, the RCI value was 23.4% lower in rosettes than stems. Structural requirements and allocation of cellular energy into maximal photosynthetic surface area (Mandoli and Briggs 1982) in rosettes is greatly different from the requirements of rigidity and solute transport in the stem tissue (Ennos 1997). Keeping in mind that the RCI measure does not determine whether preferred orientation, size or absolute crystallinity were contributing to the lower RCI value of leaves, it is evident that RCI represents a much lower crystallinity of the leaf sample. The volume fraction of cellulose in these tissues followed a similar trend with 36% lower cellulose content in leaves than stems.

When *A. thaliana* plants were grown under conditions of constant wind (thigmomorphogensis) stems had lower RCI under high wind conditions than those grown without high wind stress (Table 4.1). It is established that wind treatment results in decreased Young's modulus (stiffness of a material) (Smith and Ennos 2003), which infers a positive correlation between RCI and Young's modulus. Reports of the effect of wind on biomechanics suggest that plants are dwarfed due to investing a greater proportion of energy into mechanical reinforcement rather than surface area for photosynthesis (Read and Stokes 2006; Smith and Ennos 2003). In stems, structural changes have been reported as producing "flexure fibers" or postulated high microfibrillar angle cellulose observed under conditions of high wind to provide greater flexibility (Telewski 1989). But, crystallinity for compression wood has been shown to be lower than that of normal wood simply because the share of amorphous cell wall

components is larger in compression wood and the difference in crystallinity between normal wood and compression wood is modest (Newman 2004).

Experimental analysis of hypocotyls from dark-grown pea plants showed that the RCI decreased compared with light-grown hypocotyls (Figure 4.3C). The biophysical nature of etiolated tissues was very different from light-grown with more than double the average length of light-grown hypocotyls (3.7 cm to 9.5 cm, $P<0.001$) and the cellulose synthase array oriented from transverse to longitudinal when dark-grown seedlings were exposed to light (within 30 min, Paredez et al. 2006, Figure 4.3D). Given the results of (Stubiçar et al. 1998; Yoshida et al. 2008), the lower RCI measured in dark-grown hypocotyls may be achieved by reducing the physical length dimensions of cellulose fibrils. Or, given the experiments of Andersson et al. (2004), several factors associated with sample texture, including orientation, are likely to contribute.

In attempting to use the leaf and non-woody biomass samples for the analysis of texture by transmission geometries, several technical challenges arose. Mounting the sample into a pressed KBr opaque disk with the sample embedded was achieved but maintaining any control over fiber orientation was not. Further, X-ray penetration through the sample was not sufficient for symmetrical transmission geometries (110 and 200 A peaks were below measureable intensity). Alternatively, FTIR analysis of the light versus dark-grown pea hypocotyls distinguished between the samples based on variance in the polysaccharide fingerprint region (Kacuráková et al. 2000). Several spectral peaks in the variance plot were assigned to cellulose (Figure 4.3E). We attempted to investigate this hypothesis using live-cell imaging to compare the orientation, velocity, track length, rosette number and density of YFP::CESA6 particles at cortex in dark (transverse) versus after light exposure (longitudinal) arrays. However, only array orientation was found to significantly differ among treatments (Paredez et al. 2006). It was evident that longer maximum trajectories of YFP::CESA6 particles could be traced after light exposure induced reorientation to a longitudinal array (14.4 μm in dark to 26.8 μm after light exposure), but the average track lengths were not significantly different due to the large range and an inability to track through the z-focal plane. Since each tracks was the sum of multiple particles (YFP puncta) we assessed the particle number per track and found that within the dark-grown hypocotyl of *A. thaliana* seedlings, regardless of dark growth or brief light exposure the YFP:CESA6 density

were 0.86 and 1.05 particles per mm respectively. Given this density and their bidirectional velocity of approximately 270 $nm.min^{-1}$ (Paredez et al. 2006; DeBolt et al. 2007b) microfibril overlap along a track would perhaps be clearer in micrographs (Brown 2004).

It was evident that monocotyledons had greater foliar RCI values than the dicotyledons tested (Figure 4.2). Also, a trend of increasing RCI with increasing LMA and leaf length was measured (Figure 4.4A and B), which leans towards a possible allometric relationship (McCarthy et al. 2007). Studies on the tensile properties of plants have shown that the grasses have 5-10 times higher tensile strength than dicots for a given LMA, which suggests that the amount of fiber itself cannot account for the difference in tensile strength (Yusuke Onoda, Personal Communication). In addition to being central to plant cell shape and morphogenesis, cell walls and their biomechanical properties are thought to play a vital role in plant defense against both biotic and abiotic stress and hence have an integral role in functional plant ecology (Read and Stokes 2006). Yet, plant biomechanics are poorly understood compared with other functional traits.

Does RCI depend linearly on the crystallinity of the biomass sample? From the RCI value and experiments performed, it is arguable that the answer is no. Preferred orientation of the fibril array may in fact cause changes in the RCI consistent with finding of Andersson et al. (2004) and YFP::CESA6 experiments as can the size of cellulose crystallites (Yoshida et al. 2008) and ball milling experiments. It is noteworthy that the possibility of exploiting RCI as a trait may exist; in that lower RCI values of plant samples were far more readily turned into fermentable sugars (Weimar et al. 1995; Yoshida et al. 2008). Therefore RCI may be part of the assessment strategy useful to breeders for selection of perennial grasses with more digestible properties for forage and biofuel production.

Chapter V*

Genetic modification in cellulose-synthase reduces crystallinity and improves biochemical conversion to fermentable sugar

A sustainable human economy will require the implementation of renewable forms of energy to reduce the impacts of climate change associated with continued fossil fuel consumption (Searchinger et al. 2008). One renewable form of bioenergy that has gained consider able interest is to exploit the capacity of land plants to fix atmospheric carbon using energy from the sun to make sugar polymers (photosynthesis) (Farquhar et al. 2001). The most plentiful of these plant sugar polymers is cellulose, and it is noteworthy that plants proliferate in nearly every biome on the planet (Wright et al. 2004) and cellulose is the most abundant biopolymer on Earth (Sticklen 2008), which add to its attractiveness as a source of renewable energy. Unfortunately, cellulose polymers, referred to as microfibrils, are crystalline and highly recalcitrant to enyzmatic breakdown to form fermentable sugars that can be fermented to make alcohol for biofuel. This crystallinity presents a major technical hurdle to overcome if cost-effective biochemical conversion of lignocellulosic biomass into biofuels is to be realized.

Providing a fundamental understanding of cellulose biosynthesis may also assist in understanding how it could be more efficiently broken down to biofuel. In elongating plant tissue, cellulose deposition is generally considered to occur perpendicular to the axis of elongation, constraining lateral swelling and allowing longitudinal, or anisotropic, cell expansion (Brown 1996). The cellulose polymer is arranged in 3-nm-thick micro-fibrils (Delmer and Haigler 2002). These microfibrils are believed to consist of 8000 (primary cell wall) to 15,000 (secondary cell wall) glucose molecules (Somerville et al. 2004). Cellulose is synthesized by plasma membrane-localized proteins containing several structurally similar cellulose synthase (CESA) subunits (Arioli et al. 1998) that can be visualized as symmetrical rosettes of six globular complexes approximately 25-30 nm in diameter (Herth 1983; Brown 2004). The only known components of the

*__This chapter was originally published as: Harris D, Stork J, DeBolt S (2009)__ Genetic modification of cellulose-synthase reduces crystallinity and improves biochemical conversion to fermentable sugar. Glob Change Biol Bioenergy 1:51-61. Copyright permission was granted by the authors for inclusion in this dissertation.

CESA complex in higher plants are the CESA proteins, 10 genes of which have been identified in the sequenced genome of *Arabidopsis thaliana* (Richmond & Somerville 2000). Advances in our understanding of the required stoichiometry of CESA subunits within the CESA complex have also recently been made demonstrating that the hexameric model for CESA complex formation requires three functional CESA subunits, with CESA1 and CESA3 compulsory, whereas CESA2, 5, 6, 9 and 10 are interchangeable (Desprez et al. 2007). It has also recently been found that the plant may have a cell wall sensing mechanism, requiring THESEUS1, to provide transcriptional feedback on the integrity of the cell wall (Hématy and Höfte 2008; Hématy et al. 2007). Chemical and genetic screens for swollen organ morphology have also identified a handful of genes that participate in cellulose biosynthesis, such as the COBRA (Schindelman et al. 2001) and KORRIGAN (Lane et al. 2001: Paredez et al. 2008). However, the complexity of events contributing to activation of the CESA at the plasma membrane and its motility suggests that the list of players is far from complete.

Finally, of considerably greater potential benefit, and accordingly greater difficulty, is the possibility of changing the nature of cellulose itself. Could the cellulose synthase complex be altered to produce 'wounded' (in terms of either degree of crystallization or polymerization) cellulose more amenable to deconstruction? Would such a plant survive and thrive? (Himmel et al. 2007).

The tight bonding capacity of the hydroxyl groups via hydrogen bonding are critical to determining how the crystal structure of cellulose forms and also in directing important physical properties of cellulose materials (Nishiyama et al. 2002, 2003). It is postulated that the chains of glucosyl residues in the fibril periodically fail to coalesce into an ordered crystalline structure; these amorphous zones along the fibril length are recognized as possibly facilitating the association between hemicellulose and cellulose fibrils (Gomez et al. 2008). Indeed, the regulation of amorphous to crystalline zones in the cellulose microfibril and the potential for biological regulation has important connotations for plant design and cellulose bioconversion, but as yet this area of research is poorly understood. Herein, we demonstrate the first example of a viable low biomass-crystallinity mutant in *A. thaliana*. The mutant plant contains a point mutation in the trans- membrane region of CESA3 in the previously identified mutant *ixr1-2* (Heim et al. 1989; Heim et al. 1990). Specifically, the resulting amino acid residue change is from

threonine 942 to an isoleucine. Through combined genetic and biochemical screening analysis, with the use of X-ray diffraction studies to allocate structural information about cellulose crystallinity, we demonstrate the capacity to modulate cellulose digestibility via this straight- forward genetic modification of CESA.

Material and Methods

Chemicals

All chemicals and reagents used were of analytical grade or higher. Authentic samples of organic acids and their salts were obtained from Sigma-Aldrich, FMC-BioPolymer, Fisher Scientific, Riedel den Haan and BDH as applicable.

Plant material and sample collection

Mutants used in this study had either been previously published as, or were isolated as, homozygous T-DNA insertional alleles or point mutations screened from the ABRC stock center (Table 5.1). These plants were grown at 22ºC under a 16h light 8h dark regime in crops of 50 plants and harvested as aerial plant biomass. Four independent growing cycles and analysis were performed for top candidates.

Microscale enzymatic saccharification

Celluclast 1.5L (cellulase from *Trichoderma reesei*) and Novozyme 188 (cellobiase from *Aspergillus niger*) were purchased from Sigma-Aldrich (St Louis, MO, USA). The enzyme cocktail was obtained by mixing equal volumes of the two enzymes that contained an enzymatic activity of 486 endoglucanase units (mL^{-1} for cellulase [45.6 filter paper units (FPU) - as standardized in LAP-009] and 134 CBU mL^{-1} for cellobiase. Enzymatic saccharification of lignocellulosic material was according to the laboratory analytical procedure #009 (LAP-009) of the National Renewable Energy Laboratory (NREL). The cellulose content of mutant and wild-type *A. thaliana* plants was measured spectrophotometrically (ThermoFischer Biomate3, Madison, WI, USA) on homogeneous samples of 150 ground whole *A. thaliana* plants and sugar release values are a percentage of this total (described in detail below). Modification for the microscale experiment was made using dry biomass samples equivalent to 0.02 g cellulose. In addition, the total reaction volume was reduced to 2 mL and a range of enzyme concentrations based on cellulase activity were used including 60, 30, 15 and 7.5 FPU. The samples were positioned horizontally in an Innova 4300 incubator/shaker (New

Brunswick Scientific, New Brunswick, NJ, USA) at 50ºC while shaking at 100 rpm using a 1-inch orbit. The progress of the reaction was measured by taking representative 100 μL aliquots at 2, 4, 6, 12, 24, 72 and 168 h. Enzyme blanks and Whatman #1 filter paper were digested alongside the samples.

X-ray scattering

A. thaliana material was grown under both greenhouse and growth chamber for analysis. Plant samples were prepared by oven drying biomass at 60ºC for 36 h. Alternative temperatures for the drying regime were used, such as 37ºC for 7 days or 80ºC for 12 h followed by 110ºC for 2 h, neither of which altered the measured values in *A. thaliana* tissue (similar to Harris and DeBolt 2008). Tissue was then homogenized using an Arthur H Thomas Co Scientific grinder (Philadelphia, PA, USA) equipped with a 1mm sieve. Biomass samples were then contained in a custom built sample holder of pressed boric acid. In brief, plant material was placed into a mold, containing a sleeve and hand pressed with a solid metal plug forming a disk shape. The sleeve and plug were removed and a boric acid (Fischer, Madison, WI) base was then formed by pouring the boric acid over the bottom and sides of the sample and applying 40,000 psi of pressure to the 40 x 40 mm mold using a Carver Autopellet Press (Wabash, IN, USA). Samples were pressed to create an even horizontal surface. A Bruker-AXS Discover D8 Diffractometer (Bruker-AXS USA, Madison, WI, USA) was used for wide angle X-ray diffraction with Cu Ka radiation generated at 30 mA and 40kV. The experiments were carried out using Bragg-Brentano geometries (symmetrical reflection). Diffractograms were collected between 2º and 70º or 2º and 40º (for samples with little baseline drift), with 0.021 resolution and 2 s exposure time interval for each step. Sample rotation to redirect the X-ray beam diffraction site was achieved per replicate. The data analysis was carried out using the calculation for relative crystallinity index (RCI) = I_{002}-Iam/I_{002} x 100, where I_{002} is the maximum peak height above baseline at approximately 22.5º and I_{am} is the minimum peak height above the baseline at 18º (Weimer et al., 1995). Peaks at the 22.5º and 18º were consistent with a control of synthetic crystalline cellulose (Avicels, FMC-Biopolymer, Philadelphia, PA, USA) (Andersson et al. 2003). For assessment of experimental accuracy, the pressed samples were examined using reflective geometries at 22.5º 2θ with the sample scanned rotationally (360º) and in an arc (90º) to obtain an intensity/spatial orientation plot of a sample for which the RCI had already been established. The range of reflective intensities was then used to estimate

the accuracy of the RCI determination using a 95% cutoff across the plot range (Harris and DeBolt 2008). Three experimental replicates for mutant and wild-type biomass samples were performed. Diffractograms were collected in DIFFRAC-PLUS-XRD COMMANDER software (Bruker-AXS, Karlsruhe, Germany) and minimally processed (baseline identification, noise correction, 3D display and cropping of RCI signature region) using the EVA and TEXEVAL (Bruker-AXS) software.

Enzyme kinetics

The initial rate of sugar release using identical enzyme cocktail loadings (Celluclast 1.5 and Novozyme 188) as a function of substrate concentration was obtained by performing a similar microscale experiment as that conducted for the saccharification analysis. Dry biomass samples equivalent to sequentially increasing amounts of mutant and wild-type plant derived cellulose were mixed with enzyme (7.5 FPU) and incubated for 2h. Similar to the NREL LAP-009 saccharification experiments and using the same enzyme buffer solution, the samples were incubated in an Innova 4300 incubator/shaker (NewBrunswick Scientific) at 50 1ºC while shaking in a horizontal position at 100 rpm. The progress of the reaction was measured by taking individual aliquots at 2h and determining the glucose concentration using a Yellow Springs Instruments (YSI)–glucose analyzer standardized for glucose determination using YSI buffer and membranes purchased from YSI (Yellow Springs, OH, USA). Enzyme blanks and Whatman #1 filter paper were digested alongside the samples. The inability to exactly calculate the number of catalytic ends in the complex mixture of cell wall biomass allowed only the calculation of a relative estimation, expressed as apparent kinetics values. Hence, classical Michaelis–Menten kinetics are not determined and the *Km* and *Vmax* values are apparent *Km* and *Vmax* relative estimates. The enzyme kinetics experiment varied the concentration of substrate (cellulose) and measured enzyme velocity to determine the difference in enzyme velocities between the two substrates. These values were generated using the statistical graphing program GRAPHPAD PRISM-4 (Graphpad, La Jolla, CA, USA).

Cellulose content measurement

Crude cell walls were prepared as published previously (Reiter et al. 1993). Briefly the samples for the measurement were homogenized using an Arthur H Thomas Co Scientific grinder (Philadelphia, PA, USA) equipped with a 1 mm sieve. Twenty-five

milligram plant material were incubated in 1 mL 70% ethanol overnight at 65 °C, and washed twice with 1 mL 70% ethanol for 1 h and once with 1 mL acetone for 5 min. After washing solutions were extracted using a 1 mL pipette the samples were dried under vacuum. Cellulose content determination was essentially achieved using the methods described by Updegraff (1969): briefly, 5 mg of the dry biomass extract were weighed out in triplicates from either wild-type or mutant plants and boiled in acetic-nitric reagent (acetic acid : nitric acid : water 8 : 1 : 2) for 30 min to remove lignin and hemicellulose. The samples were allowed to cool down to room temperature and the reagents were carefully removed. The plant cell wall material was washed twice with 8 mL MQ-water and 4 mL acetone, and dried under vacuum. The cellulose samples were then hydrolyzed in 67% sulfuric acid for 1 h. The glucose content of the samples was determined by the anthrone method (Scott & Melvin, 1953). Exactly 25 mL of the sulfuric acid hydrolyzed samples were mixed with 475 mL water and 1 mL 0.3% anthrone in concentrated sulfuric acid on ice. The samples were boiled for 5 min then placed immediately back on ice. The absorbance of the samples was measured using a Bio-Mate thermo scientific spectrophotometer (Thermo Fischer, Waltham, MA, USA) set at Abs_{620} and compared with a standard curve obtained from known (10-50 mM) concentrations of glucose (the standard curve was set each time together with the reaction). The cellulose content was calculated by multiplying the measured glucose concentration of each sample by the total volume of the assay and then by the hydration correction factor of 0.9 (to correct for the water molecule added upon hydrolytic release of each glucose residue from the cellulose polymer).

High-pressure liquid chromatography (HPLC) analysis of fermentable sugars

Aliquots of the fermentable sugars released by enzymatic hydrolysis were isolated and their sugar composition quantified by HPLC according to methods of (Zhao et al. 2004). The enzymatic hydrolysates of 20 mL were injected into an eluent of 19 mM NaOH introduced at 1 mL min^{-1} using a Bio-LC HPLC (Dionex Corp., Palo Alto, CA, USA) and separated through anion exchange using a Carbo-Pac PA1 with guard column (Dionex Corp.). Signal strength from a pulsed electrochemical cell monitoring eluting sugars in column effluent amounts was estimated by numerical integration of the pulsed electrical cell monitor signal (CHROMELEON software version 6.80, Dionex Corp.). Sugars were identified and quantified by comparing their retention times and peak areas with that of known standards for glucose, xylose, galactose, fucose and rhanmose. Glucose was

quantified by comparing the sample peak areas to that of known concentration standards.

Statistical analysis

Analysis of variance was conducted using the freeware statistical software package R (Auckland, NZ, USA) to test the null hypothesis of no statistical differences in RCI values between the mutant plants and wild-type. The null hypothesis was rejected at the 0.05 level. Nonlinear regression analysis was performed using the statistics program built into GRAPHPAD PRISM.

Sequence alignment and analysis

The protein sequence for *A. thaliana* was BLAST against all plant protein sequence data using the NCBI PBLAST format (Altschul et al. 1997). Sequences with significant homology and computational annotation as putatively encoding a CESA were aligned manually.

Results

Cell wall mutant selection

To establish whether genetic mutations in genes central to cell wall synthesis could result in improved enzymatic saccharification due to a wounded or flawed cellulose fibril, previously generated *A. thaliana* plants containing homozygous T-DNA insertions or point mutations in different genes potentially involved in cellulose biosynthesis as well as plants with mutations conferring resistance to cell wall synthesis inhibitors (Table 5.1) were selected. Selections were made based on both the type of mutation, being either a T-DNA mutation or a point mutation, and the coverage of the different CESA genes in the *A. thaliana* genome as well as several mutants that we term ‘outliers’. These outliers are thought to be involved in cell wall synthesis but not directly in catalysis of UDP-glucose to cellulose (Table 5.1). The study was performed in *A. thaliana* because identifying a gene mutation that results in a wounded cellulose fibril is very fundamental in nature and has been identified as a major challenge (Somerville et al. 2004; Himmel et al. 2007; Gomez et al. 2008; Harris and DeBolt 2008). Moreover, the genetic resources that have been compiled over the past two decades provided a base of mutants with which to work. A vigorous and upright growth phenotype of the mutant plant was used as additional selection criteria. Mutants such as *eli1-1* or *cev1*

Table 5.1. Cell wall mutations in *Arabidopsis thaliana* and their source.

Gene	Mutation	Gene ID	Source
CESA1	*rsw1-2* $A_{549}V$	At4g32410	Gillmor et al J Cell Biol 2002 **156**:1003-1013
CESA2	T-DNA insertion	At4g39350	SALK 096542 (ABRC)
CESA3	*ixr1-2* $T_{942}I$	At5g44030	Scheible W-R et al PNAS 2001 **98**:10079-10084
CESA6	*ixr2-1* $R_{1064}W$	At5g64740	Desprez T et al Plant Physiol 2002 **128**:482-490
CESA6	T-DNA insertion	At5g64740	SALK 004587 (ABRC)
CESA9	T-DNA insertion	At2g21770	SALK 046455 (ABRC)
CESA10	T-DNA insertion	At2g25540	SALK 052533 (Staffan Persson)
CESA2/PRC1-1			Persson S et al PNAS 2007 **104**:15566-15571
Theseus1-3	*the1-3* T-DNA insertion	At5g54380	Hématy K et al Current Biology 2007 **17**:922-931
Theseus	5´UTR	2569-2789	Hématy K et al Current Biology 2007 **17**:922-931
CTL1	*ctl1* W_{181}Stop	At1g05850	Zhong R et al Plant Cell 2002 **14**:165-179
Cobra1-1	*cob1-1* $G_{167}R$	At5g60920	Schindelman G et al Genes Dev 2001 **15**:1115-1127
Cobra1-5	*cob1-5*	At5g60920	Schindelman G et al Genes Dev 2001 **15**:1115-1127
IRX8	*irx8* T-DNA insertion	At5g54690	Persson S et al PNAS 2005 **102**:8633-8638
Korrigan	*rsw2-1* $G_{429}R$	At5g49720	Lane DR et al Plant Physiology 2001 **126:**278-288
Korrigan	*kor16-2* T-DNA insertion	At5g49720	Nicol F et al EMBO J 1998 **17**:5563-5576
CSLC4	*cslc4*	At3g28180	Cocuron JC et al PNAS 2007 **104**:8550-8555
CSLC4/CSLC5		At3g28180/4g31590	Courtesy of J. Milne

summarized in (Robert et al. 2004), which have severe growth phenotypes due to impairment of CESA1 or CESA3, were therefore eliminated from the study. Severe phenotypic differences in growth habit were also avoided to the best of our ability. In order to control for differences in the stage of growth that might affect the results, all plants were harvested at maturity defined as the onset of senescence after seed maturity and maximal plant biomass have been reached. Harvesting at maturity was also an attempt to nullify any influence of spatial or temporal gene expression and focus on mutations that alter cellulose in the whole plant. To further reduce any bias resulting from phenotype each plant replicate was a crop of 50 plants grown under identical conditions that were dried and homogenized to create a pool.

Screening for altered digestibility

Based on the cellulose content determined for each mutant, identical cellulose loadings were analyzed for recalcitrance to saccharification after 24 h of enzymatic digestion using a commercial cellulase cocktail from *T. reesei* (Sigma-Aldrich). The results for each mutant were then compared as the percentage of cellulose converted into fermentable sugars (Figure 5.1a). In order to confirm that cellulose was being converted, the fermentable sugars released by enzymatic hydrolysis were analyzed by HPLC, which indicated that >90% of sugar was glucose. The highest saccharification efficiency was 51.2% (±0.6) measured using *ixr1-2* biomass relative to wild-type, followed by *cesa10-salk*, *cesa2-salk* and *ixr2-1*, which displayed 14.8% (±1.2), 11.4% (±1.4) and 6.3% (±0.8) higher saccharification efficiency than wild-type, respectively (Table 5.1 and Figure 5.1a). The *ixr1-2* mutant displayed greater than threefold improvement in saccharification than the next closest candidate (CESA10). A large majority of mutants analyzed displayed very similar and/or negative conversion potential relative to wild-type biomass (Figure 5.1a). Lower saccharification efficiency relative to wild-type was evident for *cobra1-1*, *cobra1-5*, *the1-3*, *CESA6-salk*, *ctl1*, *rsw2-1*, *irx8*, *korrigan16-2* and *clsC4* as well as the double mutants *clsC4/cslC5* and *cesa2/prc1-1* (Cocuron et al. 2007; Hématy et al. 2007; Lane et al. 2001; Persson et al. 2007; Persson et al. 2005; Schindelman et al. 2001; Zhong et al. 2002b) (Figure 5.1a, Table 5.1). Batch comparisons from four independent plantings of mutant *ixr1-2* vs. wild-type plants indicated that improved conversion efficiency remained at approximately 151% (Figure 5.1b). From this saccharification efficiency screen of *A. thaliana* cell wall mutants, we identified the missense mutant *ixr1-2* as the top candidate for further investigation.

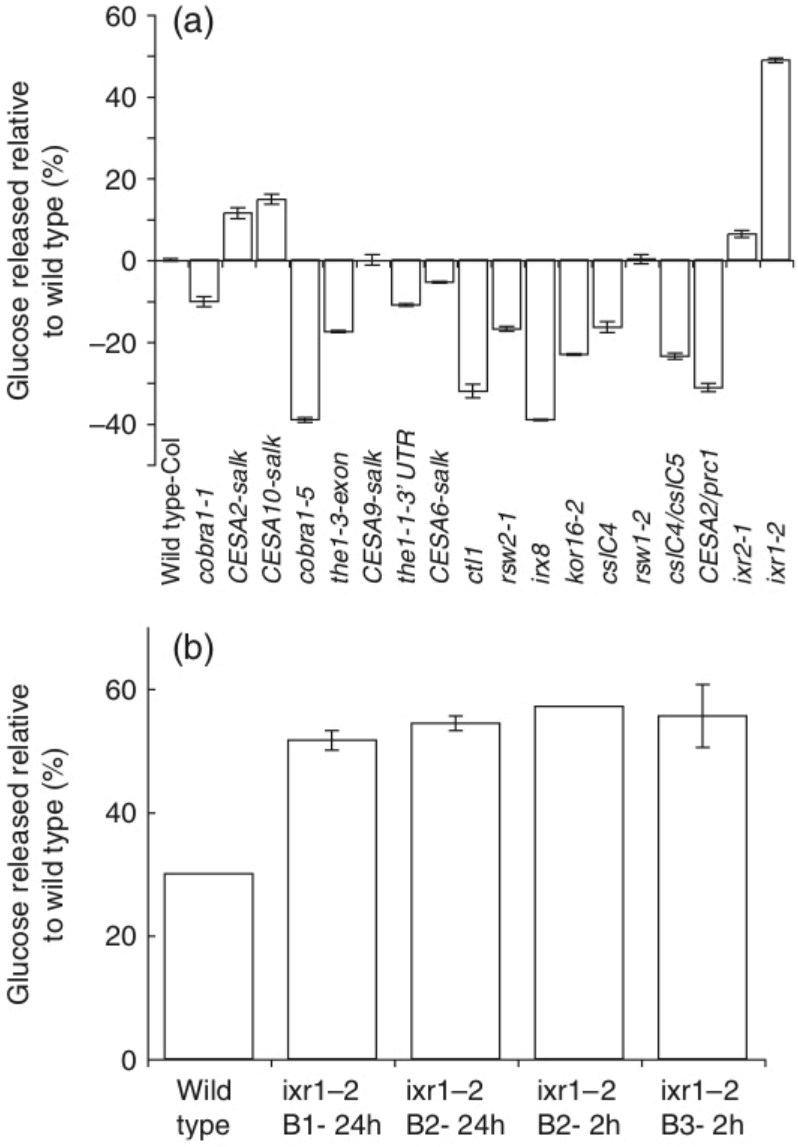

Figure 5.1. Improved biochemical conversion of dry biomass into fermentable sugars in the cell wall mutants. (a) Analysis of various *A. thaliana* plants carrying mutations in a number of genes critical to cellulose biosynthesis by saccharification efficiency using hydrolytic enzymes. The graph plots fermentable sugars released relative to the conversion rate of wild-type biomass as a percentage (n=3). (b) Batch comparison between wild-types and *ixr1-2* mutant biomass over three generations of plants (B stands for batch)

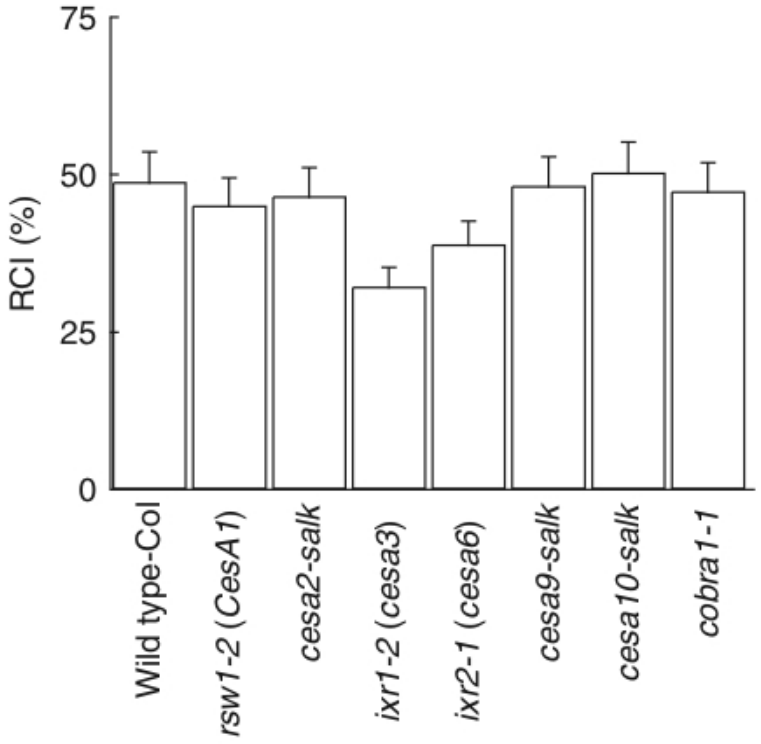

Figure 5.2. Plots of the relative crystallinity index for the biomass sample of seven different mutant plants measured by X-ray diffraction (n=3). Selected from the saccharification screen, four out of the seven mutants (*cesa2-salk*, *ixr1-2*, *ixr2-1* and *cesa10-salk*) yielded significantly more fermentable sugar than wild-type. As controls, two mutants that yielded comparable amounts to wild-type (*rsw1-2*, *cesa9-salk*) and one mutant that yielded less (*cobra1-1*) are represented.

Screening for altered cellulose structure by X-ray diffraction

A second screen for altered cellulose structure was performed on selected mutant plants identified in the saccharification efficiency screen. X-ray scattering analysis was performed to generate a RCI (Figure 5.2) that established possible changes in the orientation, size or density of the cellulose crystallites (Andersson et al. 2003; Harris and DeBolt 2008). X-ray diffraction patterns showed consistent signature peak distribution with previous published reports (Weimer et al. 1995) and these were overlayed with synthetic crystalline cellulose (Avicel) to determine the relative crystallinity index for synthetic crystalline cellulose (Weimer et al. 1995; Harris and DeBolt 2008). The experimental accuracy was approximated by determining the noise in the diffractogram using a *Phi* and *Chi* scan (360° rotational by 90° in an arc in the X-ray diffractometer) of the sample, creating an intensity/spatial orientation plot at 22.51 2y and was determined to contribute approximately 10% error, which was added variability between replicates. Experimental accuracy value does not take into account the possibility that texture of the sample influences RCI (Andersson et al. 2003). Attempts to determine sample texture by transmission geometries (Sarén et al. 2001) were not successful in the *A. thaliana* plant material. Most technically challenging was mounting the sample, X-ray penetration through the sample and orientation of the fiber axis, which was random in leaf cells and highly diverse in a heterogeneous total plant sample. A lack of texture analysis in the samples by transmission geometries does not allow us to determine the preferred orientation of crystallites within the samples, nor the size or density of crystallites. Rather, RCI provided a screening tool for sample crystallinity of which the crystalline polymer within the complex mixture of polysaccharides is cellulose. The examination of mutant alleles compared with wild-type parental lines were performed in triplicate. The RCI of wild-type parental lines was measured to be 48.9 ±4.5%. Furthermore, five out of the seven plants displayed RCI values similar to that of wild-type. Mutants analyzed were the non-conditional CESA1 allele *rsw1-2* that displayed an RCI of 44.82 ±4.9%, *cesa2-salk* 46.3% ±5.2%, CESA3 *ixr1-2* allele 31.9 ±3.4%, CESA6 *ixr2-1* allele 38.6 ±3.8%, CESA9 allele *cesa9-salk* 47.9 ±4.2%, and CESA10 allele *cesa10-salk* 50.0 ±5.2%. In addition the *cobra1-1* mutant was analyzed and was not different to wild-type (n=3) (Figure 5.2).

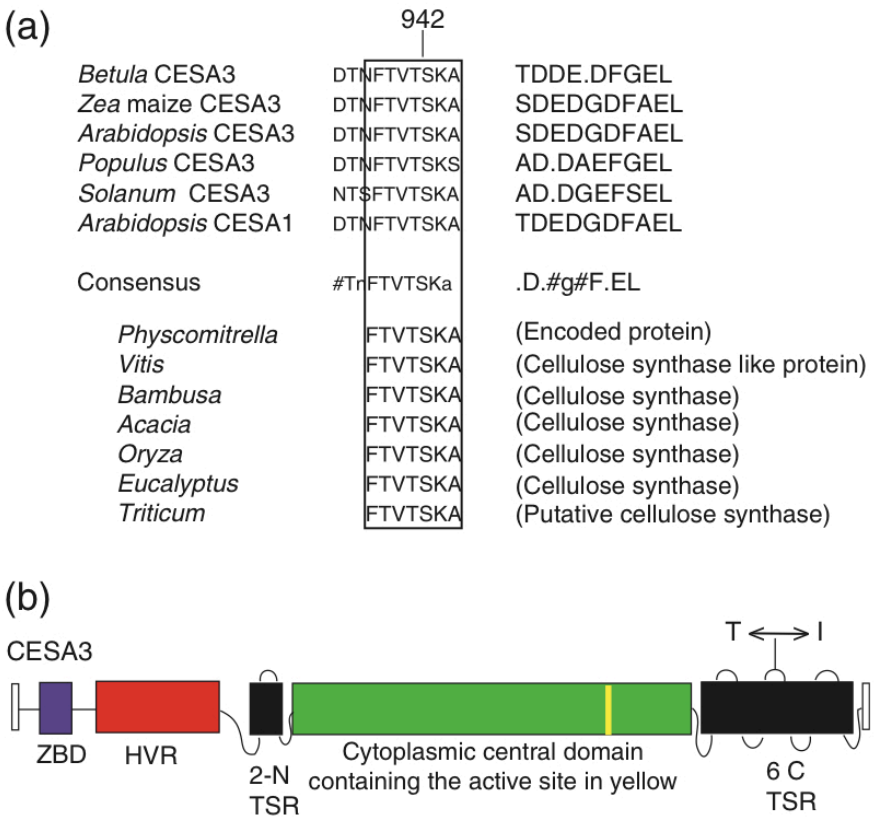

Figure 5.3. Sequence alignment and genetic mutation. (a) The region containing the *ixr1-2* mutation was compared between *A. thaliana* CESA3 and homologs from *Betula*, *Zea*, *A. thaliana*, *Solanum*, *Populus*, *Vitis*, *Bambusa*, *Acacia*, *Eucalyptus*, *Oryza*, *Triticum* and *Physcomitrella* (b) Schematic of the structure of the *CESA3* gene highlighting the region of the threonine to isoleucine mutation in the C-terminal transmembrane region (adapted from Scheible et al. 2001). (ZBD = zinc binding domain, HVR = hypervariable region, TSR = transmembrane spanning region at N-terminus and C-terminus).

Analysis of the FTVTSKA domain in higher plant genomes

CESA orthologs were identified based on homology to the CESA3 gene from *A. thaliana* and amino acid sequences examined. Orthologs were identified in many sequenced or partially sequenced plant genomes available on public databases including *Betula, Zea, A. thaliana, Solanum, Populus, Vitis, Bambusa, Acacia, Eucalyptus, Oryza and Triticum*. Analysis of sequence conservation among CESA genes revealed that the threonine-942 that was mutated to an isoleucine in the *ixr1-2* mutant occurred within a highly conserved FTVTSKA domain among all sequences analyzed. A putative ortholog from the sequenced moss *Physcomitrella patens* also contained the FTVTSKA domain (Figure 5.3). In *A. thaliana* CESA3, the FTVTSKA domain is located in a cluster of six C-terminal transmembrane spanning regions and is specifically located on the extracellular loop between transmembrane spanning regions 3 and 4 (Figure 5.3). Furthermore, analysis of the CESA protein family showed that several other CESA proteins including CESA1, CESA4 and CESA8 contained the FTVTSKA domain (Figure 5.3, data not shown).

Kinetic analysis of cellulose bioconversion in the *ixr1-2* reduced crystallinity candidate

To gain a better understanding of the increased saccharification efficiency in the *ixr1-2* mutant, a more detailed saccharification experiment was conducted to determine kinetics of the reaction by measuring eight time points from zero to 168 h and using four different enzyme concentrations ranging from 7.5 to 60 FPU. The results indicated that at the 168h time point in conditions of excessive enzyme loading (60 FPU), the fermentable sugar released was over 50% for the *ixr1-2* mutant as compared with approximately 30% for wild-type (Figure 5.4a). In addition, the *ixr1-2* mutant released a greater percentage of sugar at each time point during the reaction (Figure 5.4a–d) and more sugar was released by *ixr1-2* using the lowest enzyme concentration (7.5 FPU) than that of wild-type using the highest enzyme concentration (60 FPU) (Figure 5.4a compared with Figure 5.4d). The nature of the improved conversion efficiency was examined further by determining pseudo-apparent Michaelis–Menten kinetic parameters recognizing that there are inherent ambiguities with an insoluble substrate like cellulose and a multienzyme cellulase cocktail. Nevertheless, pseudo-apparent K*m* (K'*m*) and V*max* (V'*max*) values were significantly different between wild-type and *ixr1-2* forms of cellulose. Wild-type displayed a V'*max* of 4.18 x 10^{-6} moles min^{-1} $unit^{-1}$ $protein^{-1}$ glucose

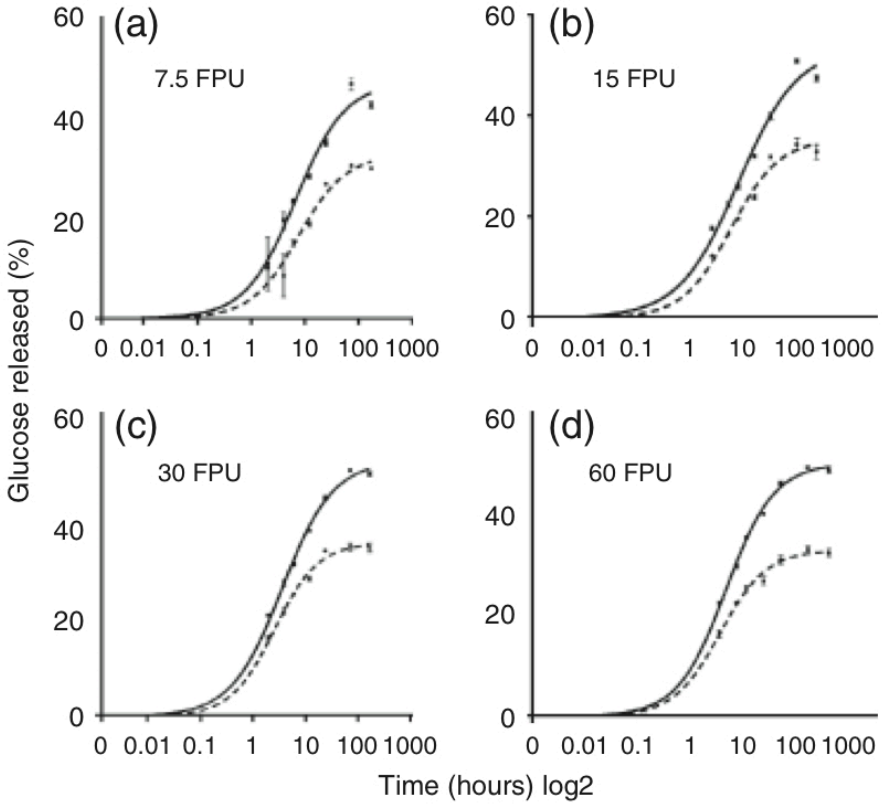

Figure 5.4. Saccharification efficiency reported as % of cellulose converted to glucose at 2, 4, 6, 12, 24, 48 and 168 h using (a) 7.5, (b) 15, (c) 30 and (d) 60 FPU of enzyme. Wild-type (dashed line) and *ixr1-2* (solid line) (error bars n=4).

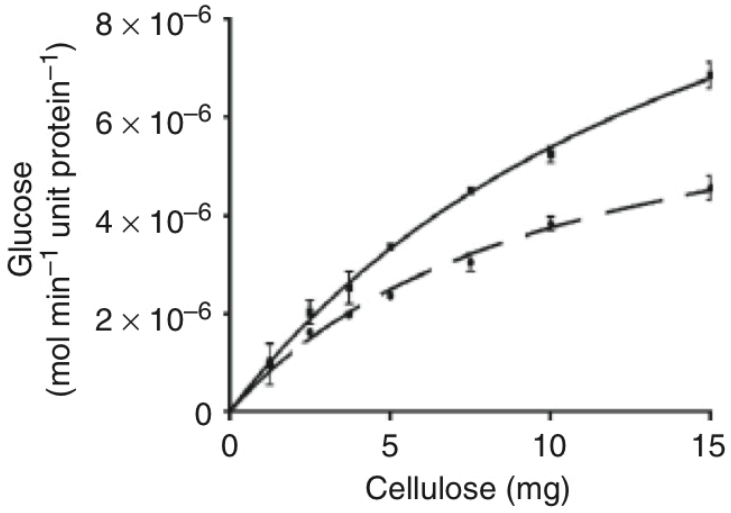

Figure 5.5. Initial rate of sugar release from biomass by the enzyme mixture as a function of cellulose concentration. Wild-type biomass closed circles and dashed line; *ixr1-2* closed squares and solid line (error bars n=3).

and K'*m* of 10.26 mg cellulose whereas *ixr1-2* displayed a V'*max* of 7.93 x 10^{-6} moles min^{-1} $unit^{-1}$ $protein^{-1}$ glucose and K'*m* of 16.55 mg cellulose. There was a 61% increase in the K'*m* for cellulose between wild-type and *ixr1-2* suggesting a significant reduction in the binding affinity for *ixr1-2* cellulose. However, the V'*max* for *ixr1-2* cellulose was 88% higher than for wild-type indicative of a higher enzymatic turnover rate as might be expected if *ixr1-2* is to be considered as a preferred substrate. A relative estimation of an apparent specificity-like constant (V'*max* /K'*m*) for wild-type was 40.7 x 10^{-3} and *ixr1-2* was 47.9 x 10^{-3} moles min^{-1} $unit^{-1}$ $protein^{-1}$ mg^{-1} (Figure 5.5), representing a 17% improvement for *ixr1-2* in the hydrolytic efficiency of the reaction.

Discussion

The overarching aim of this study was to establish whether mutations in genes central to cell wall synthesis could result in improved enzymatic saccharification efficiency of lignocellulosic biomass. This was possible due to the massive genetic infrastructure and research efforts invested in the model plant *A. thaliana* over the past two decades. A central discovery was the identification of a missense mutant in CESA3 that resulted in marked 51% improvements in saccharification efficiency relative to wild-type biomass (Figure 5.1a). Relatively minor effects on plant growth resulted from this mutation, namely *ixr1-2*, possibly due to the mutation occurring far distal to the active site in an extracellular loop between two transmembrane spanning regions (Scheible et al. 2001). Further, *ixr1-2* displayed a 34% lower relative crystallinity measurement compared with wild-type biomass; possibly providing a mechanism underlying higher saccharification efficiency. These results are discussed in detail below.

Screening for improved saccharification efficiency resulted in the identification of 4 mutants, namely *ixr1-2*, *ixr2-1*, *cesa2-salk* and *cesa10-salk* that yielded significantly more fermentable sugar than wild-type (Table 5.1 and Figure 5.1a). The *ixr1-2* mutant contains a point mutation in CESA3, which is a compulsory subunit in the cellulose synthesizing machinery (Scheible et al. 2001). Null mutations in CESA3 are embryo lethal (Somerville et al. 2004) and thus it is likely that the *ixr1-2* mutation is not completely deleterious to protein function, but more likely is altering a part of its normal structure or function. In contrast, the *ixr2-1* mutant also confers resistance to isoxaben (Desprez et al. 2002) and contains a point mutation in the CESA6 subunit. Moreover, the CESA2 and CESA10 mutants, *cesa2-salk* and *cesa10-salk*, contained T-DNA insertions

and are null mutants. These latter three plants were not selected as top candidates because CESA2 and CESA6 are partially redundant and gene expression is limited to elongating tissue (Desprez et al. 2007; Persson et al. 2007), whereas it is evident that CESA3 gene expression occurs in all tissues at all times (Persson et al. 2007). Thus, of the genetic mutations that were analyzed in this study, only one cellulose biosynthesis mutant was capable of providing a substantive improvement in the digestibility of cellulose. It is also noteworthy that a majority of the mutants analyzed displayed very similar and/or negative conversion potential relative to wild-type biomass (Figure 5.1a) and that most of these mutants are knockouts beckoning the question as to the result of over-expressing these genes. Hence, from this initial screen for conversion efficiency *ixr1-2* was identified as the top candidate due to its greater than threefold improvement in saccharification over the next closest candidate (*cesa10-salk*) and due to the intrinsic nature of CESA3 expression in all plant cells.

The determination of plant sample crystallinity through X-ray scattering analysis indicated that five of the seven mutant plants displayed RCI values similar to that of wild-type, while two of the mutants, *ixr1-2* and *ixr2-1*, were identified as having lower RCI values than wild-type (Figure 5.2). Interestingly, both of these mutants were previously identified in a forward chemical genetics screen as conferring resistance to the cellulose synthesis inhibitor isoxaben (Heim et al. 1989, 1990) and both mutant alleles displayed improved cellulose conversion efficiencies meeting the selection criteria for enhanced biofuel conversion (Figure 5.1a). Why similar mutations in different but related proteins confer isoxaben resistance, increased saccharification efficiency and reduced RCI value is not clear. With respect to the latter two characteristics, perhaps these mutations create structural changes in the proteins that alter their orientation within the CESA membrane complex, giving rise to irregular angles at which they produce and incorporate their glucan chain into the growing microfibril. This repositioning could disrupt a certain percentage of hydrogen bonding within the microfibril causing an increase in amorphous zones along the fibril length which may contribute to a reduction in RCI in the biomass sample and an increase in accessibility to enzymatic hydrolysis. In addition, the partial redundancy between CESA6 and other CESA isoforms could help explain why our data indicates that *ixr2-1* displays similar RCI and enzymatic hydrolysis characteristics as *ixr1-2* albeit not to the same extent. At a fundamental level, the RCI determination accounts only for the volume fraction of cellulose within a complex matrix

of cellular biomass. For this reason, we do not and cannot claim that absolute crystallinity of cellulose is lower, but rather that the relative crystallinity arising from the cellulose within the cell wall is lower in the *ixr1-2* and *ixr2-1* mutants. Consistent with RCI data (Figure 5.2), evidence for altered cellulose structure in the *ixr1-2* mutant was previously shown using Fourier transform infrared spectroscopy (FTIR) (Robert et al. 2004).

Kinetic analysis of the saccharification reaction indicated three areas where *ixr1-2* showed marked improvement over wild-type: fermentable sugar released at the 168 h time point was 151% that of wild-type (Figure 5.4d); at each time point a larger percent of fermentable sugar was released in *ixr1-2* compared with wild-type (Figure 5.4a–d); more sugar released using eight fold less enzyme than wild-type (Figure 5.4a compared with Figure 5.4d). At an application level, this gain in saccharification efficiency alone represents a dramatic improvement in bioconversion without costly chemical or heat pretreatment (Sticklen 2008). Further analysis of the affinity of the enzyme cocktail for the cellulosic substrate was also suggestive of altered cellulose as the appVmax/Km value indicated a 17% increase in hydrolytic efficiency when using the *ixr1-2* cellulose compared with wild-type cellulose (Figure 5.5). Hence, analysis of pseudo apparent catalytic efficiency of cellulose breakdown provided a quantitative measure that the *ixr1-2* cellulose substrate was preferred over wild-type cellulose by a cellulase cocktail.

Herein, we identify the first viable low biomass-crystallinity mutant in *A. thaliana* and demonstrate the capacity to alter the efficiency at which cellulosic biomass is converted to fermentable sugars through the genetic modification of the primary cell wall CESA3. Creating plants with low lignin has also been shown to be a viable strategy to improve the efficiency of using lignocellulosic rather than starch based biomass for biofuel production (Chen and Dixon 2007). *A. thaliana* is not a biofuel crop and therefore long-term targeted mutagenesis studies to enhance biomass to fermentable sugar conversion in mainstream biofuel crops such as maize or switchgrass are needed in order to determine whether similar enhanced bioconversion can be obtained. More fundamentally, these findings raise intriguing questions regarding the point mutation in the extracellular loop between transmembrane regions 3 and 4 at the C-terminus of CESA3. Further, what, if any, is the importance of transmembrane anchoring in establishing the correct organization of the CESA subunits within the CESA complex?

The ubiquitous nature of CESA3 orthologs in the primary cell wall of higher plants and conservation of the FTVTSKA domain (Figure 5.3) further indicates that the outcome of this study could have high value in the development of feedstock grasses for both the biofuels and forage industry. An additional point of interest pertains to secondary cell wall cellulose, which occurs as wall thickenings of woody vascular tissue (Taylor et al. 2004). Because the *ixr1-2* mutation occurs in the universally present primary cell wall CESA subunit number 3, it is quite plausible that efforts to generate the same amino acid change in the C terminal transmembrane region of the secondary cell wall CESA subunits (CESA4, 7 and 8) may provide a rational strategy to similarly improve the efficiency of biomass conversion from tree crops such as *Populus*.

Chapter VI*

Forward chemical genetic dissection of cellulose synthase structure and function

Regulation of cell and tissue morphogenesis is essential for building a multicellular organism. In plants, this is fundamentally controlled by a rigid and yet structurally dynamic cell wall that extends in a highly controlled manner to constrain cellular turgor pressure and define cell shape. The main load-bearing component of plant cell walls is cellulose, which occurs in its native form as *para*-crystalline microfibrils. These fibrils consist of multiple chains of unbranched β-1,4-glucan that aggregate via hydrogen bonds and van der Waals forces. The architecture of cellulose is thought to be controlled by the mechanism of biosynthesis, which is catalyzed by large plasma membrane (PM)-localized cellulose-synthase complexes (CSCs) that are present in all cellulose-synthesizing organisms. The CSCs utilize cytoplasmic UDP-glucose to synthesize β-1,4-glucans that are then extruded from the external face of the PM.

Central components of the CSC are the cellulose synthase A (CESA) enzymes, which are structurally conserved in bacteria (Saxena et al. 1990) and plants (Pear et al. 1996; Arioli et al. 1998). The topology of plant CESA, predicted by computational methods, is a cytoplasmic N-terminal region containing zinc-finger domains, followed by two transmembrane domains, a large cytoplasmic domain with the catalytic motifs and finally a cluster of six more transmembrane domains at the C-terminus (Delmer 1999). Three-dimensional predictions of a typical CESA suggest that the transmembrane domains anchor the protein in the PM and form a pore, either as a single polypeptide or as a CESA dimer, through which the growing glucan chain extends into the cell wall (Carpita 2010; Delmer 1999). Therefore, the CESA-facilitated unidirectional passage of the glucan chain across the PM appears to be a fundamental mechanism required for cellulose production. In *Arabidopsis thaliana*, 10 *CESA* genes have been identified (Richmond and Somerville 2000). A combination of biochemical and genetic analyses

***This chapter is currently under review as: Harris D, Corbin K, Wang T, Gutierrez R, Bertolo A, Petti C, Smilgies D-M, Estevez JM, Bonetta D, Urbanowicz B, Ehrhardt D**, **Somerville C, Rose JKC, Hong M, DeBolt S (2011)** Forward chemical genetic dissection of cellulose biosynthesis in plants. Proceeding of the National Academy of Sciences, U.S.A. Copyright permission was granted by the authors for inclusion in this dissertation.

has shown that at least three CESA subunits directly interact to form a CSC during primary (Desprez et al. 2007; Persson et al. 2007) and secondary (Taylor et al. 2003) cell wall cellulose formation. Further evidence has revealed that under oxidative conditions CESA proteins dimerize by intermolecular disulfide bonds via the zinc finger domain, although other domains are likely involved (Kurek et al. 2002; Timmers et al. 2009; Wang et al. 2006). However, the full complement of different CESA subunit interactions is unclear due to redundancy in the *CESA* gene family and separate combinations of *CESA*s that may be active in different cell types and at different times. The temperature-sensitive mutation (or homozygous allele) *rsw1-1 (CESA1)* results in primary wall deficiencies accompanied by a disappearance of rosettes from the membrane at the non-permissive temperature (Arioli et al. 1998), and strong homozygous alleles are either male gametophyte or embryo lethal (Persson et al. 2007; Gillmor et al. 2002). *CESA3* is co-expressed with *CESA1*, and null homozygous *cesa3* alleles are also male gametophyte lethal (Persson et al. 2007). CESA6 appears to be required for the elongation of hypocotyl cells in etiolated seedlings but can be partially complemented by other CESA6-related subunits such as *CESA2*, *CESA5* and *CESA9* (Desprez et al. 2007; Persson et al. 2007).

Recent experiments with CESA fused to fluorescent reporter proteins suggest that CSCs move at a constant velocity at the PM via a microtubule (MT) guidance mechanism. However, when MTs are completely depolymerized, CESA velocity remains unchanged in otherwise wild-type plants (Paredez et al. 2006; DeBolt et al. 2007a) suggesting that energy provided by glucan chain polymerization is primarily responsible for movement rather than MT motor proteins. It has recently been shown that both phytochrome regulation (Bischoff et al. 2011) and the phosphorylation status of CESA1 (Chen et al. 2010a) result in changes in the rate of YFP::CESA6 movement. Despite evidence that CESA proteins assemble into higher order complexes whose movement, and presumably biosynthetic rate, can be regulated by CESA modifications (Bischoff et al. 2011; Chen et al. 2010a), structure-function relationships between the CSC, the resulting microfibril and the expansion state of the cell are not well understood. Here, we address this challenge using forward chemical genetics. Resistance to a panel of drugs that target cellulose biosynthesis was conferred by mutations in the *CESA1* and *CESA3* C-terminal transmembrane spanning domain region, henceforth termed the TMR. We used X-ray diffraction (XRD) and ^{13}C solid-state nuclear magnetic resonance

(SSNMR) spectroscopy to show that the TMR of CESA1 and CESA3 are involved in the ordered crystallization of glucan chains in the interior of cellulose microfibrils, thereby providing evidence for a relationship between the primary structure of CESA and the architecture and organization of its product.

Materials and Methods

Plant material and growth conditions. All wild-type and mutant *A. thaliana* used were of the Columbia (Col-0) ecotype and seedlings were germinated and grown as previously described (DeBolt et al. 2007a). Inhibitors were dissolved in dimethylsufoxide (DMSO) and added to media so that DMSO never exceeded 0.1%. Isoxaben was purchased from Chem Service Inc., West Chester, PA. Chemical libraries used and screening conditions have been described in (DeBolt et al. 2007a) and supplemental on-line material. *ixr1-2* was obtained from the Arabidopsis Biological Resource Center at Ohio State University. Transgenic plants expressing various florescent protein tagged genes or gene knockouts were developed by reciprocal crossing and have been described elsewhere (Paredez et al. 2006; DeBolt et al. 2007a). Complementation of *aegeus* using the RSW1 locus was achieved by standard transformation (Clough and Bent 1998) and the F_2 population screened for segregation for susceptibility.

Cellulose content analysis and [^{14}C]-glucose incorporation assays. Total cellulose content was determined for 7-day-old dark-grown hyopcotyls and 8-week-old stems according to Updegraff (1969). For [^{14}C]-glucose incorporation assays, seeds were germinated and grown in multi-well tissue culture plates at 21°C in the dark in 2 mL of sterile, liquid MS media containing 0.5% [w/v] glucose. After 3 days, the media was replaced with fresh MS media without glucose and containing either 0.05% DMSO or 50 µM quinoxyphen. After 1 h of preincubation with or without inhibitor, 0.5 µCi/mL [^{14}C]-glucose (American Radiolabeled Chemicals Inc., St. Louis, MO) was added to each well. The seedlings were incubated for 2 h in the dark at 21°C and then washed and extracted as described Fagard et al. (2000).

Microscopy. Seedlings expressing GFP::CESA3 or YFP::CESA6 were grown in the dark for 3 d and imaged using spinning disk confocal microscopy, as described previously (Gutierrez et al. 2009) except a DMI6000 B inverted microscope with Adaptive Focus Control (Leica) was used. Cells in the upper hypocotyl were imaged at

5-s intervals for 6 min at the plasma membrane. Images were processed to minimize signal from underlying Golgi bodies and to enhance particles at the plasma membrane. A 5-frame running average was applied to the series followed by rolling ball background subtraction (2 pixel radius). Then an FFT bandpass filter was applied to enhance structures of 2-3 pixels (0.32-0.49 μm). Data were analyzed with Imaris software (Bitplane). CESA particles were detected using the Spots module (estimated diameter = 0.5 μm) and tracked using the Autoregressive Motion algorithm (maximum frame-to-frame distance = 0.067 μm, maximum gap size = 1 frame). CESA velocity was calculated as total displacement divided by duration for tracks with a duration ≥ 18 frames (90 s) and straightness ≥ 0.75. Univariate analysis of variance, with Bonferroni post hoc tests, was performed using SPSS 19 software (IBM) to compare CESA velocities from different genotypes.

Cell wall structural analysis by XRD. *A. thaliana* material was prepared and RCI determined as previously described (Harris et al. 2009) with a control of synthetic crystalline cellulose (Avicel®, FMC-Biopolymer, Philadelphia, PA, USA). Three experimental replicates for mutant and wild-type biomass samples were performed. Diffractograms were collected in Diffrac-Plus-XRD Commander software (Bruker-AXS, Karlsruhe, Germany) and minimally processed (baseline identification, noise correction and cropping of RCI signature region) using the EVA and Texeval (Bruker-AXS) software. Synchrotron X-ray scattering experiments were performed at the macromolecular crystallography beamline F1 of the Cornell High Energy synchrotron source. A high-flux wiggler X-ray beam with a photon energy of 13 keV was focused to a spot size of 20 microns using an X-ray focusing capillary with 4 mrad acceptance. Plant samples were mounted in a helium-filled enclosure to reduce air scattering. Due to the high intensity of the microbeam no further processing was necessary. A Quantum 210 area detector was placed at a distance of 120 mm from the sample and the full 2D cellulose fiber diffraction image was recorded. Data were integrated using the Fit2D software (Grenoble, France). Scherrer equation analysis was performed by fitting a Gauss peak to the 200 reflection.

Cell wall structural analysis by ^{13}C magic angle spinning SSNMR. For ^{13}C solid state magic angle NMR plants were grown in sterile media supplemented with U-^{13}C glucose and ^{15}N NH_4Cl (100 mM), and cell walls were extracted, desalted and examined by NMR

as previously described (Dick-Pérez et al. 2011). ^{13}C SSNMR spectra were measured on a Bruker Avance 600 (14.1 Tesla) spectrometer operating at resonance frequencies of 600.13 MHz for ^{1}H and 150.9 MHz for ^{13}C. A double-resonance 4 mm magic-angle-spinning (MASº probe was used to measure all spectra). Typical radio-frequency field strengths were 62-70 kHz for ^{1}H decoupling and 50 kHz for ^{13}C pulses. The samples were spun under 7 to 12 kHz MAS. ^{13}C chemical shifts were referenced to the ^{13}CO signal of α-glycine at 176.49 ppm on the TMS scale. For quantitative ^{13}C 1D experiments, the ^{13}C magnetization was created by direct excitation using a 90˚ pulse and using a long recycle delay of 20 s. To preferentially detect mobile polysaccharides, a short recycle delay of 2 s was used in the ^{13}C direct polarization experiment. ^{13}C chemical shifts were assigned by reference with the recently published result (Dick-Pérez et al. 2011) and were confirmed by 2D ^{13}C-^{13}C spin diffusion correlation experiments with a 40 ms mixing time and by 2D J-INADEQUATE experiments (Dick-Pérez et al. 2011). The latter correlates ^{13}C double-quantum chemical shifts with single-quantum chemical shifts, and gives relatively high spectral resolution.

Results

Forward chemical genetics: isolation and characterization of the cellulose biosynthesis inhibitor quinoxyphen. The herbicide quinoxyphen (Figure 6.1a**;** a structure-based analysis of analogs can be found in Figure S6.1, Table S6.1 and SI Text) was identified in a screen for compounds that inhibit cell growth anisotropy. Germination on quinoxyphen above the IC_{50} value of 1.0 μM caused severe cell and tissue swelling of the hypocotyl and upper root in *A. thaliana* seedlings (Figure 6.1b). In addition, there was a 50% inhibition of ^{14}C-glucose incorporation into crystalline cellulose in plants germinated and grown on a 5.0 μM concentration of quinoxyphen (Figure 6.1c). Clear differences in cell wall composition based on principle component analysis of FTIR spectra were detected in quinoxyphen treated seedlings (Figure S6.2a-b), as well as significant increases in the abundance of cell wall neutral sugars (Figure S6.2c). Additional analysis of seedlings exposed to quinoxyphen showed other cell wall compositional alterations, including hyper-accumulation of callose and ectopic lignin production; both common phenotypes observed following chemical inhibition of cellulose biosynthesis (Desprez et al. 2002) (Figure S6.3a-d).

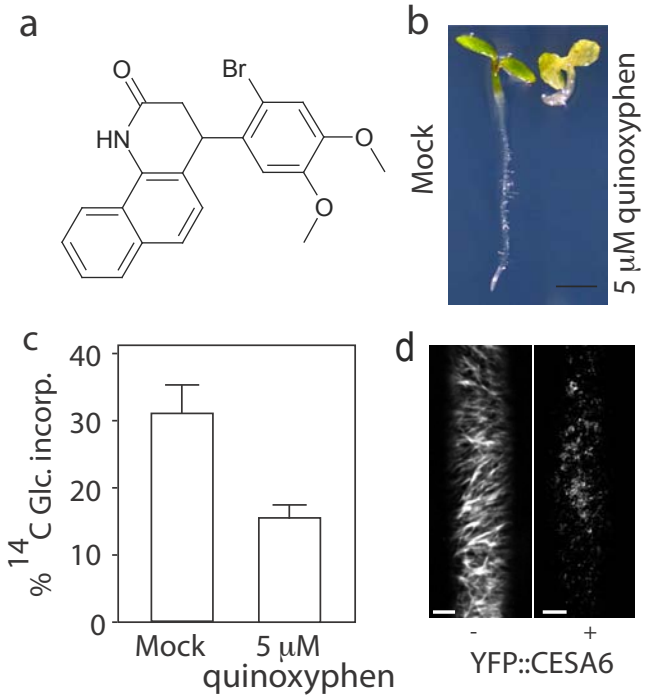

Figure 6.1. Identification of quinoxyphen as a cellulose biosynthesis inhibitor. (**a**) Structure of 4-(2-bromo-4,5-dimethoxy-phenyl)-3,4-dihydro-1H-benzo-quinolin-2-one ($C_{21}H_{18}BrNO_3$ MW 412.28), named herein quinoxyphen. (**b**) *A. thaliana* seedlings grown under continuous light for 5 days on MS agar containing 5 μM quinoxyphen (right) showed reduce growth compared with control plant (left). Scale bar 10 mm. (**c**) Incorporation of ^{14}C-glucose in the acid-insoluble fraction in wild-type treated and untreated with 5.0 μM quinoxyphen. (*P<0.001, Student's t-test, n=3). (**d**) Time lapse confocal images of YFP::CESA6 in hypocotyl cells of 3-day old etiolated plants were compared between mock control treatment and 20 μM quinoxyphen treatment revealing clearance of the PM CSCs after 120 min. Each image in panel d is an average of 60 frames taken at 5 sec intervals on the same Z plane. Scale bar, 10 μm.

In expanding *A. thaliana* hypocotyl tissue, cellulose biosynthesis can be visualized in living cells by labeling the CSC with fluorescently tagged CESA proteins. To establish a possible cause of the anisotropic growth disruption and cellulose content reduction, we used spinning disk confocal microscopy to examine the effect of quinoxyphen on the behavior of YFP-CESA6 particles in the focal plane of the PM. Consistent with previous observations following treatment with the herbicide isoxaben (Paredez et al. 2006; Gutierrez et al. 2009), labeled particles with slow and steady motility were depleted from the PM, a change visualized in time-projected images by the loss of tracks created by particle translocation (Figure 6.1d). Concurrently, label accumulated in trafficking compartments at the cell cortex, most of which were immobilized (Figure 6.1d, see Gutierrez et al. 2009 for further analysis of this redistribution syndrome). In contrast, no marked differences in morphology or general dynamics were observed in the actin (Figure S6.3e) or microtubule (Figure S6.3f) cytoskeletons after quinoxyphen treatment. Hence, we hypothesized that quinoxyphen targets cellulose biosynthesis, rather than causing broad cell toxicity, and that its mechanism of action is similar to that of isoxaben (Heim et al. 1989).

Resistance to quinoxyphen is conferred by the semi-dominant CESA1 locus. To identify possible targets of quinoxyphen, we performed a forward genetic screen and isolated an *A. thaliana* mutant showing strong resistance to quinoxyphen (>10 mM), which we named *aegeus* (Figure 6.2a). Given the similar phenotypes induced by quinoxyphen and isoxaben, as observed with live-cell imaging, we first asked whether the two drugs shared the same resistance locus. We performed an allelism test between *aegeus* and the isoxaben resistant mutant *ixr1-2* and established that the F1 crosses between the two homozygotes showed sensitivity when germinated and grown in media containing 5 μM of quinoxyphen or 10 nm of isoxaben (both lethal doses to wild-type), indicating that the two chemical resistance loci were not allelic (data not shown). In addition, homozygous *aegeus* plants displayed sensitivity to isoxaben and homozygous *ixr1-2* plants were sensitive to quinoxyphen (data not shown). Using a positional cloning approach to identify the gene conferring resistance to quinoxyphen (Figure S6.4a and Table S6.2), we found that the *aegeus* mutation corresponds to the replacement of an alanine with a valine in the fourth transmembrane spanning domain at amino acid position 903 in the C-terminal end of the CESA1 protein (Figure 6.2b-c). The mutated alanine is not highly conserved among primary cell wall CESAs, but is flanked

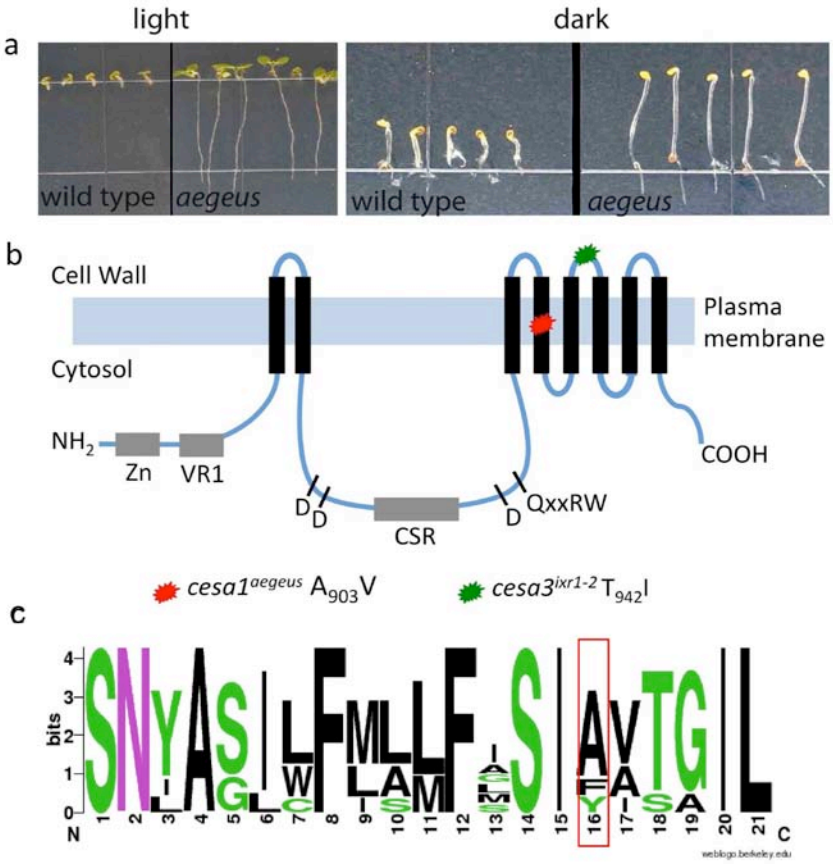

Figure 6.2. The *aegeus* mutant is resistant to quinoxyphen. (**a**) The phenotype of the *aegeus* mutant compared to wild-type when grown for 7 days in the light (left) or the dark (right) on medium containing 5 µM quinoxyphen. (**b**) The gene corresponding to the *aegeus* mutation was cloned using a map-based approach (Figure S6.3 and Table S6.2) and revealed a C to T change leading to replacement of a moderately conserved alanine residue at position 903 in the AtCESA1 protein with a valine residue (At4g3241). (**c**) Sequence logo assessment of residues in the fourth TMD of primary cell wall CESA proteins illustrates the location and conservation of the mutated alanine residue in CESA1 (red box). Amino acids are colored according to their chemical properties: polar amino acids are green, basic are blue, acidic are red and hydrophobic are black.

by several highly conserved residues (Figure 6.2c). The *aegeus* mutant displayed semi-dominant inheritance (Figure S6.4b) similar to that observed for isoxaben resistance in the *ixr* mutants (Heim et al. 1989). Both *cesa1*^{aegeus} and *cesa3*$^{ixr1\text{-}2}$ occur within the TMR of essential genes for cellulose biosynthesis in the primary wall (Figure 6.2b). Complementation of *cesa1*^{aegeus} by transformation with wild-type *CESA1* restored sensitivity to quinoxyphen (Figure S6.4c).

Generation of double drug-resistant mutants with mutations in two essential primary cell wall CESA subunits. We generated the double mutant *cesa1*^{aegeus}*/cesa3*$^{ixr1\text{-}2}$, thereby creating a primary cell wall CSC containing two essential CESA subunits with similar TMR mutations conferring drug resistances (Figure 6.3). As expected, not only did the double mutant show resistance to both quinoxyphen and isoxaben (data not shown), but also a far more pronounced dwarf phenotype than either of the single mutants (Figure 6.3a-b). Significant differences were also apparent during the first 7 days of dark-grown hypocotyl elongation (Figure 6.3c and Figure S6.5b) and in light-grown root growth (Figure S5a, c). Examination of crystalline cellulose content of mature stem (Figure 6.3d) and dark-grown hypocotyls (Figure 6.3e) revealed a significant reduction in all mutants compared with wild-type.

To dissect the structure of the cell wall in these mutants we combined neutral sugar analysis, glycosidic linkage analysis (Table S6.3 and Table S6.4) and ^{13}C SSNMR (Figure 6.4). Neutral sugar composition analysis revealed significant differences in neutral sugars as a proportion of total cell wall (Figure S6.6 and Table S6.3). In addition, although there was little to no hyper-accumulation of callose in the mutant hypocotyls (Figure S6.7a-d), similar to quinoxyphen treatment, the double mutant *cesa1*^{aegeus}*/cesa3*$^{ixr1\text{-}2}$ showed increased ectopic lignin production (Figure S6.7e-h). Quantitative ^{13}C SSNMR spectra of uniformly ^{13}C labeled cell walls indicated increased intensities of pectin and hemicellulose peaks relative to the interior cellulose C4 peak at 89 ppm for all mutants (Figure 6.4a-b). For example, the arabinan (Ara) C1 signal at 108 ppm, the galacturonic acid (GalA) and rhamnose (Rha) C1 signal at 101 ppm, and the C2/C4 signals of xyloglucan (XG) Glc, GalA, Rha, and the Ara signals at 80-83 ppm, increased markedly, consistent with linkage analysis (Figure S6.8a-b and Table S6.4). The relative amounts of glycoprotein to interior cellulose also increased in the mutants by about two fold

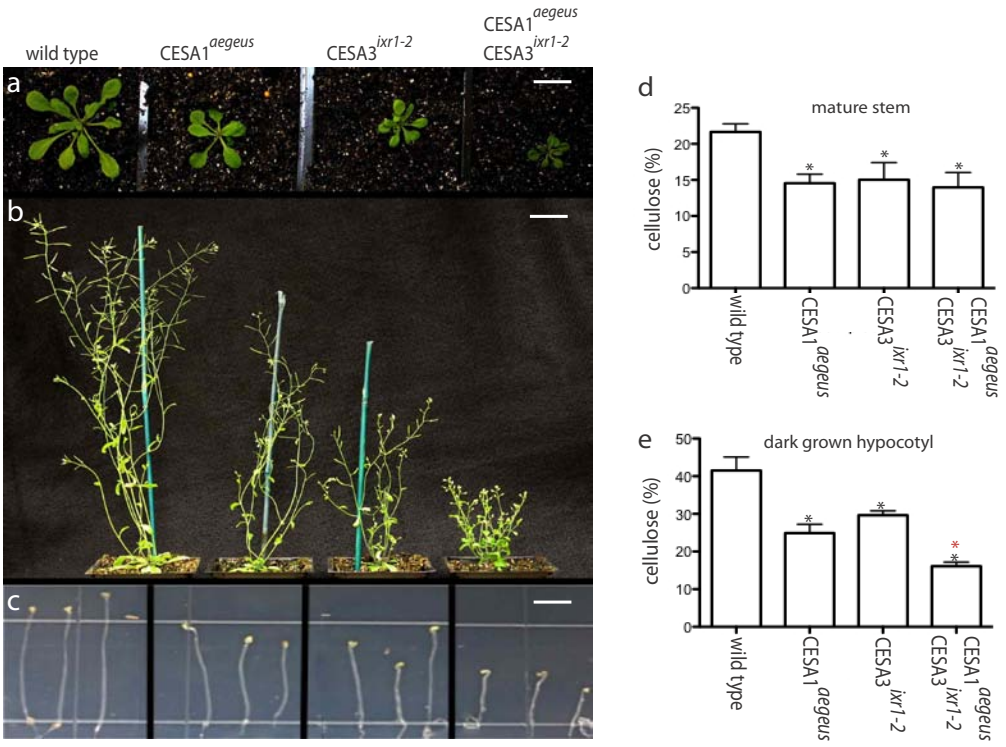

Figure 6.3. Analysis of a double mutant with mutations in CESA1 and CESA3. Viable growth of *cesa1*^{aegeus}, *cesa3*$^{ixr1\text{-}2}$ and *cesa1*^{aegeus}/*cesa3*$^{ixr1\text{-}2}$ were carefully documented. The double *cesa1*^{aegeus}/*cesa3*$^{ixr1\text{-}2}$ mutant showed a far more pronounced dwarf phenotype than single mutants from (**a**) rosette morphology to (**b**) maturity and (**c**) hypocotyl elongation. (**d**) Crystalline cellulose content of mature stems was reduced in the mutants compared to wild-type (*P<0.01 Student's t-test, n=3). (**e**) Cellulose content in dark-grown hypocotyls was reduced 40% ± 2.4, 30% ± 1.2 and 61% ±1.1 in the *cesa1*^{aegeus}, *cesa3*$^{ixr1\text{-}2}$ and *cesa1*^{aegeus}/*cesa3*$^{ixr1\text{-}2}$ respectfully, as compared to wild-type (*P<0.01 Student's t-test, n=3).

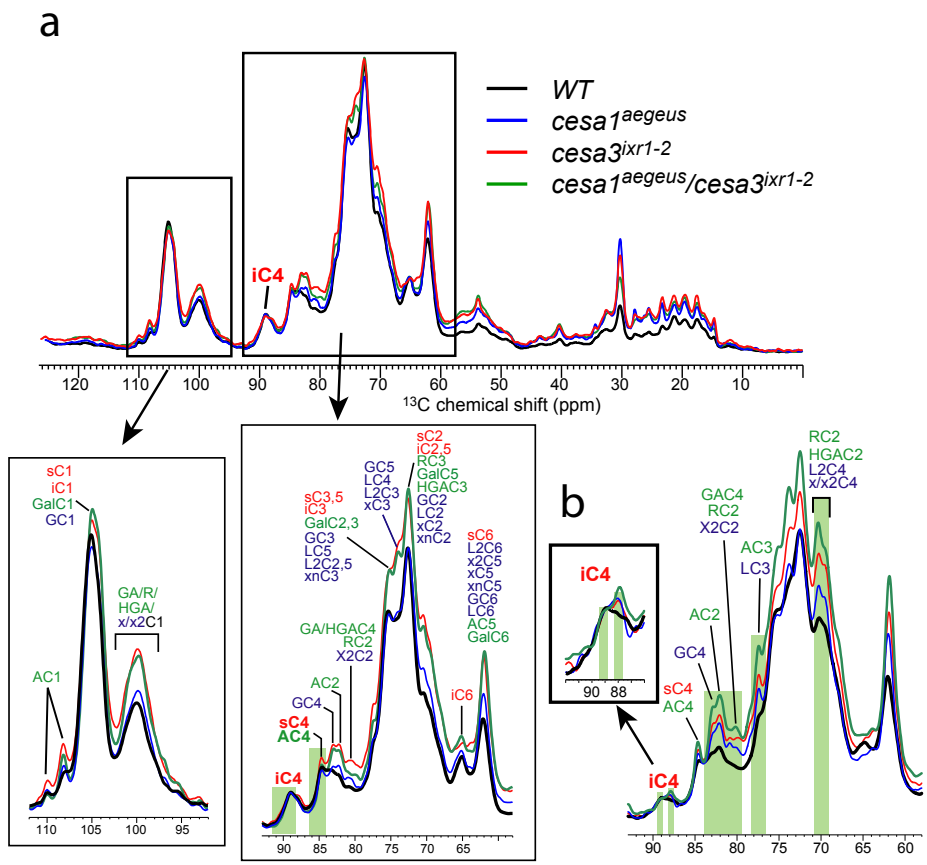

Figure 6.4. ^{13}C magic-angle-spinning SSNMR analysis of cellulose and cell wall structure in *cesa1*^{aegeus}, *cesa3*$^{ixr1\text{-}2}$ and *cesa1*^{aegeus}/*cesa3*$^{ixr1\text{-}2}$. (**a**) Quantitative ^{13}C magic-angle-spinning SSNMR spectra of wild-type and mutant cell walls. The intensity ratio of interior (88.5-91.5 ppm) to surface (84-86 ppm) cellulose C4 peaks was the lowest for the double mutant. The relative amount of hemicellulose and pectin signals to interior cellulose is significantly higher in all mutants compared to wild-type. The spectra were measured quantitatively by ^{13}C direct polarization using a long recycle delay of 20 s. (**b**) ^{13}C direct-polarization spectra measured with a short recycle delay of 2 s, which preferentially enhances the signals of mobile polysaccharides. The hemicellulose and pectin signals and the 88-ppm less-crystalline cellulose signal are increased for the mutants relative to the wild-type.

compared to wild-type. Hence, this class of mutants displays less crystalline cellulose and relative increases in pectin, hemicellulose and glycoprotein.

TMR missense mutations cause increased cellulose synthase movement in the plasma membrane. Cell wall dysfunction arising from mutation of the TMR of CESA allowed us to examine the relationship between CESA modification and CESA behavior in the PM. We concluded that the mutant CESA1 and CESA3 proteins described here are present within the CSC, and display some catalytic activity because null mutants have been documented to lose CSC rosette formation and crystalline cellulose production (*rsw1-1)* (Arioli et al. 1998) or to show male gametophytic lethality (Persson et al. 2007), respectively. We examined the *in vivo* behavior of these mutant complexes by creating double and triple mutants in stable transgenic plants expressing fluorescent reporters, and using spinning disk laser confocal microscopy to visualize the movement of the CESA subunits in living cells (proCESA3-GFP-CESA3/*cesa1*^{aegeus}, proCESA6-YFP-CESA6/*cesa3*$^{ixr1\text{-}2}$, and proCESA6-YFP-CESA6/*cesa1*^{aegeus}/*cesa3*$^{ixr1\text{-}2}$). Based on prior data suggesting that CESA movement at the PM is associated with microfibril polymerization (Paredez et al. 2006; DeBolt et al. 2007a), faster moving CESA would infer greater polymerization rates, whereas slower moving CESA would indicate a suppression of polymerization. Bidirectional trajectories of fluorescent punctae were visualized at the PM focal plane of dark-grown transgenic seedlings in all mutant combinations (epidermal cells in the upper hypocotyl, Figure 6.5a and Figure S6.8). Surprisingly, the mean velocity of labeled CESA complexes was significantly greater in *aegeus, ixr1-2* and the double mutant than in transgenic lines that carried wild-type alleles of *CESA1* and *CESA3* (P<0.0001, ANOVA with Bonferroni tests) (Figure 6.5). Previously, increased polymerization rates were observed in studies of bacterial cellulose synthesis, where the disruption of crystallization prevented microfibril assembly and caused an increased polymerization rate (Benziman et al. 1980; Haigler et al. 1980). Based on the difference in CESA behavior (Figure 6.5), and prior evidence from bacteria, we postulated that cellulose microfibril structure may be aberrant in TMR mutants, and may reflect differences in cellulose crystallization.

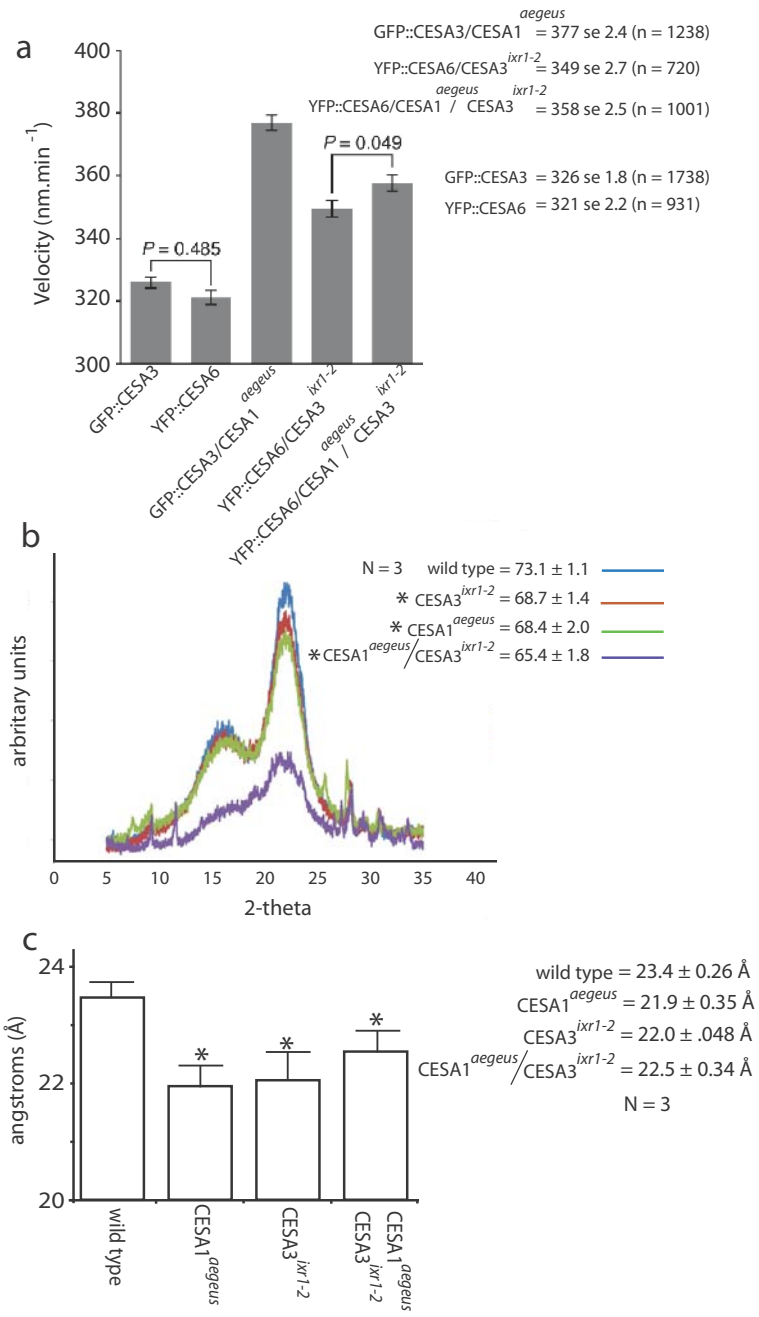

Figure 6.5. TMR mutants display cellulose structure and increased CESA particle velocity at the PM focal plane documenting feedback between structure and function. (**a**) Epidermal cells of 3-day old seedling expressing translational fusion reporters were imaged in the upper hypocotyl with spinning disk confocal microscopy (72 frames). CESA complex velocities from the indicated genotypes were compared using ANOVA with Bonferroni tests and significant difference indicated at $P<0.0001$. Each result

represents ≥720 CESA complexes from ≥10 cells from unique plants. Error bars represent SEM. (**b**) Analysis of *cesa1*^{aegeus}, *cesa3*$^{ixr1\text{-}2}$ and *cesa1*^{aegeus}/*cesa3*$^{ixr1\text{-}2}$ structural changes in the cellulose fingerprint compared between mutant plants and wild-type were initially screened by wide-angle X-ray diffraction (XRD) using Bragg-Brentano reflective geometries to obtain a relative crystallinity index (RCI) (*P<0.01 Student's t-test, n=3). (**c**) Subsequently, mutant and wild-type plants were grown to maturity and the first internode of the stem was then exposed to synchrotron X-ray analysis. Data indicated a reduction in the crystallite size (lateral dimensionality) for *cesa1*^{aegeus} of 21.9 Å ±0.35 Å, *cesa3*$^{ixr1\text{-}2}$ of 22.0 Å ±0.48 Å, *cesa1*^{aegeus}/*cesa3*$^{ixr1\text{-}2}$ of 22.5 Å ±0.34 Å as compared to 23.4 Å ±0.26 Å for wild-type (*P<0.01 Student's t-test).

TMR mutants produce structurally aberrant cellulose microfibrils. To determine whether there were differences in cellulose microfibril structure between mutant and wild-type plants, we first measured the relative crystallinity index (RCI) for each sample using X- ray diffraction (XRD). A difference in the RCI could reflect a change in the microfibril size: a reduction in microfibril width results in a larger contribution of surface glucan chains to the overall microfibril structure. A higher percentage of surface chains yields a lower relative crystallinity index both because surface chains are less constrained and because they interact with other polysaccharides, such as hemicelluloses and pectin, which distorts their hydrogen bonding. *cesa1*^{aegeus}, *cesa3*$^{ixr1\text{-}2}$ and *cesa1*^{aegeus}*/cesa3*$^{ixr1\text{-}2}$ all show significantly reduced RCI values compared to wild-type (Figure 6.5b). However, as indicated by the SSNMR analysis, the hemicellulose fraction relative to interior cellulose also increased in the mutant, which could contribute to the amorphous peak present in the XRD data and skew the RCI determination towards lower crystallinity. To obtain a more accurate estimation of the microfibril crystallinity, we examined mature stems at the first internode using high-energy synchrotron radiation XRD. This method allows the examination of intact plant samples and so disruptive grinding or chemical treatments are unnecessary. Synchrotron XRD data indicated a significant reduction in the crystallite width for *cesa1*^{aegeus}, *cesa3*$^{ixr1\text{-}2}$ and *cesa1*^{aegeus}/*cesa3*$^{ixr1\text{-}2}$ compared to wild-type (Figure 6.5c).

Further analysis of crystallite width was obtained from quantitative ^{13}C-SSNMR spectra of uniformly ^{13}C-labeled cell wall (Figure 6.4a**,** see methods for labeling protocol). Based on the intensity ratio of interior C4 (88.5 – 91.5 ppm) (iC4) to surface C4 (sC4) peak (84-86 ppm) intensities, we found that the double mutant had 8% lower crystallinity relative to wild-type (Table S6.5), while the single mutants had smaller differences from the wild-type. The mutants also displayed additional intensities in the regions of the iC4 peak, with a new 88-ppm peak that is largely absent in the wild-type spectrum (Figure S6.9). This 88-ppm peak is closer to the 85-ppm C4 peak of the more amorphous surface cellulose, suggesting that it corresponds to less crystalline cellulose. (Figure 6.4b-inset). Further, the 88-ppm intensity is preferentially enhanced in the mutant samples relative to the wild-type when the ^{13}C spectra were measured using short recycle delays to increase the intensities of dynamic polysaccharides. This suggests that the less crystalline glucan chains in the mutants are more dynamic, which is consistent with weakened hydrogen bonding and the amorphous nature of the chains. In 2D double-

quantum correlation spectra, we also observed two types of interior cellulose, which were best resolved in the CESA3^{ixr1-2} mutant but were also present in the other TMR mutants (Figure S6.9). Therefore, in the TMR mutants, the microfibrils displayed reduced width and an additional cellulose C4 peak indicative of a degree of crystallinity that is intermediate between the surface and interior cellulose of wild-type, suggesting a difference in glucan chain association during microfibril formation.

We hypothesized that cellulose with more mobile amorphous iC4 intensity might show differences in saccharification efficiency when hydrolyzed with cellulase enzymes, as cellulose crystallinity has been shown to be an important predictor of enzymatic hydrolysis rate (Hall et al. 2010). The catalytic efficiency ($_{app}V_{max}/K_m$) value showed a 32% and 49% increase in hydrolytic efficiency when using the *cesa1*^{aegeus} and *cesa1*^{aegeus}/*cesa3*$^{ixr1-2}$ cellulose extracts, respectively (Figure S6.10), consistent with our prior examination of *cesa3*$^{ixr1-2}$ (Harris et al. 2009). These saccharification data support the NMR structural information, indicating increased mobile iC4 assignments, from which we deduce that the amino acid sequence of the TMR of CESA1 and CESA3 has an important influence on cellulose microfibril architecture.

Discussion

Here, we identify a compound, quinoxyphen, which inhibits cellulose biosynthesis and characterize a resistant mutant with a missense mutation in the TMR of CESA1. Similarly, resistance to isoxaben was conferred by TMR mutations in CESA3 or CESA6 (Desprez et al. 2002; Scheible et al. 2001). Collectively, data for isoxaben and quinoxyphen resistance loci demonstrate that they occur in the TMR and confer related phenotypes on growth, cell wall composition and CESA crystallinity, but arise in association with different CESAs. A plausible mechanism to explain these data is that both drugs act to disrupt the integration of CESA into the PM (or outer face of the Golgi). These CESA subunits are unable to fold properly into the membrane or form functional proteins and thus prevent CSC formation and delivery to the PM. An alternative model is that this class of drugs inhibits the association between CESA subunits. Prior studies have shown that *rsw1* (CESA1 temperature-sensitive locus) plants grown at the non-permissive temperature fail to form CSC rosettes (Arioli et al. 1998). Live-cell imaging studies consistently show clearance of YFP::CESA6 from the PM after quinoxyphen treatment, although resistance is gained by mutations in CESA1, suggesting that CSC

disruption may involve multiple subunits. As CSC rosette assembly involves multimeric CESA associations (Taylor et al. 2003; Timmers et al. 2009; Wang et al. 2006), we propose that isoxaben and/or quinoxyphen disrupt these inter-subunit interactions. Since this drug resistance is conferred by TMR mutations, it is plausible that both the site of inhibition and subunit association occur at least partially in this region. As a resistance mechanism, a similar scenario has been observed in the case of hydrophobic sliding for drug resistance in HIV-type 1 protease (Foulkes-Murzycki et al. 2007), where drug binding affinity is displaced via mutation of residues in a TMR.

Collective studies integrating CESA mutants with SSNMR and XRD analysis of the microfibril structure provide mechanistic insights into a structure-function association during cellulose biogenesis. The amino acid sequences of the TMR of CESA1 and CESA3 influenced the glucan chain organization in the microfibril interior. We measured increased intensity of the 88-ppm peak, as well as lower crystallinity indices, which support lower H-bonding and increased proportions of amorphous zones in TMR mutant cellulose. Biochemical studies using a cellulase cocktail to digest semi-purified cellulose show that mutant cellulose was more readily enzymatically cleaved to individual glucan components, consistent with the structural determinations. Almost nothing is known about the functional significance of the TMR or the structure-function relationship between CESA and cellulose microfibril architecture. We advance three hypotheses to explain how TMR mutants create a more amorphous and mobile cellulose-like structure (Figure 6.4b). Firstly, the TMR mutations may result in completely dysfunctional CESA1 and CESA3 subunits. However, genetic data do not support this as null mutants result in male gameteophytic lethality (Persson et al. 2007). Second, the TMR may be involved in associations with other proteins in the CSC (not CESAs), which in turn play a role in microfibril assembly. However, this is only weakly supported by the nature of the *cesa1*^{aegeus} mutation, which is predicted to lie within the fourth transmembrane spanning domain; it would be necessary to invoke a conformation state for the interaction with such protein cofactors. Finally, the TMR of plant CESA proteins may act to organize the individual glucan chains and thus promote cellulose crystallinity (H-bonding) by facilitating association with other glucan chains. This model is consistent with the only reported crystal structure of a CSC, an octameric structure of the periplasmic AxCeSD subunit in the CSC of the bacterium *A. xylinum* in complex with a 5-glucose-cellulose product (Hu et al. 2010). Here, a dimer interface was necessary to facilitate passage and

proper alignment of glucan chains into a crystalline microfibril. Such a model would suggest that subtle alterations in the transmembrane helix structure via *cesa1*^{aegeus} and *cesa3*$^{ixr1\text{-}2}$ would induce changes in the organization of glucan chains via the inner side of a multimeric subunit association. Disruption of microfibril assembly induced genetically herein and pharmacologically in bacteria (Benziman et al. 1980) causes an increase in the rate of glucan chain polymerization, suggesting that the two processes are coupled and that crystallization is rate limiting. Therefore, our data revealing aberrant iC4 structure support a model whereby crystallization limits the polymerization rate of wild-type cellulose and demonstrate that these two factors can be partially decoupled.

Chapter VI
Supporting Information

Forward chemical genetic dissection of cellulose synthase structure and function

SI Text

Chemical screening conditions. Chemical libraries used and screening conditions have been described (DeBolt et al. 2007a). In brief, approximately 10 sterilized *A. thaliana* seeds were sown per well and the plates were incubated in 24 h light (50 μE/ m^2/s) at 21°C for 3 days for initial isolation of quinoxyphen. Growth was compared to control wells that contained the same amount of DMSO. Plates were visually scored after three days of growth by inspecting each well with a dissecting microscope. Structural analogs were determined using the ChemMine website (http://bioweb.ucr.edu/ChemMine) (Girke et al. 2005) and purchased from ChemBridge (San Diego, CA). Screening of these compounds for increased potency or any change in phenotype involved germinating seedlings on plates containing half-strength Murashige and Skoog (MS) mineral salts (Sigma-Aldrich, St. Louis, MO), 0.8% agar and after which grown under continuous light (200 μE/m^2/s) or in the dark at 21°C for 7 days.

Analog analysis for quinoxyphen, 4-(2-bromo-4,5-dimethoxy-phenyl)-3,4-dihydro-1H-benzo-quinolin-2-one action mechanism. To explore the basis for quinoxyphen activity and determine whether a more potent analog could be identified, a structure-based analysis was conducted using tools available through ChemMine (Girke et al. 2005) and analogs tested for their ability to inhibit root growth (Figure S6.1; analogs listed in Table S6.1). The analog study led to the observation that 5 of the 6 most active compounds contained an arylbromine group associated with a dimethoxy substitution (Figure S6.1; compounds 1, 2, 4, 5, 6). The ortho substituted bromine atom is predicted to withdraw charge from the lone aryl group; specifically, the van der Waals interaction of the relatively large bromine atom overlaps with the protons on the CH_2 group adjacent to the carbonyl. To determine whether other electron-withdrawing groups might phenocopy the aryl bromine-containing quinoxyphen, we assayed an additional set of analogs containing bromo, iodo, nitro and chloro substitutions (Figure S6.1). The substitution of

bromine with similar electron-spreading atoms resulted in compounds that also caused significantly shorter and more swollen root and hypocotyl cells. The most potent of these compounds were a 2,3-dichloro (compound 3), 2-chloro-6-fluoro (compound 7), 2-fluoro-5-bromo (compound 13), 6-nitro-1,3-benzodioxol (compound 14) or 2-chloro substitution (compound 15) (Figure S6.1a). Hence, out of 18 compounds that caused reduced root growth, 15 contained a bromo- or related electron withdrawing substitution. Overall, far greater concentrations of analogs were needed to assay inhibition of radical elongation than was required for quinoxyphen action (25 µM vs 1-5 µM), hence quinoxyphen with its specifically positioned aryl bromine was the most effective of the tested compounds for inhibition of radical elongation.

FTIR analysis. For Fourier Transform Infrared (FTIR) analysis, dried wild-type seedlings (3-day old) grown in 5.0 μM quinoxyphen were pooled and homogenized by ball milling. The powder was dried at 30°C overnight, mixed with KBr, and pressed into 13-mm pellets. Fifteen FTIR spectra for each line were collected on a Thermo Nicolet Nexus 470 spectrometer (ThermoElectric Corporation, Chicago, IL) over the range 4,000–400 cm^{-1}. For each spectrum, 32 scans were co-added at a resolution of 8 cm^{-1} for Fourier transform processing and absorbance spectrum calculation by using OMNIC software (Thermo Nicolet, Madison, WI). Spectra were corrected for background by automatic subtraction and saved in JCAMP.DX format for further analysis. Using Win-Das software (Wiley, New York), spectra were baseline-corrected and were normalized and analyzed by using the principal component (PC) analysis covariance matrix method (Kemsley 1998). Figures were processed using Sigma Plot (Microsoft, Redmond, WA).

Callose and lignin staining. Wild-type plants were grown for 5 days in the dark on one-half MS agar plates with of without supplementation of 1.0 μM quinoxyphen. Seedlings were directly spread on slides where the staining components were added followed by a coverslip. Callose staining was done with Aniline Blue Fluorochrome (Sigma-Aldrich, St Louis, MO) at a concentration of 0.1 mg ml-1 in 0.07 M sodium phosphate buffer, pH 9. Slides were kept in the dark for 1 h before observation under UV light. Phloroglucinol in a 20% hydrocholoric acid solution was used for lignin staining and slides were observed after 5 min of staining under white light.

Neutral sugar analysis of the quinoxyphen resistant mutants. Neutral sugar composition was determined by HPLC from approximately 500 dark-grown hypocotyls from each plant. Cell wall material was prepared from the hypocotyls as described (Dick-Pérez et al. 2011) and three replicates of 4 mg of air-dried cell wall material was then prepared for HPLC analysis as described (Mendu et al. 2011).

Glycosyl linkage analysis. For glycosyl linkage analysis 1 mg of each sample was prepared in triplicate. The samples were then suspended in 200 ul of dimethyl sulfoxide. The samples were then stirred for 3 days. The samples were permethylated by the treatment with sodium hydroxide and methyl iodide in dry DMSO (Ciucanu and Kerek 1984). The samples were subjected to the NaOH base for 15 minutes then methyl iodide was added and left for 45 minutes. The NaOH was then added for 15 minutes and finally more methyl iodide was added for 45 minutes. This addition of more methyl iodide and NaOH base was to insure complete methylation of the polymer. Following sample workup, the permethylated material was hydrolyzed using 2 M trifluoroacetic acid (2 h in sealed tube at 121°C), reduced with $NaBD_4$, and acetylated using acetic anhydride/trifluoroacetic acid. The resulting (PMAAs) were analyzed on an Agilent 7890 A GC interfaced to a 5975 MSD (mass selective detector, electron impact ionization mode); separation was performed on a 30 m Supelco 2330 bonded phase fused silica capillary column (York et al. 1986).

Enzymatic digestion and kinetics of cellulose saccharification efficiency. Identical loadings of semi-purified cellulose for wild-type, *cesa1*^{aegeus}, and *cesa1*^{aegeus}/*cesa3*$^{ixr1-2}$, were analyzed for recalcitrance to saccharification using a commercial cellulase cocktail and compared with the previously measured *cesa3*$^{ixr1-2}$ (Harris et al. 2009). The nature of the improved conversion efficiency was quantified by determining pseudo-apparent Michaelis–Menten kinetic parameters recognizing that there are inherent ambiguities with an insoluble substrate like cellulose and a multienzyme cellulase cocktail. Nevertheless, using this method we are able to calculate a K_{cat} value, which represents the most effective measure of substrate performance.

Statistical analyses. Crystalline cellulose content, glycosidic linkage analysis, neutral sugar composition of wild-type seedlings germinated with quinoxyphen versus mock treatment and wild-type versus mutant seedlings, root length of wild-type seedlings

germinated with the analogs versus mock treatment, hypocotyl and root length of wild-type versus mutants and the RCI values and crystallite width determined by XRD of wild-type and mutant plants were compared by two-tailed Student's t-tests. The mean velocity of labeled CESA complexes were compared between wild-type and mutants using a univariate analysis of variance, with Bonferroni post hoc tests.

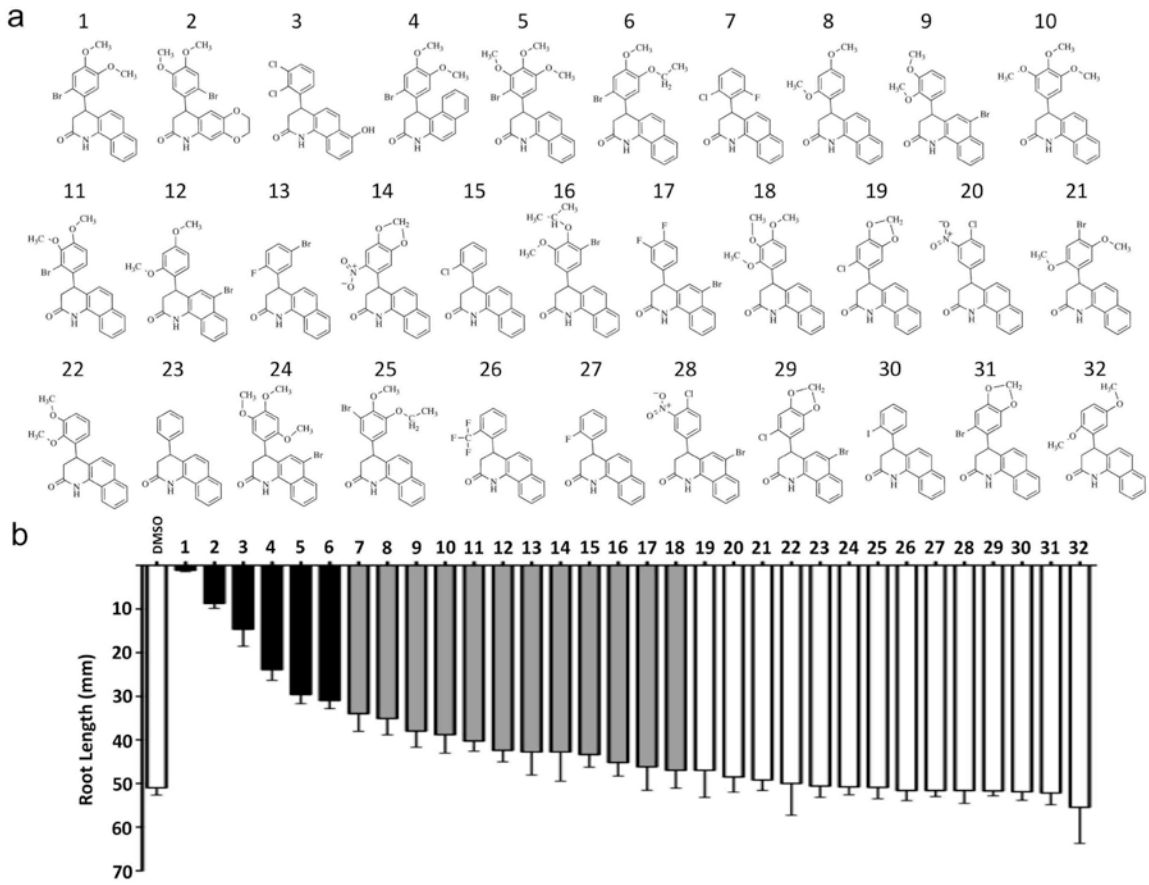

Figure S6.1. Analog analysis for quinoxyphen, 4-(2-bromo-4,5-dimethoxy-phenyl)-3,4-dihydro-1H-benzo-quinolin-2-one action mechanism. (**a**) Thirty-two commercially available analogs of quinoxyphen were identified using webtools available through ChemMine (Girke et al. 2005). (**b**) Root growth measured as radical elongation was used to assess the potency of each compound at a final concentration of 25 μM. Radical elongation was compared to control with 10 replicates per treatment (error bars indicate one standard deviation from the mean) and colored bars indicates significant reduction in vertical radical length relative to untreated control ($P<0.05$ Student's t-test). A tabulated list of ChemBridge (San Diego, CA) identification numbers and chemical formulae can be found in Table S6.1.

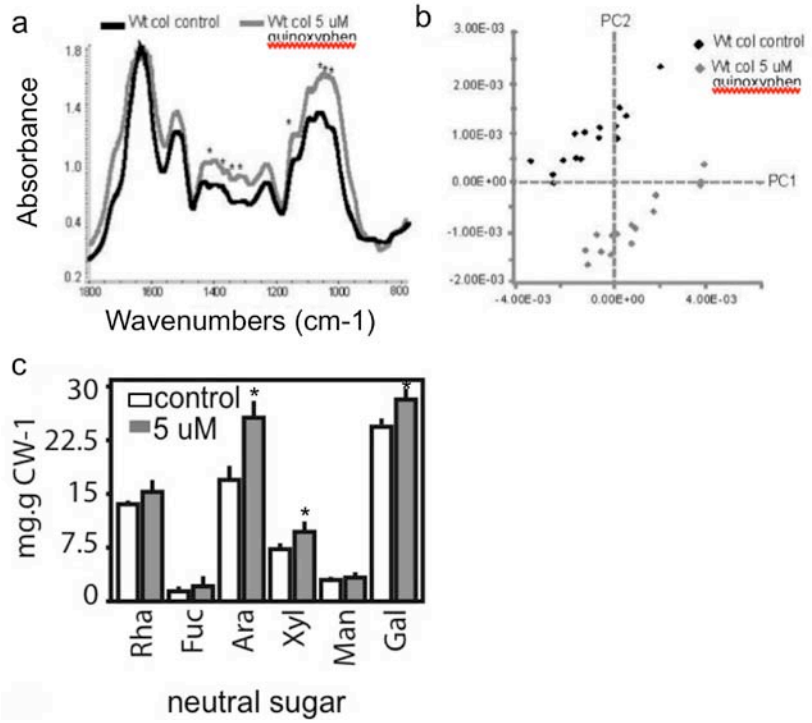

Figure S6.2. Effects on cell wall composition following quinoxyphen treatment. (**a**) The FTIR spectra of wild-type seedlings treated and untreated with 5.0 μM quinoxyphen. (**b**) In agreement with the sugar composition, principal component analysis of the FT-IR spectra from the cell walls showed a clear separation of the treated compared with the non-treated seedlings in the first two components (PC). PC 1 and PC 2 explain 93.2 % of the variability in the original IR data. Many of the differences between these two samples are present in the fingerprint region of the polysaccharides although it is difficult to assign to a single cell wall polymer. Absorbance peaks at 1032, 1073 and 1154 cm^{-1} in PC 1 and 991, 1037, 1421cm^{-1} in PC2 (not shown) are relative higher in the treated sample compared with the control. In addition, amide-I absorption peak at 1673 cm^{-1}, stronger in the control sample may reflect higher protein content. (**c**) There was an overall increase in cell wall neutral sugar content of quinoxyphen treated seedlings compared to the wild-type control. Specifically, arabinose, xylose and galactose were significantly higher in the treated seedlings. * Indicates changes were significantly different from wild-type, $P<0.05$, Student's t-test, n=3.

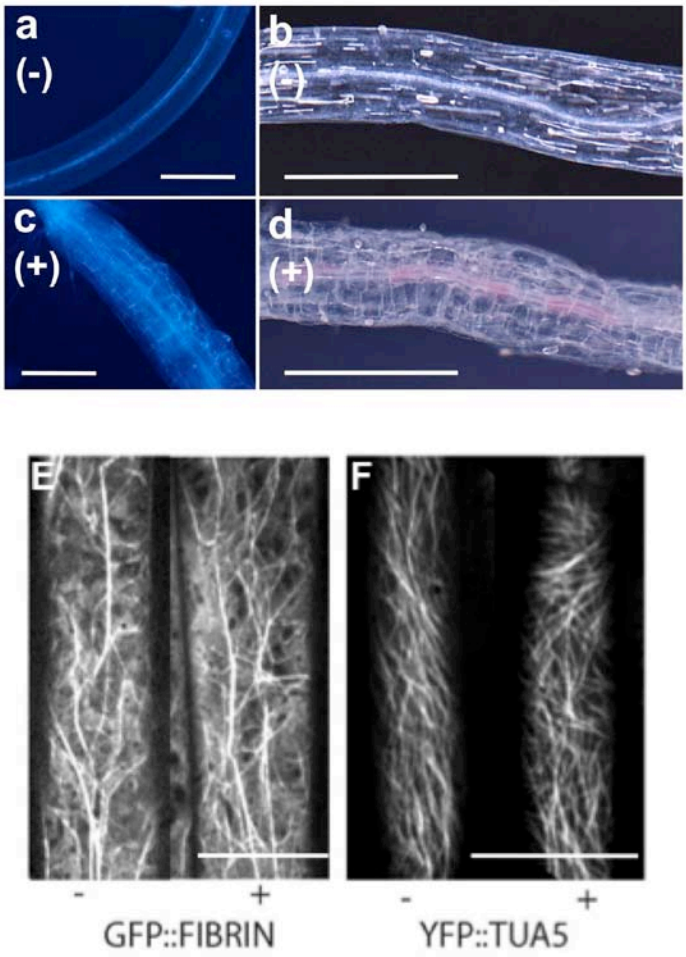

Figure S6.3. Quinoxyphen treatment causes hyper-accumulation of callose and ectopic lignin production but no change in the cytoskeleton. Dark-grown hypocotyls stained with (**a, c**) aniline blue indicate an accumulation of callose and with (**b, d**) phloroglucinol show an accumulation of lignin when wild-type seedlings are grown in the presence of 1.0 μM quinoxyphen for 5 days. Scale bar 300 mm. Quinoxyphen (20 μM) caused no change in morphology or motility of the (**e**) actin cytoskeleton (GFP::FIBRIN) or (**f**) microtubule array (YFP::TUA5). Scale bar 10 mm.

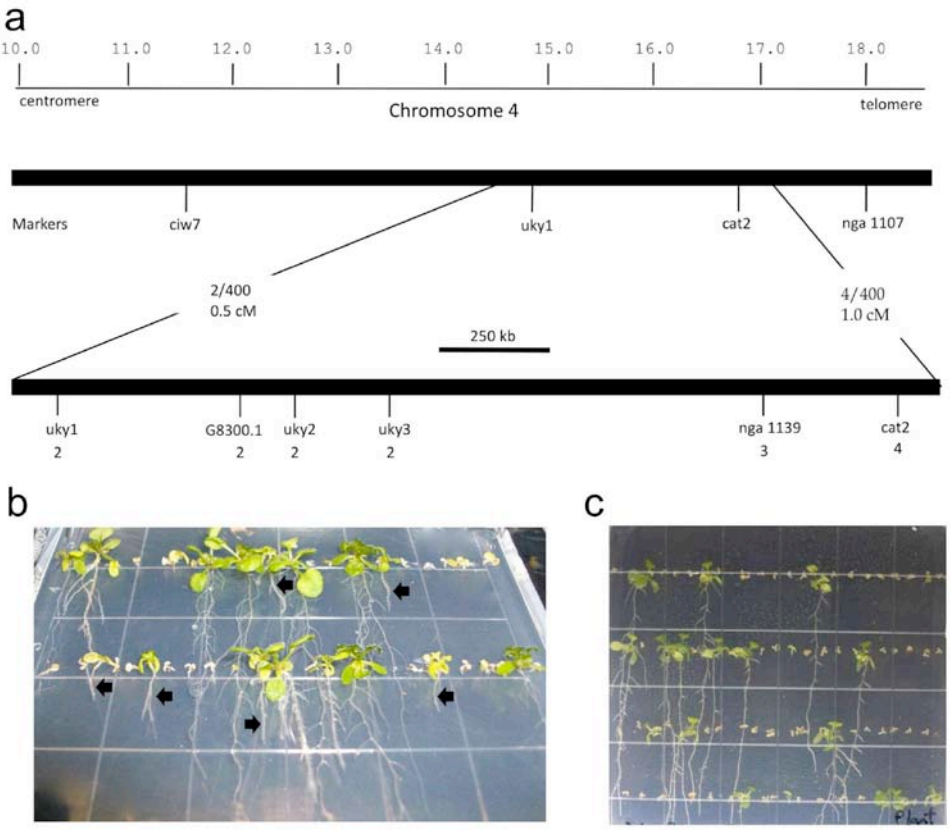

Figure S6.4. Map-based cloning of the quinoxyphen resistance locus. (**a**) Bulked segregant analysis and fine-mapping narrowed the location of the quinoxyphen resistant locus to an 830 kb region between markers UKY3 and NGA1139 that contained the *AtCESA1* gene. (**b**) Growth of seed from the F_2 mapping population indicated that heterozygote individuals possessed some degree of resistance to 5.0 μM quinoxyphen as shown by the growth of radially swollen roots (indicated with black arrow) suggesting that the *aegeus* mutation confers a semi-dominant phenotype. (**c**) To confirm that the mutation found in the *aegeus* mutant was responsible for the quinoxyphen-resistance phenotype, the wild-type *AtCESA1* gene was transformed into the *aegeus* mutant. T_2 progeny of the *aegeus* mutants transformed with the *AtCESA1* gene segregated for susceptibility on media containing 100 μM quinoxyphen, where only plants homozygous for the *aegeus* mutation can grow.

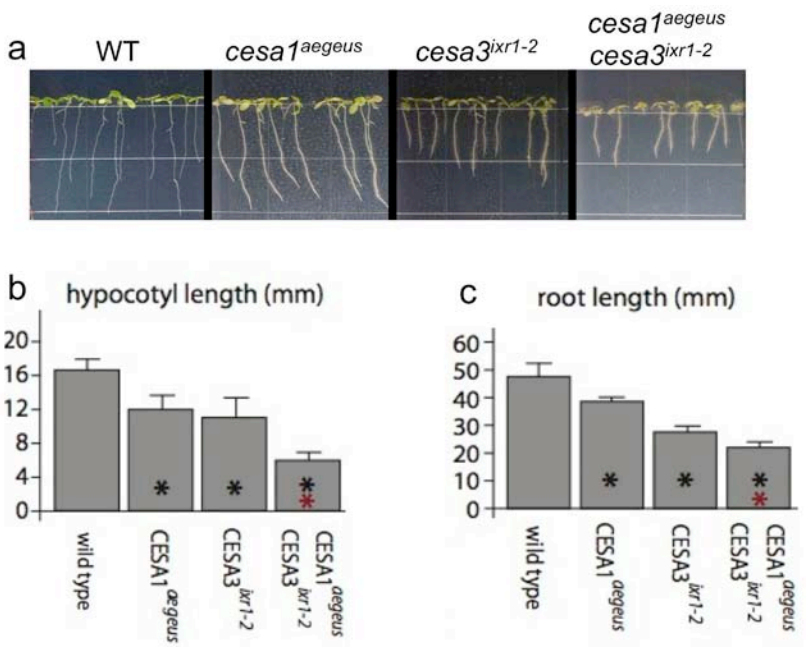

Figure S6.5. Analysis of a double mutant with mutations in CESA1 and CESA3. The double *cesa1*^{aegeus}/*cesa3*$^{ixr1-2}$ mutant showed a far more pronounced dwarf phenotype than single mutants in seedling root growth. Measurement of 7-day-old (**b**) hypocotyl and (**c**) root elongation. * Indicates changes were significantly different from wild-type, P<0.05, Student's t-test, n=10. * Indicates changes were significantly different from the single mutants, P<0.05, Student's t-test, n=10.

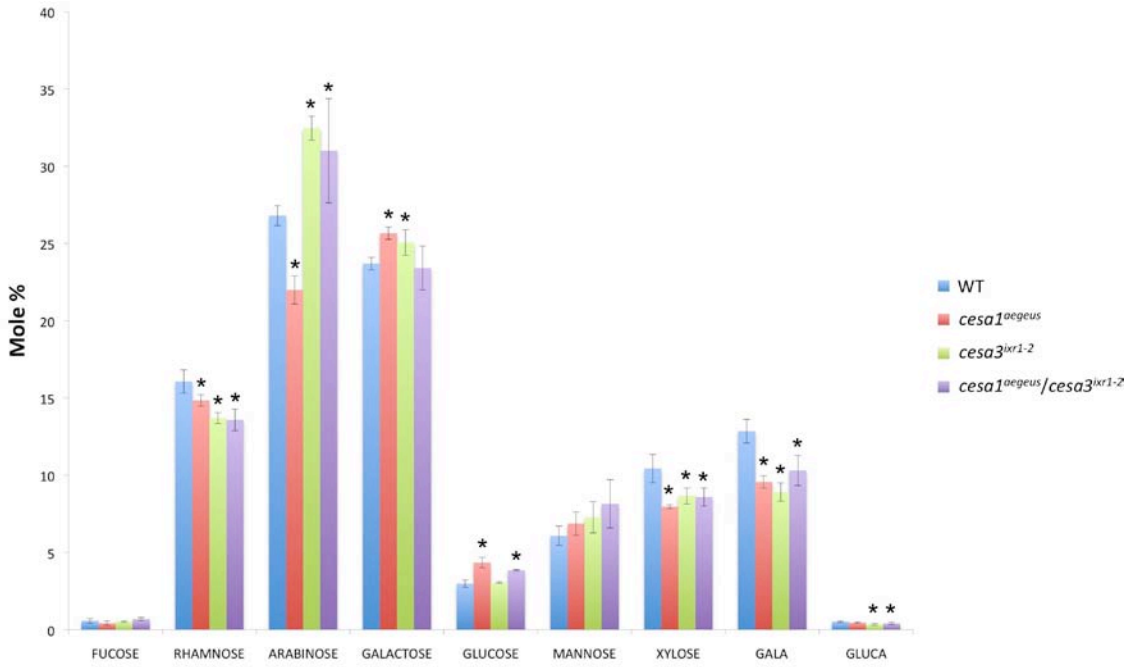

Figure S6.6. Cell wall monosaccharide analysis. There were significant percentage changes in cell wall neutral sugars between wild-type and the mutants. Specifically, *cesa1*^{aegeus} had decreased rhamnose, arabinose, xylose, and galacturonic acid, but increased in galactose and glucose. *cesa3*$^{ixr1-2}$ was decreased in rhamnose, xylose, galacturonic acid and glucuronic acid, but increased in arabinose and galactose. *cesa1*^{aegeus}*/cesa3*$^{ixr1-2}$ was decreased in rhamnose, xylose, galacturonic acid and glucuronic acid, but increased arabinose. The results are expressed in mol %. * Indicates changes were significantly different from wild-type, $P<0.05$, Student's t-test, n=3.

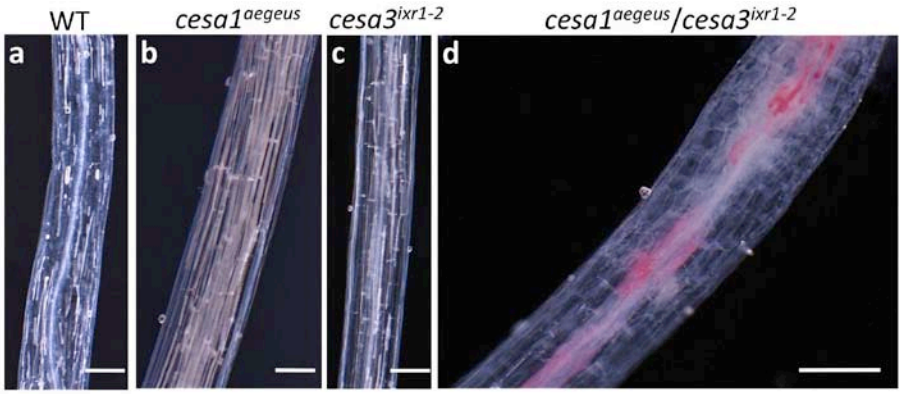

Figure S6.7. Ectopic lignin production primarily occurs in *cesa1*^{aegeus}*/cesa3*$^{ixr1-2}$. Seven-day-old dark-grown hypocotyls stained with phloroglucinol show no accumulation of lignin in (**a**) wild-type or (**b-c**) the single mutants, but strong accumulation in (**d**) *cesa1*^{aegeus}*/cesa3*$^{ixr1-2}$. Scale bar 100 mm.

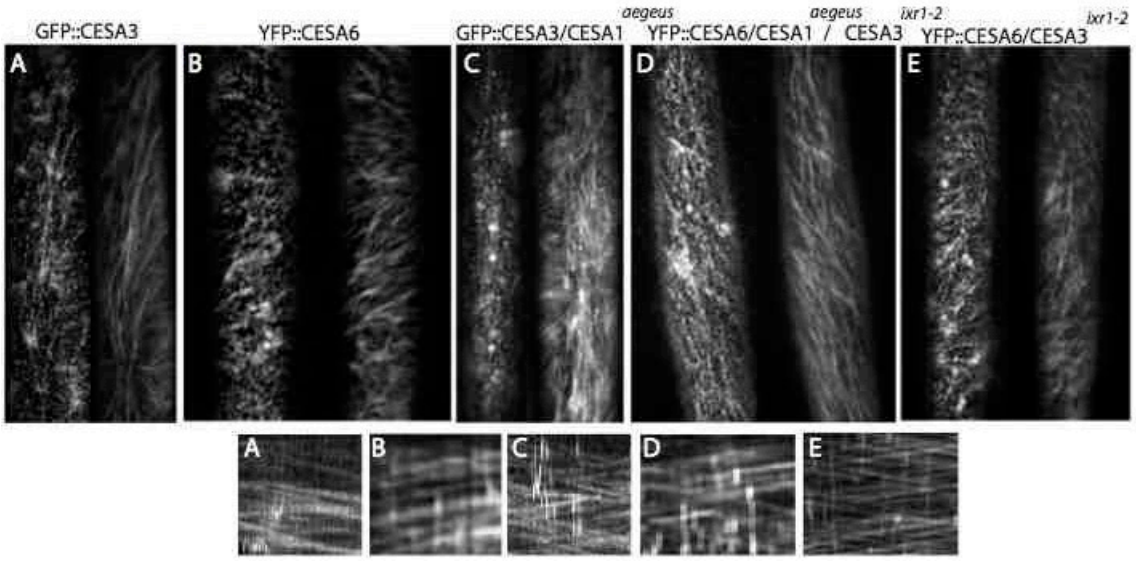

Figure S6.8. CESA motility is enhanced in *aegeus* and *ixr1-2* mutants. Transgenic seedlings expressing (**a**) GFP::CESA3, (**b**) YFP::CESA6, **(c)** GFP::CESA3- *cesa1*^{aegeus}**,** **(d)** YFP::CESA6- *cesa1*^{aegeus}/*cesa3*$^{ixr1-2}$ and **(e)** YFP::CESA6- *cesa3*$^{ixr1-2}$ were grown in the dark for 3 days. Epidermal cells in the upper hypocotyl were imaged with spinning disk confocal microscopy and are presented as both single frame images and time projections (tp) of 72 frames. Time projections are used to create kymographs for PM localized CESA documenting bidirectional velocity (inset for each panel).

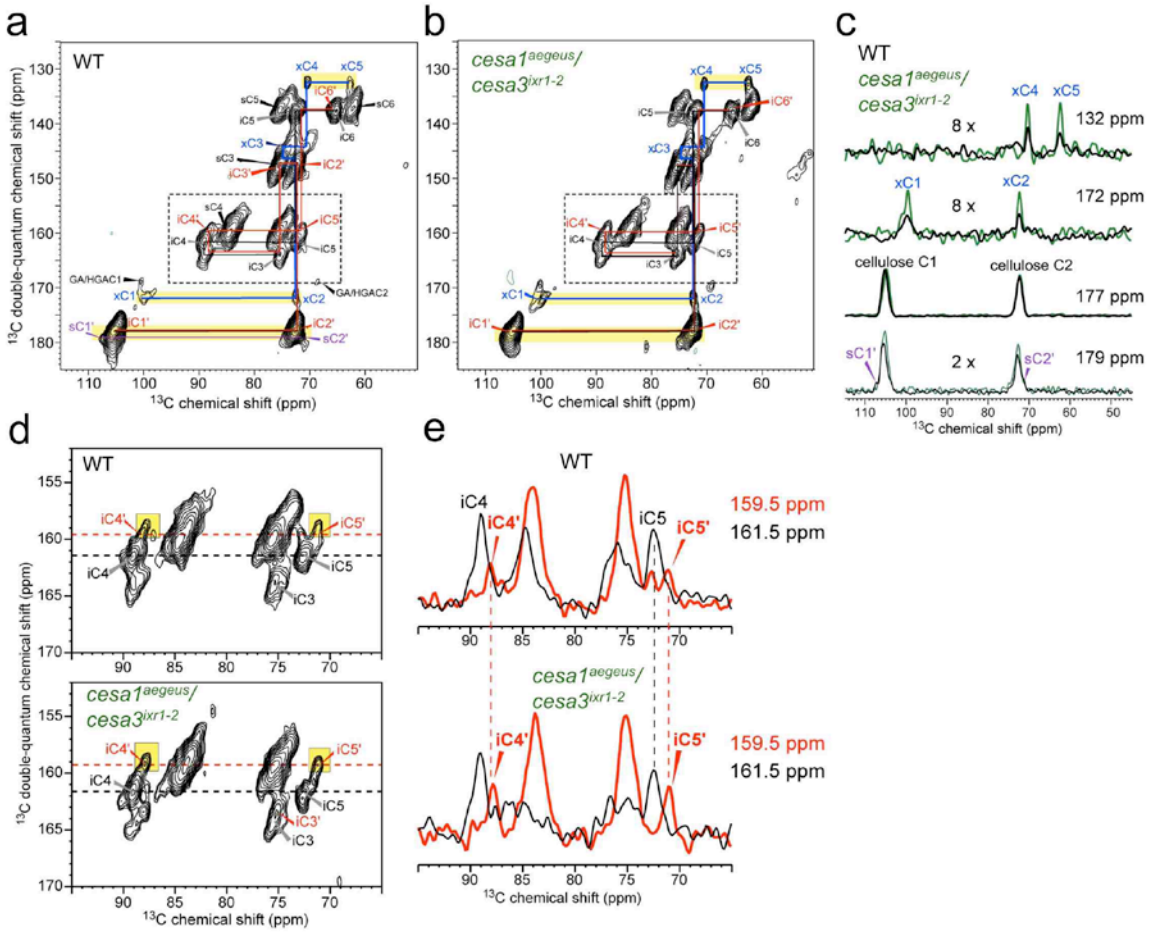

Figure S6.9. 2D ^{13}C double-quantum correlation spectra of wild-type and *cesa1*^{aegeus}*/cesa3*$^{ixr1-2}$ cell walls showing changes in the cellulose structure. (**a**) wild-type cell wall spectrum. Colored assignments denote polysaccharides whose amounts changed in the double mutant. These include xylose (blue), a modified interior cellulose (red with prime) with different C4 and C5 chemical shifts from those of regular crystalline interior cellulose, and a modified surface cellulose (purple with prime) whose C1 and C2 chemical shifts differ from those of regular surface cellulose. (**b**) *cesa1*^{aegeus}*/cesa3*$^{ixr1-2}$ spectrum. The xylose peaks increased in intensity, the modified surface cellulose signals are absent. (**c**) 1D cross sections at the specified double-quantum chemical shifts, showing the relative increase of the xylose peak intensities of *cesa1*^{aegeus}*/cesa3*$^{ixr1-2}$ compared to the wild-type cell wall and the loss of the modified surface cellulose. (**d**) Expanded C3-C4 and C4-C5 region of the 2D spectra. The C4' and C5' peaks of the modified interior cellulose are highlighted in yellow. The intensities of this species relative to the regular interior cellulose are higher in the double mutant than in the wild-type, which is further shown in the (**e**) 1D cross sections.

	Vmax	Km	Kcat
wild type	7.8	9.0	0.87
CESA1^{aegeus}	10.6	9.2	1.16 (32 % higher than WT)
CESA1^{aegeus}/CESA3^{ixr1-2}	11.8	9.1	1.30 (49 % higher than WT)

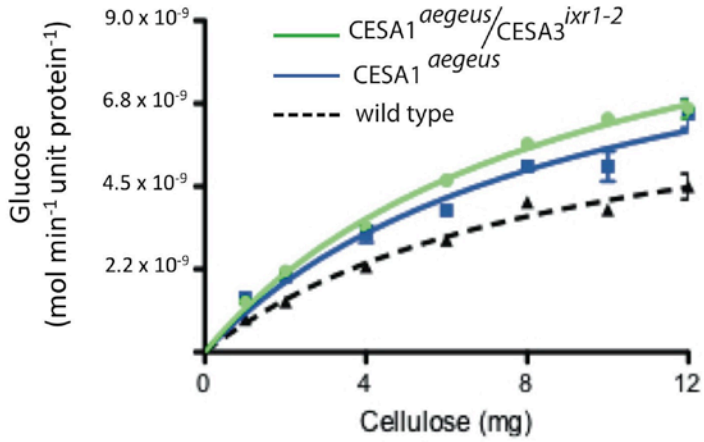

Figure S6.10. Enzymatic digestion and kinetics of cellulose saccharification efficiency in mutants containing cellulose structural variation. Pseudo-apparent K_m (K'_m) values were determined in the present study for wild-type, *cesa1*^{aegeus} *and cesa1*^{aegeus}*/cesa3*$^{ixr1-2}$ samples, corresponding to 9.0 ± 1.8 mg, 9.2 ± 2.3 mg and 9.1 ±0.9 mg cellulose respectively. Likewise, wild-type displayed a V'_{max} of 7.82 ± 0.8 × 10^{-9} moles min^{-1} $unit^{-1}$ $protein^{-1}$ glucose, *cesa1*^{aegeus} displayed a V'_{max} of 10.6 ± 1.4 × 10^{-9} moles min^{-1} $unit^{-1}$ $protein^{-1}$ glucose and *cesa1*^{aegeus}*/cesa3*$^{ixr1-2}$ displayed a V'_{max} of 11.8 ± 0.6 × 10^{-9} moles min^{-1} $unit^{-1}$ $protein^{-1}$ glucose. Comparing these measurements with the previously reported values for *cesa3*$^{ixr1-2}$ (Harris et al. 2009), the mutant cellulose represents an improvement of 17%, 32% and 49% for *cesa3*$^{ixr1-2}$, *cesa1*^{aegeus}, and *cesa1*^{aegeus}*/cesa3*$^{ixr1-2}$ respectively, in the hydrolytic efficiency of the reaction.

Table S6.1. Quinoxyphen analogs

Analog analysis of structural variations in the quinoxyphen (Q1) backbone structure and the corresponding ChemBridge (San Diego, CA) identification number. Analog potency was assessed via a radical elongation assay at a concentration of 25 μM. One asterisk indicates significantly reduced elongation compared to mock treated seedlings, $P<0.05$ Student's t-test. An increase in asterisks correlates to an increase in elongation reduction and an increase in potency.

Identification	ChemBridge ID	Structural Formulae	Potency
Q1	5771210	4-(2-bromo-4,5-dimethoxy-phenyl)-3,4-dihydro-1H-benzo-quinolin-2(1H)-one	*********
Q2	7965141	9-(2-bromo-4,5-dimethoxyphenyl)-2,3,8,9-tetrahydro[1,4]dioxino[2,3-g]quinolin-7(6H)-one	*******
Q3	8801191	4-(2,3-dichlorophenyl)-7-hydroxy-3,4-dihydrobenzo[h]quinolin-2(1H)-one	******
Q4	6045100	1-(2-bromo-4,5-dimethoxyphenyl)-1,4-dihydrobenzo[f]quinolin-3(2H)-one	*****
Q5	6433679	4-(2-bromo-3,4,5-trimethoxyphenyl)-3,4-dihydrobenzo[h]quinolin-2(1H)-one	***
Q6	7588163	4-(2-bromo-5-ethoxy-4-methoxyphenyl)-3,4-dihydrobenzo[h]quinolin-2(1H)-one	***
Q7	5967913	4-(2-chloro-6-fluorophenyl)-3,4-dihydrobenzo[h]quinolin-2(1H)-one	**
Q8	7991705	6-bromo-4-(2,4,5-trimethoxyphenyl)-3,4-dihydrobenzo[h]quinolin-2(1H)-one	**
Q9	6067149	6-bromo-4-(2,3-dimethoxyphenyl)-3,4-dihydrobenzo[h]quinolin-2(1H)-one	**
Q10	5611376	4-(3,4,5-trimethoxyphenyl)-3,4-dihydrobenzo[h]quinolin-2(1H)-one	**
Q11	6240537	4-(3-bromo-4,5-dimethoxyphenyl)-3,4-dihydrobenzo[h]quinolin-2(1H)-one	**
Q12	6240229	6-bromo-4-(2,4-dimethoxyphenyl)-3,4-dihydrobenzo[h]quinolin-2(1H)-one	*
Q13	6075657	4-(5-bromo-2-fluorophenyl)-3,4-dihydrobenzo[h]quinolin-2(1H)-one	*
Q14	5614027	4-(6-nitro-1,3-benzodioxol-5-yl)-3,4-dihydrobenzo[h]quinolin-2(1H)-one	*
Q15	5616365	4-(2-chlorophenyl)-3,4-dihydrobenzo[h]quinolin-2(1H)-one	*
Q16	7870707	4-(3-bromo-5-ethoxy-4-isopropoxyphenyl)-3,4-dihydrobenzo[h]quinolin-2(1H)-one	*
Q17	6045217	6-bromo-4-(3,4-difluorophenyl)-3,4-dihydrobenzo[h]quinolin-2(1H)-one	*
Q18	5749928	4-(2,3,4-trimethoxyphenyl)-3,4-dihydrobenzo[h]quinolin-2(1H)-one	*
Q19	5967309	4-(6-chloro-1,3-benzodioxol-5-yl)-3,4-dihydrobenzo[h]quinolin-2(1H)-one	
Q20	5971665	4-(4-chloro-3-nitrophenyl)-3,4-dihydrobenzo[h]quinolin-2(1H)-one	
Q21	6367411	4-(4-bromo-2,5-dimethoxyphenyl)-3,4-dihydrobenzo[h]quinolin-2(1H)-one	
Q22	6050276	4-(2,3-dimethoxyphenyl)-3,4-dihydrobenzo[h]quinolin-2(1H)-one	
Q23	5140892	4-phenyl-3,4-dihydrobenzo[h]quinolin-2(1H)-one	
Q24	7987555	6-bromo-4-(2,4,5-trimethoxyphenyl)-3,4-dihydrobenzo[h]quinolin-2(1H)-one	
Q25	6238513	4-(3-bromo-5-ethoxy-4-methoxyphenyl)-3,4-dihydrobenzo[h]quinolin-2(1H)-one	
Q26	5600690	4-[2-(trifluoromethyl)phenyl]-3,4-dihydrobenzo[h]quinolin-2(1H)-one	
Q27	5708748	4-(2-fluorophenyl)-3,4-dihydrobenzo[h]quinolin-2(1H)-one	
Q28	6046165	6-bromo-4-(4-chloro-3-nitrophenyl)-3,4-dihydrobenzo[h]quinolin-2(1H)-one	
Q29	6238985	6-bromo-4-(6-chloro-1,3-benzodioxol-5-yl)-3,4-dihydrobenzo[h]quinolin-2(1H)-one	
Q30	8800003	4-(2-iodophenyl)-3,4-dihydrobenzo[h]quinolin-2(1H)-one	
Q31	5602766	4-(6-bromo-1,3-benzodioxol-5-yl)-3,4-dihydrobenzo[h]quinolin-2(1H)-one	
Q32	5613923	4-(2,5-dimethoxyphenyl)-3,4-dihydrobenzo[h]quinolin-2(1H)-one	

Table S6.2. Map-based cloning PCR markers

The cleaved amplified polymorphic sequences markers uky1, uky2 and uky3 were newly created for this study by D.M.H.

Marker	BAC	Forward Primer (5' ->3')	Reverse Primer (3' ->5')	Size of PCR Product (bp)	Restriction Enzyme	Fragment Length COL / LER
uky1	F6I18	TGTGCTAGCTGGAGTTCAATGT	GTGCTAAAGGCAATTGATGAGA	434	DdeI	434 / 78, 356
uky2	F11C18	TTCTTCAGGTTGATGTGAATGG	ACACTAAATTTAAGCCGCAAGC	467	DraI	141, 325 / 467
uky3	F10M6	TGGAGTTAAGAGTTCCCCCATA	TATGTCGGTTCCTGCTTTAGGT	439	DdeI	438 / 182, 257

Table S6.3. Cell wall monosaccharide analysis

The results are expressed in mol %. * Indicates changes were significantly different from wild-type, P<0.05 Student's t-test, n=3.

Sugar	WT	*cesa1*^{aegeus}	*cesa3*$^{ixr1\text{-}2}$	*cesa1*^{aegeus} *cesa3*$^{ixr1\text{-}2}$
Fucose	0.57 ± 0.15	0.43 ± 0.14	0.53 ± 0.06	0.68 ± 0.11
Rhamnose	16.07 ± 0.75	14.84 ± 0.37*	13.70 ± 0.36*	13.58 ± 0.69*
Arabinose	26.80 ± 0.64	21.99 ± 0.91*	32.46 ± 0.78*	31.00 ± 3.37*
Galactose	23.69 ± 0.40	25.66 ± 0.40*	25.06 ± 0.83*	23.41 ± 1.42
Glucose	2.98 ± 0.24	4.35 ± 0.34*	3.04 ± 0.05	3.86 ± 0.05*
Mannose	6.08 ± 0.63	6.87 ± 0.75	7.28 ± 1.00	8.15 ± 1.56
Xylose	10.43 ± 0.91	7.96 ± 0.12*	8.66 ± 0.51*	8.59 ± 0.59*
GalA	12.85 ± 0.76	9.56 ± 0.39*	8.91 ± 0.59*	10.30 ± 0.98*
GlucA	0.53 ± 0.06	0.46 ± 0.05	0.36 ± 0.06*	0.42 ± 0.07*

Table S6.4. Glycosyl linkage analysis

The results are expressed in relative %. * Indicates changes were significantly different from wild-type, P<0.05 Student's t-test, n=3.

Linkage	WT	*cesa1*^{aegeus} *cesa3*$^{ixr1-2}$
t-Fuc	0.67 ± 0.06	0.60 ± 0.00
t-Rha	0.70 ± 0.17	0.63 ± 0.06
2-Rha	1.57 ± 0.15	1.23 ± 0.30
2,4-Rha + 2-Man + 3-Man	1.63 ± 0.06	2.20 ± 0.26*
t-Ara	0.17 ± 0.06	0.20 ± 0.00
t-Araf	2.77 ± 0.85	4.07 ±0.81
2-Araf	2.17 ± 0.64	1.97 ± 0.15
3-Araf	0.83 ± 0.25	0.80 ± 0.10
2,3,4-Ara	0.30 ± 0.14	1.05 ± 1.06
4-Arap or 5-Araf	1.87 ± 0.49	2.53 ± 0.15*
2,4-Arap or 2,5-Araf	1.40 ± 0.53	1.53 ± 0.15
3,4-Arap or 3,5-Araf	0.60 ± 0.20	0.97 ± 0.21*

Linkage	WT	*cesa1*^{aegeus} *cesa3*$^{ixr1-2}$
t-Xyl	2.93 ± 0.57	2.70 ± 0.35
4-Xyl	2.93 ± 0.21	2.27 ± 0.28*
2,4-Xyl	0.83 ± 0.06	1.00 ± 0.17
2,3,4-Xyl	0.10 ± 0.06	0.20 ± 0.14
t-Galf	0.20 ± 0.10	0.30 ± 0.00
t-Gal	3.33 ± 0.57	3.70 ± 0.35
2-Gal	1.53 ± 0.15	1.40 ± 0.30
3-Gal	8.13 ± 1.80	11.87 ± 1.46*
4-Gal	0.83 ± 0.25	1.07 ± 0.21
6-Gal	0.47 ± 0.06	0.63 ± 0.06*
2,3-Gal	0.23 ±0.06	0.33 ± 0.06
3,6-Gal	1.27 ± 0.06	2.30 ± 0.20*
4,6-Gal	0.10 ±0.00	0.17 ± 0.06
3,4,6-Gal	0.20 ± 0.10	0.27 ± 0.12

Linkage	WT	*cesa1*^{aegeus} *cesa3*$^{ixr1-2}$
t-Glc	0.53 ± 0.06	0.60 ± 0.17
2-Glc	0.67 ± 0.35	0.77 ± 0.31
4-Glc	48.97 ± 4.76	41.37 ± 2.17*
2,4-Glc	0.57 ± 0.21	0.43 ± 0.06
3,4-Glc	0.47 ± 0.15	0.40 ± 0.00
4,6-Glc	4.43 ± 0.12	3.63 ± 0.50*
3,4,6-Glc	0.13 ± 0.06	0.10 ± 0.00
2,4,6-Glc	0.13 ± 0.06	0.20 ± 0.17
2,3,6-Glc	N.D.	0.10 ± 0.00
t-Man	1.73 ± 0.38	2.40 ± 0.26*
4-Man	2.73 ± 0.21	2.17 ± 0.25*
4,6-Man	1.63 ± 0.40	1.87 ± 0.06
3,6-Man	0.37 ± 0.12	0.40 ± 0.20

Table S6.5. Relative intensities of interior and surface cellulose C4 signals of different cell walls from quantitative ^{13}C NMR spectra. *cesa1*^{aegeus}*/cesa3*$^{ixr1-2}$ cell wall exhibits a clear reduction in crystallinity.

Plants	I(iC4) 88.5 – 91.5 ppm	I(sC4) 84 – 86 ppm	I(iC4)/I(sC4)	Normalized I(iC4)/I(sC4)
WT	37.7E6	58.1E6	0.65	1.00
cesa1^{aegeus}	22.4E6	32.7E6	0.69	1.06
cesa3^{ixr1-2}	25.1E6	39.3E6	0.64	0.98
cesa1^{aegeus}/ *cesa3*$^{ixr1-2}$	19.1E6	32.0E6	0.60	0.92

References

Akin D (2007) Grass lignocellulose. Appl Biochem Biotechnol 137-140: 3-15

Alonso JM, Stepanova AN, Leisse TJ, Kim CJ, Chen H, Shinn P, Stevenson DK, Zimmerman J, Barajas P, Cheuk R, Gadrinab C, Heller C, Jeske A, Koesema E, Meyers CC, Parker H, Prednis L, Ansari Y, Choy N, Deen H, Geralt M, Hazari N, Hom E, Karnes M, Mulholland C, Ndubaku R, Schmidt I, Guzman P, Aguilar-Henonin L, Schmid M, Weigel D, Carter DE, Marchand T, Risseeuw E, Brogden D, Zeko A, Crosby WL, Berry CC, Ecker JR (2003) Genome-Wide Insertional Mutagenesis of *Arabidopsis thaliana*. Science 301: 653-657

Altschul SF, Madden TL, Schäffer AA, Zhang J, Zhang Z, Miller W, Lipman DJ (1997) Gapped BLAST and PSI-BLAST: a new generation of protein database search programs. Nucleic Acids Research 25: 3389-3402

Andersson S, Serimaa R, Paakkari T, Saranpää P, Pesonen E (2003) Crystallinity of wood and the size of cellulose crystallites in Norway spruce (*Picea abies*). Journal of Wood Science 49: 531-537

Andersson S, Serimaa R, Torkkeli M, Paakkari T, Saranpää P, Pesonen E (2000) Microfibril angle of Norway spruce [*Picea abies* (L.) Karst.] compression wood: comparison of measuring techniques. Journal of Wood Science 46: 343-349

Andersson S, Wikberg H, Pesonen E, Maunu S, Serimaa R (2004) Studies of crystallinity of Scots pine and Norway spruce cellulose. Trees - Structure and Function 18: 346-353

Andersson-Gunnerås S, Mellerowicz EJ, Love J (2006) Biosynthesis of cellulose-enriched tension wood in Populus: global analysis of transcripts and metabolites identifies biochemical and developmental regulators in secondary wall biosynthesis. Plant J 45: 144-165

Appenzeller L, Doblin M, Barreiro R, Wang H, Niu X, Kollipara K, Carrigan L, Tomes D, Chapman M, Dhugga KS (2004) Cellulose synthesis in maize: isolation and expression analysis of the cellulose synthase (CesA) gene family. Cellulose 11: 287-299

Apse MP, Aharon GS, Snedden WA, Blumwald E (1999) Salt Tolerance Conferred by Overexpression of a Vacuolar Na+/H+ Antiport in *Arabidopsis*. Science 285: 1256-1258

Arabidopsis Genome Initiative (2000) Analysis of the genome sequence of the flowering plant *Arabidopsis thaliana*. Nature 408: 796-815

Arioli T, Peng LC, Betzner AS, Burn J, Wittke W, Herth W, Camilleri C, Hofte H, Plazinski J, Birch R, Cork A, Glover J, Redmond J, Williamson RE (1998) Molecular analysis of cellulose biosynthesis in *Arabidopsis*. Science 279: 717-720

Atalla RH, VanderHart DL (1984) Native Cellulose: A Composite of Two Distinct Crystalline Forms. Science 223: 283-285

Atanassov II, Pittman JK, Turner SR (2009) Elucidating the Mechanisms of Assembly and Subunit Interaction of the Cellulose Synthase Complex of *Arabidopsis* Secondary Cell Walls. J. Biol. Chem. 284: 3833-3841

Austin RS, Vidaurre D, Stamatiou G, Breit R, Provart NJ, Bonetta D, Zhang J, Fung P, Gong Y, Wang PW, McCourt P, Guttman DS (2011) Next-generation mapping of *Arabidopsis* genes. The Plant Journal 67: 715-725

Balashov V, Preston RD (1955) Fine Structure of Cellulose and other Microfibrillar Substances. Nature 176: 64-65

Baskin TI (2001) On the alignment of cellulose microfibrils by cortical microtubules: A review and a model. Protoplasma 215: 150-171

Baskin TI, Betzner AS, Hoggart R, Cork A, Williamson RE (1992) Root morphology mutants in *Arabidopsis thaliana*. Australian Journal of Plant Physiology 19: 427-437

Beale CV, Long SP (1995) Can perennial C4 grasses attain high efficiencies of radiant energy-conversion in cool climates. Plant Cell Environ. 18: 641-650

Benfey PN, Linstead PJ, Roberts K, Schiefelbein JW, Hauser MT, Aeschbacher RA (1993) Root development in *Arabidopsis*: four mutants with dramatically altered root morphogenesis. Development 119: 57-70

Benziman M, Haigler CH, Brown RM, White AR, Cooper KM (1980) Cellulose biogenesis: Polymerization and crystallization are coupled processes in *Acetobacter xylinum*. Proceedings of the National Academy of Sciences 77: 6678-6682

Berlin A, Gilkes N, Kurabi A, Bura R, Tu MB, Kilburn D, Saddler J (2005) Weak lignin-rinding enzymes - A novel approach to improve activity of cellulases for hydrolysis of lignocellulosics. Appl Biochem Biotechnol 121: 163

Bessueille L, Bulone V (2008) A survey of cellulose biosynthesis in higher plants. Plant Biotechnology 25: 315-322

Bessueille L, Sindt N, Guichardant M, Djerbi S, Teeri TT, Bulone V (2009) Plasma membrane microdomains from hybrid aspen cells are involved in cell wall polysaccaride biosynthesis. Biochemical Journal 420: 93-103

Bhandari S, Fujino T, Thammanagowda S, Zhang D, Xu F, Joshi C (2006) Xylem-specific and tension stress-responsive coexpression of KORRIGAN endoglucanase and three secondary wall-associated cellulose synthase genes in aspen trees. Planta 224: 828-837

Bindschedler LV, Tuerck L, Maunders M, Ruel K, Petit-Conil M, Danoun S, Boudet A-M, Joseleau J-P, Bolwell GP (2007) Modification of hemicellulose content by antisense down-regulation of UDP-glucuronate decarboxylase in tobacco and its consequences for cellulose extractibility. Phytochem 68: 2635-2648

Bindschedler LV, Wheatley E, Gay E, Cole J, Cottage A, Bolwell GP (2005) Characterisation and expression of the pathway from UDP-glucose to UDP-xylose in differentiating tobacco tissue. Plant Mol Biol 57: 285-301

Binning G, Rohrer H (1986) Scanning tunneling microscopy. IBM J Res Dev 30: 355

Bischoff V, Cookson SJ, Wu S, Scheible W-R (2009) Thaxtomin A affects CESA-complex density, expression of cell wall genes, cell wall composition, and causes ectopic lignification in *Arabidopsis thaliana* seedlings. J Exp Bot 60: 955-965

Bischoff V, Desprez T, Mouille G, Vernhettes S, Gonneau M, Höfte H (2011) Phytochrome Regulation of Cellulose Synthesis in *Arabidopsis*. Current Biology 21: 1822-1827

Bisgrove SR, Kropf DL (2001) Cell wall deposition during morphogenesis in fucoid algae. Planta 212: 648-658

Biswas GCG, Ransom C, Sticklen M (2006) Expression of biologically active *Acidothermus cellulolyticus* endoglucanase in transgenic maize plants. Plant Sci 171: 617-623

Boerjan W, Ralph J, Baucher M (2003) Lignin biosynthesis. Annu Rev Plant Biol 54: 519-546

Bonawitz ND, Chapple C (2010) The Genetics of Lignin Biosynthesis: Connecting Genotype to Phenotype. Annu Rev Genet 44: 337-363

Bosca S, Barton CJ, Taylor NG, Ryden P, Neumetzler L, Pauly M, Roberts K, Seifert GJ (2006) Interactions between MUR10/CesA7-Dependent Secondary Cellulose Biosynthesis and Primary Cell Wall Structure. Plant Physiol 142: 1353-1363

Bouquin T, Mattsson O, Naested H, Foster R, Mundy J (2003) The *Arabidopsis lue1* mutant defines a katanin p60 ortholog involved in hormonal control of microtubule orientation during cell growth. J Cell Sci 116: 791-801

Bowling AJ, Brown RM (2008) The cytoplasmic domain of the cellulose-synthesizing complex in vascular plants. Protoplasma 233: 115-127

Bowling AJ, Vaughn KC (2008) Immunocytochemical characterization of tension wood: Gelatinous fibers contain more than just cellulose. Am J Bot 95: 655-663

Brett CT (2000) Cellulose microfibrils in plants: Biosynthesis, deposition, and integration into the cell wall. International Review of Cytology. Academic Press, pp 161-199

Brocard-Gifford I, Lynch TJ, Garcia ME, Malhotra B, Finkelstein RR (2004) The *Arabidopsis thaliana* ABSCISIC ACID-INSENSITIVE8 Locus Encodes a Novel Protein Mediating Abscisic Acid and Sugar Responses Essential for Growth. Plant Cell 16: 406-421

Brongniart A, Pelouze TJ, Dumas AB (1839) Rapport sur un mémoire de M. Payen, relatif à la composition de la matière ligneuse. C R Hebd Seances Acad Sci 8: 51-53

Brosse N, Sannigrahi P, Ragauskas A (2009) Pretreatment of *Miscanthus x giganteus* Using the Ethanol Organosolv Process for Ethanol Production. Ind Eng Chem Res 48: 8328-8334

Brown DM, Zeef LAH, Ellis J, Goodacre R, Turner SR (2005) Identification of novel genes in *Arabidopsis* involved in secondary cell wall formation using expression profiling and reverse genetics. Plant Cell 17: 2281-2295

Brown RM, Jr, Montezinos D (1976) Cellulose microfibrils: visualization of biosynthetic and orienting complexes in association with the plasma membrane. Proc. Natl Acad. Sci. USA 73: 143-147

Brown RM (1996) The biosynthesis of cellulose. J. Macromol. Sci. A33: 1345-1373

Brown RM (2004) Cellulose structure and biosynthesis: What is in store for the 21st century? Journal of Polymer Science Part A: Polymer Chemistry 42: 487-495

Bulone V (2007) Analysis of (1→3)-β-D-glucans and cellulose synthesized in vitro: A key step towards the characterization of glucan synthases. In: Brown RM, Saxena IM (eds) Cellulose: Molecular and Structural Biology. Springer London, pp 123-145

Burk DH, Liu B, Zhong R, Morrison WH, Ye Z-H (2001) A Katanin-like Protein Regulates Normal Cell Wall Biosynthesis and Cell Elongation. Plant Cell 13: 807-828

Burk DH, Zhong R, Ye Z-H (2007) The Katanin Microtubule Severing Protein in Plants. Journal of Integrative Plant Biology 49: 1174-1182

Burton RA, Shirley NJ, King BJ, Harvey AJ, Fincher GB (2004) The CesA Gene Family of Barley. Quantitative Analysis of Transcripts Reveals Two Groups of Co-Expressed Genes. Plant Physiol 134: 224-236

Byrne ME, Simorowski J, Martienessen RA (2002) ASYMMETRIC LEAVES1 reveals knox gene redundancy in *Arabidopsis*. Development 129: 1957-1965
Campbell JE, Lobell DB, Genova RC, Field CB (2008) The Global Potential of Bioenergy on Abandoned Agriculture Lands. Environ. Sci. Technol. 42: 5791-5794

Campbell MM, Sederoff RR (1996) Variation in Lignin Content and Composition (Mechanisms of Control and Implications for the Genetic Improvement of Plants). Plant Physiol. 110: 3-13

Canam T, Park J-Y, Yu K, Campbell M, Ellis D, Mansfield S (2006) Varied growth, biomass and cellulose content in tobacco expressing yeast-derived invertases. Planta 224: 1315-1327

Carlson TR, Vispute TP, Huber GW (2008) Green Gasoline by Catalytic Fast Pyrolysis of Solid Biomass Derived Compounds. ChemSusChem 1: 397-400

Carpita NC (1986) Incorporation of Proline and Aromatic-Amino-Acids into Cell-Walls of Maize Coleoptiles. Plant Physiol. 80: 660-666

Carpita NC (2011) Update on Mechanisms of Plant Cell Wall Biosynthesis: How Plants Make Cellulose and Other (1→4)-β-D-Glycans. Plant Physiol 155: 171-184

Carpita NC, Gibeaut DM (1993) Structural Models of Primary-Cell Walls in Flowering Plants - Consistency of Molecular-Structure with the Physical-Properties of the Walls during Growth. Plant J. 3: 1-30

Causton HC, Ren B, Koh SS, Harbison CT, Kanin E, Jennings EG, Lee TI, True HL, Lander ES, Young RA (2001) Remodeling of Yeast Genome Expression in Response to Environmental Changes. Mol Biol Cell 12: 323-337

Cavalier DM, Lerouxel O, Neumetzler L, Yamauchi K, Reinecke A, Freshour G, Zabotina OA, Hahn MG, Burgert I, Pauly M, Raikhel NV, Keegstra K (2008) Disrupting Two *Arabidopsis thaliana* Xylosyltransferase Genes Results in Plants Deficient in Xyloglucan, a Major Primary Cell Wall Component. The Plant Cell Online 20: 1519-1537

Chaffey N, Cholewa E, Regan S, Sundberg B (2002) Secondary xylem development in *Arabidopsis*: A model for wood formation. Physiol Plant 114: 594-600

Chalfie M, Tu Y, Euskirchen G, Ward W, Prasher D (1994) Green fluorescent protein as a marker for gene expression. Science 263: 802-805

Chen F, Dixon RA (2007) Lignin modification improves fermentable sugar yields for biofuel production. Nat Biotechnol 25: 759-761

Chen F, Srinivasa Reddy MS, Temple S, Jackson L, Shadle G, Dixon RA (2006) Multi-site genetic modulation of monolignol biosynthesis suggests new routes for formation of syringyl lignin and wall-bound ferulic acid in alfalfa (*Medicago sativa* L.). Plant J 48: 113-124

Chen S, Ehrhardt DW, Somerville C (2010a) Mutations of cellulose synthase (CESA1) phosphorylation sites modulate anisotropic cell expansion and bidirectional mobility of cellulose synthase. Proceedings of the National Academy of Sciences U.S.A. 107: 17188-17193

Chen X-A, Ishida N, Todaka N, Nakamura R, Maruyama J-i, Takahashi H, Kitamoto K (2010b) Promotion of Efficient Saccharification of Crystalline Cellulose by Aspergillus fumigatus Swo1. Appl Environ Microbiol 76: 2556-2561

Chen Z, Hong X, Zhang H, Wang Y, Li X, Zhu J-K, Gong Z (2005) Disruption of the cellulose synthase gene, *AtCesA8/IRX1*, enhances drought and osmotic stress tolerance in *Arabidopsis*. Plant J 43: 273-283

Cho H-T, Cosgrove DJ (2000) Altered expression of expansin modulates leaf growth and pedicel abscission in *Arabidopsis thaliana* Proc Natl Acad Sci USA 97: 9783-9788

Choe S, Fujioka S, Noguchi T, Takatsuto S, Yoshida S, Feldmann KA (2001) Overexpression of *DWARF4* in the brassinosteroid biosynthetic pathway results in increased vegetative growth and seed yield in *Arabidopsis*. Plant J 26: 573-582

Choi D, Lee Y, Cho H-T, Kende H (2003) Regulation of Expansin Gene Expression Affects Growth and Development in Transgenic Rice Plants. Plant Cell 15: 1386-1398

Chu Z, Chen H, Zhang Y, Zhang Z, Zheng N, Yin B, Yan H, Zhu L, Zhao X, Yuan M, Zhang X, Xie Q (2007) Knockout of the *AtCESA2* Gene Affects Microtubule Orientation and Causes Abnormal Cell Expansion in *Arabidopsis*. Plant Physiol 143: 213-224

Chum HL, Black SK (1990) Process for fractionating fast-pyrolysis oils, and products derived therefrom. Midwest Research Institute (Kansas City, MO), United States

Cifuentes C, Bulone V, Emons AMC (2010) Biosynthesis of Callose and Cellulose by Detergent Extracts of Tobacco Cell Membranes and Quantification of the Polymers Synthesized in vitro. Journal of Integrative Plant Biology 52: 221-233

Ciucanu I, Kerek F (1984) A simple and rapid method for the permethylation of carbohydrates. Carbohydrate Research 131: 209-217

Clough SJ, Bent AF (1998) Floral dip: a simplified method forAgrobacterium-mediated transformation of *Arabidopsis thaliana*. The Plant Journal 16: 735-743

Cocuron J-C, Lerouxel O, Drakakaki G, Alonso AP, Liepman AH, Keegstra K, Raikhel N, Wilkerson CG (2007) A gene from the cellulose synthase-like C family encodes a β-1,4 glucan synthase. Proc Natl Acad Sci USA 107: 8550-8555

Coleman HD, Ellis DD, Gilbert M, Mansfield SD (2006) Up-regulation of sucrose synthase and UDP-glucose pyrophosphorylase impacts plant growth and metabolism. Plant Biotechnol J 4: 87-101

Coleman HD, Park JY, Nair R, Chapple C, Mansfield SD (2008a) RNAi-mediated suppression of p-coumaroyl-CoA 3 '-hydroxylase in hybrid poplar impacts lignin deposition and soluble secondary metabolism. Proc Natl Acad Sci USA 105: 4501-4506

Coleman HD, Samuels AL, Guy RD, Mansfield SD (2008b) Perturbed Lignification Impacts Tree Growth in Hybrid Poplar--A Function of Sink Strength, Vascular Integrity, and Photosynthetic Assimilation. Plant Physiol 148: 1229-1237

Coleman HD, Yan J, Mansfield SD (2009) Sucrose synthase affects carbon partitioning to increase cellulose production and altered cell wall ultrastructure. Proc Natl Acad Sci USA 106: 13118-13123

Colombani A, Djerbi S, Bessueille L, Blomqvist K, Ohlsson A, Berglund T, Teeri TT, Bulone V (2004) In vitro synthesis of (1→3)-β-D-glucan (callose) and cellulose by detergent extracts of membranes from cell suspension cultures of hybrid aspen. Cellulose 11: 313-327

Cosgrove DJ (2005) Growth of the plant cell wall. Nat Rev Mol Cell Biol 6: 850-861

Coutinho PM, Henrissat B (1999) Life with no sugars? J Mol Microbiol Biotech 1: 307-308

Crowell EF, Bischoff V, Desprez T, Rolland A, Stierhof Y-D, Schumacher K, Gonneau M, Höfte H, Vernhettes S (2009) Pausing of Golgi Bodies on Microtubules Regulates Secretion of Cellulose Synthase Complexes in *Arabidopsis*. The Plant Cell 21: 1141-1154

Cutler SR, Ehrhardt DW, Griffitts JS, Somerville C (2000) Random GFP::cDNA fusions enable visualization of subcellular structures in cells of *Arabidopsis* at a high frequency. Proc. Natl Acad. Sci. USA 97: 3718-3723

Czernik S, Bridgwater AV (2005) Application of Biomass Fast Pyrolysis Oil. In: Bridgwater AV (ed) Fast Pyrolysis of Biomass: A Handbook Volume 3. CPL Press, pp. 105-120. Newbury, UK

Dai Z, Hooker BS, Anderson DB, Thomas SR (2000) Improved plant-based production of E1 endoglucanase using potato: expression optimization and tissue targeting. Mol Breed 6: 277-285

Daras G, Rigas S, Penning B, Milioni D, McCann MC, Carpita NC, Fasseas C, Hatzopoulos P (2009) The *thanatos* mutation in *Arabidopsis thaliana* cellulose synthase 3 (*AtCesA3*) has a dominant-negative effect on cellulose synthesis and plant growth. New Phytol 184: 114-126

Davies LM, Harris PJ (2003) Atomic force microscopy of microfibrils in primary cell walls. Planta 217: 283-289

DeBolt S, Campbell JE, Jr. RS, Montross M, Stork J (2009) Life cycle assessment of native plants and marginal lands for bioenergy agriculture in Kentucky as a model for south-eastern USA. Glob Chang Biol Bioenergy 1: 308-316

DeBolt S, Gutierrez R, Ehrhardt DW, Melo CV, Ross L, Cutler SR, Somerville C, Bonetta D (2007a) Morlin, an inhibitor of cortical microtubule dynamics and cellulose synthase movement. Proc. Natl Acad. Sci. USA 104: 5854-5859

DeBolt S, Gutierrez R, Ehrhardt DW, Somerville C (2007b) Nonmotile cellulose synthase subunits repeatedly accumulate within localized regions at the plasma membrane in *Arabidopsis* hypocotyl cells following 2,6-dichlorobenzonitrile treatment. Plant Physiol. 145: 334-338

Delmer DP (1999) Cellulose biosynthesis: Exciting times for a difficult field of study. Annu. Rev. Plant Physiol. Plant Molec. Biol. 50: 245-276

Delmer DP, Amor Y (1995) Cellulose biosynthesis. Plant Cell 7: 987-1000

Delmer DP, Haigler CH (2002) The Regulation of Metabolic Flux to Cellulose, a Major Sink for Carbon in Plants. Metabolic Engineering 4: 22-28

Delmer DP, Read SM, Cooper G (1987) Identification of a Receptor Protein in Cotton Fibers for the Herbicide 2,6-Dichlorobenzonitrile. Plant Physiol 84: 415-420

Demura T, Ye Z-H (2010) Regulation of plant biomass production. Curr Opin Plant Biol 13: 298-303

Desprez T, Juraniec M, Crowell EF, Jouy H, Pochylova Z, Parcy F, Höfte H, Gonneau M, Vernhettes S (2007) Organization of cellulose synthase complexes involved in primary cell wall synthesis in *Arabidopsis thaliana*. Proc Natl Acad Sci USA 104: 15572-15577

Desprez T, Vernhettes S, Fagard M, Refregier G, Desnos T, Aletti E, Py N, Pelletier S, Hofte H (2002) Resistance against herbicide isoxaben and cellulose deficiency caused by distinct mutations in same cellulose synthase isoform CESA6. Plant Physiol 128: 482-490

Dick-Pérez M, Zhang Y, Hayes J, Salazar A, Zabotina OA, Hong M (2011) Structure and Interactions of Plant Cell-Wall Polysaccharides by Two- and Three-Dimensional Magic-Angle-Spinning Solid-State NMR. Biochemistry 50: 989-1000

Din N, Gilkes NR, Tekant B, Miller RC, Warren RAJ, Kilburn DG (1991) Non-Hydrolytic Disruption of Cellulose Fibres by the Binding Domain of a Bacterial Cellulase. Nat Biotech 9: 1096-1099

Ding S-Y, Himmel ME (2006a) The Maize Primary Cell Wall Microfibril: A New Model Derived from Direct Visualization. J Agric Food Chem 54: 597-606

Djerbi S, Lindskog M, Arvestad L, Sterky F, Teeri T (2005) The genome sequence of black cottonwood (*Populus trichocarpa*) reveals 18 conserved cellulose synthase (*CesA*) genes. Planta 221: 739-746

Doblin MS, Kurek I, Jacob-Wilk D, Delmer DP (2002) Cellulose Biosynthesis in Plants: from Genes to Rosettes. Plant Cell Physiol 43: 1407-1420

Dodd AN, Salathia N, Hall A, Kevei E, Toth R, Nagy F, Hibberd JM, Millar AJ, Webb AAR (2005) Plant Circadian Clocks Increase Photosynthesis, Growth, Survival, and Competitive Advantage. Science 309: 630-633

Drake B, Prater C, Weisenhorn A, Gould S, Albrecht T, Quate C, Cannell D, Hansma H, Hansma P (1989) Imaging crystals, polymers, and processes in water with the atomic force microscope. Science 243: 1586-1589

Ebrigenova A (2006) Structural diversity and application potential of hemicelluloses. Macromol Symp 232: 1-12

Ehrhardt DW, Shaw SL (2006) Microtubule dynamics and organization in the plant cortical array Annual Review of Plant Biology 57: 859-875

Ellis C, Karafyllidis I, Wasternack C, Turner JG (2002) The *Arabidopsis* Mutant *cev1* Links Cell Wall Signaling to Jasmonate and Ethylene Responses. Plant Cell 14: 1557-1566

Engel A, Lyubchenko Y, Muller D (1999) Atomic force microscopy: a powerful tool to observe biomolecules at work. Trends in Cell Biology 9: 77-80

Ennos AR (1997) Wind as an ecological factor. Trends in Ecology & Evolution 12: 108-111

Eriksson ME, Israelsson M, Olsson O, Moritz T (2000) Increased gibberellin biosynthesis in transgenic trees promotes growth, biomass production and xylem fiber length. Nat Biotech 18: 784-788

Fagard M, Desnos T, Desprez T, Goubet F, Refregier G, Mouille G, McCann M, Rayon C, Vernhettes S, Hofte H (2000) PROCUSTE1 Encodes a Cellulose Synthase Required for Normal Cell Elongation Specifically in Roots and Dark-Grown Hypocotyls of *Arabidopsis*. Plant Cell 12: 2409-2424

Fairweather JK, Lai Kee Him J, Heux L, Driguez H, Bulone V (2004) Structural characterization by 13C-NMR spectroscopy of products synthesized in vitro by polysaccharide synthases using 13C-enriched glycosyl donors: application to a UDP-glucose: (1→3)-β-D-glucan synthase from blackberry (Rubus fruticosus) Glycobiology 14: 775-781

Fargione J, Hill J, Tilman D, Polasky S, Hawthorne P (2008) Land Clearing and the Biofuel Carbon Debt. Science 319: 1235-1238

Farquhar GD, von Caemmerer S, Berry JA (2001) Models of photosynthesis. Plant Physiol. 125: 42-45

Farrokhi N, Burton RA, Brownfield L, Hrmova M, Wilson SM, Bacic A, Fincher GB (2006) Plant cell wall biosynthesis: genetic, biochemical and functional genomics approaches to the identification of key genes. Plant Biotechnology Journal 4: 145-167

Feraru E, Feraru MI, Kleine-Vehn J, Matinière A, Mouille G, Vanneste S, Vernhettes S, Runions J, Frimi J (2011) PIN Polarity Maintenance by the Cell Wall in *Arabidopsis*. Current Biol 21: 338-343

Fischer DG, Mann J (1960) Crystalline modifications of Cellulose. Part VI. Unit cell and molecular symmetry of cellulose I. J Poly Sci 62: 189-194

Fort DA, Remsing RC, Swatloski RP, Moyna P, Moyna G, Rogers RD (2007) Can ionic liquids dissolve wood? Processing and analysis of lignocellulosic materials with 1-n-butyl-3-methylimidazolium chloride. Green Chem 9: 63-69

Foulkes-Murzycki JE, Scott WRP, Schiffer CA (2007) Hydrophobic Sliding: A Possible Mechanism for Drug Resistance in Human Immunodeficiency Virus Type 1 Protease. Structure 15: 225-233

Freudenberg K, Chen CL, Harkin JM, Nimz H, Renner H (1965) Observations on Lignin. Chem. Commun.: 224-225

Gardiner JC, Taylor NG, Turner SR (2003) Control of cellulose synthase complex localization in developing xylem. Plant Cell 15: 1740-1748

Geisler-Lee J, Geisler M, Coutinho PM, Segerman B, Nishikubo N, Takahashi J, Aspeborg H, Djerbi S, Master E, Andersson-Gunneras S, Sundberg B, Karpinski S, Teeri TT, Kleczkowski LA, Henrissat B, Mellerowicz EJ (2006) Poplar Carbohydrate-Active Enzymes. Gene Identification and Expression Analyses. Plant Physiol 140: 946-962

Gírio FM, Fonseca C, Carvalherio F, Duarte LC, Marques S, Bogel-Lukasik R (2010) Hemicelluloses for fuel ethanol: A review. Bioresource Technol 101: 4775-4800

Girke T, Cheng L-C, Raikhel N (2005) ChemMine. A Compound Mining Database for Chemical Genomics. Plant Physiol. 138: 573-577

Gomez LD, Steele-King CG, McQueen-Mason SJ (2008) Sustainable liquid biofuels from biomass: the writing's on the walls. New Phytol 178: 473-485

Goodin M, Chakrabarty R, Banerjee R, Yelton S, DeBolt S (2007) New Gateways to Discovery. Plant Physiol 145: 1100-1109

Grabber JH, Hatfield RD, Lu F, Ralph J (2008) Coniferyl Ferulate Incorporation into Lignin Enhances the Alkaline Delignification and Enzymatic Degradation of Cell Walls. Biomacromolecules 9: 2510-2516

Graham LE, Cook ME, Busse JS (2000) The origin of plants: Body plan changes contributing to a major evolutionary radiation. Proc Natl Acad Sci USA 97: 4235-4540

Gray-Mitsumune M, Blomqvist K, McQueen-Mason S, Teeri TT, Sundberg B, Mellerowicz EJ (2008) Ectopic expression of a wood-abundant expansin PttEXPA1 promotes cell expansion in primary and secondary tissues in aspen. Plant Biotechnol J 6: 62-72

Green PB (1962) Mechanism for Plant Cellular Morphogenesis. Science 138: 1404-1405

Gross GG, Stockigt J, Mansell RL, Zenk MH (1973) 3 Novel Enzymes Involved in Reduction of Ferulic Acid to Coniferyl Alcohol in Higher-Plants - Ferulate - Coa Ligase, Feruloyl-Coa Reductase and Coniferyl Alcohol Oxidoreductase. FEBS Letters 31: 283-286

Gu Y, Kaplinsky N, Bringmann M, Cobb A, Carroll A, Sampathkumar A, Baskin TI, Persson S, Somerville C (2010) Identification of a cellulose synthase-associated protein required for cellulose biosynthesis. Pro Natl Acad Sci USA 107: 12866-12871

Gutierrez R, Lindeboom JJ, Paredez AR, Emons AMC, Ehrhardt DW (2009) *Arabidopsis* cortical microtubules position cellulose synthase delivery to the plasma membrane and interact with cellulose synthase trafficking compartments. Nat. Cell Biol. 11: 797-806

Haigler C, Brown R, Benziman M (1980) Calcofluor white ST Alters the in vivo assembly of cellulose microfibrils. Science 210: 903-906

Haigler CH, Brown RM (1986) Transport of rosettes from the golgi apparatus to the plasma membrane in isolated mesophyll cells of *zinnia elegans* during differentiation to tracheary elements in suspension culture. Protoplasma 134: 111-120

Hall M, Bansal P, Lee JH, Realff MJ, Bommarius AS (2010) Cellulose crystallinity – a key predictor of the enzymatic hydrolysis rate. FEBS Journal 277: 1571-1582

Hancock JF (2006) Lipid rafts: contentious only from simplistic standpoints. Nat Rev Mol Cell Biol 7: 456-462

Harper AD, Bar-Peled M (2002) Biosynthesis of UDP-xylose. Cloning and characterization of a novel *Arabidopsis* gene family, UXS, encoding soluble and putative membrane-bound UDP-glucuronic acid decarboxylase isoforms. Plant Physiol 130: 2188-2198

Harris D, DeBolt S (2008) Relative Crystallinity of Plant Biomass: Studies on Assembly, Adaptation and Acclimation. PLoS ONE 3: e2897

Harris D, DeBolt S (2010) Synthesis, regulation and utilization of lignocellulosic biomass. Plant Biotechnol J 8: 244-262

Harris D, Stork J, DeBolt S (2009) Genetic modification in cellulose-synthase reduces crystallinity and improves biochemical conversion to fermentable sugar. Glob Chang Biol Bioenergy 1: 51-61

Haworth WN (1932) Molecular structure of cellulose and of amylose. Nature 129: 365

Hauser M-T, Benfey PN (1993) Genetic Regulation of Root Expansion in *Arabidopsis thaliana*. In: NATO-ASI Plant Molecular Biology Series (Pugdomenech P, Coruzzi G, eds) Springer-Verlag, pp. 31-40. New York

He Z-H, Fujiki M, Kohorn BD (1996) A Cell Wall-associated, Receptor-like Protein Kinase. J. Biol. Chem. 271: 19789-19793

Heazlewood JL, Verboom RE, Tonti-Filippini J, Small I, Millar AH (2007) SUBA: the *Arabidopsis* Subcellular Database. Nucleic Acid Res 35: D213-D218

Heim DR, Roberts JL, Pike PD, Larrinua IM (1989) Mutation of a Locus of *Arabidopsis thaliana* Confers Resistance to the Herbicide Isoxaben. Plant Physiol 90: 146-150

Heim DR, Roberts JL, Pike PD, Larrinua IM (1990a) A Second Locus, Ixr B1 in *Arabidopsis thaliana*, that Confers Resistance to the Herbicide Isoxaben. Plant Physiol 92: 858-861

Heim DR, Skomp JR, Tschabold EE, Larrinua IM (1990b) Isoxaben Inhibits the Synthesis of Acid Insoluble Cell Wall Materials In *Arabidopsis thaliana*. Plant Physiol 93: 695-700

Held MA, Penning B, Brandt AS, Kessans SA, Yong W, Scofield SR, Carpita NC (2008) Small-interfering RNAs from natural antisense transcripts derived from a cellulose synthase gene modulate cell wall biosynthesis in barley. Proc. Natl. Acad. Sci. USA 105: 20534-20539

Hématy K, Höfte H (2008) Novel receptor kinases involved in growth regulation. Current Opinion in Plant Biology 11: 321-328

Hématy K, Sado PE, Van Tuinen A, Rochange S, Desnos T, Balzergue S, Pelletier S, Renou JP, Hofte H (2007) A receptor-like kinase mediates the response of *Arabidopsis* cells to the inhibition of cellulose synthesis. Curr Biol 17: 922-931

Hepler PK, Newcomb EH (1964) Microtubules and fibrils in the cytoplasm of *coleus* cells undergoing secondary wall deposition. J. Cell Biol. 20: 529-533

Hermans PH (1949) Physics and Chemistry of Cellulose Fibres. Elsevier, Amsterdam

Herth W (1983) Arrays of plasma membrane "rosettes" in cellulose microfibril formation of Spirogyra. Planta 159: 347-356

Herth W (1987) Effects of 2,6-DCB on plasma membrane rosettes of wheat root cells. Naturwissenschaften 74: 556-557

Hill J, Nelson E, Tilman D, Polasky S, Tiffany D (2006) Environmental, economic, and energetic costs and benefits of biodiesel and ethanol biofuels. Proc. Natl. Acad. Sci. USA 103: 11206

Himmel ME, Ding SY, Johnson DK, Adney WS, Nimlos MR, Brady JW, Foust TD (2007) Biomass recalcitrance: Engineering plants and enzymes for biofuels production. Science 315: 804-807

Himmelspach R, Williamson RE, Wasteneys GO (2003) Cellulose microfibril alignment recovers from DCB-induced disruption despite microtubule disorganization. The Plant Journal 36: 565-575

Hogetsu T, Shibaoka H, Shimokoriyama M (1974) Involvement of cellulose synthesis in actions of gibberellin and kinetin on cell expansion. 2,6-Dicholorobenzonitrile as a new cellulose-synthesis inhibitor. Plant and Cell Physiology 15: 389-393

Holbrey JD, Seddon KR (1999) Ionic Liquids. Clean Technol Environ Policy 1: 223-236

Holland N, Holland D, Helentjaris T, Dhugga KS, Xoconostle-Cazares B, Delmer DP (2000) A Comparative Analysis of the Plant Cellulose Synthase (*CesA*) Gene Family. Plant Physiol 123: 1313-1324

Hon DNS (1994) Cellulose: a random walk along its historical path. Cellulose 1: 1-25

Honjo G, Watanabe M (1958) Examination of cellulose fiber by the low-tempearture specimen method of electron diffraction and electron microscopy. Nature 181: 326-328

Hu S-Q, Gao Y-G, Tajima K, Sunagawa N, Zhou Y, Kawano S, Fujiwara T, Yoda T, Shimura D, Satoh Y, Munekata M, Tanaka I, Yao M (2010) Structure of bacterial cellulose synthase subunit D octamer with four inner passageways. Proc. Natl Acad. Sci. USA 107: 17957-17961

Hugdahl JD, Morejohn LC (1993) Rapid and Reversible High-Affinity Binding of the Dinitroaniline Herbicide Oryzalin to Tubulin from Zea mays L. Plant Physiol 102: 725-740

Jacob-Wilk D, Kurek I, Hogan P, Delmer DP (2006) The cotton fiber zinc-binding domain of cellulose synthase A1 from *Gossypium hirsutum* displays rapid turnover in vitro and in vivo. Proc. Natl. Acad. Sci. USA 103: 12191-12196

Joshi C (2003) Xylem-specific and tension stress-responsive expression of cellulose synthase genes from aspen trees. Appl Biochem Biotechnol 105: 17-25

Joshi CP, Bhandari S, Ranjan P, Kalluri UC, Liang X, Fujino T, Samuga A (2004) Genomics of cellulose biosynthesis in poplars. New Phytol 164: 53-61

Jouanin L, Goujon T, de Nadai V, Martin MT, Mila I, Vallet C, Pollet B, Yoshinaga A, Chabbert B, Petit-Conil M, Lapierre C (2000) Lignification in transgenic poplars with extremely reduced caffeic acid O-methyltransferase activity. Plant Physiol 123: 1363-1373

Kacuráková M, Capek P, Sasinková V, Wellner N, Ebringerová A (2000) FT-IR study of plant cell wall model compounds: pectic polysaccharides and hemicelluloses. Carbohydrate Polymers 43: 195-203

Kaida R, Satoh Y, Bulone V, Yamada Y, Kaku T, Hayashi T, Kaneko TS (2009) Activation of β-Glucan Synthases by Wall-Bound Purple Acid Phosphatase in Tobacco Cells. Plant Physiol 150: 1822-1830

Kemsley EK (1998) Discriminant analysis of spectroscopic data. John Wiley and Sons, Chichester, UK

Kiedaisch B, Blanton R, Haigler C (2003) Characterization of a novel cellulose synthesis inhibitor. Planta 217: 922-930

Kilpeläinen I, Xie H, King A, Granstrom M, Heikkinen S, Argyropoulos DS (2007) Dissolution of Wood in Ionic Liquids. J Agric Food Chem 55: 9142-9148

Kimura S, Laosinchai W, Itoh T, Cui X, Linder CR, Brown R, Jr (1999) Immunogold labeling of rosette terminal cellulose-synthesizing complexes in the vascular plant vigna angularis. Plant Cell 11

Kirby AR, Gunning AP, Waldron KW, Morris VJ, Ng A (1996) Visualization of plant cell walls by atomic force microscopy. Biophysical Journal 70: 1138-1143

Kohorn BD, Kobayashi M, Johansen S, Riese J, Huang L-F, Koch K, Fu S, Dotson A, Byers N (2006) An *Arabidopsis* cell wall-associated kinase required for invertase activity and cell growth. Plant J. 46: 307-316

Kohorn BD, Johansen S, Shishido A et al (2009) Pectin activation of MAP kinase and gene expression is WAK2 dependent. Plant J 60: 974-982

Koukol J, Conn EE (1961) The Metabolism of Aromatic Compounds in Higher Plants. IV. Purification and Properties of the Phenylalanine Deaminase of *Hordeum vulgare* J Biol Chem 236: 2692-2698

Koyama M, Helbert W, Imai T, Sugiyama J, Henrissat B (1997) Parallel-up structure evidences the molecular directionality during biosynthesis of bacterial cellulose. Proc Natl Acad Sci USA 94: 9091-9095

Kubo M, Udagawa M, Nishikubo N, Horiguchi G, Yamaguchi M, Ito J, Mimura T, Fukuda H, Demura T (2005) Transcription switches for protoxylem and metaxylem vessel formation. Genes Dev. 19: 1855-1860

Kudlicka K, Brown RM (1997) Cellulose and callose biosynthesis in higher plants (I. Solubilization and Seperation of (1→3)- and (1→4)-β-glucan synthase activities from mung bean. Plant Physiol 115: 643-656

Kudlicka K, Brown RM, Li L, Lee JH, Shin H, Kuga S (1995) β-glucan synthesis in the cotton fiber (IV. In vitro assembly of the cellulose 1 allomorph. Plant Physiol 107: 111-123

Kudlicka K, Lee JH, Brown RM, Jr. (1996) A Comparative Analysis of in Vitro Cellulose Synthesis from Cell-Free Extracts of Mung Bean (Vigna radiata, Fabaceae) and Cotton (Gossypium hirsutum, Malvaceae). American Journal of Botany 83: 274-284

Kurek I, Kawagoe Y, Jacob-Wilk D, Doblin M, Delmer D (2002) Dimerization of cotton fiber cellulose synthase catalytic subunits occurs via oxidation of the zinc-binding domains. Proc. Natl. Acad. Sci. USA 99: 11109-11114

Lai Kee Him J, Pelosi L, Chanzy H, Putaux J-L, Bulone V (2001) Biosynthesis of (1→3)-β-d-glucan (callose) by detergent extracts of a microsomal fraction from *Arabidopsis thaliana*. European Journal of Biochemistry 268: 4628-4638

Lai Kee Him J, Chanzy H, Muller M, Putaux J-L, Imai T, Bulone V (2002) In vitro versus in vivo cellulose microfibrils from plant primary wall synthases: structural differences. J Biol Chem 277: 36931-36939

Lally D, Ingmire P, Tong H-Y, He Z-H (2001) Antisense Expression of a Cell Wall-Associated Protein Kinase, WAK4, Inhibits Cell Elongation and Alters Morphology. Plant Cell 13: 1317-1332

Lane D, Wiedemeier A, Peng L, Hofte H, Vernhettes S, Desprez T, Hocart C, Birch R, Baskin T, Burn J (2001) Temperature sensitive alleles of RSW2 link the KORRIGAN endo-1,4-beta-glucanase to cellulose synthesis and cytokinesis in *Arabidopsis thaliana*. Plant Physiol 126: 278 - 288

Lapierre C, Pollet B, Petit-Conil M, Toval G, Romero J, Pilate G, Leple JC, Boerjan W, Ferret V, De Nadai V, Jouanin L (1999) Structural alterations of lignins in transgenic poplars with depressed cinnamyl alcohol dehydrogenase or caffeic acid O-methyltransferase activity have an opposite impact on the efficiency of industrial kraft pulping. Plant Physiol 119: 153-163

Ledbetter MC, Porter KR (1963) A "microtubule" in plant cell fine structure The Journal of Cell Biology 19: 239-250

Lee C, Teng Q, Huang W, Zhong R, Ye Z-H (2009) The F8H glycosyltransferase is a functional paralog of FRA8 involved in glucuronoxylan biosynthesis in *Arabidopsis*. Plant Cell Physiol 50: 812-827

Lee C, Zhong R, Richardson EA, Himmelsbach DS, McPhail BT, Ye Z-H (2007) The PARVUS gene is expressed in cells undergoing secondary wall thickening and is essential for glucuronoxylan biosynthesis. Plant Cell Physiol 48: 1659-1672

Lertpiriyapong K, Sung ZR (2003) The elongation defective mutant of *Arabidopsis* is impaired in the gene encoding a serine-rich secreted protein. Plant Mol Biol 53: 581-595

Levy I, Shani Z, Shoseyov O (2002) Modification of polysaccharides and plant cell wall by endo-1,4-[beta]-glucanase and cellulose-binding domains. Biomol Eng 19: 17-30

Li L, Zhou YH, Cheng XF, Sun JY, Marita JM, Ralph J, Chiang VL (2003) Combinatorial modification of multiple lignin traits in trees through multigene cotransformation. Proc Natl Acad Sci USA 100: 4939-4944

Li X, Weng JK, Chapple C (2008) Improvement of biomass through lignin modification. Plant J 54: 569-581

Liang H, Frost CJ, Wei X, Brown NR, Carlson JE, Tien M (2008) Improved Sugar Release from Lignocellulosic Material by Introducing a Tyrosine-rich Cell Wall Peptide Gene in Poplar. CLEAN – Soil, Air, Water 36: 662-668

Lichtenberg D, Goñi FM, Heerklotz H (2005) Detergent-resistant membranes should not be identified with membrane rafts. Trends in Biochemical Sciences 30: 430-436

Liepman AH, Nairn CJ, Willats WGT, Sorensen I, Roberts AW, Keegstra K (2007) Functional Genomic Analysis Supports Conservation of Function Among Cellulose Synthase-Like A Gene Family Members and Suggests Diverse Roles of Mannans in Plants. Plant Physiol 143: 1881-1893

Liu Y, Schieving F, Stuefer JF, Anten NPR (2007) The effects of mechanical stress and spectral shading on the growth and allocation of ten genotypes of a stoloniferous plant. Annals of Botany 99: 121-130

Loria R, Kers J, Joshi M (2006) Evolution of Plant Pathogenicity in *Streptomyces*. Annu. Rev. Phytopathol. 44: 469-487

Lovins A (2004) How America can free itself of oil - profitably. Fortune 150: 70-72

Lynd LR, Wyman CE, Gerngross TU (1999) Biocommodity Engineering. Biotechnol Prog 15: 777-793

MacKay JJ, O'Malley DM, Presnell T, Booker FL, Campbell MM, Whetten RW, Sederoff RR (1997) Inheritance, gene expression, and lignin characterization in a mutant pine deficient in cinnamyl alcohol dehydrogenase. Proc Natl Acad Sci USA 94: 8255-8260

Madson M, Dunand C, Li X, Verma R, Vanzin GF, Caplan J, Shoue DA, Carpita NC, Reiter W-D (2003) The MUR3 Gene of *Arabidopsis* Encodes a Xyloglucan

Galactosyltransferase That Is Evolutionarily Related to Animal Exostosins. The Plant Cell Online 15: 1662-1670

Mandoli DF, Briggs WR (1982) Optical properties of etiolated plant tissues. Proc Natl Acad Sci USA 79: 2902-2906

Mansfield SD, Mooney C, Saddler JN (1999) Substrate and Enzyme Characteristics that Limit Cellulose Hydrolysis. Biotechnol Prog 15: 804-816

Marrinan HJ, Mann J (1956) Infrared spectra of the crystalline modifications of cellulose. Journal of Polymer Science 21: 301-311

McCann M, Roberts K (1991) Architecture of the primary cell wall. In: Lloyd CW (ed) The Cytoskeletal Basis of Plant Growth and Form. Academic Press, London, pp 109-129

McCarthy MC, Enquist BJ, Kerkhoff AJ (2007) Organ Partitioning and Distribution across the Seed Plants: Assessing the Relative Importance of Phylogeny and Function. International Journal of Plant Sciences 168: 751-761

McCarthy RL, Zhong R, Z-H Y (2009) MYB83 is a direct target of SND1 and acts redundantly with MYB46 in the regulation of secondary cell wall biosynthesis in *Arabidopsis*. Plant Cell 50: 1950-1964

McQueen-Mason S, Cosgrove DJ (1994) Disruption of hydrogen-bonding between plant-cell wall polymers by proteins that induce wall extension. Proc Natl Acad Sci USA 91: 6574-6578

Meinke DW (1985) Embryo-lethal mutants of *Arabidopsis thaliana*: analysis of mutants with a wide range of lethal phases. Theoretical and Applied Genetics 69: 543-552

Mellerowicz EJ, Baucher M, Sundberg B, Boerjan W (2001) Unravelling cell wall formation in the woody dicot stem. Plant Mol. Biol. 47: 239-274

Mellerowicz EJ, Sundberg B (2008) Wood cell walls: biosynthesis, developmental dynamics and their implications for wood properties. Curr Opin Plant Biol 11: 293-300

Mendu V, Griffiths J, Persson S, Stork J, Downie B, Voiniciuc C, Haughn G, DeBolt S (2011) Subfunctionalization of cellulose synthases in seed coat epidermal cells mediate secondary radial wall synthesis and mucilage attachment. Plant Physiology 157: 441-453

Meyer KH, Misch L (1937) Position des atomes dans le nouveau modele spatial de la cellulose. Sur la constitution de la partie cristallisee de la cellulose VI. Helv Chim Acta 20: 232-244

Mitchell RAC, Dupree P, Shewry PR (2007) A Novel Bioinformatics Approach Identifies Candidate Genes for the Synthesis and Feruloylation of Arabinoxylan. Plant Physiol 144: 43-53

Mitsuda N, Iwase A, Yamamoto H, Yoshida M, Seki M, Shinozaki K, Ohme-Takagi M (2007) NAC transcription factors, NST1 and NST3, are key regulators of the formation of secondary walls in woody tissues of *Arabidopsis*. Plant Cell 19: 270-280

Mitsuda N, Seki M, Shinozaki K, Ohme-Takagi M (2005) The NAC transcription factors NST1 and NST2 of Arabidopsis regulate secondary wall thickenings and are required for anther dehiscence. Plant Cell 17: 2993-3006

Mizuta S, Brown RM (1992) Effects of 2,6-dichlorobenzonitrile and Tinopal LPW on the structure of the cellulose synthesizing complexes of Vaucheria hamata. Protoplasma 166: 200-207

Montezinos D, Delmer DP (1980) Characterization of inhibitors of cellulose synthesis in cotton fibers. Planta 148: 305-311

Morejohn LC (1991) The molecular pharmacology of plant tubulin and microtubules. In: Lloyd CW (ed) The Cytoskeletal Basis of Plant Growth and Form. Academic Press, London, pp 29-55

Morris VJ, Gunning AP, Kirby AR (1999) Atomic force microscopy for biologist. Imperial College Press, London

Mosier N, Wyman C, Dale B, Elander R, Lee YY, Holtzapple M, Ladisch M (2005) Features of promising technologies for pretreatment of lignocellulosic biomass. Bioresour. Technol. 96: 673-686

Mouille G, Robin S, Lecomte M, Pagant S, Hofte H (2003) Classification and identification of *Arabidopsis* cell wall mutants using Fourier-Transform InfraRed (FT-IR) microspectroscopy. Plant J 35: 393-404

Mueller S, Brown R, Jr (1980) Evidence for an intramembrane component associated with a cellulose microfibril-synthesizing complex in higher plants. J. Cell Biol. 84: 315-326

Muller M, Hori R, Itoh T, Sugiyama J (2002) X-ray Microbeam and Electron Diffraction Experiments on Developing Xylem Cell Walls. Biomacromolecules 3: 182-186

Mutwil M, Debolt S, Persson S (2008) Cellulose synthesis: a complex complex. Current Opinion in Plant Biology 11: 252-257

Nakashima J, Chen F, Jackson L, Shadle G, Dixon RA (2008) Multi-site genetic modification of monolignol biosynthesis in alfalfa (*Medicago sativa*): effects on lignin composition in specific cell types. New Phytol 179: 738-750

Nass LL, Pereira PAA, Ellis D (2007) Biofuels in Brazil: An Overview. Crop Sci 47: 2228-2237

Newman RH (2004) Homogeneity in cellulose crystallinity between samples of Pinus radiata wood. Holzforschung 58: 91-96

Nicol F, His I, Jauneau A, Vernhettes S, Canut H, Hofte H (1998) A plasma membrane-bound putative endo-1 ;4-beta-D-glucanase is required for normal wall assembly and cell elongation in *Arabidopsis*. EMBO J. 17: 5563-5576

Nidetzky B, Zachariae W, Gercken G, Hayn M, Steiner W (1994) Hydrolysis of cellooligosaccharides by *Trichoderma reesei* cellobiohydrolases: Experimental data and kinetic modeling. Enzyme Microb. Technol. 16: 43-52

Niklas KJ, Cobb ED (2008) Evidence for "diminishing returns" from the scaling of stem diameter and specific leaf area. American Journal of Botany 95: 549-557

Nishikawa S, Ono S (1913) Transmission of X-rays through fibrous, lamellar and granular substances. Proceedings of the Tokyo Mathematico-Physical Society 7: 131-138

Nishiyama Y, Langan P, Chanzy H (2002) Crystal structure and hydrogen-bonding system in cellulose 1β from synchrotron X-ray and neutron fiber diffraction. J Am Chem Soc 124: 9074-9082

Nishiyama Y, Sugiyama J, Chanzy H, Langan P (2003) Crystal structure and hydrogen bonding system in cellulose 1α from synchrotron X-ray and neutron fibre diffraction. J Am Chem Soc 125: 14300-14306

NSF (2008) Breaking the chemical and engineering barriers to lignocellulosic biofuels: Next generation hydrocarbon biorefineries. In: Huber G (ed). University of Massachusetts Amherst, National Science Foundation, Chemical, Bioengineering, Environmental, and Transport Systems Division, Washington, D.C.

Nühse TS, Stensballe A, Jensen ON, Peck SC (2004) Phosphoproteomics of the *Arabidopsis* plasma membrane and a new phosphorylation site database. Plant Cell 16: 2394-2405

O'Connell A, Holt K, Piquemal J, Grima-Pettenati J, Boudet A, Pollet B, Lapierre C, Petit-Conil M, Schuch W, Halpin C (2002) Improved Paper Pulp from Plants with Suppressed Cinnamoyl-CoA Reductase or Cinnamyl Alcohol Dehydrogenase. Transgenic Res 11: 495-503

O'Sullivan A (1997) Cellulose: the structure slowly unravels. Cellulose 4: 173-207
Okuda K, Li L, Kudlicka S, Kuga S, Brown R, Jr (1993) β-Glucan synthesis in the cotton fiber (I. Identification of β-1,4- and β-1,3-glucans synthesized in vitro). Plant Physiol 101: 1131-1142

Oraby H, Venkatesh B, Dale B, Ahmad R, Ransom C, Oehmke J, Sticklen M (2007) Enhanced conversion of plant biomass into glucose using transgenic rice-produced endoglucanase for cellulosic ethanol. Transgenic Res 16: 739-749

Pagant S, Bichet A, Sugimoto K, Lerouxel O, Desprez T, McCann M, Lerouge P, Vernhettes S, Hofte H (2002) KOBITO1 Encodes a Novel Plasma Membrane Protein Necessary for Normal Synthesis of Cellulose during Cell Expansion in *Arabidopsis*. Plant Cell 14: 2001-2013

Pan GX, Spencer L, Leary GJ (1999) Reactivity of Ferulic Acid and Its Derivatives toward Hydrogen Peroxide and Peracetic Acid. J Agric Food Chem 47: 3325-3331

Paredez AR, Persson S, Ehrhardt DW, Somerville CR (2008) Genetic Evidence That Cellulose Synthase Activity Influences Microtubule Cortical Array Organization. Plant Physiol. 147: 1723-1734

Paredez AR, Somerville CR, Ehrhardt DW (2006) Visualization of cellulose synthase demonstrates functional association with microtubules. Science 312: 1491-1495

Park J-Y, Canam T, Kang K-Y, Ellis D, Mansfield S (2008) Over-expression of an *Arabidopsis* family A sucrose phosphate synthase (SPS) gene alters plant growth and fibre development. Transgenic Res 17: 181-192

Pauly M, Keegstra K (2008a) Cell-wall carbohydrates and their modification as a resource for biofuels. Plant J. 54: 559-568

Payen A (1838) Memoire sur la composition du tissu propre des plantes et du ligneux. C R Hebd Seances Acad Sci 7: 1052-1056

Pear JR, Kawagoe Y, Schreckengost WE, Delmer DP, Stalker DM (1996) Higher plants contain homologs of the bacterial celA genes encoding the catalytic subunit of cellulose synthase. Proc. Natl. Acad. Sci. USA 93: 12637-12642

Pedersen JF, Vogel KP, Funnell DL (2005) Impact of Reduced Lignin on Plant Fitness. Crop Sci 45: 812-819

Peña MJ, Zhong R, Zhou G-K, Richardson EA, O'Neil MA, Darvill AG, York WS, Ye Z-Y (2007) *Arabidopsis irregular xylem8* and *irregular xylem9*: implications for the complexity of glucuronoxylan biosynthesis. Plant Cell 19: 546-563

Peng L, Xiang F, Roberts E, Kawagoe Y, Greve LC, Kreuz K, Delmer DP (2001) The Experimental Herbicide CGA 325'615 Inhibits Synthesis of Crystalline Cellulose and Causes Accumulation of Non-Crystalline β-1,4-Glucan Associated with CesA Protein. Plant Physiol 126: 981-992

Perrin RM, DeRocher AE, Bar-Peled M, Zeng W, Norambuena L, Orellana A, Raikhel NV, Keegstra K (1999) Xyloglucan Fucosyltransferase, an Enzyme Involved in Plant Cell Wall Biosynthesis. Science 284: 1976-1979

Persson S, Paredez A, Carroll A, Palsdottir H, Doblin M, Poindexter P, Khitrov N, Auer M, Somerville CR (2007) Genetic evidence for three unique components in primary cell-wall cellulose synthase complexes in *Arabidopsis*. Proc Natl Acad Sci USA 104: 15566-15571

Persson S, Wei H, Milne J, Page GP, Somerville C (2005) Identification of genes required for cellulose synthesis by regression analysis of public microarray data sets. Proc Natl Acad Sci USA 102: 8633-8638

Pieslinger AM, Hoepflinger MC, Tenhaken R (2010) Cloning of Glucuronokinase from *Arabidopsis thaliana*, the Last Missing Enzyme of the myo -Inositol Oxygenase Pathway to Nucleotide Sugars J Biol Chem 285: 2902-2910

Piñeiro G, Jobbágy EG, Baker J, Murray BC, Jackson RB (2009) Set-asides can be better climate investment than corn ethanol. Ecol. Appl. 19: 277-282

Piston F, Uauy C, Fu L, Langston J, Labavitch J, Dubcovsky J (2010) Down-regulation of four putative arabinoxylan feruloyl transferase genes from family PF02458 reduces ester-linked ferulate content in rice cell walls. Planta 231: 677-691

Porchia AC, Sorensen SO, Scheller HV (2002) Arabinoxylan Biosynthesis in Wheat. Characterization of Arabinosyltransferase Activity in Golgi Membranes. Plant Physiol 130: 432-441

Pu Y, Jiang N, Ragauskas AJ (2007) Ionic Liquid as a Green Solvent for Lignin. J Wood Chem Technol 27: 23-33

Puri VP (1984) Effect of crystallinity and degree of polymerization of cellulose on enzymatic saccharification. Biotechnology and Bioengineering 26: 1219-1222

Qian X, Ding S-Y, Nimlos MR, Johnson DK, Himmel ME (2005) Atomic and Electronic Structures of Molecular Crystalline Cellulose Ib: A First-Principles Investigation. Macromolecules 38: 10580-10589

Raes J, Rohde A, Christensen JH, Van de Peer Y, Boerjan W (2003) Genome-Wide Characterization of the Lignification Toolbox in *Arabidopsis*. Plant Physiol 133: 1051

Ragauskas AJ, Williams CK, Davison BH, Britovsek G, Cairney J, Eckert CA, Frederick WJ, Jr., Hallett JP, Leak DJ, Liotta CL, Mielenz JR, Murphy R, Templer R, Tschaplinski T (2006) The Path Forward for Biofuels and Biomaterials. Science 311: 484-489

Rajangam AS, Kumar M, Aspeborg H, Guerriero G, Arvestad L, Pansri P, Brown CJ-L, Hober S, Blomqvist K, Divne C, Ezcurra I, Mellerowicz E, Sundberg B, Bulone V, Teeri TT (2008) MAP20, a Microtubule-Associated Protein in the Secondary Cell Walls of Hybrid Aspen, Is a Target of the Cellulose Synthesis Inhibitor 2,6-Dichlorobenzonitrile. Plant Physiol. 148: 1283-1294

Ralph J, Akiyama T, Kim H, Lu F, Schatz PF, Marita JM, Ralph SA, Reddy MSS, Chen F, Dixon RA (2006) Effects of Coumarate 3-Hydroxylase Down-regulation on Lignin Structure. J Biol Chem 281: 8843-8853

Ralph J, Kim H, Lu F, Grabber JH, Leple JC, Berrio-Sierra J, Derikvand MM, Jouanin L, Boerjan W, Lapierre C (2008) Identification of the structure and origin of a thioacidolysis marker compound for ferulic acid incorporation into angiosperm lignins (and an indicator for cinnamoyl CoA reductase deficiency). Plant J 53: 368-379

Ralph J, Lundquist K, Brunow G, Lu F, Kim H, Schatz PF, Marita JM, Hatfield RD, Ralph SA, Christensen JH, Boerjan W (2004) Lignins: Natural polymers from oxidative coupling of 4-hydroxyphenylpropanoids. Phytochem Rev 3: 29

Ransom C, Balan V, Biswas G, Dale B, Crockett E, Sticklen M (2007) Heterologous Acidothermus cellulolyticus 1,4-β-endoglucanase E1 produced within the corn biomass converts corn stover into glucose. Appl Biochem Biotechnol 137-140: 207-219

Read J, Stokes A (2006) Plant biomaechanics in an ecological context. American Journal of Botany 93: 1546-1565

Reddy MSS, Chen F, Shadle G, Jackson L, Aljoe H, Dixon RA (2005) Targeted down-regulation of cytochrome P450 enzymes for forage quality improvement in alfalfa (*Medicago sativa* L.). Proc Natl Acad Sci USA 102: 16573-16578

Regalbuto JR (2009) Cellulosic Biofuels--Got Gasoline? Science 325: 822-824

Reiter W-D, Chapple C, Somerville CR (1993) Altered Growth and Cell Walls in a Fucose-Deficient Mutant of *Arabidopsis*. Science 261: 1032-1035

Reiter W-D, Chapple C, Somerville CR (1997) Mutants of *Arabidopsis thaliana* with altered cell wall polysaccharide composition. The Plant Journal 12: 335-345

Richmond T (2000) Higher Plant Cellulose Synthases. Genome Biol 1: 30011-30016

Richmond TA, Somerville CR (2000) The Cellulose Synthase Superfamily. Plant Physiology 124: 495-498

Righelato R, Spracklen DV (2007) ENVIRONMENT: Carbon Mitigation by Biofuels or by Saving and Restoring Forests? Science 317: 902

Rippert P, Puyaubert J, Grisollet D, Derrier L, Matringe M (2009) Tyrosine and Phenylalanine Are Synthesized within the Plastids in *Arabidopsis*. Plant Physiol 149: 1251-1260

Robert S, Mouille G, Höfte H (2004) The mechanism and regulation of cellulose synthesis in primary walls: lessons from cellulose-deficient *Arabidopsis* mutants. Cellulose 11: 351-364

Robert S, Raikhel Natasha V, Hicks Glenn R (2008) Powerful Partners: *Arabidopsis* and Chemical Genomics. The *Arabidopsis* Book. The American Society of Plant Biologists, pp 1-16

Roelofsen PA, Houwink AL (1953) Architecture and growth of the primary wall in some plant hairs and in the Phycomyces sporangiophore. Acta Bot Neerl 2: 218-225

Roudier F, Fernandez AG, Fujita M, Himmelspach R, Borner GHH, Schindelman G, Song S, Baskin TI, Dupree P, Wasteneys GO, Benfey PN (2005) COBRA, an *Arabidopsis* Extracellular Glycosyl-Phosphatidyl Inositol-Anchored Protein, Specifically Controls Highly Anisotropic Expansion through Its Involvement in Cellulose Microfibril Orientation. Plant Cell 17: 1749-1763

Rowen JW, Hunt CM, Plyler EK (1947) Absorption Spectra in the Detection of Chemical Changes in Cellulose and Cellulose Derivatives Textile Res J 17: 504-511

Rudolph U, Gross H, Schnepf E (1989) Investigations of the turnover of the putative cellulose-synthesizing particle “rosettes” within the plasma membrane of Funaria hygrometrica protonema cells. Protoplasma 148: 57-69

Saloheimo M, Paloheimo M, Hakola S, Pere J, Swanson B, Nyyssonen E, Bhatia A, Ward M, Penttila M (2002) Swollenin, a *Trichoderma reesei* protein with sequence similarity to the plant expansins, exhibits disruption activity on cellulosic materials. Eur. J. Biochem. 269: 4202-4211

Sampathkumar A, Lindeboom JJ, Debolt S, Gutierrez R, Ehrhardt DW, Ketelaar T, Persson S (2011) Live-cell imaging Reveals Structural Associations between the Actin and Microtubule Cytoskeleton in Arabidopsis. The Plant Cell 23: 2302-2313

Sarén M-P, Serimaa R, Andersson S, Paakkari T, Saranpää P, Pesonen E (2001) Structural Variation of Tracheids in Norway Spruce (*Picea abies* [L.] Karst.). Journal of Structural Biology 136: 101-109

Sarkar P, Bosneaga E, Auer M (2009) Plant cell walls throughout evolution: towards a molecular understanding of their design principles. J. Exp. Bot. 60: 3615-3635

Sato S, Kato T, Kakegawa K, Ishii T, Liu Y-G, Awano T, Takabe K, Nishiyama Y, Kuga S, Sato S, Nakamura Y, Tabata S, Shibata D (2001) Role of the putative membrane-bound endo-1-4-beta-glucanase KORRIGAN in cell elongation and cellulose synthesis in *Arabidopsis thaliana*. Plant Cell Physiol 42: 251-263

Saxena I, Lin F, Brown RM (1990) Cloning and sequencing of the cellulose synthase catalytic subunit gene of *Acetobacter xylinum*. Plant Molecular Biology 15: 673-683

Scalbert A, Monties B, Lallemand J-Y, Guittet E, Rolando C (1985) Ether linkage between phenolic acids and lignin fractions from wheat straw. Phytochemistry 24: 1359-1362

Scheible W-R, Fry B, Kochevenko A, Schindelasch D, Zimmerli L, Somerville S, Loria R, Somerville CR (2003) An *Arabidopsis* Mutant Resistant to Thaxtomin A, a Cellulose Synthesis Inhibitor from *Streptomyces* Species. The Plant Cell 15: 1781-1794

Scheible W-R, Pauly M (2004) Glycosyltransferases and cell wall biosynthesis: novel players and insights. Curr Opin Plant Biol 7: 285-295

Scheible WR, Eshed R, Richmond T, Delmer D, Somerville CR (2001) Modifications of cellulose synthase confer resistance to isoxaben and thiazolidinone herbicides in *Arabidopsis Ixr1* mutants. Proc Natl Acad Sci USA 98: 10079-10084

Scheller HV, Ulvskov P (2010) Hemicelluloses. Annu Rev Plant Biol 61: 263-289

Schindelman G, Morikami A, Jung J, Baskin TI, Carpita NC, Derbyshire P, McCann MC, Benfey PN (2001) COBRA encodes a putative GPI-anchored protein, which is polarly localized and necessary for oriented cell expansion in *Arabidopsis*. Genes Dev 15: 1115-1127

Searchinger T, Heimlich R, Houghton RA, Dong F, Elobeid A, Fabiosa J, Tokgoz S, Hayes D, Yu T-H (2008) Use of U.S. Croplands for Biofuels Increases Greenhouse Gases Through Emissions from Land-Use Change. Science 319: 1238-1240

Sedbrook JC (2004) MAPs in plant cells: delineating microtubule growth dynamics and organization. Current Opinion in Plant Biology 7: 632-640

Segal L, Creely JJ, Martin AE, Conrad CM (1959) An empirical method for estimating the degree of crystallinity of native cellulose using the X-ray diffractometer. Textile Research Journal 29: 786-794

Seifert GJ (2004) Nucleotide sugar interconversions and cell wall biosynthesis: how to bring the inside to the outside. Curr Opin Plant Biol 7: 277-284

Senderowicz AMJ, Kaur G, Sainz E, Laing C, Inman WD, Rodriguez J, Crews P, Malspeis L, Grever MR, Sausville EA, Duncan KLK (1995) Jasplakinolide's Inhibition of the Growth of Prostate Carcinoma Cells In Vitro With Disruption of the Actin Cytoskeleton. Journal of the National Cancer Institute 87: 46-51

Shani Z, Dekel M, Tsabary G, Goren R, Shoseyov O (2004) Growth enhancement of transgenic poplar plants by overexpression of *Arabidopsis thaliana* endo-1,4–β-glucanase (cel1). Mol Breed 14: 321-330

Shaw SL, Kamyar R, Ehrhardt DW (2003) Sustained Microtubule Treadmilling in *Arabidopsis* Cortical Arrays. Science 300: 1715-1718

Shen H, Yin Y, Chen F, Xu Y, Dixon R (2009) A Bioinformatic Analysis of NAC Genes for Plant Cell Wall Development in Relation to Lignocellulosic Bioenergy Production. BioEnergy Res 2: 217-232

Shoseyov O, Shani Z, Levy I (2006) Carbohydrate Binding Modules: Biochemical Properties and Novel Applications. Microbiol Mol Biol Rev 70: 283-295

Singh S, Fischer U, Singh M, Grebe M, Marchant A (2008) Insight into the early steps of root hair formation revealed by the *procuste1* cellulose synthase mutant of *Arabidopsis thaliana*. BMC Plant Biol 8: 57

Smidansky E, Martin J, Hannah C, Fischer A, Giroux M (2003) Seed yield and plant biomass increases in rice are conferred by deregulation of endosperm ADP-glucose pyrophosphorylase. Planta 216: 656-664

Smith AM, Stitt M (2007) Coordination of carbon supply and plant growth. Plant Cell Environ 30: 1126-1149

Smith VC, Ennos AR (2003) The effects of air flow and stem flexure on the mechanical and hydraulic properties of the stems of sunflowers Helianthus annus L. Journal of Experimental Botany 54: 845-849

Somerville C (2006) Cellulose Synthesis in Higher Plants. Annu Rev Cell Dev Biol 22: 53-78

Somerville C, Bauer S, Brininstool G, Facette M, Hamann T, Milne J, Osborne E, Paredez A, Persson S, Raab T, Vorwerk S, Youngs H (2004) Toward a Systems Approach to Understanding Plant Cell Walls. Science 306: 2206-2211

Sorensen A, Teller PJ, Hilstrom T, Ahring BK (2008) Hydrolysis of Miscanthus for bioethanol production using dilute acid presoaking combined with wet explosion pre-treatment and enzymatic treatment. Bioresour Technol 99: 6602-6607

Spring DR (2005) Chemical genetics to chemical genomics: small molecules offer big insights. Chem Soc Rev 34: 472-482

Staudinger H (1926) Die Chemie der organischen hochmolekularen Stoffe im Sinne der Kekuléschen Strukturlehre. Ber Deut Chem Ges 59: 3019

Sticklen MB (2008) Plant genetic engineering for biofuel production: towards affordable cellulosic ethanol. Nat. Rev. Genet. 9: 433-443

Stone B, Clarke A (1992) Chemistry and biology of 1,3-β-glucans. La Trobe University Press, Melbourne, Australia

Stork J, Harris D, Griffiths J, Williams B, Beisson F, Li-Beisson Y, Mendu V, Haughn G, DeBolt S (2010) CELLULOSE SYNTHASE9 Serves a Nonredundant Role in Secondary Cell Wall Synthesis in *Arabidopsis* Epidermal Testa Cells. Plant Physiol 153: 580-589

Stork J, Montross M, Smith R, Schwer L, Chen W, Reynolds M, Phillips T, Coolong T, DeBolt S (2009) Regional examination shows potential for native feedstock options for cellulosic biofuel production. Glob Chang Biol Bioenergy: 10

Stubiçar N, Šmit I, Stubiçar M, Tonejc A, Jánosi A, Schurz J, Zipper P (1998) An X-ray Diffraction Study of the Crystalline to Amorphous Phase Change in Cellulose During High-Energy Dry Ball Milling. Holzforschung 52: 455-458

Šturcová A, His I, Apperley DC, Sugiyama J, Jarvis MC (2004) Structural Details of Crystalline Cellulose from Higher Plants. Biomacromolecules 5: 1333-1339

Sugimoto K, Himmelspach R, Williamson RE, Wasteneys GO (2003) Mutation or drug-dependent microtubule disruption causes radial swelling without altering parallel cellulose microfibril deposition in *Arabidopsis* root cells. Plant Cell 15: 1414-1429

Sullivan JT (1955) Cellulose and Lignin in Forage Grasses and Their Digestion Coefficients. J Anim Sci 14: 710-717

Swenson NG, Enquist BJ (2008) The relationship between stem and branch wood specific gravity and the ability of each measure to predict leaf area. American Journal of Botany 95: 516-519

Szyjanowicz PMJ, McKinnon I, Taylor NG, Gardiner J, Jarvis MC, Turner SR (2004) The irregular xylem 2 mutant is an allele of korrigan that affects the secondary cell wall of *Arabidopsis thaliana*. The Plant Journal 37: 730-740

Tan H, Yang R, Sun W, Wang S (2009) Peroxide-Acetic Acid Pretreatment To Remove Bagasse Lignin Prior to Enzymatic Hydrolysis. Ind Eng Chem Res 49: 1473-1479

Tanaka K, Murata K, Yamazaki M, Onosato K, Miyao A, Hirochika H (2003) Three Distinct Rice Cellulose Synthase Catalytic Subunit Genes Required for Cellulose Synthesis in the Secondary Wall. Plant Physiol 133: 73-83

Taylor NG (2007) Identification of cellulose synthase AtCesA7 (IRX3) in vivo phosphorylation sites—a potential role in regulating protein degradation. Plant Mol. Biol. 64: 161-171

Taylor NG, Laurie S, Turner SR (2000) Multiple Cellulose Synthase Catalytic Subunits Are Required for Cellulose Synthesis in *Arabidopsis*. Plant Cell 12: 2529-2540

Taylor NG, Scheible WR, Cutler S (1999) The *irregular xylem3* locus of *Arabidopsis* encodes a cellulose synthase required for secondary cell wall synthesis. Plant Cell 11: 769-779

Taylor NG, Gardiner JC, Whiteman R, Turner SR (2004) Cellulose synthesis in the *Arabidopsis* secondary cell wall. Cellulose 11: 329-338

Taylor NG, Howells RM, Huttly AK, Vickers K, Turner SR (2003) Interactions among three distinct CesA proteins essential for cellulose synthesis. Proc Natl Acad Sci USA 100: 1450-1455

Teeäär R, Serimaa R, Paakkarl T (1987) Crystallinity of cellulose, as determined by CP/MAS NMR and XRD methods. Polymer Bulletin 17: 231-237

Telewski FW (1989) Structure and function of flexure wood in *Abies fraseri*. Tree Physiology 5: 113-121

Teymouri F, Alizadeh H, Laureano-Pérez L, Dale B, Sticklen M (2004) Effects of ammonia fiber explosion treatment on activity of endoglucanase from *Acidothermus cellulolyticus* in transgenic plant. Appl Biochem Biotechnol 116: 1183-1191

Thimm JC, Burritt DJ, Ducker WA, Melton LD (2000) Celery (*Apium graveolens* L.) parenchyma cell walls examined by atomic force microscopy: effect of dehydration on cellulose microfibrils. Planta 212: 25-32

Tian G-W, Mohanty A, Chary SN, Li S, Paap B, Drakakaki G, Kopec CD, Li J, Ehrhardt D, Jackson D, Rhee SY, Raikhel NV, Citovsky V (2004) High-Throughput Fluorescent Tagging of Full-Length *Arabidopsis* Gene Products in Planta. Plant Physiol. 135: 25-38

Tilman D, Reich PB, Knops JMH (2006) Biodiversity and ecosystem stability in a decade-long grassland experiment. Nature 441: 629

Timmers J, Vernhettes S, Desprez T, Vincken J-P, Visser RGF, Trindade LM (2009) Interactions between membrane-bound cellulose synthases involved in the synthesis of the secondary cell wall. FEBS Letters 583: 978-982

Triplett B, Timpa J (1995) Characterization of cell-wall polymers from cotton ovule culture fiber cells by gel permeation chromatography. In Vitro Cell Dev Biol Plant 31: 171-175

Turner SR, Somerville CR (1997) Collapsed Xylem Phenotype of *Arabidopsis* Identifies Mutants Deficient in Cellulose Deposition in the Secondary Cell Wall. Plant Cell 9: 689-701

Updegraff DM (1969) Semimicro determination of cellulose inbiological materials. Analytical Biochemistry 32: 420-424

Urbanowicz BR, Catala C, Irwin D, Wilson DB, Ripoll DR, Rose JKC (2007) A tomato endo-beta-1,4-glucanase, SlCel9C1, represents a distinct subclass with a new family of carbohydrate binding modules (CBM49). J Biol Chem 282: 12066-12074

Valdivia RH, Schekman R (2003) The yeasts Rho1p and Pkc1p regulate the transport of chitin synthase III (Chs3p) from internal stores to the plasma membrane. Proc. Natl. Acad. Sci. USA 100: 10287-10292

van der Wel NN, Putman CAJ, van Noort SJT, de Grooth BG, Emons AMC (1996) Atomic force microscopy of pollen grains, cellulose microfibrils, and protoplasts. Protoplasma 194: 29-39

Vanholme R, Demedts B, Morreel K, Ralph J, Boerjan W (2010) Lignin Biosynthesis and Structure. Plant Physiol 153: 895-905

Vergara CE, Carpita NC (2001) Beta-D-Glycan synthases and the *CesA* gene family: lessons to be learned from the mixed-linkage (1 -> 3),(1 -> 4)beta-D-glucan synthase. Plant Mol. Biol. 47: 145-160

Verica JA, He Z-H (2002) The Cell Wall-Associated Kinase (WAK) and WAK-Like Kinase Gene Family. Plant Physiol. 129: 455-459

Vermerris W, Saballos A, Ejeta G, Mosier NS, Ladisch MR, Carpita NC (2007) Molecular Breeding to Enhance Ethanol Production from Corn and Sorghum Stover. Crop Sci 47: S-142-S-153

Viëtor RJ, Newman RH, Ha M-A, Apperley DC, Jarvis MC (2002) Conformational features of crystal-surface cellulose from higher plants. The Plant Journal 30: 721-731

Vile D, Garnier É, Shipley B, Laurent G, Navas M-L, Roumet C, Lavorel S, Díaz S, Hodgson JG, Lloret F, Midgley GF, Poorter H, Rutherford MC, Wilson PJ, Wright IJ (2005) Specific leaf area and dry matter content estimate thickness in laminar leaves. Annals of Botany 96: 1129-1136

Vispute TP, Zhang H, Sanna A, Xiao R, Huber G (2010) Renewable chemical commodity feedstocks from integrated catalytic processing of pyrolysis oils. Science 330: 1222-1227

Vitousek PM, Turner DR, Kitayama K (1995) Foliar Nutrients During Long-Term Soil Development in Hawaiian Montane Rain Forest. Ecology 76: 712-720

Wagner TA, Kohorn BD (2001) Wall-Associated Kinases Are Expressed throughout Plant Development and Are Required for Cell Expansion. Plant Cell 13: 303-318

Wang J, Howles PA, Cork A, Birch R, Williamson RE (2006) Chimeric proteins suggest that the catalytic and/or C-terminal domains give CesA1 and CesA3 access to their specific sites in the cellulose synthase of primary walls. Plant Physiol 142: 685-695

Wasteneys GO, Galway ME (2003) Remodeling the cytoskeleton for growth and form: An Overview with Some New Views. Annual Review of Plant Biology 54: 691-722

Wasteneys GO, Yang Z (2004) New Views on the Plant Cytoskeleton. Plant Physiology 136: 3884-3891

Webb M, Jouannic S, Foreman J, Linstead P, Dolan L (2002) Cell specification in the *Arabidopsis* root epidermis requires the activity of ECTOPIC ROOT HAIR 3 , a katanin-p60 protein. Development 129: 123-131

Weimer PJ, Hackney JM, French AD (1995) Effects of chemical treatments and heating on the crystallinity of celluloses and their implications for evaluating the effect of crystallinity on cellulose biodegradation. Biotechnology and Bioengineering 48: 169-178

Weng J-K, Li X, Stout J, Chapple C (2008) Independent origins of syringyl lignin in vascular plants. Proc Natl Acad Sci USA 105: 7887-7892

Wightman R, Marshall R, Turner SR (2009) A Cellulose Synthase-Containing Compartment Moves Rapidly Beneath Sites of Secondary Wall Synthesis. Plant Cell Physiol. 50: 584-594

Wightman R, Turner SR (2008) The roles of the cytoskeleton during cellulose deposition at the secondary cell wall. Plant J. 54: 794-805

Willats W, McCartney L, Mackie W, Knox J (2001) Pectin: cell biology and prospects for functional analysis. Plant Mol. Biol. 47: 9-27

Williamson RE, Burn JE, Birch R, Baskin TI, Arioli T, Betzner AS, Cork A (2001) Morphology of a cellulose-deficient mutant of *Arabidopsis thaliana*. Protoplasma 215: 116-127

Woodcock DW, Shier AD (2003) Does canopy position affect wood specific gravity in temperate forest trees? Annals of Botany 91: 529-537

Wright IJ, Ackerly DD, Bongers F, Harms KE, Ibarra-Manriquez G, Paz H, Pitman NCA, Poorter L, Silman MR, Vriesendorp CF, Webb CO, Westobu M, Wright SJ (2007) Relationship among ecologically important dimensions of plant trait variation in seven neotropical forests. Annals of Botany 99: 1003-1015

Wright IJ, Clifford HT, Kidson R, Reed ML, Rice BL, Westoby M (2000) A survey of seed and seedling characters in 1744 Australian dicotyledon species: cross-species trait correlations and correlated trait-shifts within evolutionary lineages. Biological Journal of the Linnean Society 69: 521-547

Wright IJ, Reich PB, Westoby M, Ackerly DD, Baruch Z, Bongers F, Cavender-Bares J, Chapin T, Cornelissen JHC, Diemer M, Flexas J, Garnier E, Groom PK, Gulias J, Hikosaka K, Lamont BB, Lee T, Lee W, Lusk C, Midgley JJ, Navas M-L, Niinemets U, Oleksyn J, Osada N, Poorter H, Poot P, Prior L, Pyankov VI, Roumet C, Thomas SC, Tjoelker MG, Veneklaas EJ, Villar R (2004) The worldwide leaf economics spectrum. Nature 428: 821-827

Wu A-M, Hörnblad E, Voxeur A, Gerber L, Rihouey C, Lerouge P, Marchant A (2010) Analysis of the *Arabidopsis* IRX9/IRX9-L and IRX14/IRX14-L pairs of glycosyltransferase genes reveals critical contributions to biosynthesis of the hemicellulose glucuronoxylan. Plant Physiol 153: 542-554

Wu A-M, Rihouey C, Seveno M, Hörnblad E, Singh SK, Matsunaga T, Ishii T, Lerouge P, Marchant A (2009) The *Arabidopsis* IRX10 and IRX10-LIKE glycosyltransferases are critical for glucuronoxylan biosynthesis during secondary cell wall formation. Plant J 57: 718-731

Yang C, Xu Z, Song J, Conner K, Vizcay Barrena G, Wilson ZA (2007) *Arabidopsis* MYB26/MALE STERILE35 Regulates Secondary Thickening in the Endothecium and Is Essential for Anther Dehiscence. Plant Cell 19: 534-548

Yoneda A, Higaki T, Kutsuna N, Kondo Y, Osada H, Hasezawa S, Matsui M (2007) Chemical Genetic Screening Identifies a Novel Inhibitor of Parallel Alignment of Cortical Microtubules and Cellulose Microfibrils. Plant Cell Physiol 48: 1393-1403

Yoneda A, Ito T, Higaki T, Kutsuna N, Saito T, Ishimizu T, Osada H, Hasezawa S, Matsui M, Demura T (2010) Cobtorin target analysis reveals that pectin functions in the deposition of cellulose microfibrils in parallel with cortical microtubules. The Plant Journal 64: 657-667

York WS, Darvill AG, McNeil M, Stevenson TT, Albersheim P (1986) Isolation and characterization of plant cell walls and cell wall components. In: Arthur Weissbach HW (ed) Methods in Enzymology. Academic Press, pp 3-40

York WS, O'Neill MA (2008) Biochemical control of xylan biosynthesis -- which end is up? Current Opinion in Plant Biology 11: 258-265

Yoshida M, Liu Y, Uchida S, Kawarada K, Ukagami Y, Ichinose H, Kaneko S, Fukuda K (2008) Effects of Cellulose Crystallinity, Hemicellulose, and Lignin on the Enzymatic Hydrolysis of Miscanthus sinensis to Monosaccharides. Bioscience, Biotechnology, and Biochemistry 72: 805-810

Zablackis E, York WS, Pauly M, Hantus S, Reiter W-D, Chapple CCS, Albersheim P, Darvill A (1996) Substitution of L-Fucose by L-Galactose in Cell Walls of *Arabidopsis mur1*. Science 272: 1808-1810

Zabotina OA, Malm E, Drakakaki G, Bulone V, Raikhel N (2008a) Identification and Preliminary Characterization of a New Chemical Affecting Glucosyltransferase Activities Involved in Plant Cell Wall Biosynthesis. Mol Plant 1: 977-989

Zabotina OA, Van De Ven WTG, Freshour G, Drakakaki G, Cavalier D, Mouille G, Hahn MG, Keegstra K, Raikhel NV (2008b) *Arabidopsis* XXT5 gene encodes a putative α-1,6-xylosyltransferase that is involved in xyloglucan biosynthesis. The Plant Journal 56: 101-115

Zakzeski J, Bruijnincx PCA, Jongerius AL, Weckhuysen BM (2010) The Catalytic Valorization of Lignin for the Production of Renewable Chemicals. Chem Rev 110: 3552-3599

Zeng W, Chatterjee M, Faik A (2008) UDP-Xylose-stimulated glucuronyltransferase activity in wheat microsomal membranes: characterization and role in glucurono(arabino)xylan biosynthesis. Plant Physiol 147: 78-91

Zhang YHP, Lynd LR (2004) Toward an aggregated understanding of enzymatic hydrolysis of cellulose: Noncomplexed cellulase systems. Biotechnol Bioeng 88: 797-824

Zhao T-Y, Thacker R, Corum JW, Snyder JC, Meeley RB, Obendorf RL, Downie B (2004) Expression of the maize GALACTINOL SYNTHASE gene family: (I) Expression of two different genes during seed development and germination. Physiologia Plantarum 121: 634-646

Zhong R, Burk DH, Morrison WH, Ye Z-H (2002a) A Kinesin-Like Protein Is Essential for Oriented Deposition of Cellulose Microfibrils and Cell Wall Strength. The Plant Cell Online 14: 3101-3117

Zhong R, Demura T, Ye Z-H (2006) SND1, a NAC Domain Transcription Factor, Is a Key Regulator of Secondary Wall Synthesis in Fibers of *Arabidopsis*. Plant Cell 18: 3158-3170

Zhong R, Kays SJ, Schroeder BP, Ye Z-H (2002b) Mutation of a Chitinase-Like Gene Causes Ectopic Deposition of Lignin, Aberrant Cell Shapes, and Overproduction of Ethylene. Plant Cell 14: 165-179

Zhong R, Morrison WH, III, Freshour GD, Hahn MG, Ye Z-H (2003) Expression of a Mutant Form of Cellulose Synthase AtCesA7 Causes Dominant Negative Effect on Cellulose Biosynthesis. Plant Physiol 132:786-795

Zhong R, Peña MJ, Zhou G-K, Nairn CJ, Wood-Jones A, Richardson EA, Morrison WH, III, Darvill AG, York WS, Ye Z-H (2005) Arabidopsis Fragile Fiber8, Which Encodes a Putative Glucuronyltransferase, Is Essential for Normal Secondary Wall Synthesis. Plant Cell 17: 3390-3408

Zhong R, Richardson EA, Ye ZH (2007a) The MYB46 transcription factor is a direct target of SND1 and regulates secondary wall biosynthesis in *Arabidopsis*. Plant Cell 19: 2776-2792

Zhong R, Ye Z-H (2007) Regulation of cell wall biosynthesis. Curr. Opin. Plant Biol. 10: 564-572

Zhong RQ, Richardson EA, Ye ZH (2007b) Two NAC domain transcription factors, SND1 and NST1, function redundantly in regulation of secondary wall synthesis in fibers of *Arabidopsis*. Planta 225: 1603-1611

Zhou J, Lee C, Zhong R, Ye Z-H (2009) MYB58 and MYB63 Are Transcriptional Activators of the Lignin Biosynthetic Pathway during Secondary Cell Wall Formation in *Arabidopsis*. Plant Cell 21: 248-266

Zhou Q, Baumann MJ, Piispanen PS, Teeri TT, Brumer H (2006) Xyloglucan and xyloglucan endo-transglycosylases (XET): Tools for ex vivo cellulose surface modification. Biocatalysis Biotransformation 24

Zhou Q, Greffe L, Baumann MJ, Malmström E, Teeri TT, Brumer H (2005) The use of xyloglucan as a molecular anchor for the elaboration of polymers from cellulose surfaces: a general route for the design of biocomposites. Macromolecules 38: 3547-3549

Zhou Q, Rutland MW, Teeri TT, Brumer H (2007) Xyloglucan in cellulose modification. Cellulose 14: 625–641

Ziegelhoffer T, Raasch JA, Austin-Phillips S (2001) Dramatic effects of truncation and sub-cellular targeting on the accumulation of recombinant microbial cellulase in tobacco. Mol Breed 8: 147-158

Ziegler MT, Thomas SR, Danna KJ (2000) Accumulation of a thermostable endo-1,4-β-D-glucanase in the apoplast of *Arabidopsis thaliana* leaves. Mol Breed 6: 37-46

Zuo J, Niu Q-W, Nishizawa N, Wu Y, Kost B, Chua N-H (2000) KORRIGAN, an Arabidopsis Endo-1,4-{beta}-Glucanase, Localizes to the Cell Plate by Polarized Targeting and Is Essential for Cytokinesis. Plant Cell 12: 1137-1152

Vita

Darby M. Harris
Date of Birth: November 2, 1971
Place of Birth: Durham, North Carolina

Education

Ph.D. Candidate in Plant Physiology/Molecular Biology/Biochemistry, University of Kentucky, Lexington, KY
M.S. Biology, 2005, Western Carolina University, Cullowhee, NC
B.A. *magna cum laude*, French/minor History, 2001, Western Carolina University, Cullowhee, NC
B.S. Biology/minor Chemistry, 1997, Western Carolina University, Cullowhee, NC

Employment

2008 – present	Ph.D. Candidate and Research Assistant in the laboratory of Dr. Seth DeBolt, University of Kentucky, Lexington, KY
2007 – 2008	Examination Evaluator, Measurement Incorporated, Durham, NC
2005 – 2006	Part-time Instructor, Biology Department, Western Carolina University, Cullowhee, NC
2004 – 2005	M.S. Student and Teaching Assistant, Biology Department, Western Carolina University, Cullowhee, NC
2004	Upward Bound Summer Science Instructor, Sylva, NC
2003 – 2004	Customer Service Rep, Farnam Custom Products, Arden, NC
2002	Upward Bound Summer Science Instructor, Sylva, NC
2001 – 2002	Biology Teacher, Smoky Mt High School, Sylva, NC
2001	French Instructor, SW Community College, Sylva, NC
2000 – 2001	Teaching Assistant, Modern Foreign Languages Department, Western Carolina University, Cullowhee, NC

Publications (peer-reviewed)

°First author or co-first authorship

Harris D°, Corbin K, Wang T, Gutierrez R, Bertolo A, Petti C, Smilgies D-M, Estevez JM, Bonetta D, Urbanowicz B, Ehrhardt D, **Somerville C, Rose JKC, Hong M, DeBolt S** (2011) Forward chemical genetic dissection of cellulose biosynthesis in plants. Proceeding of the National Academy of Sciences, U.S.A. (In review)

Mendu V, Stork S, Harris D, DeBolt S (2011) Cellulose synthesis in two secondary cell wall processes in a single cell type. Plant Signaling and Behavior **6**: 1638-1643.

Joshi C, Thammannagowda S, Fujino T, Gou J-Q, Avci U, Haigler C, McDonnell L, Mansfield S, Mengesha B, Carpita N, Harris D, DeBolt S, Peter G (2011) Perturbation of wood cellulose synthesis causes pleiotropic effects in transgenic Aspen. Molecular Plant **4**: 331-345.

Stork J°, Harris D°, Griffiths J, Williams B, Beisson F, Li-Beissons Y, Mendu V,

Haughn G, DeBolt S (2010) CELLULOSE SYNTHASE9 serves a nonredundant role in secondary cell wall synthesis in *Arabidopsis* epidermal testa cells. Plant Physiology **153**: 580-589.

Harris D°, Bulone V, Ding S-Y, Debolt S (2010) Tools for cellulose analysis in plant cell walls. Plant Physiology **153**: 420-426.

Harris D° & DeBolt S (2010) Synthesis, regulation and utilization of lignocellulosic biomass. Plant Biotechnology Journal **8**: 244-262.

Harris D°, Stork J, DeBolt S (2009) Genetic modification in cellulose-synthase reduces crystallinity and improves biochemical conversion to fermentable sugar. Global Change Biology: Bioenergy **1**: 51-61.

Harris D° & DeBolt S (2008) Relative crystallinity of plant biomass: studies on assembly, adaptation and acclimation. PLoS ONE **3**: e2897.

Harris DM°, Myrick TL, Rundle SJ (1999) The *Arabidopsis* homolog of yeast Tap42 and mammalian α4 binds to the catalytic subunit of protein phosphatase 2A and is induced by chilling. Plant Physiology **121**: 609-617.

Latorre KA, Harris DM, Rundle SJ (1997) Differential expression of three *Arabidopsis* genes encoding the B' regulatory subunit of protein phosphatase 2A. European Journal of Biochemistry **245:** 156-163.

Book Chapters

Harris D° & DeBolt S (2011) The use of small molecules to dissect and manipulate the cytoskeleton and biosynthesis of the plant cell wall. In *Plant Chemical Biology* (Overvoorde P & Audenaert D, eds), John Wiley & Sons, Ltd, Chichester, UK. (In press).

Harris D°, Petti C, DeBolt S (2011) The synthesis, regulation and modification of lignocellulosic biomass as a resource for biofuels and bioproducts. In *Advanced Biofuels and Bioproducts* (Lee JW, ed), New York: Springer Science+Business Media, LLC (In press).

Patent

DeBolt S, Stork J, Harris D (Provisional patent UKRF 1595) Invention title: Improved conversion of lignocellulosic biomass to fermentable sugars by altering the high-order structure of cellulose via genetic modification of cellulose synthase genes (2008).

Presentations/Abstracts/Awards

Seminar Speaker, Ph.D. Exit Seminar, Plant Physiology Seminar Series, University of Kentucky, Department of Plant and Soil Sciences, Lexington, KY, November 9, 2011. Presentation title: “Forward chemical genetic dissection of cellulose biosynthesis in plants.”

Seminar Speaker, Plant Physiology Seminar Series, University of Kentucky, Department of Plant and Soil Sciences, Lexington, KY, April 8, 2011. Presentation title: "Cellulose microfibril structural variants in *Arabidopsis*."
Invited Seminar Speaker, Paul Burton Seminar Series, Western Carolina University, Department of Biology, Cullowhee, NC, Oct 1, 2010. Presentation title: "The molecular and chemical dissection of cellulose biosynthesis and its application towards biofuel and biochemical production."
Seminar Speaker, The University of Kentucky Center for Ecology, Evolution and Behavior Spring Research Symposium, Lexington, KY, May 14, 2010. Presentation title: "Modifications of lignocellulosic biomass for conversion to biofuels and bioproducts."
Seminar Speaker and Best Presentation Award Recipient, University of Kentucky Graduate Student Interdisciplinary Conference, Lexington, KY, April 9, 2010. Presentation title: "Genetic modification in cellulose-synthase reduces crystallinity and improves biochemical conversion to fermentable sugar."
Gamma Sigma Delta Inductee, Agricultural Honor Society, Kentucky Chapter, March 2010.
Student Voice Representative and Travel Grant Recipient for the University of Kentucky College of Agriculture, National Agricultural Biotechnology Conference 21 "Adapting Agriculture to Climate Change" at the University of Saskatchewan, Saskatoon, Saskatchewan Canada, June 24-26, 2009.
***Seminar Speaker and Most Outstanding Graduate Student Presentation Award Recipient**, The Plant Cell Walls Gordon-Kenan Graduate Research Seminar held in conjunction with the 2009 Plant Cell Walls Gordon Research Conference at Bryant University, Smithfield, RI, Aug 2-7, 2009. Presentation title: "Genetic modification in cellulose-synthase reduces crystallinity and improves biochemical conversion to fermentable sugar."
*This is the #1 International Conference in the field of Plant Cell Wall research
Seminar Speaker, Plant Physiology Seminar Series, University of Kentucky, Department of Plant and Soil Sciences, Lexington, KY, Feb 6, 2009. Presentation title: "Molecular and chemical dissection of cellulose biosynthesis."
Student Voice Representative and Travel Grant Recipient for the University of Kentucky College of Agriculture, National Agricultural Biotechnology Conference 20 "Reshaping American Agriculture to Meet its Biofuel and Biopolymer Roles" at The Ohio State University, Columbus Ohio, June 3-5, 2008.
Masters Thesis Presentation/Defense, Department of Biology, Western Carolina University, Cullowhee, NC, April 15, 2005. Presentation title: "The identification and characterization of a novel protein that interacts with the catalytic subunit of *Arabidopsis thaliana* protein phosphatase 2A." Advisor: Dr. Sabine J. Rundle
Outstanding Graduate Student Teaching Award 2004-2005, Department of Biology, Western Carolina University, Cullowhee, NC.
Graduate Research Conference Presenter, Thesis Research, Western Carolina University, Cullowhee, NC, March 19, 1998.
Poster Presenter, American Society of Plant Physiology Conference, Madison, Wisconsin. June 27-July 1, 1998. Poster title: "Differential expression of three *Arabidopsis* genes encoding the B' regulatory subunit of protein phosphatase 2A."

Undergraduate Research Student Mentoring

The DeBolt Lab NSF-funded Mentoring Program exposes high school seniors and college undergraduates to scientific research while also allowing graduate students and post-docs a chance to develop mentoring skills. Students mentored directly by me:

Megan Reynolds, Northern Kentucky University, Summer 2008
Rachael Strang, Hanover College, Summer 2009
Kendall Corbin, University of Kentucky Agricultural Biotechnology Program. Fall 2009-Spring 2011
Eliana Geissingworth, Sayre High School, Lexington, KY, Summer 2010
Rachel Crowley, Dunbar High School, Lexington, KY, Spring 2011
Undergraduate Presentations/Research/Awards

Most Outstanding French Major 1999-2000, Department of Modern Foreign Languages, Western Carolina University.
Phi Sigma Iota Inductee, International Foreign Language Honor Society, Western Carolina University Chapter, March 2000.
Undergraduate Research Conference Presentation: Albert Camus: L'Étranger, Department of Modern Foreign Languages, Spring 2000, Western Carolina University
Undergraduate Research Conference Presentation: Intellectual Reparations: The Exploitation and Denial Programs of German Science and Technology after World War II, Department of History, Spring 2000, Western Carolina University.
Undergraduate Senior Thesis: Detection of Protein-Protein Interaction of the Catalytic Subunit of *Arabidopsis* PP2A and Novel Subunits and/or Substrates, Department of Biology, Spring 1997, Western Carolina University
Undergraduate Research Conference Presentation: Senior Thesis Research, Department of Biology, Spring 1997, Western Carolina University
Research in Chemistry: Isolation and Characterization of a Natural Product: Maltol from Fraser Fir Foliage, Department of Chemistry, Fall 1996, Western Carolina University.
Undergraduate Research Grant Recipient, Department of Biology, 1996-1997, Western Carolina University.
Organic Chemistry Tutor, Department of Chemistry, 1996-1997, Western Carolina University.
Genetics Tutor, Department of Biology via Student Support Services, 1996-1997, Western Carolina University.
General Chemistry Tutor, Department of Chemistry, 1995-1996, Western Carolina University.